THE MAGNETISM AND COORDINATION CHEMISTRY OF MONONUCLEAR AND POLYNUCLEAR COMPLEXES OF COPPER(II) AND OTHER FIRST ROW TRANSITION METAL IONS DERIVED FROM OPEN-CHAIN DIAZINE (N-N) LIGANDS

ZHIQIANG XU

The Magnetism and Coordination Chemistry of Mononuclear and Polynuclear Complexes of Copper(II) and other First Row Transition Metal Ions Derived from Open-Chain Diazine (N-N) Ligands

by

Zhiqiang Xu, B.Sc., M.Sc.

A thesis submitted to the

School of Graduate Studies

in partial fulfilment of the

requirements for the degree

Doctor of Philosophy

Department of Chemistry

Memorial University of Newfoundland

St. John's **Newfoundland**

ABSTRACT

This thesis describes the structures and the magnetic properties of the first row transition metal complexes containing open-chain diazine (N-N) moieties. The purpose of the research is to establish a magnetostructural correlation involving the N-N single bond bridge and to investigate the coordination chemistry of open-chain diazine ligands to the first row transition metal ions. A relevant literature search is presented in Chapter 1.

Chapter 1 describes a general introduction to magnetic exchange in polynuclear copper complexes and a general review of the coordination chemistry of diazine (N_2) bridged complexes. In Chapter 2, seventeen dicopper(II) complexes with five open-chain diazine ligands (PAHAP, PMHAP, PHMAP, PHAAP and PYPZ) are reported, in which the two copper(II) centers are bridged by a single N-N bond only. The X-ray structures of one ligand and twelve dinuclear copper(II) complexes were determined. Changing the ligands, together with varying the coligands leads to a situation where the dihedral angle between the copper planes can be varied from 75° to 168.5°. For small angles (less than 80°) ferromagnetic coupling prevails, whereas at larger angles antiferromagnetic exchange is observed between the copper(II) centers. The exchange integrals (-2J) vary from -24.4 to 210 cm^{-1}. This is associated with the degree of alignment of the nitrogen *p* orbitals in the diazine bridge, and is supported by molecular orbital calculations on the complexes and appropriate models. Chapter 3 deals mainly with dinuclear copper(II) complexes containing two ligands bridging two metal centers. The dinuclear copper(II) complexes containing two N-N single bonds have no or very weak coupling because of orbital

orthogonality and the twisting of the two copper planes around these two N-N single bonds. A dicopper complex containing mixed diazine bridges (pyridazine/N-N) shows weak antiferromagnetic coupling, and since the diazine unit in the aromatic ring system bridges two copper centers in an orthogonal manner, this net antiferromagnetic coupling occurs only through the open-chain diazine bridge. A tetranuclear copper complex contains two pairs of dicopper(II) centers bridged orthogonally by two μ_2-1,1-azide anions with each pair of copper(II) centers bridged by one N-N single bond and one μ_2-1,1-azide with a 119° azide bridge angle. The dihedral angle about the N-N single bond is 54°, which indicates either no coupling or weak ferromagnetic coupling *via* such a bridge. Therefore, the strong antiferromagnetic coupling ($-2J = 246\ cm^{-1}$) occurs only through the μ_2-1,1-azide bridges between each pair of copper(II) centers, giving the first genuine example contradicting the spin polarization mechanism associated with azide bridges. In Chapter 4, a series of spiral-like dinuclear complexes of Mn(II), Fe(II), Fe(III), Co(II), Co(III) and Ni(II) ions containing three N-N single bonds with a formula $[L_3M_2].(X)n.mH_2O$ (L = PAHAP, PZHPZ; X = ClO_4 or NO_3; n = 4, 6) and a seven-coordinate Fe(III) complex are discussed. The X-ray structures of six of these complexes have been determined. Variable-temperature magnetic properties, electrochemistry and spectra are discussed. Chapter 5 discusses the synthesis, structural and magnetic properties of some mononuclear and polynuclear first row transition metal complexes of the open-chain diazine ligands. The X-ray structures of eight complexes were determined. Two new coordination modes for open-chain diazine ligands have been

found. In the last chapter, a general conclusion about coordination modes, magnetostructural correlations, etc. of the open-chain diazine complexes is made.

Acknowledgements

First of all, I would like to give my thanks to my supervisor, University Research Professor Laurence K. Thompson for his advice and encouragement, patience and financial support during the course of the research and for his help with variable temperature magnetic studies and some of the MO calculations. His assistance and patience in the process of the writing of this thesis are gratefully acknowledged. As well, I would like to acknowledge the advice and support of the other members of my supervisory committee, Dr. C. Jablonski and Dr. P. Georghiou.

Special thanks are extended to Mr. D. O. Miller, Dr. H. J. Clase and Dr. J. N. Bridson of the Department of Chemistry, Memorial University of Newfoundland, Dr. Andres E. Goeta and Prof. Judith A. K. Howard of the Department of Chemistry, University of Durham, and Dr. Glenn P. A. Yap at the University of Windsor for the X-ray structure determinations.

My thanks are also due to the Department of Chemistry, and School of Graduate Studies of Memorial University of Newfoundland for financial support during the course of this study. I would like to acknowledge all of my colleagues in the Thompon research group. Special thanks are extended to Mr. Christopher L. Sheppard for his help in using some computer programs and all other help as well, Dr Santokh S. Tandon, Dr. Makoto Handa and Dr. Craig Metthews for their kindness, very valuable suggestions and for making the time in chemistry enjoyable. In addition, thanks go to Mr. Murray K. Park for helping me to use the IR and RT magnetic instruments.

Thanks are also extended to all the students, staff and faculty of the Department of Chemistry, who have made my years at Memorial a good experience to remember.

Finally, I would like to mostly thank my wife for her understanding, support, encouragement and love, and for her care of our son.

Table of Contents

List of Tables

List of Figures

List of Abbreviations and Symbols

R	residual factor
s	local spin quantum number
S	dimer spin quantum number
Z'	dimer lattice coordination number
α	torsion angle, bridging angle, rotational angle
α_o	angle of accidental orthogonality
γ	dihedral angle between MN_2C_2 five-membered chelate rings
β	electronic Bohr magneton
χ	magnetic susceptibility
Δ	energy difference between symmetric and antisymmetric MO's
ε	molar extinction coefficient
ε_i	energy of molecular orbital i
Φ	molecular orbital
μ_{eff}	effective magnetic moment
θ	Curie-Weiss or Weiss-like correction
ρ	fraction of paramagnetic impurity
Ψ	Heitler-London (two-electron) wavefunction
PAH	2-Pyridylamide-hydrazone
PAHAP	Bis(picolinamide) Azine

PAHOX	2,3-Butanedione monoxime picolinamidrazone
PHAAP	Picolinamide-picolinhydrazone
PHMAP	6-Methyl-2-pyridinecarboaldehyde picolinamidrazone
PMHAP	2-Acetylpyridine picolinamidrazone
PTS	3-(2-Pyridyl)-5-(2-hydroxyphenyl)-1,2,4-triazoline
PYPZ	(2'-Pyrazinecarboxamide)-picolinamide Azine
PZHPZ	Bis(2'-pyrazinecarboxamide) Azine

CHAPTER 1. General Introduction

1. 1 Introduction to the magnetic exchange in polynuclear copper(II) complexes

1.1.1 Magnetic properties of polynuclear copper(II) complexes

The magnetic properties of a polynuclear complex involving paramagnetic metal ions are in general totally different from the sum of the magnetic properties of each metal ion fragment separately [1]. To interpret these results, magnetic exchange interactions are considered. These may arise by direct exchange between the closely spaced paramagnetic centers, leading to diamagnetism, or by superexchange [2], in which the intervening bridging atoms or molecules (often diamagnetic in their ground state) are capable of transmitting the magnetic exchange interaction. The superexchange can be divided into two categories: ferromagnetic and antiferromagnetic, according to the mode of spin interaction between the metal centers [3, 4]. The magnetic behaviour of materials has been widely explored from both experimental and theoretical points of view [5-12].

In dinuclear copper(II) complexes, both metal centers A and B (**Figure 1-1**) each have one unpaired electron with effective electron spin s denoted as s_A and s_B and associated with spin angular momentum M_s. The interaction between A and B leads to two molecular states, namely a spin singlet S = 0 and spin triplet S = 1 with a singlet-triplet

energy gap denoted by 2J [1, 3, 4], which is called the isotropic exchange coupling constant (**Figure 1-1**) [13]. **Figure 1-1** also shows the axial zero-field splitting D (anisotropic spin-spin interaction) and the rhombic zero-field splitting E due to the second-order spin-orbit coupling. The anisotropic spin-spin interaction leads to a much smaller energy gap compared with isotropic exchange. If S = 0 is the ground state, J is negative and the interaction is antiferromagnetic. If S = 1 is the ground state, J is positive and the interaction is ferromagnetic.

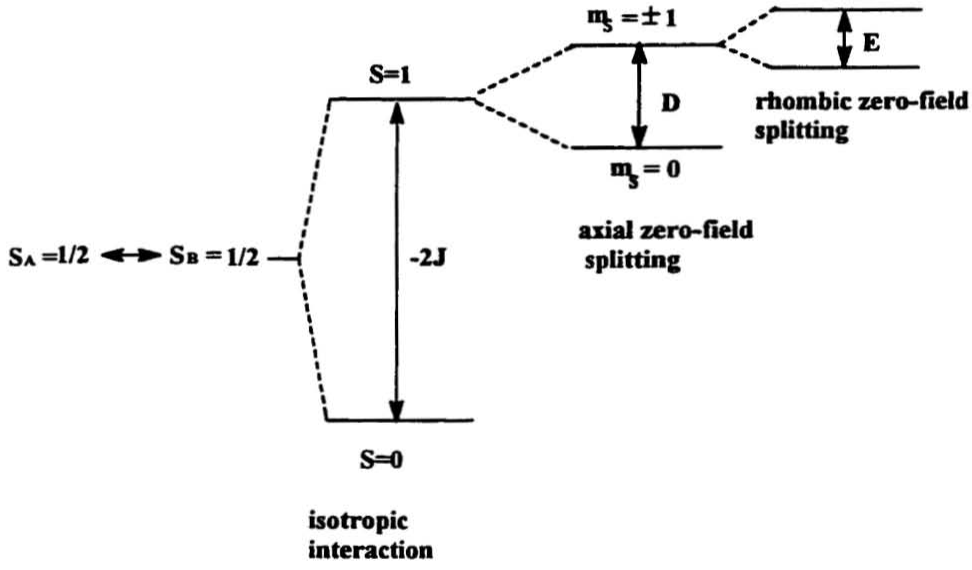

Figure 1-1. Schematic representation of the low-lying states in a dinuclear copper(II) complex A-B.

Based on two assumptions [1, 11] (1) the interaction is weak enough in order for the S = 0 and S = 1 states to be properly described by Heitler-London wavefunctions built from the magnetic orbitals and (2) the metal-metal charge transfer configuration of the type A^+-B^- or A^--B^+ is much too high in energy to couple significantly with the ground configuration A-B, the net measured exchange J_T may be expressed in a relatively simple way as the sum of two components: an antiferromagnetic negative component J_{AF} and a positive ferromagnetic component J_F.

$$J_T = J_{AF} + J_F \quad \text{with}$$

$$J_{AF} = -2S(\Delta^2 - \delta^2)^{1/2} \text{ and}$$

$$J_F = 2j$$

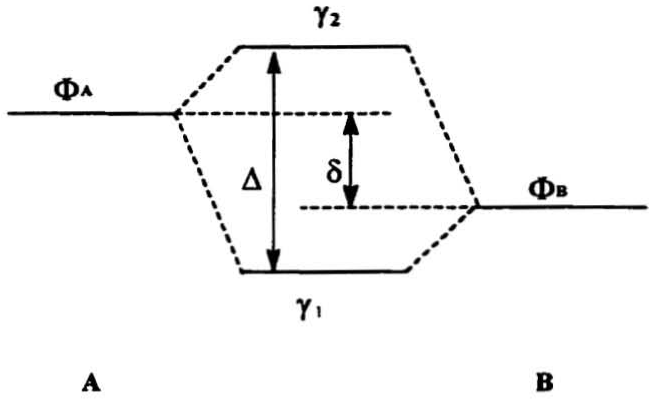

Figure 1-2. Relative energies of the magnetic orbitals Φ_A, Φ_B and molecular orbitals γ_1, γ_2 built from these magnetic orbitals in a dissymmetrical dinuclear copper(II) complex A-B.

The difference in energy between the two singly occupied molecular orbitals γ_1 and γ_2 for the triplet state of A-B, built from the magnetic orbitals Φ_A and Φ_B is represented by Δ. The energy difference between the two magnetic orbitals Φ_A and Φ_B (**Figure 1-2**) is represented by δ. S (overlap integral between the magnetic orbitals Φ_A, Φ_B) and j (the two-electron exchange integral) are given by

$$S = \int_{space} \rho(i) d\iota_i \qquad \text{and}$$

$$j = \int_{space} \rho(i)\rho(j)/r_{ij} d\iota_i d\iota_j$$

where $\rho(i)$ (overlap density) is defined as

$$\rho(i) = \Phi_A(i)\Phi_B(i)$$

If the A and B fragments are identical (symmetrical, so, δ is zero), J_{AF} is reduced to

$$J_{AF} = -2\Delta S$$

Several factors can affect the spin communication. The major factors include: (1) geometry at the metal centers [14]; (2) angle at the bridge [15]; (3) number of atoms in the bridge (distance between the metals) [16]; (4) identity and polarizing power of the bridging and non-bridging atoms bound to the metal [17]; (5) the presence or absence of

orthogonal bridge interactions [14, 17]; (6) the fused aromatic ring capacitor effect [18-20]; (7) spin polarization effects [17-21]. All of these factors are demonstrated very well by copper (II) polynuclear complexes.

The correlation of magnetic properties with these electronic and structural factors is so important that it has allowed magnetochemistry to provide a means for the preliminary characterization of the active sites of bioactive molecules (i.e. hemocyanin, hemerythrin, ribonucleotide reductase, cytochrome c oxidase etc.) [22, 23] and in catalytic processes [24-28].

1.1.2 The detection of magnetic exchange interactions by temperature dependent magnetic susceptibility measurements

For a mononuclear paramagnetic compound, molar magnetic susceptibility follows the Curie Law (**eqn. 1-1**).

$$\chi_m = \frac{Ng^2\beta^2}{3kT}(S(S+1)) \quad \text{.....[1-1]}$$

For a dinuclear compound A-B, a temperature dependent magnetic susceptibility measurement allows a good determination of the J-values because this technique can detect an energy separation down to about 1 cm^{-1}. By using the isotropic (Heisenberg) exchange Hamilitonian ($\hat{S}_A$ and $\hat{S}_B$ are the local spin quantum operators):

$$\hat{H} = -2J(\hat{S}_A \cdot \hat{S}_B)$$

the molar magnetic susceptibility is given by the population-weighted average of the susceptibility of the energy levels [29] (**eqn. 1-2**).

$$\chi_m = \frac{N\Sigma_i \left(\left(E_{i(1)}^2 / kT \right) - 2E_{i(2)} \right) \exp\left(-E_{i(0)} / kT\right)}{\Sigma_i \exp\left(-E_{i(0)} / kT\right)} \quad \text{.....[1-2]}$$

Where $E_{i(0)}$ is the energy of the level **i** in the absence of a magnetic field. $E_i(1)$ and $E_i(2)$ are the coefficients of the first and second order Zeeman effects respectively. When a sample is placed in a magnetic field, the first order Zeeman effect splits each level symmetrically into 2S+1 component levels ranging in energy from -gβS to +gβS, while the result of the second order Zeeman effect is to make a temperature independent contribution to χ_m. Therefore, the equation reduces to **(eqn. 1-3)** [30]

$$\chi_m = \frac{Ng^2\beta^2}{3kT} \left(\frac{\Sigma_i S(S+1)(2S+1)\exp\left(-E_{i(0)} / kT\right)}{\Sigma_i (2S+1)\exp\left(-E_{i(0)} / kT\right)} \right) + N\alpha \quad \text{.....[1-3]}$$

where $N\alpha$ is a term which accounts for temperature independent paramagnetism.

For two s = 1/2 copper (II) centers, and considering two factors 1) that copper(II) complexes normally contain a small amount of paramagnetic impurity and 2) non-localized intermolecular spin interactions are commonly observed, the molar magnetic susceptibility χ_m (per metal) can be given as

$$\chi_m = \frac{Ng^2\beta^2}{k(T-\theta)} \left[\frac{1}{3 + \exp\left(-2J / kT\right)} \right] (1-\rho) + \left(\frac{Ng^2\beta^2}{4kT} \right) \rho + N\alpha \quad \text{.....[1-4]}$$

where ρ is the fraction of paramagnetic impurity and θ is the Weiss-like correction which accounts for intermolecular interactions. This equation is called the modified Bleaney-Bowers equation [31], and is used to fit the variable-temperature magnetic susceptibility data for all new dicopper(II) complexes described in this thesis.

1.1.3 Antiferromagnetic interactions, ferromagnetic interactions and magnetostructural correlations

Antiferromagnetic coupling , in a dicopper system involving a spin singlet ground state and a spin triplet excited state, is comparatively common and has been extensively studied. However, ferromagnetic coupling is quite uncommon. The orthogonality of the interacting magnetic orbitals, which could be strict or accidental, leads to $\Delta = 0$, or in other words, a ferromagnetic interaction.

In the strict orthogonal interaction cases, the famous examples are represented by $[CuVO[(fsa)_2en](CH_3OH)]$ and $[CuCr[(fsa)_2en](H_2O)_2]Cl.3H_2O$ ($H_4(fsa)_2en$ = N,N'-bis(2-hydroxy-3-carboxybenzylidene)-1,2-diaminoethane) **(Figure 1-3)** [11,32]. The magnetic orbitals Φ_{Cu} in the above two complexes are d_{xy} and are partially delocalized towards the

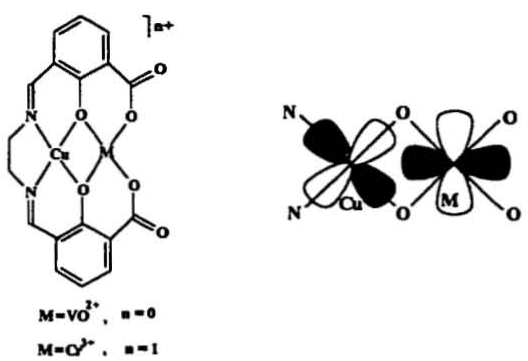

Figure 1-3. Structural and molecular orbital representation of $[CuVO[(fsa)_2en](CH_3OH)]$ and $[CuCr[(fsa)_2en](H_2O)_2]Cl.3H_2O$ with $H_4(fsa)_2en$ = N,N'-bis(2-hydroxy-3-carboxybenzylidene)-1,2-diaminoethane.

N and O atoms surrounding the copper due to the σ -type antibonding overlap, while the magnetic orbital Φ_{VO} or Φ_{Cr} is $d_{x^2-y^2}$ and is partially delocalized towards the O atoms but involves the π-type antibonding overlap. Therefore , the overlap integral between Φ_{Cu} and Φ_{VO} or Φ_{Cr} is zero (J_{AF} is zero) and the singlet-triplet energy gap J is given by

$$J_T = J_F + J_{AF} = 2j$$

which is positive. The ferromagnetic coupling is confirmed by magnetic property measurements.

By the same mechanism, some long distance ferromagnetic coupling systems were also found in the following two examples: A very weak ferromagnetic coupling was found in a trinuclear copper (II) complex through a very long bridging $[CuCl_4]^{2-}$ anion, which has a distorted square pyramidal structure (**Figure 1-4**) [33]; and a rather strong ferromagnetic coupling was observed in a phthalato-bridged copper(II) trinuclear complex having a long Cu-Cu separation (6.7 Å) *via* a Cu-Cl-Cu-Cl-Cu pathway [34].

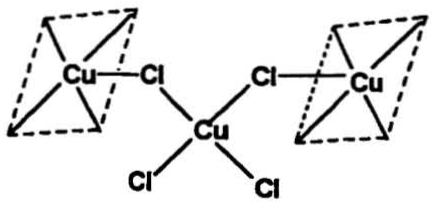

Figure 1-4. Strict orthogonal interaction in a trinuclear complex bridged by $[CuCl_4]^{2-}$.

In the case of accidental orthogonality, the occurrence is not directly related to the symmetry of the complex. For very peculiar values of the structural parameters, the molecular orbitals for the system can become accidentally degenerate and the energy gap

Δ becomes zero. Any structural deformation will lead to the disappearance of this accidental orthogonality. The well documented system is $[L_2Cu(OH)_2CuL_2]^{2+}$, which has a planar structure (**Figure 1-5**). Both experimental studies (by Hatfield et al. [35, 36]) and

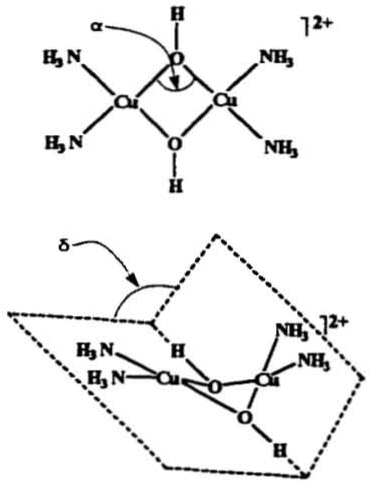

Figure 1-5. The model compounds used by Kahn and co-workers to calculate the dependence of J_{AF} on bridging angle (α) and dihedral angle (δ).

theoretical studies (by Kahn et al. [7, 37, 38]) show that the energy difference between the two copper (II) magnetic orbitals varies with the Cu-OH-Cu bridging angle α. Based on experimental data, Hatfield et al [35, 36] obtained a very good linear correlation:

$$2J(cm^{-1}) = -74\alpha \text{ (degrees)} + 7270 \quad \text{.....[1-5]}$$

When α is larger than 97.5° the J_{AF} component is predominant and the observed coupling is antiferromagnetic. When $\alpha = 97.5°$, $J_{AF} = 0$ and a ferromagnetic interaction is observed. However, for certain angles $\alpha < 97.5°$, J_{AF} should become the dominant component and an antiferromagnetic interaction will theoretically be observed again. A similar correlation was found by Merz and Haase [39] in the Cu-$(OR')_2$-Cu system:

$$2J(cm^{-1}) = -82\alpha \text{ (degrees)} + 7857 \quad \text{.....[1-6]}$$

A magnetostructural correlation for phenoxide bridged dinuclear copper(II) macrocycles has recently been proposed by Thompson et al. [15] , which is somewhat analogous to that for the hydroxide bridge system.

While the magnetostructural correlation holds for planar Cu-$(OH)_2$-Cu compounds, it does not hold if the molecule is bent along the O-O axis. Kahn et al. [10] studied theoretically the dependence of -2J on dihedral angle (δ) for the hydroxide bridged system, where δ is the angle created by bending the molecule about the O-O axis (**Figure 1-5**). The MO calculations showed that by bending the molecule from planar (δ = 180°) to larger dihedral distortions (δ < 180°), the energy gap ΔE between the triplet molecular orbitals becomes drastically smaller, which means that for the hydroxide bridge, J_{AF} becomes more positive (smaller in magnitude) as δ increases from a planar to a dihedrally distorted structure and that $2J$ will increase for deviations from planarity.

Accidental orthogonality and ferromagnetic exchange coupling also have been observed in mixed bridged systems, such as Cu(II)-RO/(μ_2-1,3)RCO_2-Cu(II) [40-44]

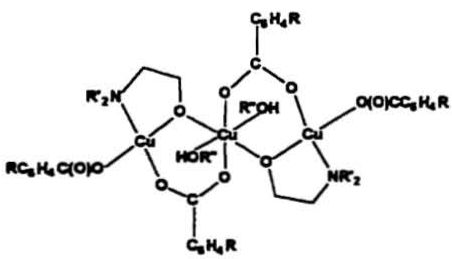

Figure 1-6. Schematic representation of accidental orthogonality in trinuclear copper(II) complexes bridged by RO/RCO_2(μ_2-1,3).

(**Figure 1-6**). In such systems, the angle between the central copper magnetic plane and the terminal copper magnetic planes varies with changes in the size of R" groups.

In addition to the orthogonality of the magnetic orbitals, both spin polarization by ligands like N_3^-, NCS^-, NCO^- etc., bridging in an end-on manner, and orbital counter-complementarity effects, also lead to a ferromagnetic interaction.

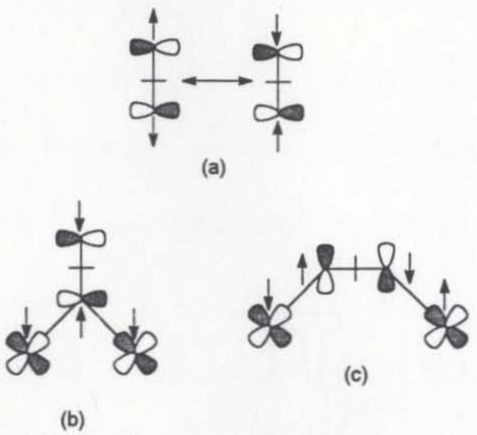

Figure 1-7 Molecular orbital representation of the spin-polarization mechanism (a) free N_3^-, (b) μ_2-1,1- N_3^- in a dicopper(II) complex (c) μ_2-1,3- N_3^- in a dicopper(II) complex.

The spin polarization effect was proposed to explain the observed ferromagnetism in μ_2-1,1-azide bridged dinuclear copper(II) complexes. The ferromagnetism results through the interaction between the two copper(II) d_{xy} metallic orbitals and the π_g MO on the azide, while the μ_2-1,3-azide bridge leads to an antiferromagnetic interaction **(Figure 1-7)**.

The spin polarization effect was proposed in the early 1980's by Kahn [17, 21] to account for the magnetic properties of these μ_2-1,1-azide bridged copper(II) complexes with Cu-N_3^--Cu angles in the range 97.5°-105.5°[45-47]. According to the extended Hückel MO calculations [46], in this angle range the energy gap between the two molecular orbitals constructed from the d_{xy} magnetic orbitals in the triplet state and appropriate symmetry orbitals on the bridging ligands was considered to be very small. Therefore the observed net ferromagnetic coupling is reasonable. It was also suggested that ferromagnetism should prevail for all azide bridge angles. However, recent studies in Thompson's group [48] showed that antiferromagnetic μ_2-1,1-azide bridged dinuclear copper(II) complexes also can be produced with some dinucleating N_4 diazine ligands, which can generate a very large range of azide bridge angles (98.3-124.1°). In some cases, very strong antiferromagnetic coupling ($-2J > 900$ cm^{-1}) [49, 50] has been observed. Detailed studies showed that when the azide bridge angle exceeds 108, the azide bridge is responsible for antiferromagnetic coupling. So, the μ_2-1,1-azide bridge can enter an antiferromagnetic realm. Therefore the spin polarization mechanism may be inappropriate, or may only be applied in small angle systems. The question of an antiferromagnetic realm for the μ_2-1,1-azide bridge in dinickel(II) [51] or other dimetal systems still remains.

The orbital counter-complementarity effect has been well demonstrated by a chain compound $[Cu_2(\mu_2\text{-}1,1\text{-}N_3)_2(\mu_2\text{-}1,3\text{-}NO_3)_2(\mu_2\text{-}1,3\text{-}Me_3NCH_2COO_2)_2]_n$ (**Figure 1-8**) reported by Thompson et al [52] and Mak et al. [53]. In this compound, every pair of copper(II) centers is bridged by μ_2-1,1-azide and μ_2-1,3-carboxylate groups in the equatorial plane.

The nitrates bridge the copper(II) centers axially in an alternating *trans* mode throughout the chain. The copper(II) magnetic ground states ($d_{x^2-y^2}$) are based on the equatorial planes, so the exchange interactions would be expected to happen only through the azide and

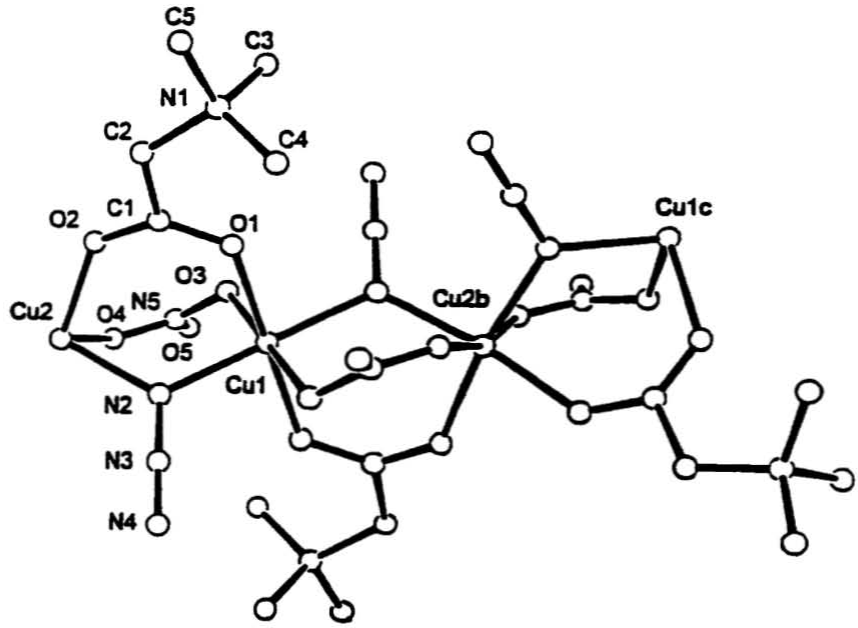

Figure 1-8. Segment of the chain structure of $[Cu_2(\mu_2\text{-}1,1\text{-}N_3)_2(\mu_2\text{-}1,3\text{-}NO_3)_2(\mu_2\text{-}1,3\text{-}Me_3NCH_2COO_2)_2]_n$.

the carboxylate bridges. The apical nitrate bridges will contribute very little to the exchange since they are orthogonal. The azide bridge angle in this compound is 119.5(2)°, which is much larger than 108°. Therefore, the expected coupling in this compound, based on the azide bridge alone, should be antiferromagnetic. Actually, variable temperature magnetic susceptibility studies reveal dominant intrachain ferromagnetism ($J = 26\ cm^{-1}$).

This result has been satisfactorily explained by using extended Hückel molecular orbital calculations on simple model compounds [52].

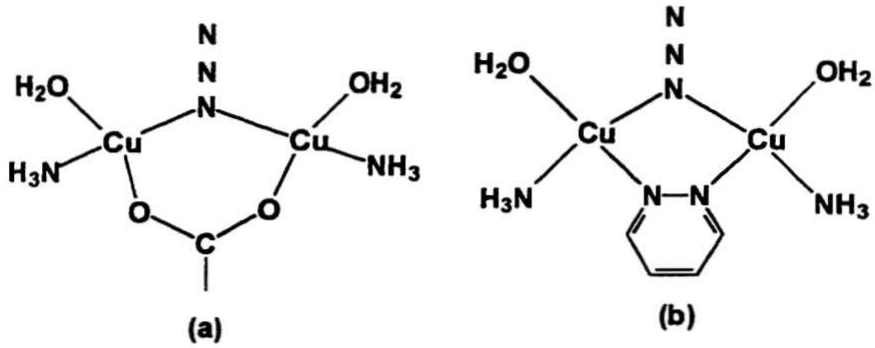

Figure 1-9. Schematic representation for the model compounds bridged (Cu-N_3^--Cu angle is 120° in both cases) by μ_2-1,1-azide/μ_2-1,3 -carboxylate (**a**) and μ_2-1,1-azide/μ_2-1,2-diazine (**b**).

The calculation for model compound **a** (**Figure 1-9**) shows exactly a situation where the ferromagnetic term becomes dominant, due to the orbital counter-complementarity effect [52]. On the contrary, if the carboxylate group was replaced by a diazine (e.g. pyridazine) or hydroxide, the calculations, using model compound **b** (**Figure 1-9**), showed that the energy gap between the two frontier orbitals would increase compared with that of a monobridged μ_2-1,1-azide, μ_2-1,2-diazine or μ_2-OH complex. This gives an explanation for the larger antiferromagnetic interaction observed in such systems.

It was also noted that the orbital counter-complementarity effect is responsible for

explaining the weak or even ferromagnetic [44] coupling in the Cu(II) ($d_{x^2-y^2}$)-(R'O$^-$, R' = alkyl, H)/(μ_2-1,3)RCO$_2^-$- Cu(II)($d_{x^2-y^2}$) system.

1.2 Polynuclear copper(II) complexes with N_2 diazine bridges in conjugated aromatic ligands

N_2 diazine bridges in some conjugated aromatic heterocyclic ligands can bring two copper(II) centers into close proximity and generate intramolecular exchange between the two copper centers *via* the π system of the heterocyclic ligand. This varies with the nature of the diazine ligand. Extensive studies have revealed that in the dinuclear copper(II) complexes involving pyrazine, pyrimidine and other related bridges, where the heterocyclic nitrogen donor centers are arranged at the 1,4 and 1,3 ring positions [54], very weak intramolecular antiferromagnetic interactions were observed (**Figure 1-10**).

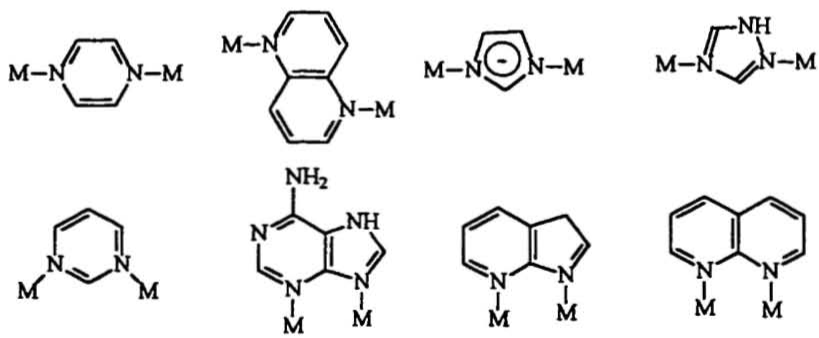

Figure 1-10. Examples of weak coupling *via* M-diazine-M links.

However, for some heterocyclic diazine ligands with a 1,2-heterocyclic nitrogen arrangement, moderate to strong antiferromagnetic coupling has been observed depending on the identity of the ligand (**Figure 1-11**) [18-20, 55-68]. For essentially planar bis-(N_4) ligand complexes in which the magnetic orbital is $d_{x^2-y^2}$, the -2J values are in the order of pyridazine/phthalazine (450-550 cm^{-1}) [18, 61 ,65, 66] > pyrazolate (200-430 cm^{-1}) [55-57] > triazolate (200-240 cm^{-1}) [58, 61] > 4-aminotriazole (< 220 cm^{-1}) [59, 67] (**Table 1-1**) [68].

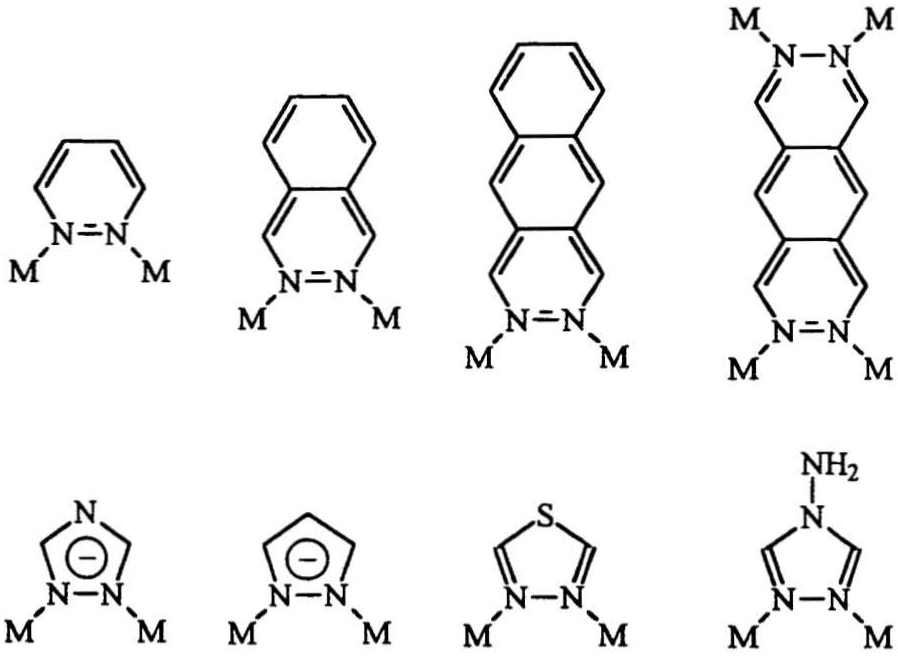

Figure 1-11. Moderate to strong antiferromagnetic coupling *via* M-1,2-diazine-M links.

Table 1-1. Magnetic and structural data of doubly diazine bridged dinuclear copper(II) (Cu_2N_8) complexes.

Compound	-2J(cm^{-1})	Cu...Cu(Å)	Cu-N(Å) (diazine)	Cu-N(Å) (peripheral)	Cu-O(Å) (axial)	Ref.
$[Cu_2(DPYH)_2(H_2O)_2(ClO_4)_2]$	536(2)	3.760(2)	2.027(5) 2.014(6)	1.977(7) 1.974(6)	2.310(6) 2.554(6)	63
$[Cu_2(DHPH)_2(H_2O)_2(ClO_4)_2]$ $(ClO_4)_2$	489(1)	3.729	1.981(7) 1.965(8)	1.966(8) 2.019(7)	2.351(7) 2.615(12)	18
$[Cu_2(DPAP)_2](BPh_4)_2$	428	3.903(2)	1.929(4) 1.906(3)	2.028(3) 2.108(4)		55
$[Cu_2(BAMPZ)_2Br_2]$	384.0	3.947(4)	1.88(2) 1.96(1)	2.07(1)		69
$[Cu_2(BPYPZ)_2(H_2O)_2(NO_3)_2]$ $2H_2O$	361.8	4.044	1.954(5) 1.942(5)	2.074(5) 2.092(5)	2.22	57
$[Cu_2(BPT)_2(CF_3SO_3)_2(H_2O)_2]$	236(20)	4.085(1)	1.942(3) 1.936(3)	2.082(3) 2.087(3)	2.376(3) 2.802(4)	61
$[Cu_2(AAMT)_2(H_2O)_2Br_2]$	220(2)	4.069(7)	1.950(3) 1.937(3)	2.032(3) 2.043(2)	2.647(3)	59

(Note: For structures of the ligands see " **Figure 1-12**")

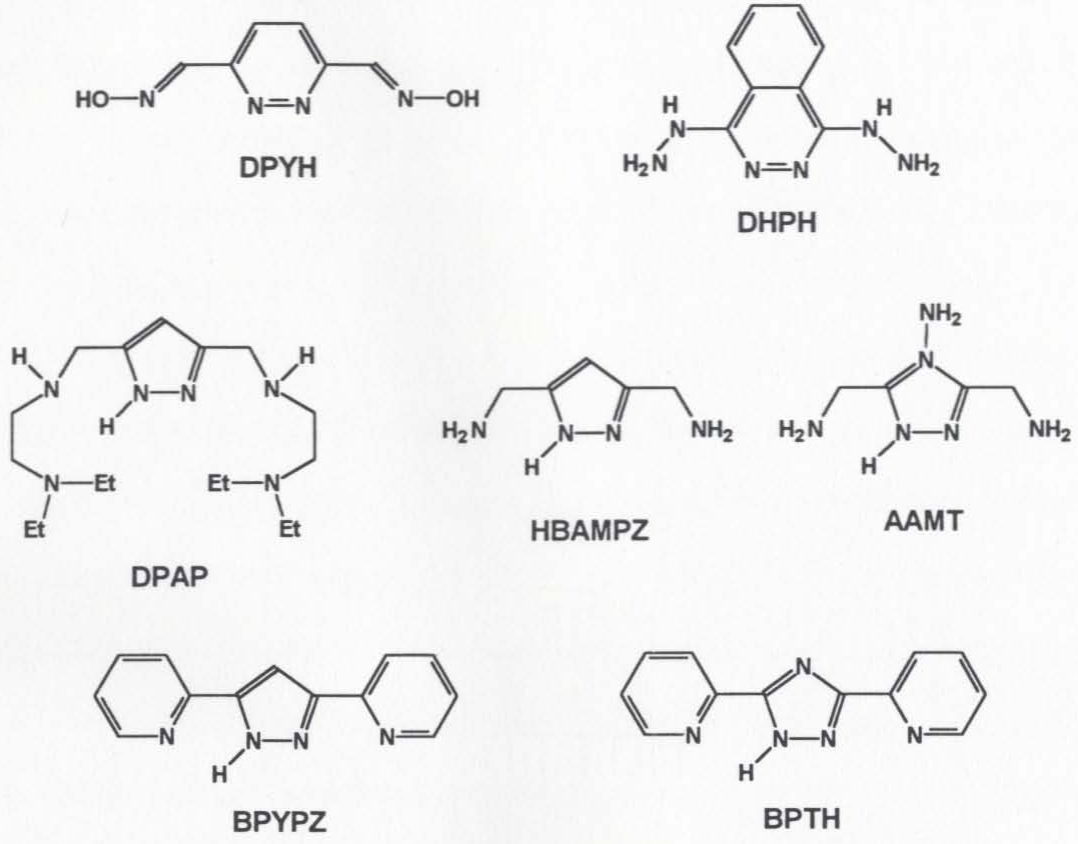

Figure 1-12. Schematic representation of the diazine ligands.

Detailed studies comparing the six-membered heterocyclic ligands pyridazine and phthalazine showed that the antiferromagnetic coupling was generally stronger *via* a pyridazine bridge than via a phthalazine bridge, because of a capacitor effect (fused aromatic rings) [18-20]. For the five membered heterocycles the antiferromagnetic

coupling was generally weaker compared with that in the pyridazine or phthalazine bridged systems because the five membered ligand geometry forces the copper(II) ions to be further apart. Considering the polarizing power of the extra electronegative nitrogen within the same rings, which limits the exchange among the five-membered ring diazine systems, the pyrazolate propagates the antiferromagnetic exchange more efficiently than 1,2,4-triazole, 1,2,4-triazolate or 4-amino-1,2,4-triazole.

A very interesting phenomenon has been observed in some heterocyclic bis-diazine copper complexes, when the coordination geometry is changed. Koningsbruggen et al. [13, 57, 59, 60, 65, 70] investigated the magneto-structural correlations for dinuclear doubly N_1, N_2-1,2,4-triazole bridged copper(II) complexes and found that the J value and the N-Cu-N angle (**Figure 1-13**) have a linear relationship, like the case observed for planar dihydroxo-bridged copper(II) compounds. When the N-Cu-N angle decreases, the J value dramatically increases to a maximum, with N-Cu-N = 90°.

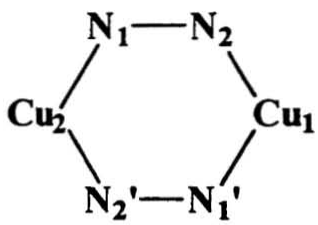

Figure 1-13. Topology of the atoms constituting the bridging network in doubly N1,N2-1,2,4-triazole bridged dinuclear copper(II) compounds.

Theoretically, to obtain an effective propagation of superexchange the N-Cu-N angle and Cu-N-N angle should be 90° and 126° respectively, because only in such a way can the electron delocalization occur effectively via the nitrogen atoms.

However, a surprising result [71] was obtained in a heterocyclic bis-diazine complex $[Cu_2(PTP)_2Cl](ClO_4)_3$ (PTP=3,6-bis(2-pyridylthio)pyridazine) in which the copper N_4 planes are canted symmetrically toward an apical chlorine bridge to form a boat conformation. The antiferromagnetic exchange does not diminish significantly because of this boat conformation, and is comparable to that observed for the planar complex $[Cu_2(DHPH)_2(H_2O)_2](ClO_4)_4$. This observation is supported by a theoretical study on a model complex $[Cu_2(PYZ)_2Cl_4]^{2-}$, which showed that J_{AF} value was insensitive to the twisting of the copper planes relative to the pyrazolate plane, but contrasts with another study on roof-shaped bis-(hydroxo)-bridged dicopper(II) model complexes in which J_{AF} diminishes with the decreasing of the dihedral angle between the copper planes [10,72] (see **Figure 1-5**).

1.3 Copper(II) complexes with open-chain diazine ligands

As mentioned above, the dicopper(II) complexes containing a diazine moiety incorporated in a heterocyclic ring system have been studied extensively. The main conclusion is that the diazine in aromatic heterocyclic ligands generally can fix two metal centers in close proximity to provide an antiferromagnetic exchange pathway and the J_{AF} value is generally insensitive to the change of the coordination environment, even though a slight change of -2J value has been observed in the 1,2,4-triazole bridged dinuclear

copper(II) system. The literature dealing with dicopper(II) compounds containing open-chain diazine ligands is rather limited [13, 73-76].

Compared with the diazine moiety in heterocyclic ring systems the N_2 diazine linkages in open-chain systems are much more flexible (see **Figure 1-14**) and provide

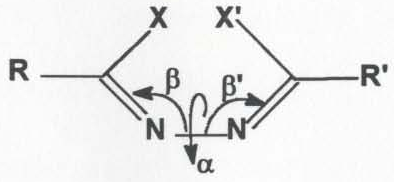

Figure 1-14. Flexibilities in open-chain diazine systems.

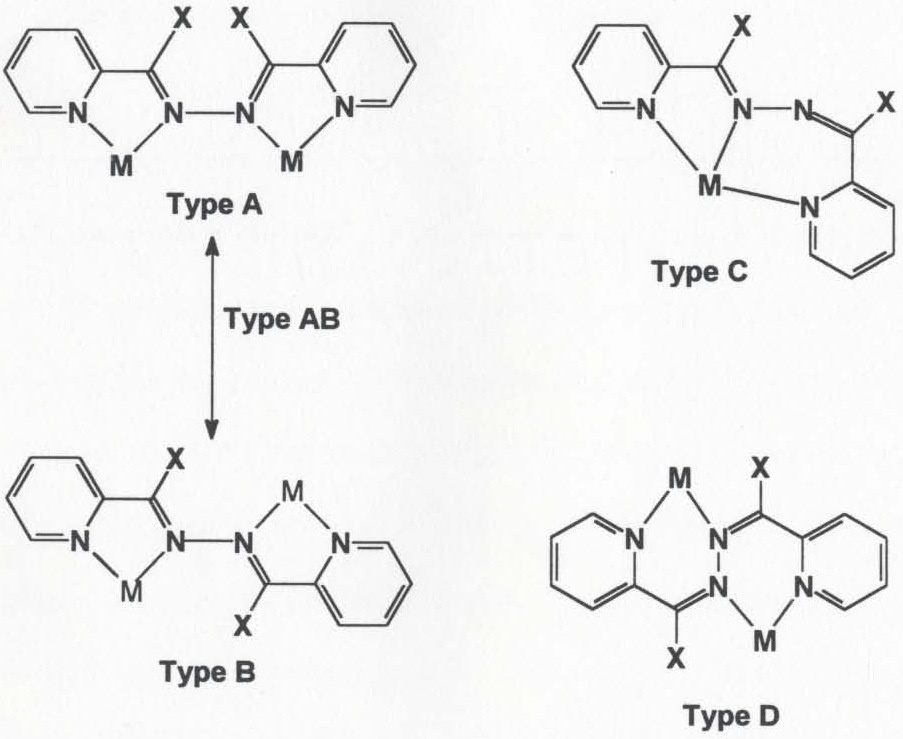

Figure 1-15. Topological variation of open-chain diazine ligands and their coordination modes.

a very interesting topological variation. Depending on R, R', X, X' and the metal ions, coordination modes will vary with the changes in two types of angles, namely the torsion angle (α) about the N-N linkage and bend angles around the two nitrogen atoms (β or β'). The limiting situations of the changes of these two types of angles are noted in **Figure 1-15** when R = R' = Py and X = X'. All these types are defined either for ligands or their complexes based on the arrangement of the ligands.

Type D (*cis-cis* conformation) complexes have not yet been found because the *cis-cis* conformation is believed to be sterically unstable. For the same reason the limiting situation of the *trans-trans* conformation **Type A** has not yet been observed either [77, 78].

A couple of **Type C** (*cis-trans* conformation) copper(II) complexes have been structurally documented. In 1983, O'Connor et al. [79] reported a PMK copper(II) complex with general formula $Cu(PMK)(NO_3)_2$ (PMK see **Figure 1-16**) which exhibits no significant magnetic coupling over the temperature range of 6-300 K because it consists of isolated monomers. In 1984 Thompson et al. [80] described an example of an IMAA (**Figure 1-16**) copper(II) complex, which has an analogous structure to that of $[Cu(PMK)(NO_3)_2]$. The only difference between these two complexes from the structural point of view is that the stereochemistry at the copper centre is closer to a square-pyramid in $[Cu(IMAA)Br_2]H_2O$, and closer to trigonal-pyramidal in $[Cu(PMK)(NO_3)_2]$. The structural index τ ($\tau = (\beta - \alpha)/60$, β and α are the two largest bond angles) proposed by Addison et al. [81] for $[Cu(IMAA)Br_2].H_2O$ is 0.2, but 0.53 for $[Cu(PMK)(NO_3)_2]$.

Another two mononuclear copper complexes, $[CuBr_2(HL)]H_2O$ and [Cu(HPCT)(PCT)] (NCS) (HPCT, **Figure 1-16**) also involve **Type C** conformation [82, 83].

If there are appropriate donors included in R or R' (**Fig. 1-14**), the **Type C** (*cis-trans)* conformation can generate binuclear complexes. Abraham et al. [84] reported

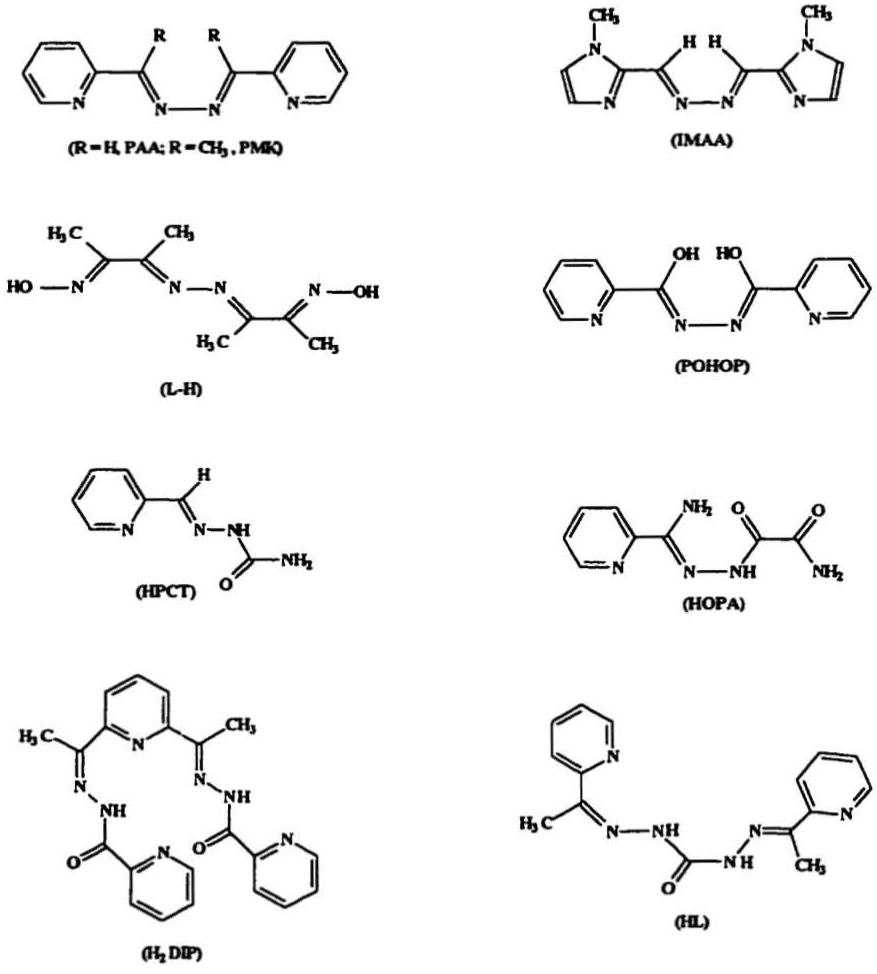

Figure 1-16. Schematic representation of some open-chain diazine ligands.

a dinuclear copper complex of a polydentate diacetylazine dioxime ligand (L-H, **Figure 1-16**). The structure shows that the nearly planar (L-H) group behaves as a bridging tetradentate ligand. Each copper has a distorted square-pyramidal coordination including three N donors from two oximes and an azine, and one O donor from each oxime. ESR spectroscopy shows that the copper(II) centers are highly coupled through the N-O bridges. Another dinuclear copper(II) complex containing a *cis-trans* diazine moiety of the ligand HPCT was reported by Rojo et al. [85]. In this complex, two copper centers were bridged by two S atoms from thiocyanate and it exhibits very weak antiferromagnetic coupling because Cu-S-Cu is close to 90° (87.0°).

A mixed case of *cis-trans* **(Type C)** and *trans-trans* **(Type AB)** conformations was found by Mangia et al. [86] in a tetranuclear copper complex $[Cu_2(DIP)Cl_2]_2(H_2O)_2$ and its analogous compounds [87] containing the 2,6-diacetylpyridine-bis-(picolinoyl- hydrazone) dianion (H_2DIP, **Figure 1-16**). In the complex, two crystallographically independent metal ions are linked by diazine moieties originating from the octadentate DIP ligand. The **Type C** (*cis-trans*) conformation has a 235° bend angle (β) and the **Type B** (*trans-trans*) conformation has a torsion angle (α) of about 90°. There is no report of the magnetic properties of this complex. Another mixed case was reported recently by Pelizzi et al. [88]. X-ray crystallographic analysis shows that the copper complex $[Cu_2(HL)Cl_3(H_2O)].1.5H_2O$ (HL = bis(methyl-2-pyridyl ketone carbono-hydrazone, **Figure 1-16**) is dinuclear. The copper complex centers have a mixed conformation of *cis-trans* **(Type C)** and trans-trans **(Type B)**, and an almost planar arrangement of two $d_{x^2-y^2}$

copper(II) centers linked by a N-N bond. This complex exhibits strong antiferromagnetic coupling ($-2J = 213.3\ cm^{-1}$).

A number of **Type B** copper(II) complexes have been reported including di-, tri- and tetra-nuclear cases [89]. A typical **Type B** dinuclear copper(II) complex was reported by Lagrenée et al. [90]. The X-ray structure shows a dinuclear complex of the ligand, (2-pyridoyl) pyridine carbohydrazide (abbreviated as POHOP, **Figure 1-16**) obtained by opening of the oxadiazole ring in 2,5-bis(2-pyridyl)-1,3,4-oxadiazole *via* a hydrolysis mechanism. Bacchi et al. [91] reacted a hydrazone derivative, di-2-pyridyl ketone [phenyl (semicarbazono)acetyl] hydrazone with $CuCl_2$ in ethanol and obtained another dinuclear copper complex of **Type B**. The two copper centers in both cases are bridged by an open-chain diazine moiety solely in the trans-trans (**Type B**) conformation with α = 180°. Therefore, the two copper(II) centers in these two complexes might have strong coupling compared with the result observed in $[Cu_2(HL)Cl_3(H_2O)]1.5H_2O$ [92]. Unfortunately, there are no studies on magnetic properties reported.

Two dinuclear copper(II) complexes containing a **Type B** diazine ligand, in which only one nitrogen was coordinated, were reported by Ainscough et al. [92] and Koningsbruggen et al. [13, 93]. But in such dinuclear complexes the two copper centers are linked by hydrogen bonds or by a $[SiF_6]^{2-}$ group, and no significant coupling could be observed in these cases. If there are some appropriate donors in the ligands, strong coupling can be generated *via* other bridges (i.e. N_3^-, PhO^-). Some complexes of this type

have been reported by Koh et al. [84], Wang et al. [95] **(Figure 1-17 A)** and Murray et al. [96].

Only one trinuclear copper complex containing a compartmental trinucleating trans-trans open ring diazine ligand **(Figure 1-17 B)** has been reported [97]. Three copper centers in the complex have square-pyramidal structures and are bridged by two trans-trans diazines **(Type B)**. However the central copper(II) is quite distorted ($\tau = 0.44$) [97].

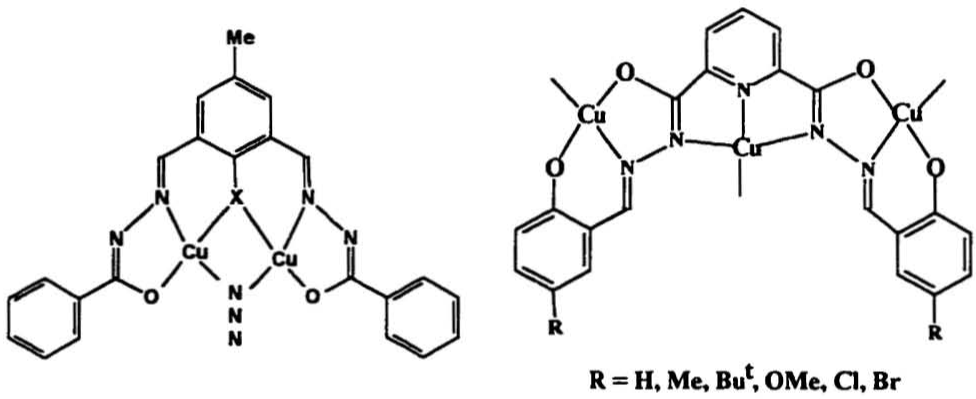

A **B**

Figure 1-17. **Type B** complex without donor site at R (see **Figure 1-14**) hence N-N cannot act as a bridge (A); Schematic representation of a series of compartmental trinucleating ligands (B).

Even though the central copper(II) ion is still far from a purely trigonal-bipyramidal chromophore, such distortion would have a significant effect on the magnetic coupling. The magnetic simulations of the experimental data gave magnetic parameters $g = 2.10$, $J =$

-50 cm^{-1}, θ = -0.65 K and $N\alpha$ = $-270*10^{-6}$ cm^{-1} mol^{-1}. Compared with the result in a *cis-trans* and *trans-trans* mixed diazine dicopper(II) complex reported by Pelizzi et al. [88], the trigonal bipyramidal distortion around the central copper(II) ion inhibits the magnetic coupling.

A very interesting structural type is the intermediate one between **Type A** and **Type B**, defined as **Type AB** ($0° < \alpha < 180°$). Until now only two structurally characterized copper(II) complexes of this type have been reported. A magnetostructurally characterized dicopper(II) complex $[Cu_2(PMK)Cl_4]$ (PMK see **Figure 1-16**) was reported by O'Connor et al. [79] in which the copper planes form a folded square planar conformation with an torsion angle (α) of 70.8°. This complex exhibits weak antiferromagnetic coupling ($-2J$ = 52 cm^{-1}). A cyclic tetranuclear copper(II) complex of an asymmetric hydrazone ligand N,N'-imidopicolinyloxamyl hydrazine $[Cu(OPA)]_4(NO_3)_4 \cdot 8H_2O$ (HOPA see **Figure 1-16**) reported by Koningsbruggen et al. [98] has a 90° torsion angle between the copper square planes, and shows a negligible exchange interaction between the metal centers. It seems that when the torsion angle between the copper magnetic planes decreases, the antiferromagnetic coupling for polynuclear copper(II) complexes containing **Type AB** diazine moieties also decreases, based on the results of magnetic property studies on these two complexes and $[Cu_2(HL)Cl_3(H_2O)].1.5H_2O$ [86]. However it is not possible to reach any conclusion from these limited examples concerning a magnetostructural correlation based on torsion angle (α).

1.4 Scope of the thesis

The literature search for open-chain diazine ligands and their copper(II) complexes shows that although a handful of open-chain diazine bridged copper(II) complexes has been structurally characterized, variable-temperature magnetic and related structural

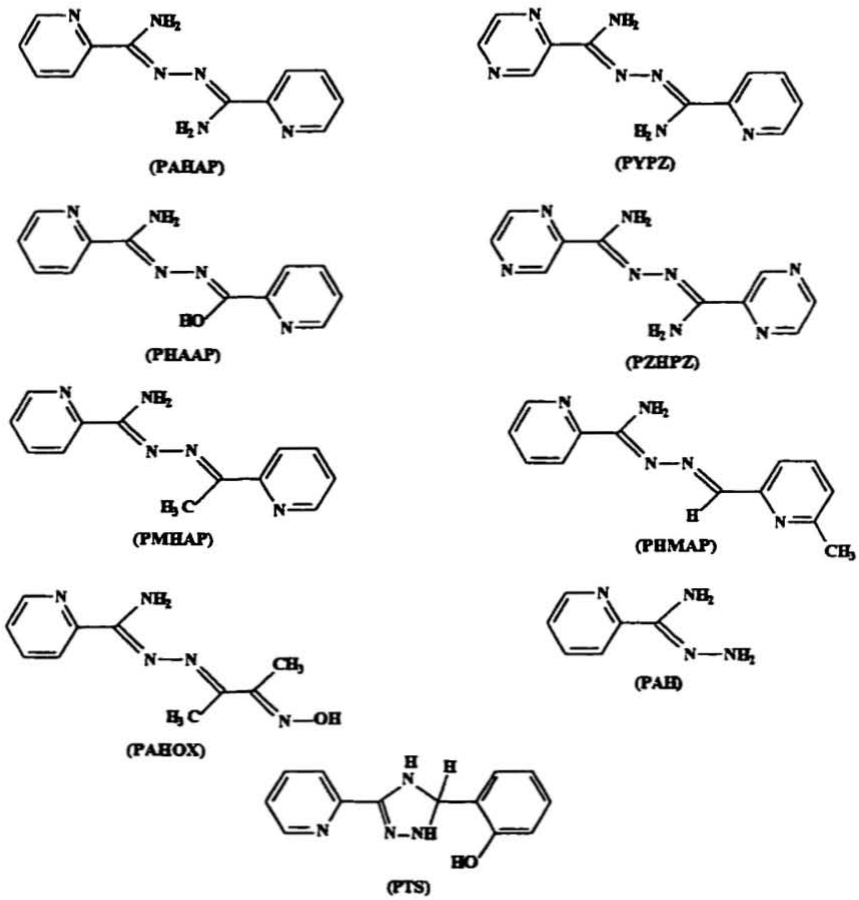

Figure 1-18. Open-chain diazine ligands studied in this thesis.

studies on such complexes are very limited. This thesis describes an extensive investigation of the coordination chemistry of copper(II), as well as other first row transition metal ions, with members of this class of open-chain diazine ligands, and focuses on magnetostructural correlations for dinuclear copper(II) complexes. To achieve these goals, a series of open-chain diazine ligands (**Figure 1-18**) and their complexes were synthesized which contain NH_2 or OH groups at the X or X' positions (see **Figure 1-14**). Compared with related ligands, such as PAA [73-76] and PMK [79], the ligands have several beneficial features: 1) The replacement of H or methyl in PAA or PMK by NH_2 or OH groups will possibly lead to the complexes being more soluble in polar solvents; 2) The NH_2 or OH groups will stabilise the ligands via super-conjugation effects, in other words, such ligands would have less reducing ability to e.g. Cu(II); 3) From the magnetic point of view, the NH_2 or OH groups can change the torsion angle (α) between two metal magnetic planes *via* either H-bonding or steric effects, which will affect the magnetic interaction drastically; 4) From the organic chemistry point of view, further organic reactions could take place at the NH_2 or OH groups leading to additional ligand functionality and extended coordination chemistry; 5) NH_2 or OH groups in the ligands could provide more coordination possibilities with formation of polynuclear complexes. These ligands present an unusual arrangement of potential donor sites, with many possible mononucleating and dinucleating coordination modes. The ligand PAHAP as well as PHAAP has the potential for hexadentate coordination in a binuclear complex. Several possible modes for PAHAP involving pyridine and/or diazine and/or amino groups are

illustrated in **Scheme 1-1**. Despite the similar coordination modes of PAHAP and PHAAP it can have another mode as shown in **Scheme 1-2**, which shows that the hydroxyl group in the ligand can lose a proton and bridge two metal centers. PMHAP and PHMAP have

Scheme 1-1

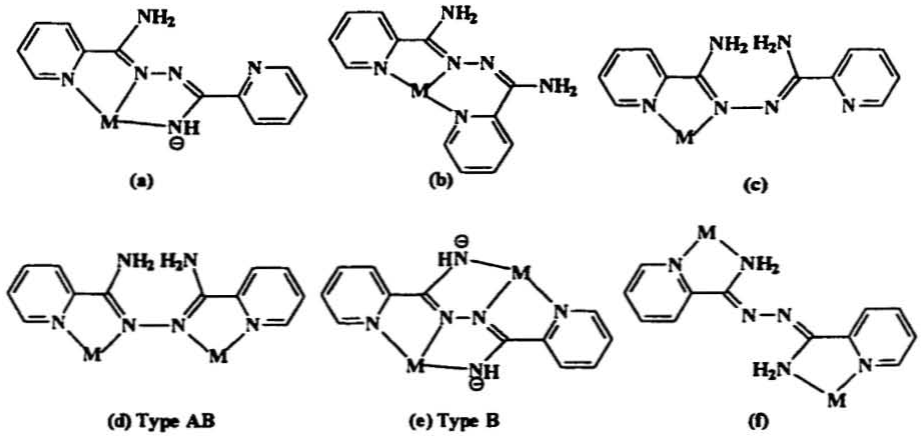

Scheme 1-2

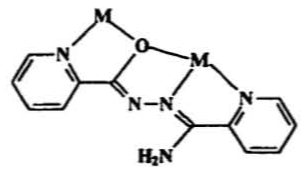

similar coordination modes and have the potential for pentadentate coordination in a binuclear complex. Another dinucleating mode for these two ligands is the intermediate

Type AB. PYPZ may have similar coordination modes to that of PAHAP, with the exception that it contains one more nitrogen donor at the fourth position of the pyrazine ring, which can provide additional coordination possibilities. PAHOX not only contains an open-chain diazine unit but also an oxime group which could act in a monodentate fashion at the N site or as an N-O bridge.

In Chapter 2, dicopper(II) complexes with five open-chain diazine ligands (PAHAP, PMHAP, PHMAP, PHAAP and PYPZ, **Figure 1-18**) are presented, in which the two copper(II) centers are bridged by a single N-N bond only. Changing the ligands, together with varying co-ligands leads to a situation where the torsion angle between the copper planes can be varied over a very large range. The comparison of magnetic exchange integrals and the torsion angles between the copper magnetic planes for these complexes has allowed us to establish magnetostructural correlations for open-chain diazine bridged dicopper(II) systems.

Chapter 3 deals mainly with dinuclear copper(II) complexes containing two open-chain diazine ligands (PAHAP, PMHAP, PYPZ, **Figure 1-18**) bridging two metal centers. The variable-temperature magnetic property studies on such complexes will be presented, and a comparison of the propagation of the exchange interaction *via* one N-N single bond and two N-N single bond linkages will be made. In this chapter, the studies on a most unusual tetranuclear copper(II) complex bridged by N-N single bonds from the open-chain diazine ligand and μ_2-1,1- azide will be also presented.

Chapter 4 describes a series of spiral homodinuclear complexes of Mn(II), Fe(II), Fe(III), Co(II), Co(III) and Ni(II) ions containing three N-N single bond bridges with a formula $[L_3M_2].(X)_n.mH_2O$ (L=PAHAP, PZHPZ, **Figure 1-18**; X=ClO_4 or NO_3; n = 4, 6) and an unusual seven-coordinate Fe(III) mononuclear complex. The X-ray structures, variable-temperature magnetic properties, electrochemistry and UV/vis, ^1H NMR spectra are discussed.

Chapter 5 focuses on a more extensive investigation of the coordination chemistry of the open-chain diazine ligands (PHAAP, PAHAP, PAHOX, PAH, **Figure 1-18**). An analysis of the crystal structures of a series of mononuclear and polynuclear first row transition metal complexes is presented. ^1H NMR spectra of diamagnetic complexes and the magnetic properties of the paramagnetic polynuclear complexes will be discussed.

In the last chapter, a general conclusion about coordination modes, magnetostructural correlations, etc. of the open-chain diazine complexes will be made. Some suggestions with regard to the future work in this field are given.

1.5 Analyses - spectroscopic and physical measurements

UV/VIS SPECTRA

Electronic spectra were recorded as Nujol mulls and in solution using a Cary 5E spectrometer.

INFRARED SPECTROSCOPY (IR)

Infrared spectra were recorded as Nujol mulls using a Mattson Polaris FT-IR instrument.

MASS SPECTRA

Mass spectra were obtained using a VG micromass 7070HS spectrometer.

ELEMENTAL ANALYSES

C, H, N determinations were performed by the Canadian Microanalytical Service, Delta, B.C., Canada.

MAGNETIC MEASUREMENTS

Room temperature magnetic moments were measured using a Cahn 7600 Faraday balance and variable temperature magnetic data (4-305K) were obtained using an Oxford Instruments Superconducting Faraday Susceptometer with a Sartorius 4432 microbalance. A main solenoid field of 1.5 T and a gradient field of 10 T m^{-1} were employed. Calibrations were carried out with $HgCo(NCS)_4$ and temperature errors were determined with [TMEN][$CuCl_4$] (TMEN=$(CH_3)_2HNCH_2CH_2NH(CH_3)_2^{2+}$) [99].

ESR SPECTROSCOPY

ESR spectra were recorded with a Bruker ESP 300 X-band spectrometer at room temperature.

ELECTROCHEMICAL MEASUREMENTS

Cyclicvoltammetry was performed at room temperature in H_2O and dimethyl-formamide (DMF) (spectroquality grade dried over molecular sieves), under O_2 free conditions, using a BAS CV-27 voltammograph and a BAS XY recorder. A three electrode system was used in which the working electrode and counter electrode were glassy-carbon and platinum respectively, with a standard calomel (SCE) reference electrode. The

supporting electrolytes were KNO_3 for aqueous solution and tetra- ethylammonium nitrate (TEAN) for DMF solution. All potentials ($E_{1/2}$ values) are reported versus the standard calomel electrode (SCE).

MELTING POINTS

Melting points were measured on a Fisher-Johns melting point apparatus and are uncorrected.

^{1}H NMR

^{1}H NMR spectra were obtained with a General Electric 300-NB spectrometer with tetramethylsilane (TMS) as an internal standard.

1.6 Safety note

Both perchlorate and azide compounds are potentially explosive and should be treated with care and used only in small quantities. In particular, $Cu(N_3)_2$ and many other simple ionic metal azides are explosive, so care must be taken to avoid using an excess amount of metal salt and azide during the preparation of the metal complexes. All azide and perchlorate complexes reported herein were tested by controlled mechanical impact to ensure their stability.

CHAPTER 2 Dinuclear Copper(II) Complexes Bridged by One N-N Single Bond Only

2.1 Introduction

As mentioned previously, the literature references to copper(II) complexes containing open-chain diazine ligands are very limited. Such diazine moieties in the ligands are much more flexible compared with those incorporated in heterocyclic compounds, and generate many coordination modes. **Type B** systems exhibit moderately strong exchange coupling with -2J value of about 210 cm^{-1}, while with **Type AB** diazine bridge systems, which have a twisted conformation, variable exchange coupling pathways exist, i.e. -2J = 53 cm^{-1} in $[Cu(PMK)Cl_4]$ [79], and no coupling in $[Cu(OPA)]_4(NO_3)_4.8H_2O$ [98]. Therefore, systematic studies on the structures and magnetic properties of this type of polynuclear copper(II) complex represent an interesting step forward towards the understanding of magnetic exchange propagation *via* this kind of diazine bridge. Therefore, this chapter presents a study of a series of binuclear copper(II) complexes of the following diazine ligands, including their syntheses, structures, magnetic properties and MO modelling. The ligands PAHAP, PMHAP, PHMAP, PHAAP and PYPZ were synthesized by **Scheme 2-1**.

Scheme 2-1

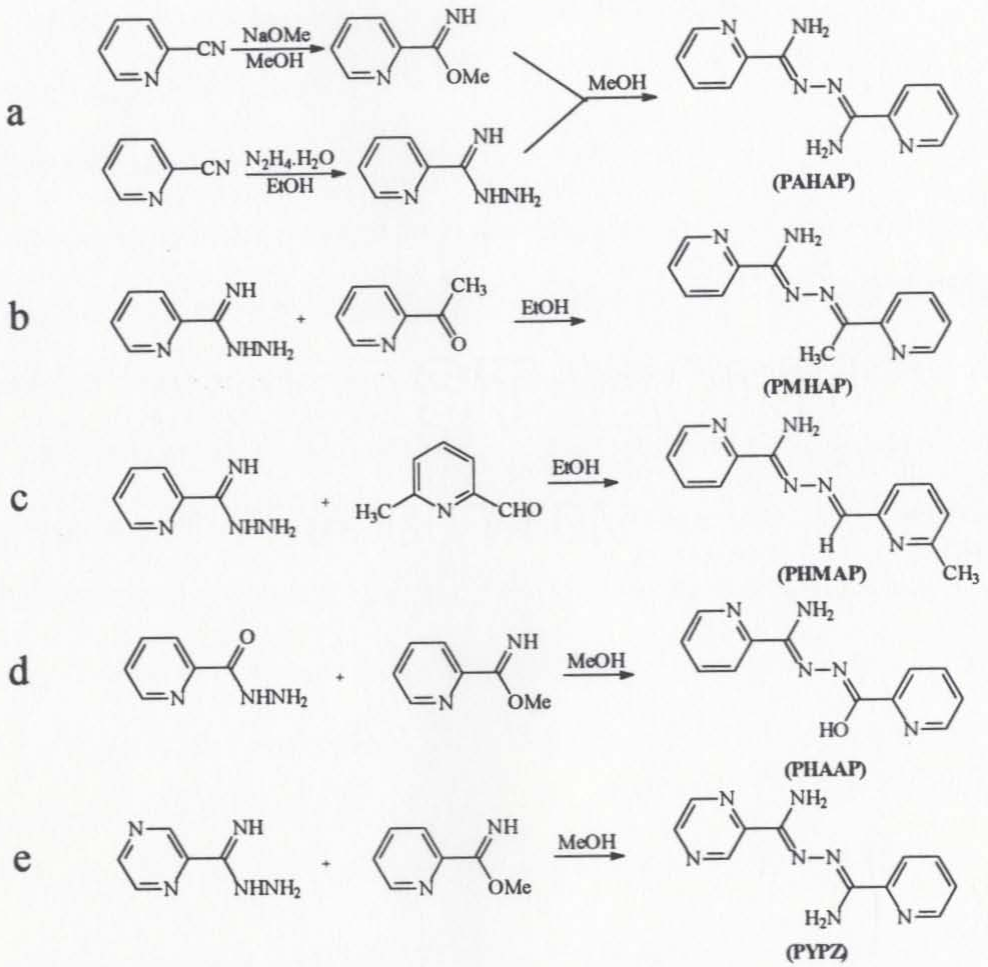
a
NaOMe
MeOH
MeOH
N2H4.H2O
EtOH
(PAHAP)
b
EtOH
(PMHAP)
c
EtOH
(PHMAP)
d
MeOH
(PHAAP)
e
MeOH
(PYPZ)

2.2 Experimental

2.2.1 Materials

Commercially available solvents and chemicals were used without further purification.

2.2.2 Measurements

Analysis, spectroscopic and physical measurements (see Chapter 1)

2.2.3 Synthesis of the ligands

PAHAP (picolinamide azine)

This compound was prepared by a procedure different from that reported in the literature [100], with an improved yield. 2-cyanopyridine (20.8 g, 0.200 mol) was reacted with a solution of sodium methoxide, generated by addition of sodium metal (0.46 g, 0.020 mol) to dry methanol (200 mL), at room temperature for 12 hr to yield the methyl ester of iminopicolinic acid [98]. Picolinamide hydrazone [101] (27.6 g, 0.200 mol) was added to the solution of iminopicolinic acid ester in situ and the resulting clear solution was refluxed for 24 hrs. Cooling to room temperature produced yellow crystals (yield 40.8 g, 85.0%), which were recrystalized from ethanol and characterized by C, H, N analysis, MS, ^{1}H NMR and mp. (mp. 210°C; lit. 210-211°C).

PMHAP

Picolinamide hydrazone [100] (13.6 g, 0.100 mol) was reacted with 2-acetyl pyridine (12.1 g, 0.100 mol) in boiling absolute ethanol (50 mL) for 4 hrs. The resulting solution was cooled to room temperature, whereupon, yellow crystals were obtained (yield 17.9 g, 80.0%, mp. 117-118°C). Mass spectrum (major mass peak; m/z): 239 (M), 224

(M-CH_3), 161, 133, 108, 78. Infrared spectrum, $\nu_{C=N}$ 1613 cm^{-1}, ν_{NH} 3465 cm^{-1}, 3318 cm^{-1}. Anal. calcd. for $C_{13}H_{13}N_5$: C, 65.26; H, 5.48; N, 29.27. Found: C, 65.26; H, 5.48; N, 29.42.

PHMAP

Picolinamide hydrazone [100] (13.6 g, 0.100 mol) was added to a boiling solution of 6'-methyl-2-pyridine carboxaldehyde (12.1 g, 0.100 mol) in absolute ethanol (60 mL). The resulting solution was refluxed for 4 hrs. On cooling to room temperature, yellow crystals formed (yield 19 g, 80%, mp. 125-126°C). Mass spectrum (major mass peak; m/z): 239 (M), 238 (M-H), 208, 147, 134, 119, 106, 79. Infrared spectrum, $\nu_{C=N}$ 1618 cm^{-1}, 1604 cm^{-1}, ν_{NH} 3484, 3455, 3362, 3300 cm^{-1}. Anal. calcd. for $C_{13}H_{13}N_5$: C, 65.26; H, 5.48; N, 29.27. Found: C, 65.29; H, 5.46; N, 29.30.

PHAAP

13.7 g (0.100 mol) picolinic hydrazide, made from ethyl picolinate by reacting with hydrazine hydrate in methanol at room temperature, was added to a 100 mL methanol solution containing 0.11 mol of the methyl ester of iminopicolinic acid. The clear solution was refluxed for 6 hrs. Cooling the solution to room temperature produced a pale yellow crystalline product (yield 85-90%, mp. 215-216°C). Mass spectrum (major mass peak; m/z): 241(M), 224, 223 (M-NH_3 and M-H_2O respectively), 194, 163, 107, 79. Infrared spectrum, $\nu_{C=N}$ 1602 cm^{-1}, $\nu_{C=O}$ 1667 cm^{-1}, ν_{NH} 3305, 3167 cm^{-1}. Anal. calcd. for $C_{12}H_{11}N_5O$: C, 59.75; H, 4.60; N, 29.21. Found: C, 59.73; H, 4.58; N, 29.34.

PYPZ

PYPZ was made in a similar fashion to that of PAHAP, using 2-pyrazinamide hydrazone instead of picolinamide hydrazone, with a 90% yield (mp. 212-214°C). Mass spectrum (major mass peak; m/z): 241(M), 225, 224 (M-NH_2) 196, 195, 163, 162, 121, 120, 106, 105, 80, 79. Infrared spectrum, $\nu_{C=N}$ 1606 cm^{-1}, ν_{NH} 3408, 3301 cm^{-1}. Anal. calcd. for $C_{11}H_{11}N_7$: C, 54.77; H, 4.60; N, 40.67. Found: C, 54.97; H, 4.53; N, 41.19.

2.2.4 Synthesis of the complexes

$[Cu_2(PAHAP)Cl_4].H_2O$ (1)

PAHAP (0.24 g, 1.0 mmol) was added to an aqueous solution (30 mL) of $CuCl_2.2H_2O$ (0.34 g, 2.0 mmol), and the mixture was stirred for several minutes at room temperature until the ligand dissolved. The deep green solution was filtered and the filtrate was allowed to stand at room temperature for several days. Dark green crystals, suitable for an X-ray structural determination formed; these were filtered off, washed quickly with water and air-dried (yield 90%). Anal. calcd. for $[Cu_2(C_{12}H_{12}N_6)Cl_4].H_2O$: C, 27.34; H, 2.68; N, 15.94. Found: C, 27.45; H, 2.63; N, 16.12.

$[Cu_2(PAHAP)Cl_4]$ (2)

This complex was prepared as brown crystals, which were suitable for an X-ray structural determination, in a similar way to that of 1, with the exception that a 2-fold excess of copper chloride was used. Yield 92%. Anal. calcd. for $[Cu_2(C_{12}H_{12}N_6)Cl_4]$: C, 28.31; H, 2.37; N, 16.50. Found: C, 28.37; H, 2.38; N, 16.57.

$[Cu_2(PAHAP)Br_4].H_2O$ (3)

This complex was prepared in a similar manner to **1**, using copper(II) bromide, and was obtained as brown crystals (92%), suitable for an X-ray structural determination. Anal. calcd. for $[Cu_2(C_{12}H_{12}N_6)Br_4].H_2O$: C, 20.44; H, 2.00; N, 11.92. Found: C, 20.55; H, 1.98; N, 11.92.

$[Cu_2(PAHAP)(H_2O)_6](NO_3)_4$ (4)

This complex was also prepared in a similar manner to **1**, using copper(II) nitrate (yield 80%), forming deep green crystals suitable for an X-ray structural determination. Anal. calcd. for $[Cu_2(C_{12}H_{12}N_6)(H_2O)_{5.5}](NO_3)_4$: C, 20.17; H, 3.24; N, 19.60. Found: C, 20.22; H, 3.03; N, 19.46. The X-ray sample, which was not vacuum-dried, was shown to have four strongly and two weakly coordinated water molecules.

$[Cu_2(PAHAP\text{-}H)(N_3)_2(NO_3)]$ (5)

This compound was prepared as olive green microcrystals by addition of an aqueous solution of sodium azide to an aqueous solution of **4**. Anal. calcd. for $[Cu_2(C_{12}H_{11}N_6)(N_3)_2(NO_3)]$: C, 28.07; H, 2.14; N, 35.45. Found: C, 28.19; H, 2.18; N, 36.04.

$[Cu_2(PAHAP)(NCS)_4(DMF)_2].2DMF$ (6)

Complex **4** (0.72 g, 1.0 mmol) was dissolved in 40 mL deionized water and added slowly with stirring to a solution of KSCN (0.58 g, 6.0 mmol) dissolved in water (30 mL). A yellow-green precipitate formed immediately, which was allowed to stand overnight, filtered and washed with deionized water and dried under vacuum. Green crystals, suitable

for X-ray determination, were obtained by diffusion of ether into a DMF/MeOH (1:1) solution of the precipitate (yield 90%). Anal. calcd. for $[Cu_2(C_{12}H_{12}N_6)(NCS)_4(DMF)_2]$ .2DMF: C, 37.71; H, 4.52; N, 22.00. Found: C, 37.47; H, 4.37; N, 22.30.

$[Cu_2(PAHAP)(NCO)_4].2DMF$ (7)

Compound 7 was prepared as olive green microcrystals in a similar manner to compound 6 in 85% yield, by using KOCN instead of KSCN. Anal. calcd. for $[Cu_2(C_{12}H_{12}N_6)(NCO)_4].2DMF$: C, 38.76; H, 3.82; N, 24.66. Found: C, 38.30; H, 3.19; N, 24.66.

$[Cu_2(PAHAP)(Bipy)_2(NO_3)_2].(NO_3)_2.4H_2O$ (8)

Bipy (0.312 g, 2.00 mmol) was added to a solution of compound 4 (0.72 g, 1.0 mmol) dissolved in 20 mL deionized water, forming a clear green solution after a few minutes. The solution was filtered and allowed to stand at room temperature for a few days. Deep green crystals, suitable for structure analysis, formed which were filtered off and dried in air (yield 61%). Anal. calcd. for $[Cu_2(C_{12}H_{12}N_6)(C_{10}H_8N_2)_2(NO_3)_2].(NO_3)_2$ $.4H_2O$: C, 38.44; H, 3.63; N, 19.61. Found: C, 38.40; H, 3.35; N, 19.65.

$[Cu_2(PAHAP)(Glyn\text{-}H)_2(NO_3)(H_2O)](NO_3).3H_2O$ (9)

Glycine (0.15 g, 2.0 mmol) was neutralised by addition of a solution of KOH (2.0 mmol in 5 mL H_2O) and added to a solution of compound 4 (0.72 g, 1.0 mmol) dissolved in 15 mL deionized water, with the formation of a deep green solution. The solution was filtered and allowed to stand for 3 days. Dark blue crystals formed, which were suitable for structural analysis (yield 84.4%) Anal. calcd. for $[Cu_2(C_{12}H_{12}N_6)(C_2H_4NO_2)_2](NO_3)_2$.

$4H_2O$: C, 26.96; H, 3.83; N, 19.60. Found: C, 27.01; H, 3.98; N, 19.68.

$[Cu_2(PAHAP)(Aln\text{-}H)_2(H_2O)_2]\ (NO_3)_2.3H_2O$ **(10)**

This compound was prepared as dark blue, rod like crystals in a procedure similar to that for **9**, except for the use of *d,l*-alanine instead of glycine (yield 89.8%). Anal. calcd. for $[Cu_2(C_{12}H_{12}N_6)(C_3H_6NO_2)_2\ (H_2O)_2\ ](NO_3)_2.3H_2O$: C, 28.54; H, 4.52; N, 18.49. Found: C, 28.26; H, 4.43; N, 18.39.

$[Cu_2(PAHAP)(ACAC\text{-}H)_2](NO_3)_2$ **(11)**

This compound was prepared as dark blue crystals in a similar manner to **9** using sodium acetylacetonate (NaACAC). Yield 0.60 g (80.8%). Anal. calcd. for $[Cu_2(C_{12}H_{12}N_6)(C_5H_7O_2)_2](NO_3)_2$: C, 38.32; H, 3.80; N, 16.24. Found: C, 38.28; H, 3.84; N, 16.29.

$[Cu_2(PMHAP\text{-}H)(NO_3)_3]$ **(12)**

A hot solution of PMHAP (0.24 g, 1.0 mmol) in dichloromethane (10 mL) was added to a hot solution $Cu(NO_3)_2.3H_2O$ (0.60 g, 2.5 mmol) in methanol (20 mL), and the resulting solution was allowed to stand at room temperature overnight. Dark green crystals formed, which were suitable for X-ray structure determination (yield 0.45 g, 81%). Anal. calcd. for $[Cu_2(C_{13}H_{12}N_5)(NO_3)_3]$: C, 28.32; H, 2.19; N, 20.32. Found: C, 28.30; H, 2.31; N, 20.29.

$[Cu_2(PMHAP)(H_2O)_2(NO_3)_2]\ (NO_3)_2$ **(13)**

This compound was prepared as green crystals in a similar procedure to that of compound **4** (71%), using PMHAP instead of PAHAP. The crystals lose weakly

coordinated water and lattice water on drying. Anal. calcd. for $[Cu_2(C_{13}H_{13}N_5)(H_2O)_2(NO_3)_2](NO_3)_2$: C, 24.00; H, 2.63; N, 19.37. Found: C, 23.68; H, 2.43; N, 19.09.

$[Cu_2(PHMAP\text{-}H)(MeOH)(H_2O)(NO_3)_3]$ **(14)**

PHMAP (0.24 g, 1.0 mmol) was dissolved in acetonitrile (10 mL) and added to a hot solution of $Cu(NO_3)_2.3H_2O$ (0.53 g, 2.2 mmol) in methanol (20 mL). The resulting dark green solution was filtered and the filtrate allowed to stand at room temperature overnight. Dark green, almost black, crystals formed which were filtered off, washed with methanol and dried in air (yield 0.51 g, 84.8%). Anal. calcd. for $[Cu_2(C_{13}H_{12}N_5)(H_2O)(MeOH)(NO_3)_3]$: C, 27.96; H, 3.02; N, 18.63. Found: C, 27.59; H, 2.95; N, 18.96.

$[Cu_2(PHAAP\text{-}H)(Br)_3(H_2O)]$ **(15)**

PHAAP (0.241 g, 1.00 mmol) was suspended in a solution of copper(II) bromide (0.67g, 3.0 mmol) in 20 mL deionized water at room temperature. To the mixture, 10 mL ethanol was added. A clear solution formed, which was filtered and allowed to stand at room temperature for a few days. Black crystals formed, which were filtered off and dried in air (yield 0.50 g, 71%). Anal. calcd. for $[Cu_2(C_{12}H_{10}N_5O)(H_2O)(Br)_3]$: C, 23.06; H, 1.94; N, 11.20. Found: C, 23.69; H, 1.74; N, 11.42.

$[Cu_2(PYPZ)Cl_4].H_2O$ **(16)**

PYPZ (0.241 g, 1.00 mmol) was added to an aqueous solution of copper(II) chloride (0.68 g, 4.0 mmol) in 20 mL water, and the mixture was stirred for several minutes at room temperature until the ligand dissolved. The deep green solution was filtered, and the filtrate was allowed to stand at room temperature for several days. Dark

green, diamond shaped crystals formed, which were suitable for an X-ray structural determination. These were filtered off, washed quickly with cold deionized water, and air dried (yield 80%). Anal. calcd. for $[Cu_2(C_{11}H_{11}N_7)Cl_4].H_2O$: C, 25.00; H, 2.48; N, 18.56. Found: C, 24.67; H, 2.48; N, 18.20.

$[Cu_2(PYPZ)Br_4].H_2O$ (17)

This compound was prepared similarly to **16**, using copper(II) bromide instead of copper(II) chloride, and was obtained as brown crystals (yield 80%). Anal. calcd. for $[Cu_2(C_{11}H_{11}N_7)Br_4].H_2O$: C, 18.71; H, 1.86; N, 13.88. Found: C, 18.94; H, 1.83; N, 14.07.

2.2.5 Crystallographic data collection and refinement of the structures

PAHAP

A yellow crystal of approximate dimensions 0.35 × 0.25 × 0.40 mm was transferred to a Rigaku AFC6S diffractometer with graphite-monochromatized Mo Kα radiation. The diffraction intensities were collected at 26.1 °C by using the $\omega - 2\theta$ scan technique to a $2\theta_{max}$ value of 50.1°. A total of 2533 reflections were measured and 1229 were considered significant with $I_{net} > 2.0\ \sigma\ (I_{net})$. The intensities of three representative reflections, which were measured after every 150 reflections, remained constant throughout the data collection, indicating crystal and electronic stability (no decay correction was applied). An empirical absorption correction, based on azimuthal scans of several reflections, was applied, which resulted in transmission factors ranging from 0.97 to 1.00. The data were corrected for Lorentz and polarisation effects. The cell parameters

were obtained from the least-squares refinement of the setting angles of 23 carefully centred reflections with 2 θ in the range 20.1-26.3°.

The structure was solved by direct methods [102, 103]. All atoms except hydrogens were refined anisotropically. Hydrogen atoms were optimized by positional refinement with isotropic thermal parameters set 20% greater than those of their bonded partners at the time of their inclusion. However, they were fixed for the final round of refinement. The final cycle of full-matrix least-squares refinement was based on 1229 observed reflections ($I > 2.00\sigma(I)$) and 164 variable parameters and converged with unweighted and weighted agreement factors of $R = \Sigma||F_o|-|Fc||/\Sigma|F_o| = 0.045$ and $R_w = [(\Sigma w(|F_o|-|F_c|)^2/ \Sigma wF_o^2]^{1/2} = 0.038$. The maximum and minimum peaks on the final difference Fourier map correspond to 0.14 and - 0.19 electron $Å^{-3}$, respectively. Neutral atom scattering factors [104] and anomalous-dispersion terms [105, 106], were taken from the usual sources. All calculations were performed with the TEXSAN [107] crystallographic software package using a VAX 3100 work station. Abbreviated crystal data are given in **Table 2-1**.

$[Cu_2(PAHAP)Cl_4].H_2O$ (**1**), $[Cu_2(PAHAP)Br_4].H_2O$ (**3**), $[Cu_2(PAHAP)(H_2O)_6](NO_3)_4$(**4**), $[Cu_2(PAHAP)(Glyn\text{-}H)_2(NO_3)(H_2O)](NO_3).3H_2O$ (**9**), $[Cu_2(PAHAP)(Aln\text{-}H)_2(NO_3)_2].5H_2O$ (**10**), and $[Cu_2(PYPZ)Cl_4].H_2O$ (**16**). The data collections and structure solutions for these crystals were carried out in a manner similar to that for PAHAP. Bromine Br(3) in **3** exhibited some positional disorder and was modelled with two (80/20)

components. Only one hydrogen associated with the lattice water molecule could be found in difference maps. Abbreviated crystal data for those crystals are given in **Table 2-1.**

$[Cu_2(PMHAP\text{-}H)(NO_3)_3]$ **(12)**

The crystals of **12** are green. A single crystal of **12** of dimensions 0.20 × 0.10 × 0.10 mm was transferred to a Siemens Smart three-circle diffractometer, equipped with a CCD area detector using graphite-monochromatized Mo Kα radiation, and controlled by a pentium based PC running the SMART software package [108]. ω-scans were used in such a way that an initial 180° scan range consisting of 0.3° intervals is followed by three further 120°, 180° and 120°scans with ϕ offsets of 88, 180 and 268°, respectively. This strategy samples the sphere of reciprocal space up to 2θ = 56.62°. Cell parameters were refined using the centroid values of 300 reflections with 2θ angles up to 56.62°. Raw frame data were integrated using the SAINT [109] programme. The structure was solved by direct methods [110]. An empirical absorption correction was applied to the data using the programme SADABS [111]. Abbreviated crystal data are listed in **Table 2-1**.

$[Cu_2(PAHAP)(NCS)_4(DMF)_2].2DMF$ **(6)**, $[Cu_2(PAHAP)(Bipy)_2(NO_3)_2].(NO_3)_2.4H_2O$ **(8)**, $[Cu_2(PAHAP)(ACAC\text{-}H)_2](NO_3)_2$ **(11)**, $[Cu_2(PHMAP)(MeOH)(H_2O)(NO_3)_3]$ **(14)**, $[Cu_2(PHAAP)(Br)_3(H_2O)]$ **(15)**. Crystal data collection and structure refinement for these crystals were carried out in a similar manner to that for **12**. Abbreviated crystal data for all of these complexes are given **Table 2-1**. The elemental analysis of a bulk sample of **6** clearly indicates the presence of four DMF molecules, but only the coordinated ones are clearly defined in the X-ray structural analysis. The components of the lattice could not be

modelled successfully but the binuclear complex itself is however clearly defined. We assume that in this unusual case the batch of **6** used for elemental analysis and structural analysis may differ slightly, but we are confident by comparison of infrared spectra that the complex itself is the same in each sample.

Despite repeated attempts at the structural solution of **8**, and measuring diffraction data for a second crystal, and also repeating the structural determination using a Rigaku AFC6S diffractometer, the lattice nitrates, which are clearly evident from the elemental analysis of the crystallographic sample, and other physical data, do not show up clearly in the refinement. The structural features of the binuclear cation are clearly revealed, with eminently sensible parameters for a binuclear copper(II) complex of this sort, and so the absence of the nitrates is considered to be due to less than optimal crystal quality. The structures of both **6** and **8** are considered as preliminary at this point, but the structures of the main fragments are clearly revealed.

Note in **Table 2-1**:

Rigaku data; * Siemens Smart data

$\mathbf{R} = \Sigma||F_o| - |F_c||/\Sigma|F_o|$, $\mathbf{R_w} = [(\Sigma(|F_o| - |F_c|)^2/\Sigma wF_o^2)]^{1/2}$

$\mathbf{R1} = \Sigma||F_o| - |F_c||/\Sigma|F_o|$, $\mathbf{wR_2} = [\Sigma[w(|F_o|^2 - |F_c|^2)^2/\Sigma[w(|F_o|^2)^2]]^{1/2}$

⊗: Preliminary structure

Table 2-1. Summary of crystallographic data for the ligand PAHAP and complexes **1, 3, 4, 6, 8-12, 14-16**.

Compound	PAHAP[#]	1[#]	3[#]
chemical formula	$C_{12}H_{12}N_6$	$C_{12}H_{14}N_6OCl_4Cu_2$	$C_{12}H_{14}N_6OBr_4Cu_2$
formula wt.	240.27	527.19	703.98
space group	Pbca (#61)	C2/c (#15)	C2/c (#15)
a (Å)	19.845(4)	26.732 (6)	27.336 (2)
b(Å)	13.178(5)	8.670 (9)	8.859(4)
c(Å)	9.483(8)	16.436(4)	16.795(3)
α(deg)	90	90	90
β(deg)	90	100.88(2)	100.78(1)
γ(deg)	90	90	90
V (Å^3)	2480 (4)	3741 (6)	3996 (3)
ρ_{calcd}(gcm^{-3})	1.287	1.872	2.340
Z	8	8	8
μ(cm^{-1})	0.79	28.72	100.75
λ	0.71069	0.71069	0.71069
T, K	299(1)	299(1)	299(1)
R1(R)	0.045(R)	0.029(R)	0.037(R)
wR2(R_w)	0.038(R_w)	0.025(R_w)	0.030(R_w)

Table 2-1. (contd.) Summary of crystallographic data for the ligand PAHAP and complexes **1, 3, 4 , 6, 8-12, 14-16.**

Compound	$4^{\#}$	$6^{*,\otimes}$	$8^{\#,\otimes}$
chemical formula	$C_{12}H_{24}N_{10}O_{18}Cu_2$	$C_{22}H_{30.32}Cu_2N_{12}O_{4.16}S_4$	$C_{32}H_{28}Cu_2N_{12}O_6$
formula wt.	723.47	784.76	803.74
space group	C2/c (#15)	C2/c	Pcca
a (Å)	20.983(4)	36.7978(9)	13.9286(8)
b(Å)	7.505(4)	15.7510(3)	12.5106(8)
c(Å)	17.219(3)	16.1358(4)	24.578(1)
α(deg)	90	90	90
β(deg)	104.22 (1)	114.992(1)	90
γ(deg)	90	90	90
V ($Å^3$)	2628(1)	8476.7(3)	4282(4)
$\rho_{calcd}(gcm^{-3})$	1.828	1.230	1.247
Z	4	8	4
$\mu(mm^{-1})$	1.718	1.239	1.044
λ	0.71069	0.71073	0.71073
T, K	299(1)	298(2)	298(2)
R1(R)	0.048(R)	0.0582	0.0547(R)
wR2(R_w)	0.053(R_w)	0.1494	0.1296(R_w)

Table 2-1. (contd.) Summary of crystallographic data for the ligand PAHAP and complexes **1, 3, 4 , 6, 8-12, 14-16.**

Compound	9#	10#	11*
chemical formula	$C_{16}H_{24}N_{10}O_{12}Cu_2$	$C_{18}H_{40}Cu_2N_{10}O_{15}$	$C_{22}H_{32}Cu_2N_8O_{13}$
formula wt.	675.53	763.66	743.64
space group	PI	PI	$P2_1/c$
a (Å)	11.506(12)	17.603(4)	17.226(3)
b(Å)	12.525(18)	18.378(4)	12.260(2)
c(Å)	10.319(4)	10.742(4)	14.795(3)
α(deg)	94.47(7)	93.44(3)	90
β(deg)	106.58(5)	93.19(3)	100.208(3)
γ(deg)	114.55(9)	62.98(2)	90
V ($Å^3$)	1263(2)	3071(2)	3075(2)
$\rho_{calcd}(gcm^{-3})$	1.776	1.652	1.607
Z	2	4	4
$\mu(mm^{-1})$	1.765	1.469	1.459
λ	0.71073	0.71069	0.71073
T, K	150(2)	299(2)	293(2)
R1(R)	0.0538	0.060(R)	0.0263
wR2(R_w)	0.1257	0.048(R_w)	0.0620

Table 2-1. (contd.) Summary of crystallographic data for the ligand PAHAP and complexes **1, 3, 4 , 6, 8-12, 14-16.**

Compound	12*	14*
chemical formula	$C_{13}H_{12}N_8O_9Cu_2$	$C_{14}H_{18}N_8O_{11}Cu_2$
formula wt.	551.39	601.44
space group	PĪ	PĪ
a (Å)	7.838(1)	7.4754(1)
b(Å)	8.015(3)	8.7340(1)
c(Å)	15.655(4)	17.9942(2)
α(deg)	99.81(3)	84.690(1)
β(deg)	101.74(2)	83.190(1)
γ(deg)	94.52(2)	66.885(1)
V (Å^3)	942.2(4)	1071.54(2)
ρ_{calcd}(gcm^{-3})	1.943	1.864
Z	2	2
μ(cm^{-1})	23.28	2.062
λ (Å)	0.71073	0.71073
T, K	298(2)	150(2)
R1(R)	0.0708	0.0483
wR2(R_w)	0.1563	0.1038

Table 2-1. (contd.) Summary of crystallographic data for the ligand PAHAP and complexes **1, 3, 4 , 6, 8-12, 14-16**.

Compound	15*	16#
chemical formula	$C_{12}H_{13}N_5O_2Cu_2Br_4$	$C_{11}H_{13}N_7Cu_2Cl_4O$
formula wt.	705.99	528.17
space group	$P2_1/c$	C2/c(#15)
a (Å)	15.1463(3)	26.754(3)
b(Å)	18.1847(4)	8.466(3)
c(Å)	6.8554(2)	16.334(3)
α(deg)	90	90
β(deg)	92.7450(10)	100.94(1)
γ(deg)	90	90
V (Å^3)	1886.02(8)	3632(1)
ρ_{calcd}(gcm^{-3})	2.3176	1.931
Z	4	8
μ(cm^{-1})	8.64	8.458
λ (Å)	0.71073	1.54178
T, K	298 (2)	299(1)
R1(R)	0.048	0.058(R)
wR2(R_w)	0.1173	0.039(R_w)

2.3 Results and discussion

2.3.1 Structures

PAHAP

The structure of PAHAP is illustrated in **Figure 2-1**, and relevant bond distances and bond angles are listed in **Table 2-2**. The molecule is essentially flat and has a *trans* configuration. The dihedral angle between the least squares planes including the atom groups N(1)-C(5)-C(6)-N(2)-N(3) and N(6)-C(8)-C(7)-N(5)-N(4) is 6.2°. The nitrogen-nitrogen bond N(3)-N(4) (1.424 (3) Å) can be formally defined as a single bond, and compares closely with the N-N bond distance in hydrazine (1.47 Å). The sum of the angles at C(6) and C(7) are 360.0° and 359.9° respectively, so the CN bonds C(6)-N(3) and C(7)-N(4) (1.287(3) and 1.295(3) Å respectively) are considered to have full double bond character. Intramolecular contacts between the amine hydrogen atoms attached to N(2) and N(5) and adjacent sp^2 nitrogen N(1), N(4) and N(3), N(6) respectively are too long to be considered as hydrogen bonds. Considering the repulsion between lone pair electrons of sp^2 N(1) and N(3) and that of sp^2 N(4) and N(6) due to the planar structure, the overall trans configuration is therefore due mainly to steric repulsion effects. An examination of intermolecular contacts reveals only two of possible significance between N(4) and N(6) and hydrogens bonded to N(5)' and N(2)' respectively (N-H 2.183 Å and 2.179 Å respectively), but these are clearly weak.

Table 2-2. Interatomic distances (Å) and angles (Deg.) for PAHAP.

N(2)-C(6)	1.343(4)	N(3)-N(4)	1.424(3)
N(3)-C(6)	1.287(3)	N(4)-C(7)	1.295(3)
N(5)-C(7)	1.347(4)		
N(2)-C(6)-C(5)	116.1(3)	N(4)-N(3)-C(6)	110.9(2)
N(3)-C(6)-C(5)	117.7(3)	N(3)-N(4)-C(7)	111.9(2)
N(4)-C(7)-N(5)	124.9(3)	N(4)-C(7)-C(8)	117.2(3)
N(5)-C(7)-C8)	117.8(3)	N(2)-C(6)-N(3)	126.2(3)

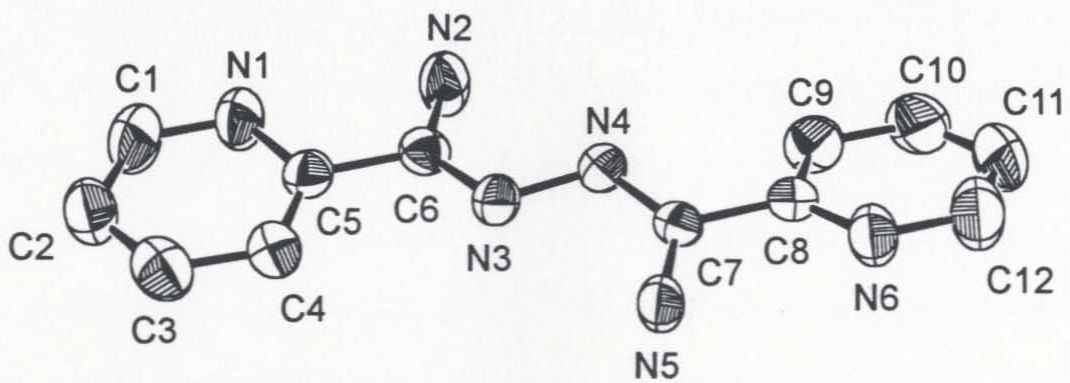

Figure 2-1. Structural representation of PAHAP with hydrogen atoms omitted (40% probability thermal ellipsoids).

$[Cu_2(PAHAP)Cl_4].H_2O$ (1)

The structure of **1** is illustrated in **Figure 2-2**, and relevant bond distances and angles are listed in **Table 2-3**. Two copper(II) ions are bound to one PAHAP ligand each via a pyridine and diazine nitrogen in a twisted structure, with nominal four coordination being completed at each copper centre by two chlorines. Cu-N and Cu-Cl distances are normal for equatorial coordination to copper(II). The diazine nitrogen-nitrogen bond distance (N(2)-N(3)) is 1.411(4) Å, implying single bond character, and largely unchanged from the free ligand. The C=N bonds (C(6)-N(2) and C(7)-N(3); 1.305(4) and 1.304(4) Å respectively) are essentially the same as those in PAHAP. However the sum of the angles at N(2) and N(3) (354.7°, 349.7° respectively) implies slight pyramidal distortion at these centers.

The two copper planes do not adopt a *trans-trans* (**Type B** as defined in Chapter 1) conformation about the C=N bonds, as might have been expected, but instead adopt a folded conformation, **Type AB**, with an acute angle between the planes. Molecular models suggest that a type B structure would be unlikely, because of steric constraints associated with the terminal chlorines and the amine groups. One significant factor responsible for the acute folding is considered to be a long intramolecular axial contact between Cu(2) and Cl(2) (3.080(3) Å), which effectively locks the two copper planes in place, creating a square-pyramidal geometry at Cu(2) (**Figure 2-2**). An analysis of intermolecular contacts reveals that two molecules are joined together via a long contact between Cu(1) and Cl(1) (3.066 Å) on an adjacent molecule, so that the complex is in reality a weakly associated

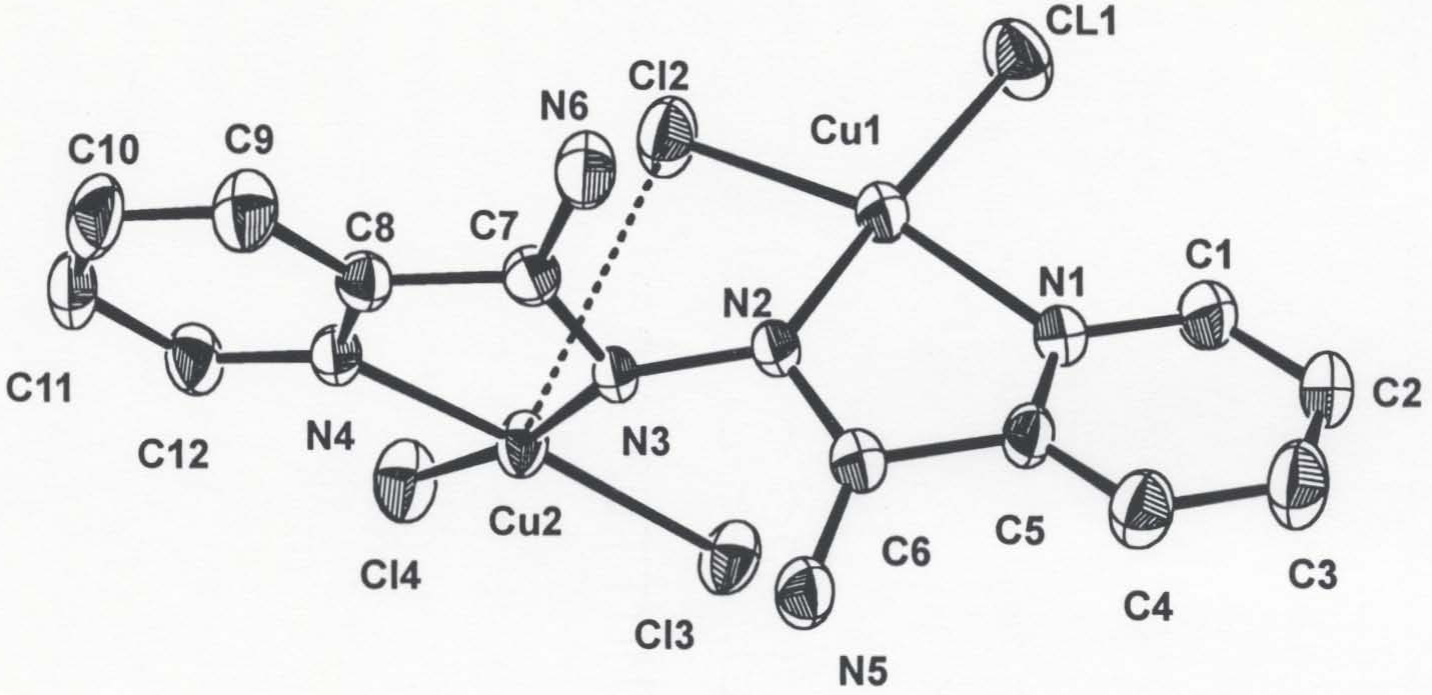

Figure 2-2. Structural representation of $[Cu_2(PAHAP)Cl_4].H_2O$ (**1**) with hydrogen atoms omitted (40% probability thermal ellipsoids).

Table 2-3 Interatomic distances (Å) and angles (Deg.) relevant to the copper coordination spheres and the ligand in $[Cu_2(PAHAP)Cl_4].H_2O$ (1).

Cu(1)-Cl(1)	2.233(1)	Cu(2)-Cl(3)	2.258(1)
Cu(1)-Cl(2)	2.257(2)	Cu(2)-Cl(4)	2.265(2)
Cu(1)-N(1)	2.027(3)	Cu(2)-N(3)	1.992(3)
Cu(1)-N(2)	1.984(3)	Cu(2)-N(4)	2.026(3)
N(5)-C(6)	1.321(4)	N(6)-C(7)	1.323(4)
N(2)-N(3)	1.411(4)	N(2)-C(6)	1.305(4)
N(3)-C(7)	1.304(4)	Cu(1)-Cu(2)	3.845(1)
Cl(1)-Cu(1)-Cl(2)	93.85(7)	Cl(3)-Cu(2)-Cl(4)	93.82(5)
Cl(1)-Cu(1)-N(1)	94.6(1)	Cl(3)-Cu(2)-N(3)	93.44(9)
Cl(1)-Cu(1)-N(2)	171.91(9)	Cl(3)-Cu(2)-N(4)	170.62(9)
Cl(2)-Cu(1)-N(1)	165.32(9)	Cl(4)-Cu(2)-N(3)	170.45(9)
Cl(2)-Cu(1)-N(2)	92.7(1)	Cl(4)-Cu(2)-N(4)	93.52(9)
N(1)-Cu(1)-N(2)	80.0(1)	N(3)-Cu(2)-N(4)	80.0(1)
N(2)-C(6)-N(5)	126.3(3)	N(2)-C(6)-C(5)	113.6(3)
N(5)-C(6)-C(5)	120.1(3)	N(3)-C(7)-N(6)	125.5(3)
N(3)-C(7)-C(8)	114.7(3)	N(6)-C(7)-C(8)	119.8(3)
N(3)-N(2)-C(6)	115.5(3)	N(2)-N(3)-C(7)	114.2(3)
Cu(1)-N(2)-N(3)	123.1(2)	Cu(1)-N(2)-C(6)	116.1(2)
Cu(2)-N(3)-N(2)	121.0(2)	Cu(2)-N(3)-C(7)	114.5(2)

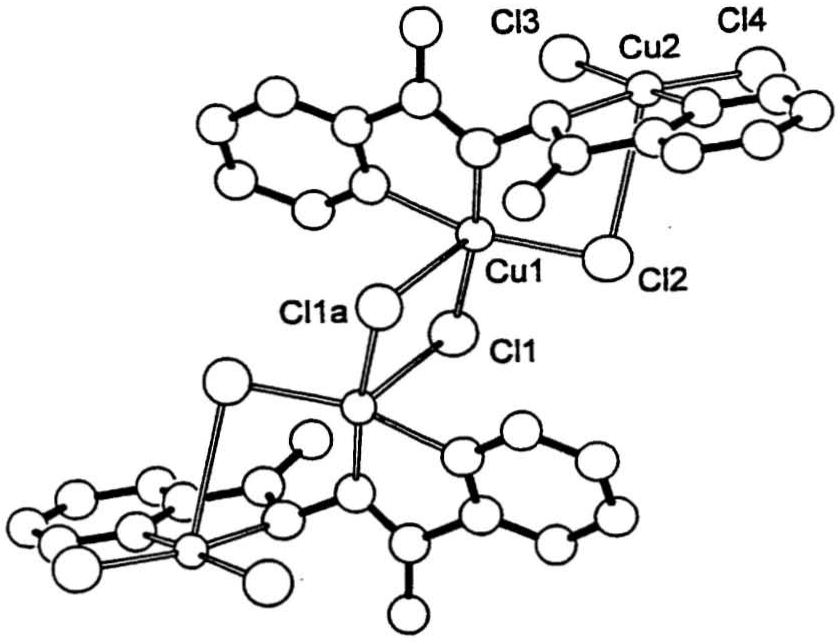

Figure 2-3. Sructural representation of the weakly associated dimer in $[Cu_2(PAHAP)Cl_4].H_2O$ (**1**).

tetranuclear dimer (**Figure 2-3**). The twist of the copper CuN_2Cl_2 planes can best be visualized in terms of the 77.1° dihedral angle between the planes Cu(1)-N(1)-C(5)-C(6) -N(2) and Cu(2)-N(4)-C(8)-C(7)-N(3). The resulting copper-copper separation (3.845(1) Å) is quite long, as would be expected. The lattice water molecule is not involved in coordination to copper. It can be concluded therefore that the molecular twist in $[Cu_2(PAHAP)Cl_4].H_2O$ (**1**) is the result of a balance between steric factors, principally associated with the chlorines and NH_2 groups on the ligand, and the weak axial interaction between Cu(2) and Cl(2).

$[Cu_2(PAHAP)Br_4].H_2O$ (3)

The structure of **3** is illustrated in **Figure 2-4** and relevant bond distances and angles are listed in **Table 2-4.** The structure is very similar to that of **1**, with two essentially planar copper (II) centers bound in a twisted cis-conformation. Deviations of the atoms in the N_2Br_2 donor sets are < 0.24 Å from their least-squares planes, with Cu(1) displaced by 0.0160 Å, and Cu(2) displaced by 0.0364 Å from their respective planes. The dihedral angle between the copper planes, as defined by the two CuN_2C_2 chelate rings is 75.02°, in close agreement with that in **1**. Cu-N distances are normal, and Cu-Br distances are close to 2.4 Å. The Cu-Cu separation (3.826(1) Å) is almost identical to that in **1**. The Cu(1)-Br(4) distance (3.107(1) Å) is very close to the intramolecular chlorine bridging contact in **1**, and so it is reasonable to assume a similar bridging situation in **3**. The Cu(2)-Br(2) distance (3.611(1) Å) is much too long for a second bridge. Intermolecular contacts involving potential bromine bridges are also too long to be significant (> 3.24 Å), and so **3** is considered to be an essentially isolated binuclear species. The similarity in fold angles for **1** and **3** is considered to result from the similar weak halogen bridged structural arrangement. Br(3) was modelled as two components in a disordered situation with an 80/20 composition. The residual electron density close to Br(3)A could not be sensibly accounted for in any other way.

Table 2-4. Interatomic distances (Å) and angles (Deg.) relevant to the copper coordination spheres and the ligand in $Cu_2(PAHAP)Br_4].H_2O$ (**3**).

Br(1)-Cu(1)	2.401(1)	N(5)-C(6)	1.334(8)
Br(2)-Cu(1)	2.402(1)	N(6)-C(7)	1.339(8)
Br(3A)-Cu(2)	2.362(2)	N(2)-N(3)	1.416(6)
Br(3B)-Cu(2)	2.39(2)	N(2)-C(6)	1.298(8)
Br(4)-Cu(2)	2.398(1)	N(3)-C(7)	1.282(8)
Cu(1)-N(1)	2.025(5)	Cu(1)-Cu(2)	3.826(1)
Cu(1)-N(2)	1.992(5)	Cu(2)-N(3)	1.991(6)
Cu(2)-N(4)	2.020(6)		
Br(1)-Cu(1)-Br(2)	93.12(4)	Br(1)-Cu(1)-N(1)	94.5(2)
Br(1)-Cu(1)-N(2)	171.6(2)	Br(2)-Cu(1)-N(1)	169.6(2)
Br(2)-Cu(1)-N(2)	93.3(1)	N(1)-Cu(1)-N(2)	79.9(2)
Br(3A)-Cu(2)-Br(4)	92.1(1)	Br(3A)-Cu(2)-N(3)	172.2(2)
Br(3A)-Cu(2)-N(4)	95.6(2)	Br(4)-Cu(2)-N(3)	93.4(2)
Br(4)-Cu(2)-N(4)	168.3(2)	N(3)-Cu(2)-N(4)	79.9(2)

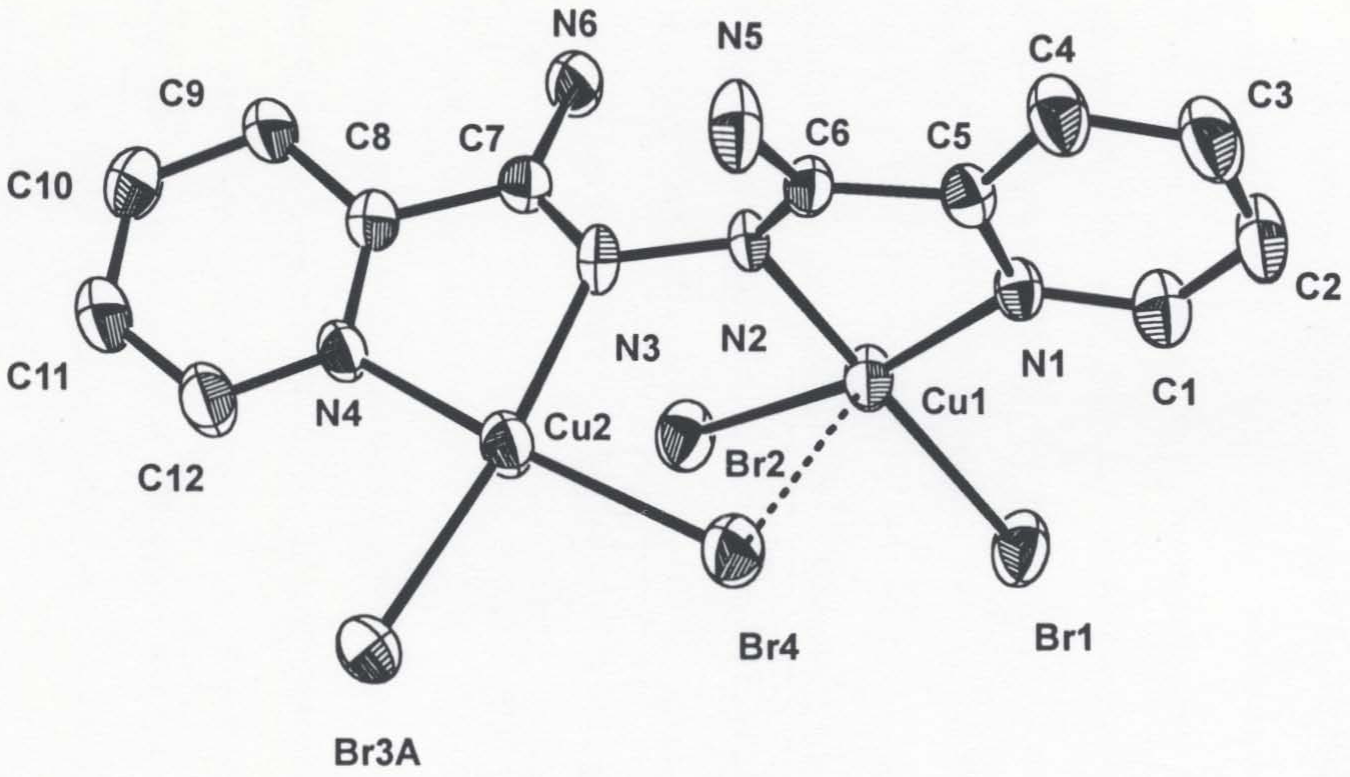

Figure 2-4. Structural representation of $[Cu_2(PAHAP)Br_4].H_2O$ (**3**) with hydrogen atoms and Br (3B) omitted (40% probability thermal ellipsoids).

$[Cu_2(PAHAP)(H_2O)_6](NO_3)_4$ (4)

The structure of **4** is illustrated in **Figure 2-5**, and relevant bond distances and angles are listed in **Table 2-5**. The two distorted six-coordinated copper ions are bound to PAHAP in a similar manner to **1**, with a twisted arrangement of the copper basal planes about the N-N bond, which clearly has single bond character (N(2)-N(2)' 1.430(8) Å). The C=N bond lengths (C(6)-N(2) 1.292(7) Å) are the same as those in PAHAP, and the sum of the angles at N(2) (359.6°) indicates that there is no pyramidal distortion at this donor centre. Three water molecules are bound to each copper (II) ion, two with short contacts in the basal plane (Cu(1)-O(1) 1.954(4) Å; Cu(1)-O(2) 1.980(4) Å), and one in the axial position (Cu(1)-O(9) 2.392(5) Å). A much longer contact to a nitrate oxygen (Cu(1)-O(4) 2.724(5) Å) indicates that a nitrate is semi-coordinated as a weak sixth ligand. The copper atom is displaced slightly from the mean N_2O_2 basal plane towards O(9) by 0.0367 Å.

The molecular twist in **4** about the N-N bond is substantially larger than in **1** and **3**. The dihedral angle between the least-squares planes Cu(1)-N(2)-C(6)-C(5)-N(1) and Cu(1)a-N(2)a-C(5)a-N(1)a is 100.2°, indicating a significant opening of the complex along the N-N bond in comparison with **1** and **3**. **Figure 2-6** illustrates a projection of **4** viewed along the N-N bond. This gives a reasonable representation of the angle between the copper magnetic planes, and explains why the Cu-Cu separation (4.389(2) Å) is so much larger than in **1** and **3**.

The most significant difference between **3**, **5** and **6** rests with the different ligands in the copper equatorial plane, and the presence of an axial, non-bridging water ligand (O(9)) in **6**. Steric repulsions between the coordinated water molecules at each metal centre, and also with the NH_2 groups, combined with the absence of a bridging ligand interaction, would reasonably allow the copper planes to move further apart until a balance between these repulsive forces was achieved. However such an effect cannot necessarily be considered in isolation, and in this case hydrogen bonding interactions should also be taken into account. Several hydrogen bonding contacts (X---H < 1.9 Å) have been identified (H(20A)-O(6) 1.824 Å, H(3NA)-O(8) 1.871 Å, H(90A)-O(7) 1.832 Å, H(90B)-O(5) 1.782 Å, H(10A)-O(3) 1.863 Å, H(10B)-O(3)1.800 Å, H(3NA)-O(8) 1.871 Å), all of which have X---H---Y angles in the range 153-175°. These are illustrated in **Figure 2-5**. Nitrate N(5) is involved in the most contacts, and provides significant links between the binuclear complex ions through the shortest interaction (O(2)-O(6) 2.724(8) Å). Other contacts through O(7) and N(4) are also involved in intermolecular contacts to water molecules O(1) and O(9). These hydrogen bonding interactions are possibly of significance in creating intermolecular spin exchange pathways (*vide supra*), but may also influence the twist between the copper equatorial coordination planes.

Table 2-5. Interatomic distances (Å) and angles (Deg.) relevant to the copper coordination spheres and the ligand in $[Cu_2(PAHAP)(H_2O)_6](NO_3)_4$ **(4)**.

Cu(1)-O(1)	1.954(4)	Cu(1)-N(1)	2.000(5)
Cu(1)-O(2)	1.980(4)	Cu(1)-N(2)	1.952(4)
Cu(1)-O(9)	2.392(5)	Cu(1)-O(4)	2.724(5)
C(5)-C(6)	1.495(7)	N(2)-N(2)a	1.430(8)
N(2)-C(6)	1.292(7)	N(3)-C(6)	1.306(7)
Cu(1)-Cu(1)a	4.389(2)		
O(2)-Cu(1)-N(1)	173.4(2)	O(1)-Cu(1)-O(2)	91.9(2)
O(2)-Cu(1)-N(2)	93.2(2)	O(1)-Cu(1)-N(1)	94.6(2)
N(1)-Cu(1)-N(2)	80.4(2)	O(1)-Cu(1)-N(2)	172.6(2)
N(2)-C(6)-C(5)	113.7(5)	N(2)-C(6)-N(3)	125.9(5)
Cu(1)-N(2)-N(2)a	125.8(4)	N(3)-C(6)-C(5)	120.4(5)
N(2)-N(2)a-C(6)	116.3(5)	Cu(1)-N(2)-C(6)	117.5(4)

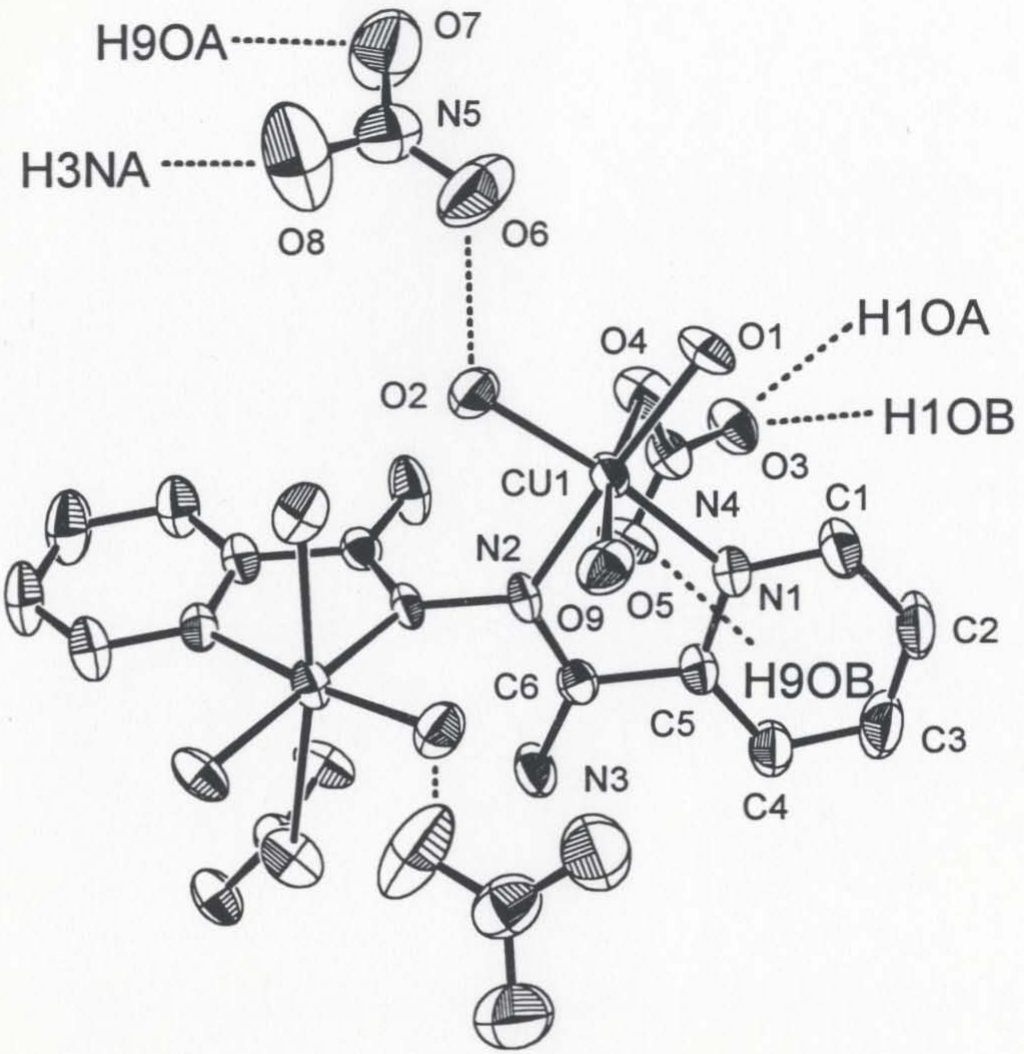

Figure 2-5. Structural representation of $[Cu_2(PAHAP)(H_2O)_6](NO_3)_4$ (**4**) with hydrogen atoms omitted (40% probability thermal ellipsoids). Significant hydrogen bonding contacts are shown (dotted lines).

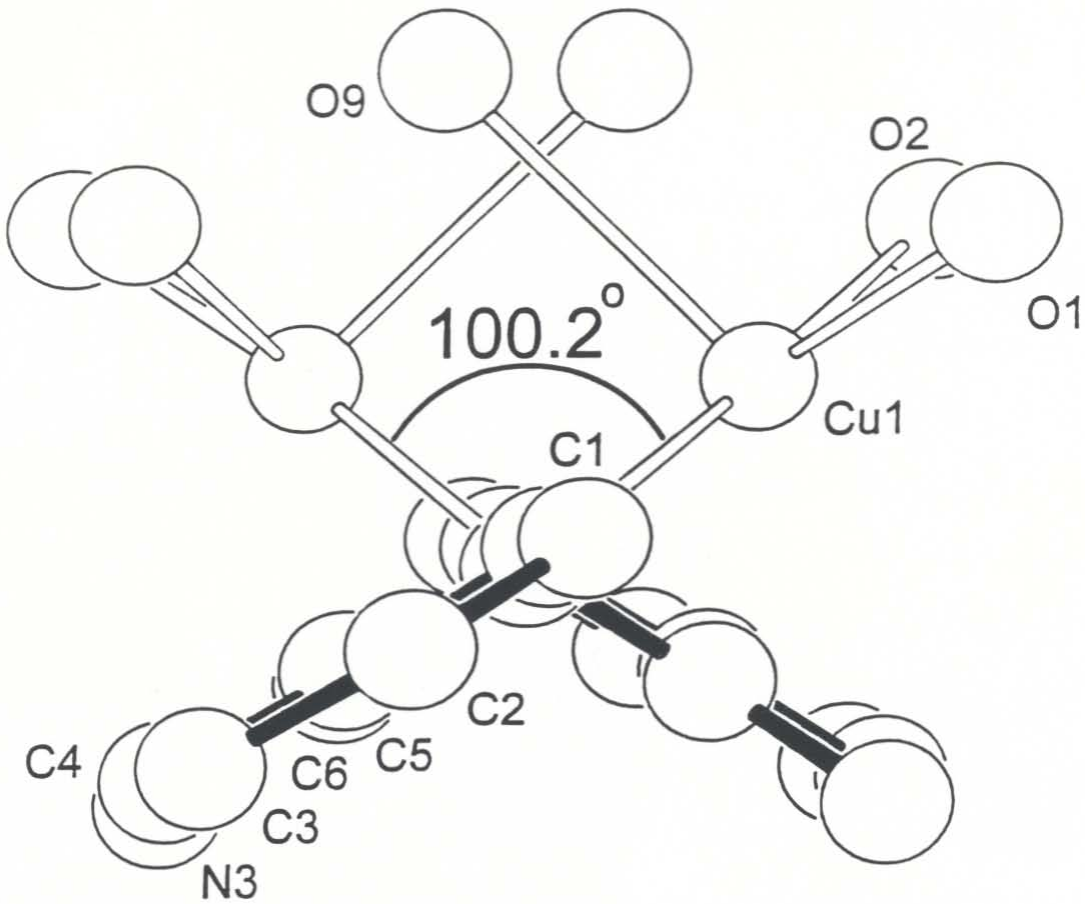

Figure 2-6. Structural representation of $[Cu_2(PAHAP)(H_2O)_6](NO_3)_4$ (**4**) viewed along an axis close to that of the N-N bond.

$[Cu_2(PAHAP)(NCS)_4(DMF)_2].2DMF$(6)

The preliminary structure of **6** is illustrated in **Figure 2-7**, and some relevant bond distances and angles are listed in **Table 2-6**. The dinuclear complex has a twisted structure with the two copper(II) square-pyramids bridged by the N-N diazine unit. Two isothiocyanates are bound in *cis* positions to the copper basal planes with two PAHAP nitrogens occupying the other basal sites. The NH_2 groups on PAHAP remain uncoordinated. Equatorial Cu-N distances are quite short (< 2.03 Å) with somewhat longer contacts to the axial DMF molecules (Cu(2)-O(2) 2.337(5) Å, Cu(1)-O(1) 2.229(5) Å). Some positional disorder was observed for S(13), and it has been modelled with two 50% site occupancies. The copper centers are separated by 4.453 Å, and the two copper planes are twisted about the N-N bond by a dihedral angle of 103.6° (angle between the least squares planes defined by Cu(1)-N(1)-C(5)-C(6)-N(2) and Cu(2)-N(4)-C(11)-C(12)-N(5)).

Table 2-6. Interatomic distances (Å) and angles (Deg.) relevant to the copper coordination spheres and the ligand in $[Cu_2(PAHAP)(NCS)_4(DMF)_2]$ .2DMF(6).

Cu(1)-N(13)	1.919(7)	Cu(2)-N(15)	1.964(7)
Cu(1)-N(14)	1.962(7)	Cu(2)-N(5)	2.009(5)
Cu(1)-N(2)	2.019(5)	Cu(2)-N(4)	2.017(6)
Cu(1)-N(1)	2.025(5)	Cu(2)-O(2)	2.337(5)
Cu(1)-O(1)	2.229(5)	Cu(1)-Cu(2)	4.453(3)
Cu(2)-N(16)	1.954(8)	N(2)-N(5)	1.407(7)
N(16)-Cu(2)-N(15)	93.6(3)	N(13)-Cu(1)-N(14)	93.9(3)
N(16)-Cu(2)-N(5)	92.9(2)	N(13)-Cu(1)-N(2)	92.5(2)
N(15)-Cu(2)-N(5)	169.4(3)	N(14)-Cu(1)-N(2)	161.5(2)
N(16)-Cu(2)-N(4)	169.9(3)	N(13)-Cu(1)-N(1)	169.1(2)
N(15)-Cu(2)-N(4)	93.1(3)	N(14)-Cu(1)-N(1)	92.3(2)
N(5)-Cu(2)-N(4)	79.4(2)	N(2)-Cu(1)-N(1)	79.0(2)
N(16)-Cu(2)-O(2)	94.7(2)	N(13)-Cu(1)-O(1)	94.2(2)
N(15)-Cu(2)-O(2)	97.0(2)	N(14)-Cu(1)-O(1)	101.1(3)
N(5)-Cu(2)-O(2)	90.8(2)	N(2)-Cu(1)-O(1)	95.7(2)
N(4)-Cu(2)-O(2)	91.9(2)	N(1)-Cu(1)-O(1)	93.3(2)

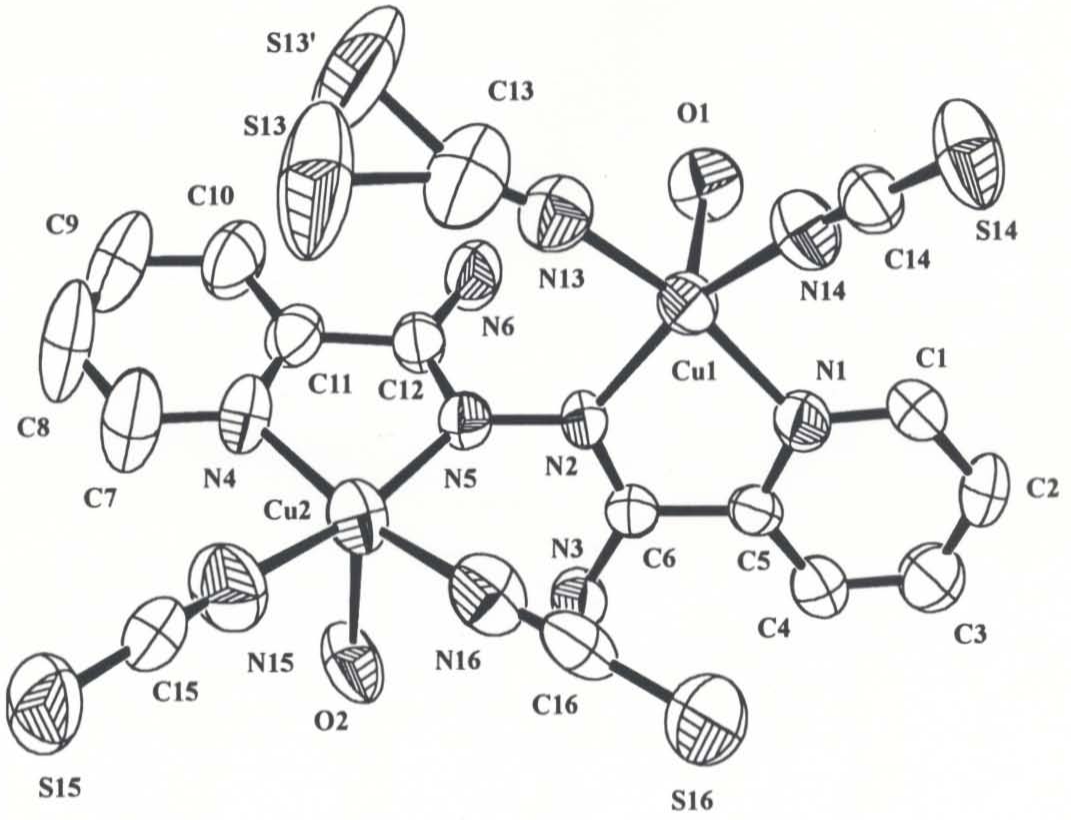

Figure 2-7. Structural representation of $[Cu_2(PAHAP)(NCS)_4(DMF)_2].2DMF$ (**6**) with hydrogen atoms omitted (40% probability thermal ellipsoids).

$[Cu_2(PAHAP)(Bipy)_2(NO_3)_2].(NO_3)_2.4H_2O$ (**8**)

The structure of the cationic fragment of **8** is illustrated in **Figure 2-8**, and relevant bond distances and angles are listed in **Table 2-7**. The dinuclear complex involves two distorted five-coordinate copper(II) centers each with two PAHAP nitrogens (pyridine and diazine), two bipyridine nitrogens and a terminal nitrate ligand. The bidentate Bipy ligands have short copper-nitrogen distances with Cu-N(1) (2.132(5) Å) slightly longer than Cu-N(2) (1.998(5) Å). The copper ion geometry is in between a square-pyramid and a trigonal-bipyramid, and using the distortion index established by Addison [75] ($\tau = (\beta - \alpha)/60$; $\beta = 179.0°$, $\alpha = 144.3°$) a value of 0.58 suggests that a distorted trigonal bipyramid is the most appropriate stereochemical description. The axial direction would then be defined by N(2)-Cu-N(3). The molecular twist around the N-N bond is much more pronounced with a much larger dihedral angle (119.8°) between the copper-$N_{diazine}$-$N_{pyridine}$ planes (as indicated by the angle between the Cu-N(3)-C(15)-C(16)-N(4) plane and the symmetry related least-squares plane). This results because there is a major steric effect between the two Bipy ligands, and they align themselves roughly parallel, effectively twisting the two copper planes about the N-N bond in an attempt to keep the planar Bipy ligands a safe distance from each other. The relatively large twist angle around the N-N bond leads to quite a large Cu-Cu separation (4.229 Å), when compared with $[Cu_2(PAHAP)Cl_4].H_2O$ (**1**).

Table 2-7. Interatomic distances (Å) and angles (Deg.) relevant to the copper coordination spheres and the ligand in $[Cu_2(PAHAP)(Bipy)_2(NO_3)_2].(NO_3)_2.4H_2O$ (**8**).

	Cu-N(3)	1.989(5)	
	Cu-N(2)	1.998(5)	
	Cu-N(4)	2.016(5)	
	Cu-N(1)	2.132(5)	
	Cu-O(1)	2.140(5)	
	Cu-Cu(a)	4.229	
	N(4)-N(4a)	1.416(9)	
N(3)-Cu-N(2)	179.0(2)	N(4)-Cu-N(1)	126.6(2)
N(3)-Cu-N(4)	80.7(2)	N(3)-Cu-O(1)	89.3(2)
N(2)-Cu-N(4)	98.6(2)	N(2)-Cu-O(1)	90.8(2)
N(3)-Cu-N(1)	100.2(2)	N(4)-Cu-O(1)	144.3(2)
N(2)-Cu-N(1)	80.7(2)	N(1)-Cu-O(1)	88.8(2)

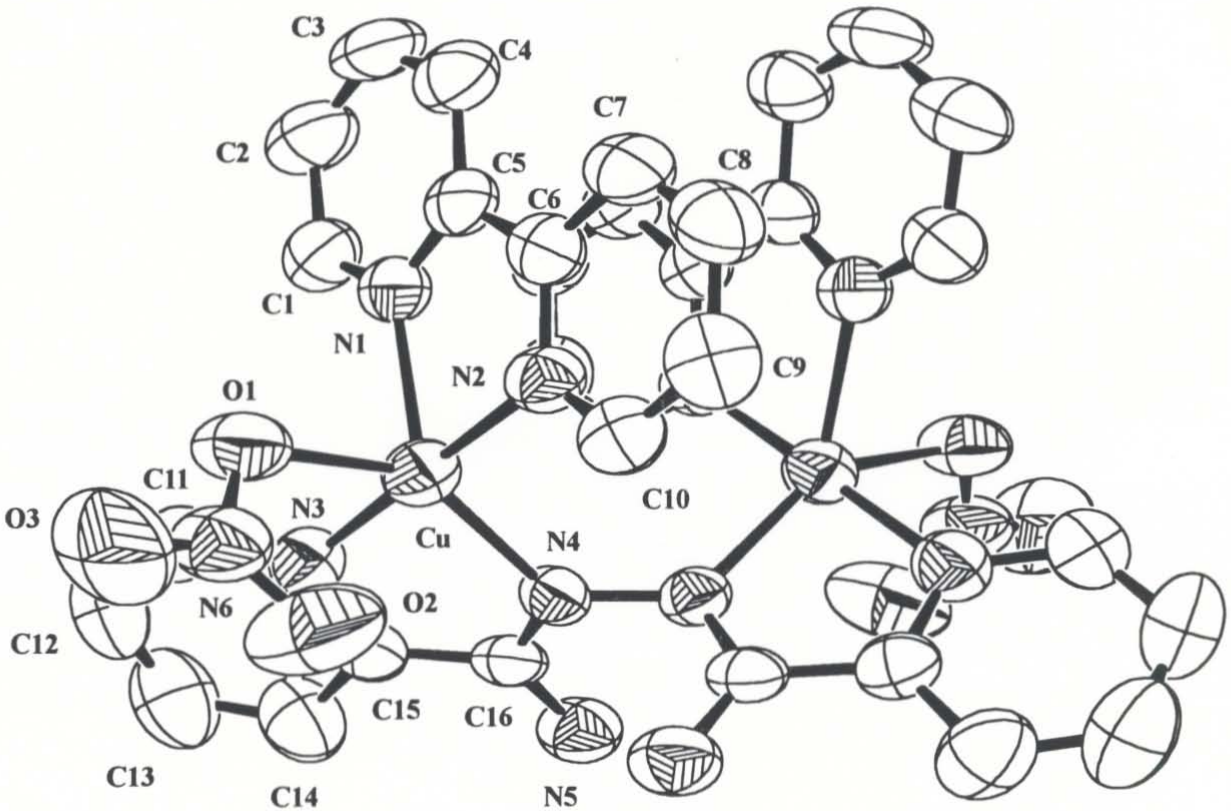

Figure 2-8. Structural representation of $[Cu_2(PAHAP)(Bipy)_2(NO_3)_2].(NO_3)_2.4H_2O$ (**8**) with hydrogen atoms omitted (40% probability thermal ellipsoids).

$[Cu_2(PAHAP)(Glyn\text{-}H)_2(NO_3)(H_2O)](NO_3).3H_2O$ (9)

The structure of **9** is illustrated in **Figure 2-9**, and bond distances and angles relevant to the copper coordination spheres are given in **Table 2-8**. The metal centers are square-pyramidal with a copper-copper separation of 4.412(4) Å. The basal donor set comprises a diazine and pyridine nitrogen pair along with the amino acid NO pair, within plane distances < 2.0 Å. Longer axial contacts to O(31) (Cu(1)-O(31) 2.548(4) Å) belonging to a nitrate, and a water molecule (Cu(2)-O(50) 2.374(8) Å) complete the five-coordination. The copper basal planes are twisted around the N-N bridge with a dihedral angle of 85.2(2)° between the least-squares planes Cu(1)-N(1)-C(5)-C(6)-N(2) and Cu(2)-N(5)-C(7)-C(8)-N(6) (torsion angle Cu(1)-N(2)-N(5)- Cu(2) 90.8(4)°).

Table 2-8. Interatomic distances (Å) and angles (Deg.) relevant to the copper coordination spheres and the ligand in $[Cu_2(PAHAP)(Glyn\text{-}H)_2(NO_3)(H_2O)](NO_3).3H_2O$ (**9**).

Cu(1)-O(1)	1.935(5)	Cu(2)-O(3)	1.967(4)
Cu(1)-N(7)	1.970(6)	Cu(2)-N(8)	1.977(5)

contd.

Cu(1)-N(1)	1.975(5)	Cu(2)-N(5)	1.985(5)
Cu(1)-N(2)	1.978(6)	Cu(2)-N(6)	1.987(5)
Cu(1)-O(31)	2.548(5)	Cu(2)-O(50)	2374(8)
Cu(1)-Cu(2)	4.412(4)	N(2)-N(5)	1.409(6)

O(1)-Cu(1)-N(7)	85.2(2)	O(1)-Cu(1)-N(1)	94.4(2)
N(7)-Cu(1)-N(1)	172.9(2)	O(1)-Cu(1)-N(2)	169.1(2)
N(7)-Cu(1)-N(2)	100.9(2)	N(1)-Cu(1)-N(2)	80.7(2)
O(3)-Cu(2)-N(8)	85.10(19)	O(3)-Cu(2)-N(5)	170.1(2)
N(8)-Cu(2)-N(5)	99.6(2)	O(3)-Cu(2)-N(6)	94.66(19)
N(8)-Cu(2)-N(6)	179.6(2)	N(5)-Cu(2)-N(6)	80.7(2)
O(3)-Cu(2)-O(50)	93.4(2)	N(8)-Cu(2)-O(50)	91.2(3)
N(5)-Cu(2)-O(50)	95.2(2)	N(6)-Cu(2)-O(50)	88.4(3)

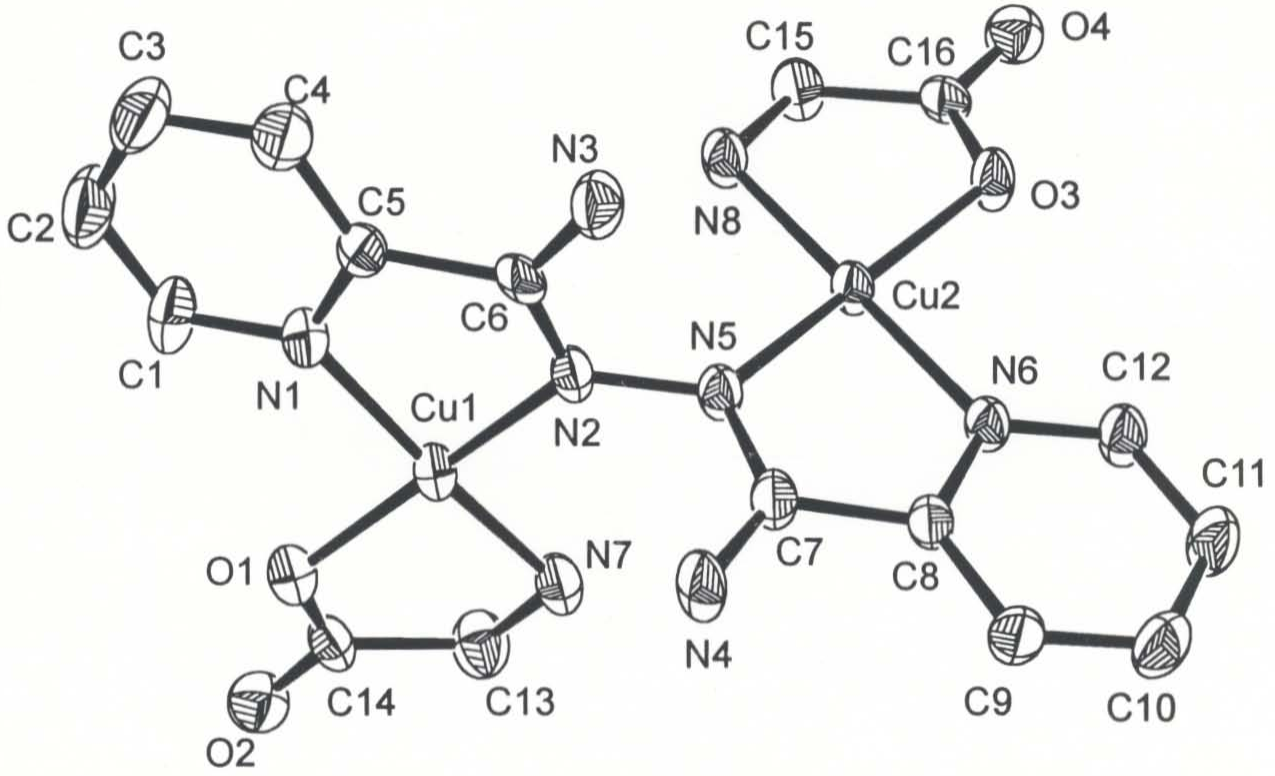

Figure 2-9. Structural representation of $[Cu_2(PAHAP)(Glyn\text{-}H)_2(NO_3)(H_2O)](NO_3).3H_2O$ (**9**) with hydrogen atoms and weakly bonded axial ligands omitted (40% probability thermal ellipsoids).

$[Cu_2(PAHAP)(Aln\text{-}H)_2(H_2O)_2]\ (NO_3)_2.3H_2O$ **(10)**

Two crystallographically independent, but very similar, molecules have been found in **10**. **Figure 2-10a** illustrates the structure of one molecule, and **Figure 2-10b** illustrates the expanded view of the coordination cores. Bond distances and angles relevant to the copper coordination spheres are given in **Table 2-9**. The copper(II) centers are close to square-pyramidal with short equatorial contacts (< 2.0 Å) to an N_3O in-plane donor set, and weak axial coordination by two water molecules (e.g. Cu(1)-O(5) 2.428(4) Å, Cu(2)-O(6) 2.325(4) Å, Cu(3)-O(11) 2.492(5) Å, Cu(4)-O(12) 2.417(4) Å). The copper basal planes are twisted about the diazine N-N bond with dihedral angles of 85.9(4)° between the least-squares planes Cu(1)-N(1)-C(5)-C(6)-N(3) and Cu(2)-N(4)-C(7)-C(8)-N(6) (torsion angle Cu(1)-N(3)-N(4)-Cu(2) 87.8(4)°) and 89.1(4)° between the least-squares planes Cu(3)-N(9)-C(23)-C(24)-N(11) and Cu(4)-N(12)-C(25)-C(26)-N(14) (torsion angle Cu(3)-N(11)-N(12)-Cu(4) 86.8(4)°). The copper atoms are separated by 4.392(4) Å (Cu(1)-Cu(2)) and 4.379(4) Å (Cu(3)-Cu(4)).

Table 2-9. Interatomic distances (Å) and angles (Deg.) relevant to the copper coordination spheres and the ligand in $[Cu_2(PAHAP)(Aln\text{-}H)_2(H_2O)_2]\ (NO_3)_2.3H_2O$ **(10)**.

Cu(1)-O(1)	1.936(3)	Cu(1)-N(1)	1.993(4)
Cu(1)-N(3)	1.973(4)	Cu(1)-N(7)	2.010(4)

contd.

Cu(2)-O(3)	1.959(3)	Cu(2)-N(4)	1.977(4)
Cu(2)-N(6)	1.994(4)	Cu(2)-N(8)	1.977(4)
Cu(3)-O(7)	1.957(3)	Cu(3)-O(11)	2.492(5)
Cu(3)-N(9)	1.972(4)	Cu(3)-N(11)	1.975(4)
Cu(3)-N(15)	1.965(4)	Cu(4)-O(9)	1.940(3)
Cu(4)-N(12)	1.984(4)	Cu(4)-N(14)	1.995(4)
Cu(4)-N(16)	1.975(4)	N(3)-N(4)	1.418(4)
N(11)-N(12)	1.400(4)	Cu(1)-Cu(2)	4.392(4)
Cu(3)-Cu(4)	4.379(4)		
O(1)-Cu(1)-N(1)	93.3(1)	O(1)-Cu(1)-N(3)	173.3(2)
O(1)-Cu(1)-N(7)	84.1(1)	N(1)-Cu(1)-N(3)	80.5(1)
N(1)-Cu(1)-N(7)	168.6(2)	N(3)-Cu(1)-N(7)	101.4(2)
O(3)-Cu(2)-N(4)	166.6(2)	O(3)-Cu(2)-N(6)	96.7(1)
O(3)-Cu(2)-N(8)	84.2(1)	N(4)-Cu(2)-N(6)	80.6(1)
N(4)-Cu(2)-N(8)	97.5(1)	N(6)-Cu(2)-N(8)	175.3(2)
O(7)-Cu(3)-O(11)	89.6(1)	O(7)-Cu(3)-N(9)	95.9(1)
O(7)-Cu(3)-N(11)	169.2(2)	O(7)-Cu(3)-N(15)	84.5(1)
O(11)-Cu(3)-N(9)	82.3(2)	O(11)-Cu(3)-N(11)	100.1(2)
O(11)-Cu(3)-N(15)	95.3(2)	N(9)-Cu(3)-N(11)	80.9(1)
N(9)-Cu(3)-N(15)	177.5(2)	N(11)-Cu(3)-N(15)	99.1(1)

contd.

O(9)-Cu(4)-N(12)	174.2(2)	O(9)-Cu(4)-N(14)	93.9(1)
O(9)-Cu(4)-N(16)	83.7(1)	N(12)-Cu(4)-N(14)	80.9(1)
N(12)-Cu(4)-N(16)	101.1(1)	N(14)-Cu(4)-N(16)	170.7(2)

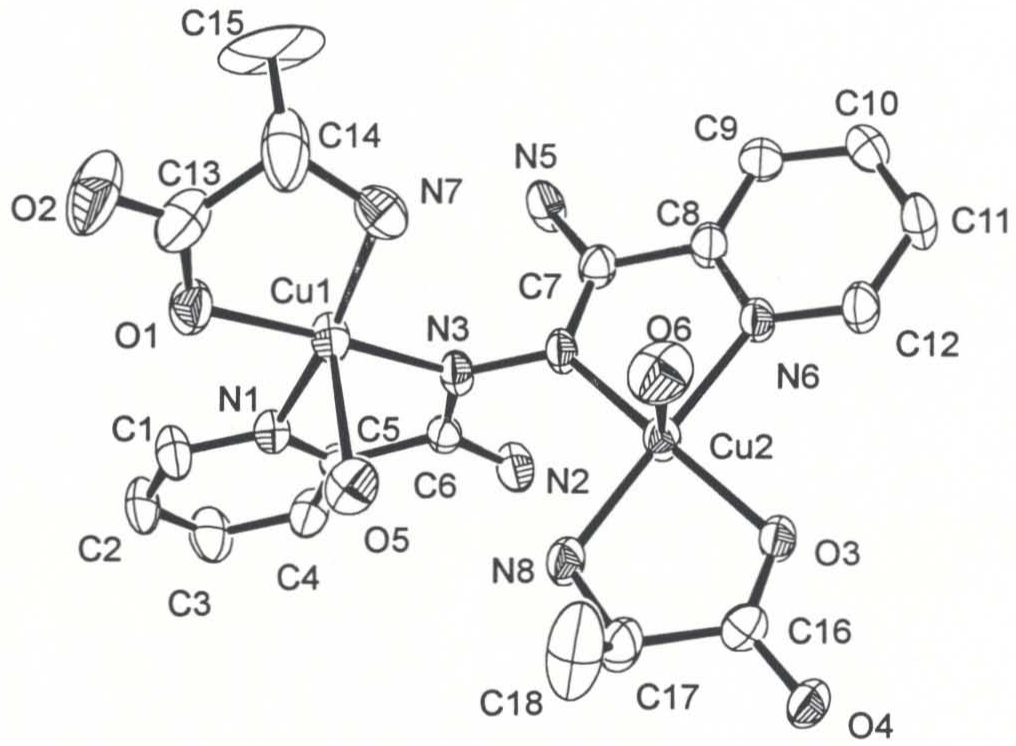

Figure 2-10a. Structural representation of $[Cu_2(PAHAP)(Aln\text{-}H)_2(H_2O)_2](NO_3)_2.3H_2O$ **(10)** with hydrogen atoms omitted (40% probability thermal ellipsoids).

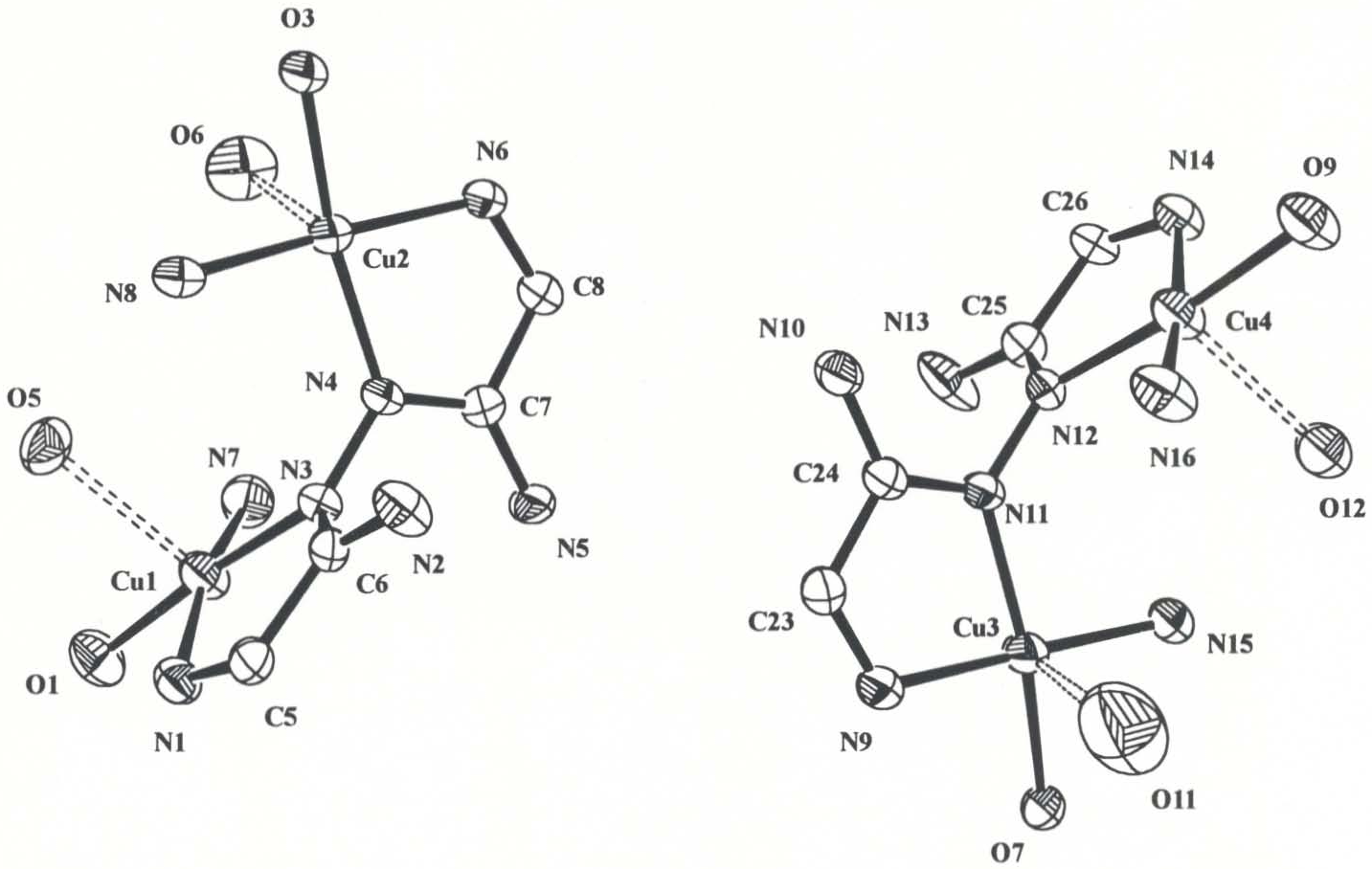

Figure 2-10b. Expanded view of the coordination cores in $[Cu_2(PAHAP)(Aln\text{-}H)_2(H_2O)_2]\ (NO_3)_2.3H_2O$ (**10**).

$[Cu_2(PAHAP)(ACAC\text{-}H)_2(H_2O)_2](NO_3)_2$ **(11)**

The structure of the cationic fragment of **11** is illustrated in **Figure 2-11a**. **Figure 2-11b** illustrates the expanded view of the coordination cores and the intramolecular hydrogen-bonding contacts in **11**. The relevant bond distances and angles are listed in **Table 2-10**. The dinuclear complex involves two square-pyramidal copper(II) centers. The two copper(II) centers are bound by short equatorial contacts to the PAHAP ligand *via* a pyridine and diazine nitrogen, and to a pentanedionate *via* its two oxygens in a twisted structure. The five-coordination at Cu(1) and Cu(2) is completed by weakly coordinated H_2O molecules in an axial position (Cu(1)-O(3) 2.3686(14) Å). Cu(2)-O(6) 2.440(2)Å). One of the nitrates is semi-coordinated to Cu(2) via O(9) (Cu(2)-O(9) 2.688(2) Å). The $H_2O(6)$ is involved in the intramolecular hydrogen-bonding contacts.

The copper basal planes are twisted about the diazine N-N bond with a dihedral angle of 82.04° between the least-squares planes Cu(1)-N(1)-C(5)-C(6)-N(3) and Cu(2)-N(6)-C(8)-C(7)-N(4) (torsion angle Cu(1)-N(3)-N(4)-Cu(2) 87.48°). The copper atoms are separated by 4.360(2) Å.

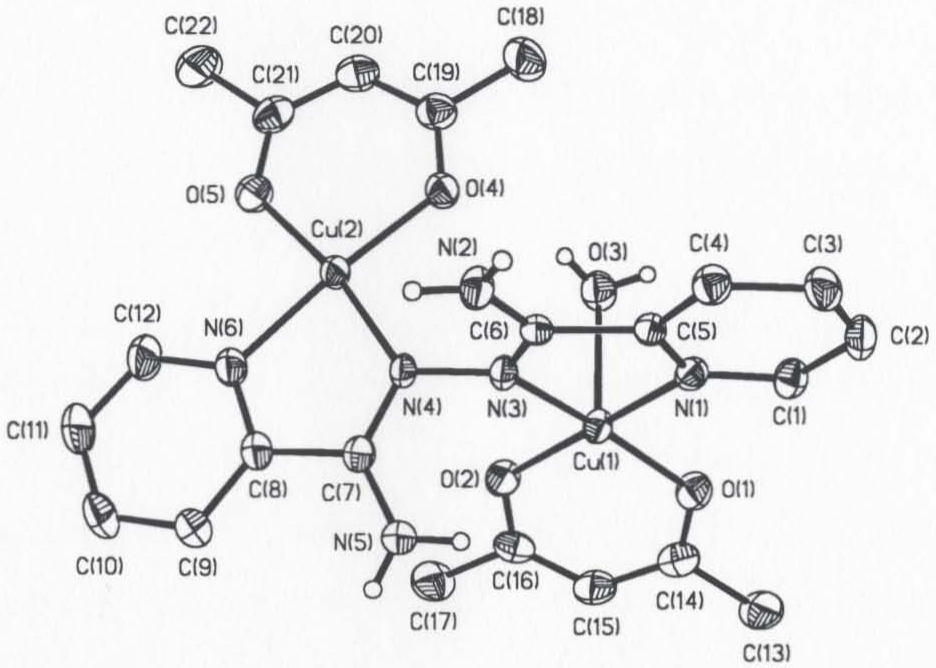

Figure 2-11a. Structural representation of $[Cu_2(PAHAP)(ACAC\text{-}H)_2(H_2O)_2](NO_3)_2$ (**11**) with hydrogen atoms and weakly coordinated $H_2O(6)$ omitted (40% probability thermal ellipsoids).

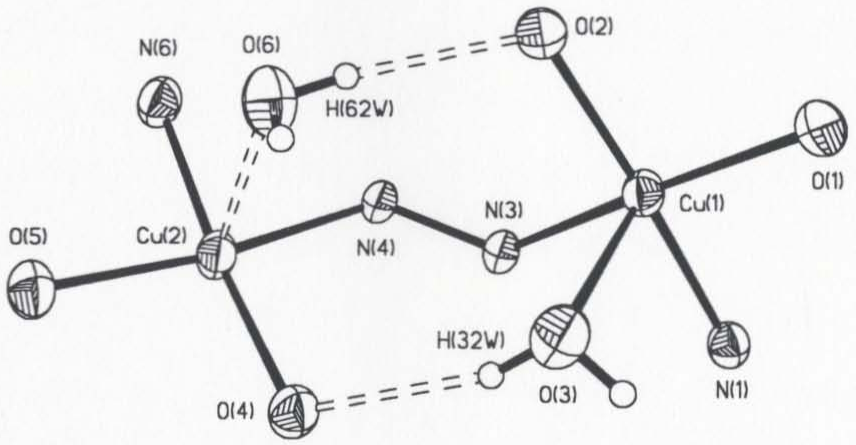

Figure 2-11b. Intramolecular hydrogen-bonding contacts in **11**.

Table 2-10. Interatomic distances (Å) and angles (Deg.) relevant to the copper coordination spheres and the ligand in $[Cu_2(PAHAP)(ACAC\text{-}H)_2(H_2O)_2](NO_3)_2$ (**11**).

Cu(1)-O(1)	1.9142(12)	Cu(1)-O(2)	1.9314(13)
Cu(1)-N(3)	1.9766(14)	Cu(1)-N(1)	2.004(2)
Cu(1)-O(3)	2.3686(14)	Cu(2)-O(5)	1.9189(13)
Cu(2)-O(4)	1.9461(13)	Cu(2)-N(4)	1.9974(14)
Cu(2)-N(6)	2.018(2)	Cu(2)-O(6)	2.440(2)
Cu(1)-Cu(2)	4.360(2)	N(3)-N(4)	1.407(2)
O(1)-Cu(1)-O(2)	93.83(5)	N(3)-Cu(1)-O(3)	91.72(6)
O(1)-Cu(1)-N(3)	166.31(6)	N(1)-Cu(1)-O(3)	92.89(5)
O(2)-Cu(1)-N(3)	92.73(6)	O(5)-Cu(2)-O(4)	94.62(6)
O(1)-Cu(1)-N(1)	92.43(6)	O(5)-Cu(2)-N(4)	169.75(6)
O(2)-Cu(1)-N(1)	170.58(6)	O(4)-Cu(2)-N(4)	95.28(5)
N(3)-Cu(1)-N(1)	79.71(6)	O(5)-Cu(2)-N(6)	90.60(6)
O(1)-Cu(1)-O(3)	99.92(5)	O(4)-Cu(2)-N(6)	174.62(6)
O(2)-Cu(1)-O(3)	92.94(5)	N(4)-Cu(2)-N(6)	79.56(6)

$[Cu_2(PMHAP\text{-}H)(NO_3)_3]$ **(12)**

The structure of **12** is illustrated in **Figure 2-12**, and relevant bond distances and angles are listed in **Table 2-11**. The ligand PMHAP binds two copper centers in a *trans*-structure **(Type B)**, and acts in a quinquedentate fashion with Cu(1) coordinated to pyridine (N(1)), diazine (N(2)) and amino nitrogens (N(3)), and Cu(2) bound to diazine (N(4)) and pyridine (N(5)) nitrogens. The presence of only three nitrates indicates that the ligand has become deprotonated at N(3), which shows the presence of just one proton. Each copper atom has four short equatorial bonds (< 2 Å), and longer contacts to nitrate oxygens (Cu(1)-O(3) 2.489(4) Å; Cu(2)-O(9) 2.544(4) Å). The Cu(1)-N(3) distance (1.916(5) Å) is very short, as would be expected. The stereochemistry at both copper centers is best described as distorted square-pyramidal, despite the nominal tetrahedral distortion at Cu(2) (N(4)-Cu(2)-O(4) 156.2 (2)°; N(5)-Cu(2)-O(7) 148.5(2)°).

The *trans*-ligand arrangement is effectively locked into place by the coordination of the deprotonated anionic nitrogen N(3) to Cu(1). This leads to a large copper-copper separation (4.778(4) Å), and an almost flat structure, with a dihedral angle between the least-squares planes N(1)-C(5)-C(6)-N(2)-Cu(1) and N(4)-C(13)-C(12)-N(5)-Cu(2) of 165.2°.

Table 2-11. Interatomic distances (Å) and angles (Deg.) relevant to the copper coordination spheres and the ligand in $[Cu_2(PMHAP\text{-}H)(NO_3)_3]$ **(12)**.

Cu(1)-N(3)	1.916(5)	Cu(2)-O(7)	1.991(4)
Cu(1)-N(2)	1.948(4)	N(2)-C(6)	1.287(6)
Cu(1)-N(1)	1.966(5)	N(2)-N(4)	1.389(6)
Cu(1)-O(1)	1.990(4)	N(3)-C(13)	1.303(6)
Cu(2)-O(4)	1.968(4)	N(4)-C(13)	1.359(6)
Cu(2)-N(5)	1.970(4)	C(5)-C(6)	1.496(7)
Cu(2)-N(4)	1.971(4)	C(12)-C(13)	1.490(7)
Cu(1)-O(3)	2.489(4)	Cu(2)-O(9)	2.544(4)
Cu(1)-Cu(2)	4.778(4)		
N(3)-Cu(1)-N(2)	80.3(2)	N(4)-Cu(2)-O(4)	156.1(2)
N(3)-Cu(1)-N(1)	161.0(2)	N(5)-Cu(2)-O(7)	148.5(2)
N(2)-Cu(1)-N(1)	81.6(2)	O(4)-Cu(2)-N(5)	91.8(2)
N(3)-Cu(1)-O(1)	99.4(2)	N(5)-Cu(2)-N(4)	82.6(2)
N(2)-Cu(1)-O(1)	177.3(2)	O(4)-Cu(2)-O(7)	95.4(2)
N(1)-Cu(1)-O(1)	98.4(2)	N(4)-Cu(2)-O(7)	101.5(2)
O(1)-Cu(1)-O(3)	55.7(2)		

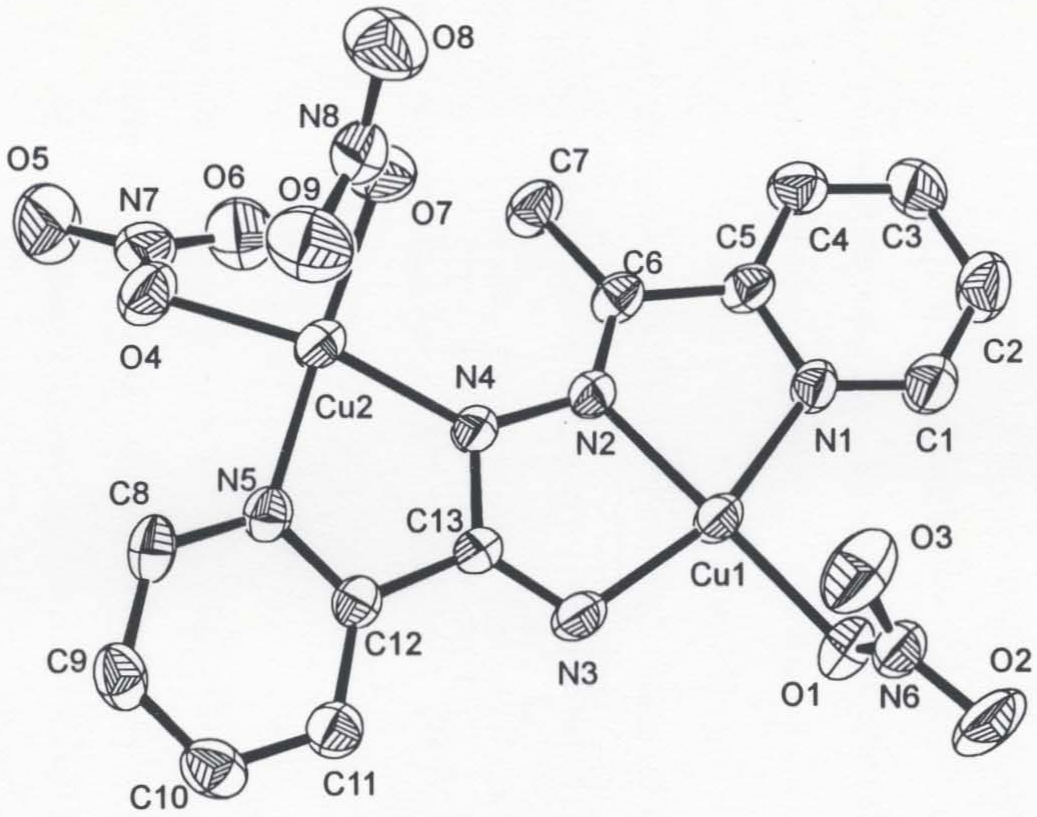

Figure 2-12. Structural representation of $[Cu_2(PMHAP\text{-}H)(NO_3)_3]$ (**12**) with hydrogen atoms omitted (50% probability thermal ellipsoids).

$[Cu_2(PHMAP\text{-}H)(MeOH)(H_2O)(NO_3)_3]$ **(14)**

The structure of **14** is illustrated in **Figure 2-13**, and relevant bond distances and angles are listed in **Table 2-12**. The ligand PHMAP acts in a pentadentate fashion with all nitrogens acting as donors to the two five-coordinate copper(II) centers in a *trans-trans* conformation (**Type B**). Cu(1) binds to pyridine and diazine nitrogens N(1) and N(3) respectively, and Cu(2) is bound to pyridine, diazine and amino nitrogens N(5), N(4) and N(2) respectively. N(2) is deprotonated. Two nitrates are bound terminally to Cu(2) and one to Cu(1), with the fourth and fifth coordination site at Cu(1) occupied by water and methanol molecules, respectively. The nitrate bound to Cu(1) is disordered, and was modeled as two nitrates with a total occupancy of 1. The stereochemistry at both Cu(1) and Cu(2) is best described as distorted square-pyramidal with τ values [81] of 0.35 and 0.26 respectively. The effect of this arrangement is to lock the ligand into an almost planar *trans-trans* configuration because of the coordination of N(2), coupled with the sp^2 character at C(6), N(3), N(4) and C(7). The dihedral angle between the least-squares planes Cu(1)-N(1)-C(5)-C(6)-N(3) and Cu(2)-N(5)-C(8)-C(7)-N(4) is 168.3°. The Cu(1)-Cu(2) separation (4.759(1) Å) is large as would be expected.

Three short intermolecular contacts link the complexes in a 2-dimensional network. This is illustrated in **Figure 2-14**, and shows the binuclear units linked head to tail in a chain arrangement by H-bonding interactions between nitrate oxygen O(9) and methanol oxygen O(2) (O(2)-O(9) 2.749(4) Å), and water oxygen O(1) and nitrate oxygen O(6)

Table 2-12. Interatomic distances (Å) and angles (Deg.) relevant to the copper coordination spheres and the ligand in $[Cu_2(PHMAP\text{-}H)(MeOH)(H_2O)(NO_3)_3]$ **(14)**.

Cu(1)-N(3)	1.955(3)	Cu(2)-N(2)	1.963(4)
Cu(1)-O(31)	1.971(11)	Cu(2)-N(5)	2.042(3)
Cu(1)-O(32)	2.00(5)	Cu(2)-O(6)	2.049(3)
Cu(1)-O(1)	2.007(3)	Cu(2)-O(9)	2.215(3)
Cu(1)-N(1)	2.016(3)	Cu(1)-Cu(2)	4.759(1)
Cu(1)-O(2)	2.153(4)	N(3)-N(4)	1.368(4)
Cu(2)-N(4)	1.944(3)		
N(3)-Cu(1)-O(31)	172.7(3)	N(3)-Cu(1)-O(32)	172.0(9)
N(3)-Cu(1)-O(1)	92.78(12)	O(31)-Cu(1)-O(1)	94.0(3)
O(32)-Cu(1)-O(1)	88.0(13)	N(3)-Cu(1)-N(1)	80.25(12)
O(31)-Cu(1)-N(1)	95.0(3)	O(32)-Cu(1)-N(1)	95.4(13)
O(1)-Cu(1)-N(1)	151.69(13)	N(3)-Cu(1)-O(2)	92.1(2)
O(31)-Cu(1)-O(2)	86.4(2)	O(32)-Cu(1)-O(2)	95.8(9)
O(1)-Cu(1)-O(2)	94.11(14)	N(1)-Cu(1)-O(2)	113.4(2)
N(4)-Cu(2)-N(2)	79.45(14)	N(4)-Cu(2)-N(5)	81.16(12)
N(2)-Cu(2)-N(5)	160.10(14)	N(4)-Cu(2)-O(6)	144.54(13)
N(2)-Cu(2)-O(6)	97.71(14)	N(5)-Cu(2)-O(6)	100.69(11)
N(4)-Cu(2)-O(9)	125.54(12)	N(2)-Cu(2)-O(9)	90.60(14)
(5)-Cu(2)-O(9)	97.03(12)	O(6)-Cu(2)-O(9)	89.63(10)

(O(1)-O(6) 2.732(4) Å), with the chains cross-linked by another H-bonding contact between nitrate oxygen O(10) and water oxygen O(1) (O(1)-O(10) 2.753(4) Å). Corresponding O-H-O angles fall in the range 160-177°.

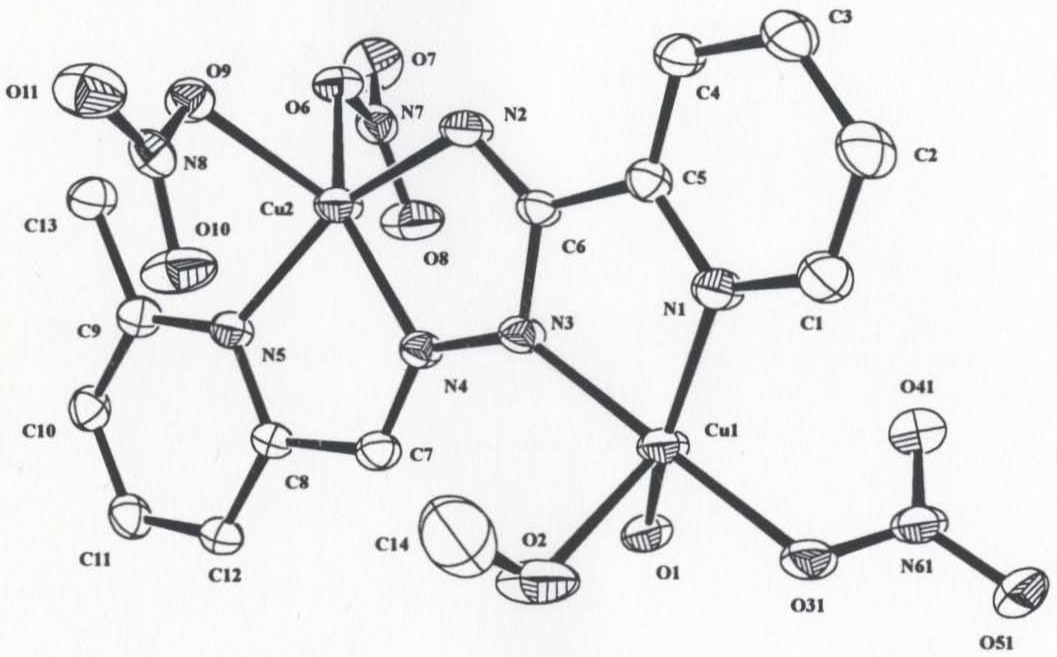

Figure 2-13. Structural representation of $[Cu_2(PHMAP\text{-}H)(MeOH)(H_2O)(NO_3)_3]$ (**14**) with hydrogen atoms omitted (50% probability thermal ellipsoids).

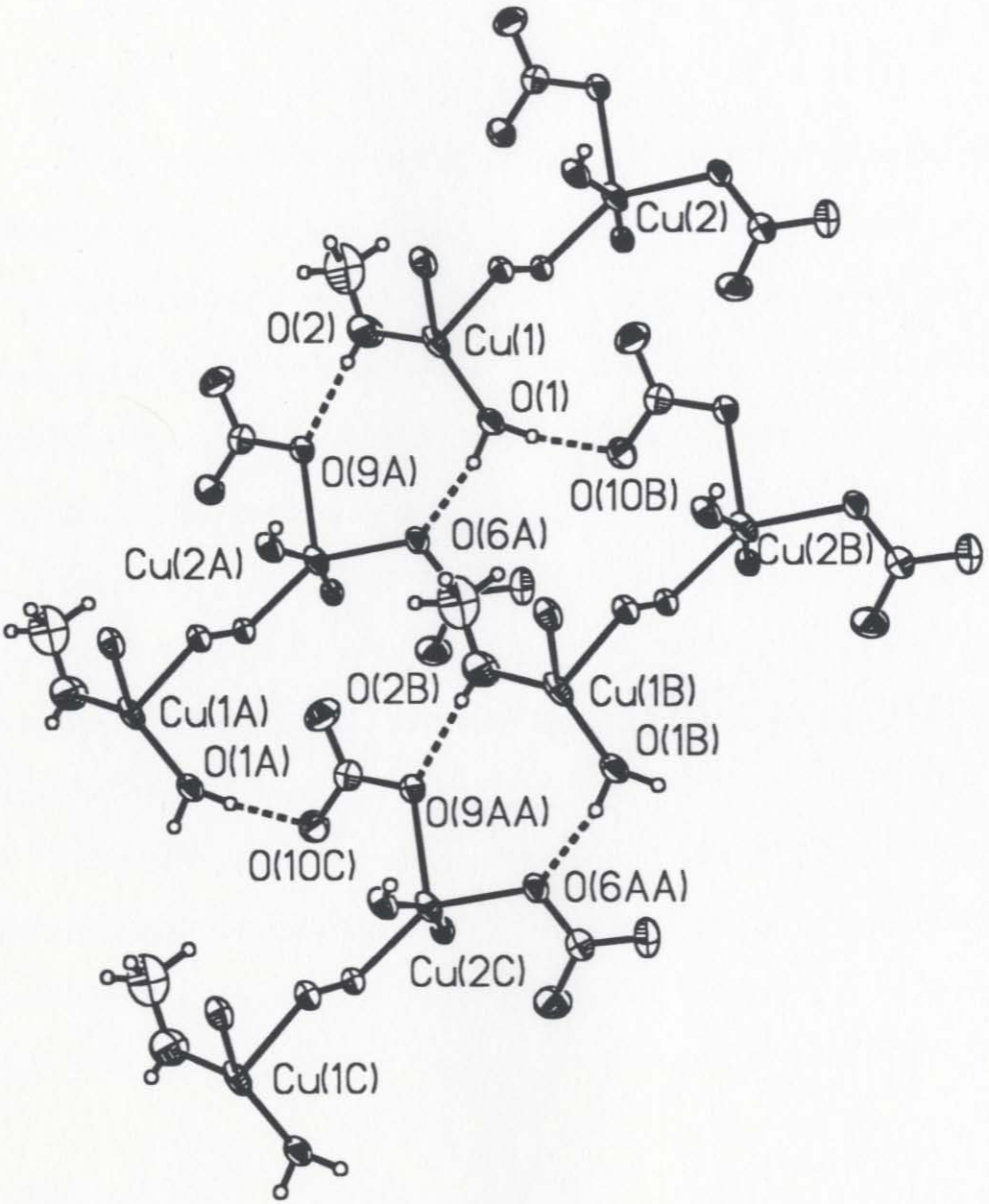

Figure 2-14. Chain structure of compound **14**.

$[Cu_2(PHAAP)(Br)_3(H_2O)]$ **(15)**

The structure of **15** is illustrated in **Figure 2-15** and relevant bond distances and angles are listed in **Table 2-13.** The ligand PHAAP also acts in a pentadentate fashion like PMHAP and PHMAP in complex **12** and **14**, with N1, N4 (from pyridine rings); N2, N3 (from diazine) and deprotonated O(1) as donors to the four-coordinate copper(II) centre (Cu(1)) and five-coordinate copper(II) centre (Cu(2)) in a *trans-trans* conformation (quasi **Type B**). The Cu(1) centre is close to square-planar with four normal bonds (Cu(1)-Br(1) 2.3208(8) Å; Cu(1)-O(1) 1.978(4) Å; Cu(1)-N(4) 1.996(5) Å; Cu(1)-N(3) 1.917(4) Å), while the Cu(2) centre is close to square-pyramidal with four short equatorial contacts (Cu(2)-N(1) 2.029(5) Å; Cu(2)-N(2) 2.002(4) Å; Cu(2)-O(4) 1.991(5) Å; Cu(2)-Br(3) 2.3967(9) Å).

The dihedral angle between the least-squares planes Cu(1)-N(4)-C(8)-C(7)-N(3) and Cu(2)-N(1)-C(1)-C(6)-N(2) is 153.2°. The expected large Cu(1)-Cu(2) separation (4.717(4) Å) is comparable with that found in complex **12** and **14**.

Table 2-13. Interatomic distances (Å) and angles (Deg.) relevant to the copper coordination spheres and the ligand in $[Cu_2(PHAAP)(Br)_3(H_2O)]$ (**15**).

Cu(1)-Br(1)	2.3208(8)	Cu(1)-N(3)	1.917(4)
Cu(1)-O(1)	1.978(4)	Cu(1)-N(4)	1.996(5)
Cu(2)-Br(2)	2.7212(9)	Cu(2)-Br(3)	2.3967(9)
Cu(2)-O(4)	1.991(5)	Cu(2)-N(2)	2.002(4)
Cu(2)-N(1)	2.029(5)	N(2)-N(3)	1.389(6)
C(6)-O(1)	1.280(7)	C(6)-N(2)	1.328(7)
C(7)-N(5)	1.311(7)	C(7)-N(3)	1.312(7)
Cu(1)-Cu(2)	4.717(4)		
N(3)-Cu(1)-O(1)	81.1(2)	N(3)-Cu(1)-N(4)	81.3(2)
O(1)-Cu(1)-N(4)	160.3(2)	N(3)-Cu(1)-Br(1)	167.65(14)
O(1)-Cu(1)-Br(1)	99.53(12)	N(4)-Cu(1)-Br(1)	99.58(13)
O(4)-Cu(2)-N(2)	168.3(2)	O(4)-Cu(2)-N(1)	93.2(2)
N(2)-Cu(2)-N(1)	80.0(2)	O(4)-Cu(2)-Br(3)	87.77(14)
N(2)-Cu(2)-Br(3)	93.84(13)	N(1)-Cu(2)-Br(3)	152.19(14)
O(4)-Cu(2)-Br(2)	94.1(2)	N(2)-Cu(2)-Br(2)	95.95(13)
N(1)-Cu(2)-Br(2)	95.29(14)	Br(3)-Cu(2)-Br(2)	112.37(3)

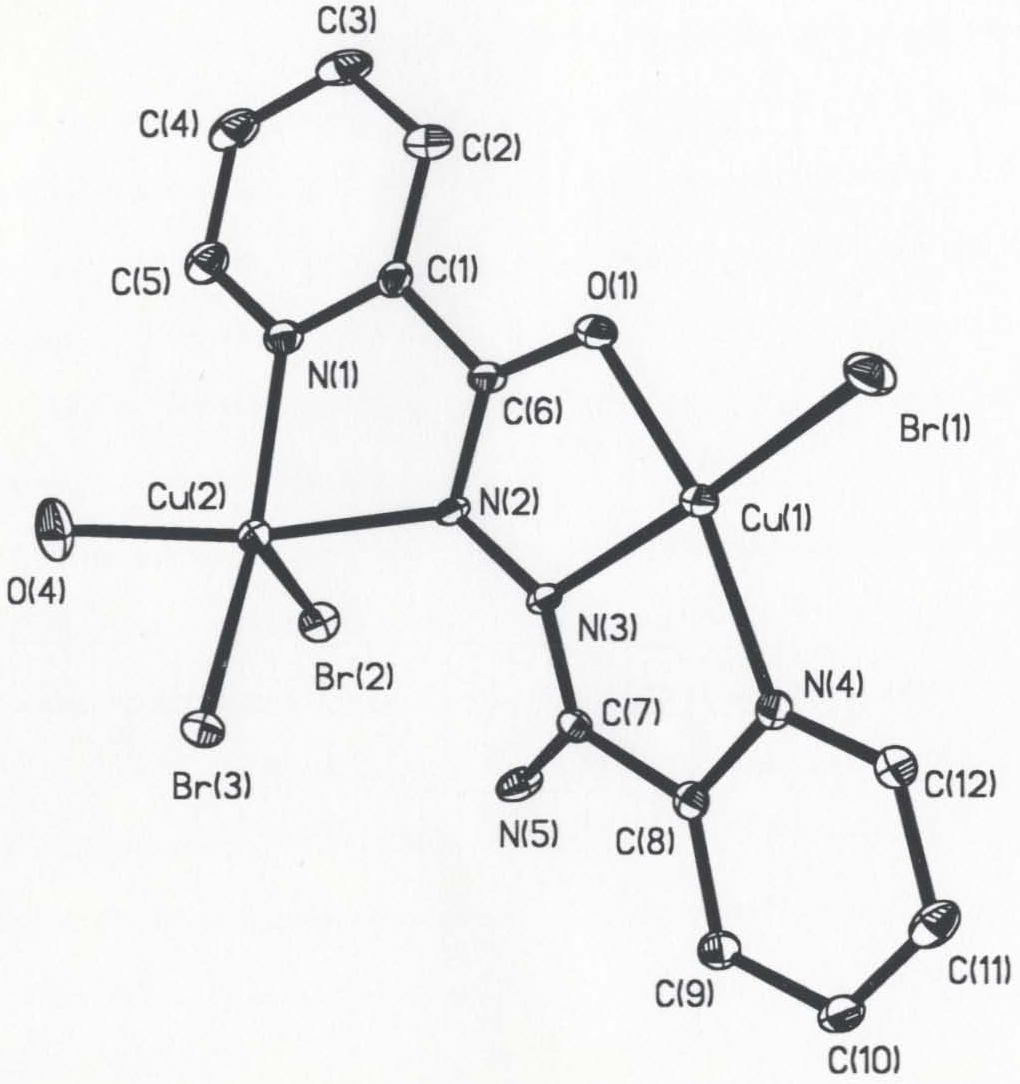

Figure 2-15. Structural representation of $[Cu_2(PHAAP)(Br)_3(H_2O)]$ (**15**) with hydrogen atoms omitted (50% probability thermal ellipsoids).

$[Cu_2(PYPZ)Cl_4].H_2O$ **(16)**

The structure of **16** is depicted in **Figure 2-16**, and relevant bond distances and angles are listed in **Table 2-14**. The structure is very similar to that of **1**, in which the Cu(1) centre is bound to one pyridine nitrogen (N(1)) and one diazine nitrogen (N(2)), while the Cu(2) centre is coordinated by one pyrazine nitrogen (N(6)) and one diazine nitrogen (N(4)) with nominal four-coordination being completed at each copper centre by two chlorines. The Cu-N and Cu-Cl distances are normal for equatorial coordination to copper(II) and comparable to those in **1**.

The two copper planes (e.g. Cu(1)-N(1)-C(5)-C(6)-N(2) and Cu(2)-N(6)-C(8)-C(7)-N(4)) are twisted about the N(3)-N(4) bond vector with a dihedral angle of 79.68°. The major factor for this acute twisting rests with the steric constraints associated with the terminal chlorines and the amine groups as mentioned for **1** and the long intramolecular axial contact between Cu(1) and Cl(3) (3.111(2) Å). The weak intermolecular contacts *via* Cl(4) and Cl(4a) (in adjacent molecule) dimerize the molecule in the same manner as in **1** (Cu(2)-Cl(4)a 2.979(2) Å). The copper-copper separation is 3.831(2) Å which is very similar to that in **1**.

The bond distances and bond angles in the NH_2-C=N framework of the ligand PYPZ in this complex are very close to those found in **1**, which contains a very similar ligand, suggesting that the free nitrogen atom in the pyrazine ring does not provide any significant effects to the coordination properties of the ligand. However, recent studies on

coordination reaction of this complex with $PtCl_4^{2-}$ show that this external nitrogen can be coordinated.

Table 2-14. Interatomic distances (Å) and angles (Deg.) relevant to the copper coordination spheres and the ligand in $[Cu_2(PYPZ)Cl_4].H_2O$ (**16**).

Cu(1)-Cl(1)	2.243(2)	Cu(1)-Cl(2)	2.263(1)
Cu(1)-N(1)	2.033(3)	Cu(1)-N(2)	1.996(3)
Cu(2)-Cl(3)	2.243(1)	Cu(2)-Cl(4)	2.238(1)
Cu(2)-N(4)	1.977(3)	Cu(2)-N(6)	2.040(4)
N(2)-N(4)	1.426(4)	Cu(1)-Cu(2)	3.831(2)
Cl(1)-Cu(1)-Cl(2)	94.19(5)	Cl(1)-Cu(1)-N(1)	93.3(1)
Cl(1)-Cu(1)-N(2)	168.9(1)	Cl(2)-Cu(1)-N(1)	171.0(1)
Cl(2)-Cu(1)-N(2)	93.9(1)	N(1)-Cu(1)-N(2)	79.4(1)
Cl(3)-Cu(2)-Cl(4)	93.94(5)	Cl(3)-Cu(2)-N(4)	93.3(1)
Cl(3)-Cu(2)-N(6)	166.65(9)	Cl(4)-Cu(2)-N(4)	172.1(1)
Cl(4)-Cu(2)-N(6)	93.2(1)	N(4)-Cu(2)-N(6)	80.2(1)

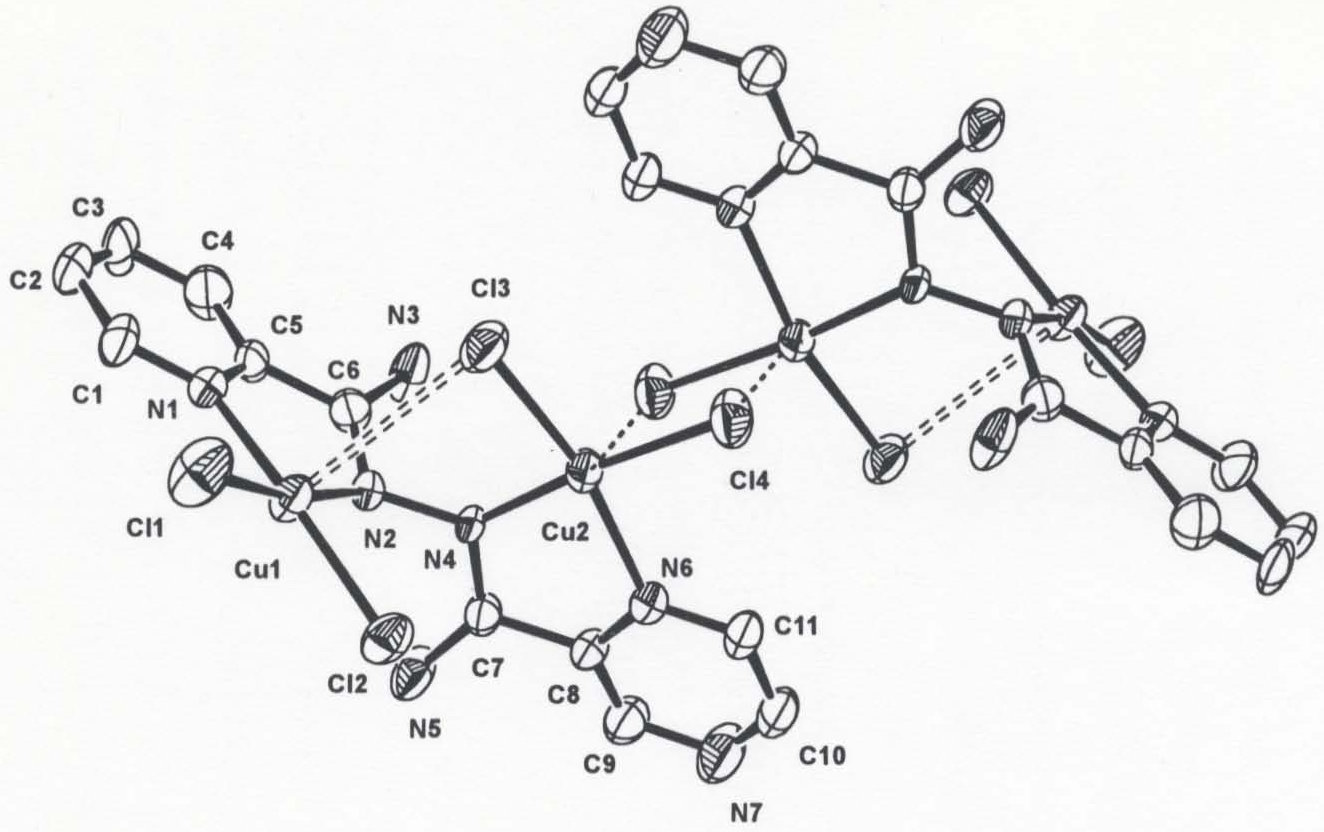

Figure 2-16. Structural representation of $[Cu_2(PYPZ)Cl_4].H_2O$ (**16**) and its weak dimer association with hydrogen atoms omitted (50% probability thermal ellipsoids).

2.3.2 Spectroscopy

All of the complexes exhibit rather complex infrared absorption patterns above 3100 cm^{-1} associated with both NH and/or OH vibrations (**Table 2-15**). The ligand PAHAP has prominent NH absorptions at 3470 and 3268 cm^{-1}. A sharp doublet at 3566, 3500 cm^{-1} for **1** is associated with the lattice water molecule, while a broad, strong absorption envelope at 3346-3150 cm^{-1} can be assigned to NH stretch. The NH vibrations can be clearly identified in **2**, which has no water, and show up as two pairs of peaks at 3353, 3309 cm^{-1} and 3231, 3189 cm^{-1}, suggesting the possibility of two different environments for the NH_2 groups in **2**. The bromide complex **3** clearly shows the presence of lattice water with a sharp doublet at 3579 and 3503 cm^{-1}, and a rather complex absorption envelope in the range 3140-3340 cm^{-1} associated with NH absorptions. Strong broad bands at 3338 and 3160 cm^{-1} are assigned to NH stretch. A sharp single nitrate combination [112] band at 1763 cm^{-1} indicates that the nitrates are essentially ionic in nature in **4**. The azide complex **5** has a sharp single NH band at 3372 cm^{-1} and a broader absorption at 3100-3200 cm^{-1}, consistent with a single NH proton at a deprotonated centre, and an NH_2 group. Azide bands at 2092 and 2031 cm^{-1} are consistent with terminally bound azide [113], probably in a local C_{2v} environment. A weak band at 1750 cm^{-1} indicates the presence of nitrate, but it is difficult to determine its role. Based on its infrared spectral information together with its UV/vis and magnetic properties, compound

Table 2-15. Infrared spectral and structural data of dicopper(II) complexes **1-17**.

compound	IR (cm^{-1})	Cu-N($_{py}$ or $_{pyr}$)
$[Cu_2(PAHAP)Cl_4].H_2O$ **(1)**	3566,3500 (H_2O); 3346-3150 (ν_{NH2});	2.027(3)
	1662, 1641 ($\nu_{C=N}$) ; 1022 (Py)	2.026(3)
$[Cu_2(PAHAP)Cl_4]$ **(2)**	3353, 3309, 3231, 3189 (ν_{NH2}); 1664, 1639 ($\nu_{C=N}$) ; 1020(Py)	
$[Cu_2(PAHAP)Br_4].H_2O$ **(3)**	3578,3503(H_2O); 3340-3140(ν_{NH2});	2.025(5)
	1657,1636($\nu_{C=N}$); 1021(Py)	2.020(6)
$[Cu_2(PAHAP)(H_2O)_6]$ $(NO_3)_4$ **(4)**	3493(H_2O); 3338,3160 (ν_{NH2}); 1664, 1644 ($\nu_{C=N}$) ; 1027(Py); 1763(NO_3^-) 2092,2031(N_3^-)	2.000(5)
$[Cu_2(PAHAP\text{-}H)(N_3)_2$ $(NO_3)]$**(5)**	3372(ν_{NH^-}); 3200-3100(br, ν_{NH_2});1666($\nu_{C=N}$); 1015 (Py); 1750 (NO_3^-, coordinated)	
$[Cu_2(PAHAP)(NCS)_4$ $(DMF)_2].2DMF$**(6)**	3328,3176(ν_{NH2}); 2100,2083,2059(SCN^-); 1639(s.and br.$\nu_{C=N}$, $\nu_{C=O}$ of DMF); 1025(Py)	2.025 2.017
$[Cu_2(PAHAP)(NCO)_4]$ .2DMF**(7)**	3363,3266,3164(ν_{NH2}); 2215(NCO^-); 1679 ($\nu_{C=O}$ of uncoordinated DMF); 1025(Py)	
$[Cu_2(PAHAP)(Bipy)_2$ $(NO_3)_2].(NO_3)_2.4H_2O$ **(8)**	3500(H_2O); 3329,3175(ν_{NH2});1672,1648 ($\nu_{C=N}$);1748(NO_3^-); 1031,1013(Py)	1.989(5)
$[Cu_2(PAHAP)(Glyn\text{-}H)_2$ $(NO_3)(H_2O)](NO_3).3H_2O$ **(9)**	3500 (H_2O); 3363-3130 (ν_{NH2}); 1684, 1639 ($\nu_{C=N}$);1742 (vw. NO_3^-); 1603, 1407(RCO_2^-, unidentate)1035 (Py);	1.978(6) 1.987(5)

Table 2-15. (contd.) Infrared spectral and structural data of dicopper(II) complexes **1-17**.

compound	IR (cm^{-1})	Cu-N($_{py}$ or $_{pyr}$)
$[Cu_2(PAHAP)(Aln\text{-}H)_2(H_2O)_2](NO_3)_2.3H_2O$ (**10**)	3470(H_2O); 3366,3300,3256,3129(ν_{NH2} of PAHAP and glycinate); 1684,1650 ($\nu_{C=N}$); 1031(Py); 1763-1736 (vw. NO_3^-); 1609, 1410(RCO_2^-, unidentate)	1.993(4) 1.994(4) 1.972(4) 1.995(4)
$[Cu_2(PAHAP)(ACAC\text{-}H)_2(H_2O)_2](NO_3)_2$ (**11**)	3360-3140(ν_{NH2}); 1757(NO_3^-);1684,1657 ($\nu_{C=N}$); 1583(coordinate$\nu_{C=O}$);1020 (Py)	2.004(2) 2.018(2)
$[Cu_2(PMHAP\text{-}H)(NO_3)_3]$ (**12**)	3376(ν_{NH}-); 1770,1757,1724(uni- and bidentate NO_3^-); 1602($\nu_{C=N}$); 1010(Py)	1.966(4) 1.970(4)
$[Cu_2(PMHAP)(H_2O)_2(NO_3)_2](NO_3)_2$(**13**)	3520(H_2O); 3370-3150(ν_{NH2}); 1762, 1753 (free and unidentate NO_3^-); 1678(ν_{NH2}); 1028,1026(Py)	
$[Cu_2(PHMAP\text{-}H)(NO_3)_3(MeOH)(H_2O)]$ (**14**)	3347(ν_{NH}-); 3600(H_2O); 1777,1744,1735(sh), 1721(sh),1712(NO_3^-); 1607($\nu_{C=N}$); 1007(Py)	2.016(3) 2.042(3)
$[Cu_2(PHAAP)(Br)_3(H_2O)]$ (**15**)	3550(H_2O); 3368-3172(multiplet,ν_{NH2}); 1667($\nu_{N\text{-}C=O}$); 1607($\nu_{C=N}$); 1022 (Py, br.)	1.996(5) 2.029(5)
$[Cu_2(PYPZ)Cl_4].H_2O$ (**16**)	3570(H_2O); 3340-3160(ν_{NH2}); 1662, 1639($\nu_{C=N}$); 1023 (py); 1044(Pyr)	2.033(3) 2.040(4)
$[Cu_2(PYPZ)Br_4].H_2O$ (**17**)	3574(H_2O); 3350-3161(ν_{NH2}); 1658, 1635($\nu_{C=N}$); 1028(py); 1042(Pyr)	

Scheme 2-2

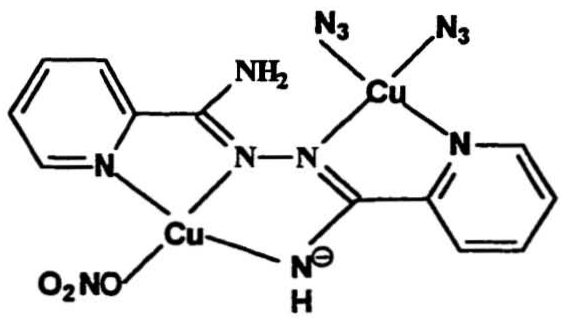

5 might have a **Type B** structure like **12**, **14** and **15** (see **Scheme 2-2**). Compound **6** exhibits two ν_{NH} infrared bands at 3328 and 3176 cm^{-1} associated with the NH_2 groups in PAHAP, and three prominent $\nu_{C\equiv N}$ bands at 2100, 2083 and 2059 cm^{-1} consistent with the *cis*-arrangement of two isothiocyanates at each copper centre [114]. A broad, strong absorption at 1639 cm^{-1} is associated with both coordinated and lattice DMF. The isocyanate complex **7** has a sharp single band at 3164 cm^{-1} and a doublet band at 3364, 3266 cm^{-1} associated with the NH_2 group in PAHAP, and only one strong and sharp ν_{CN} band at 2215 cm^{-1} consistent with the *cis*-arrangement of two isocyanates at each copper centre. The 2215 cm^{-1} band is so strong that other bands, expected to appear as a result of local symmetry are not observed. A sharp band at 1679 cm^{-1}, which does not appear in compound **6**, clearly is associated with lattice DMF. Complex **8** exhibits two ν_{NH} bands at 3329 and 3175 cm^{-1} associated with the NH_2 groups in PAHAP, a broad band at 3500 cm^{-1} due to lattice water and a prominent nitrate band [112] at 1748 cm^{-1}. At least two nitrate

combination bands [112] would be expected, associated with the lattice and coordinated nitrates, but very strong ν_{CN} bands at 1672 and 1648 cm^{-1} dominate this region. The infrared spectra of **9** and **10** above 3100 cm^{-1} are dominated by bands associated with water (3500 cm^{-1} in **9** and 3512 cm^{-1} in **10**) and NH_2 groups in PAHAP and glycinate (3363-3120 cm^{-1}) in **9** and alaninate (3366-3129 cm^{-1}) in **10**. Nitrate combination bands located at 1742 cm^{-1} (shoulder) for **9** and 1736 cm^{-1} (shoulder) for **10** are associated with ionic nitrate, and bands at 1603, 1407 cm^{-1} for **9** and 1609, 1410 cm^{-1} for **10** can be assigned as monodentate carboxylate absorption bands [115]. The ν_{NH} bands are observed in the infrared spectrum of **11** (3360-3140 cm^{-1}), confirming the existence of free NH_2 groups. Nitrate combination bands (lattice and weakly coordinated) are observed at 1757 cm^{-1} [112]. The strong 1583 cm^{-1} band is associated with the coordinated C=O groups of 1,3-pentanedionates [116]. The ligand PAHAP has two prominent NH_2 absorptions at 3465 and 3318 cm^{-1}. The PMHAP complex **12** shows just one sharp NH absorption at 3376 cm^{-1}, associated with the hydrogen bound to N(3), and no absorption associated with water. Three prominent nitrate combination bands are observed at 1770, 1757 and 1724 cm^{-1}, consistent with the presence of both monodentate and bidentate nitrate, although two bands are usually observed in each case [112]. Another PMHAP complex **13** isolated from aqueous solution shows a broad band at 3520 cm^{-1} due to coordinated water and a broad absorption at 3370-3150 cm^{-1} associated with the NH_2 group. The 1762 and 1753 cm^{-1} bands are associated with the presence of lattice and coordinated nitrates [112]. A single ν_{NH} band at 3347 cm^{-1} in the infrared spectrum of **14** confirms the deprotonation at

N(3) and the anionic nature of the ligand, and a broad shoulder at 3600 cm^{-1} is associated with the coordinated water molecule. A complex group of nitrate bands is observed (1777, 1744, 1735 (sh), 1721 (sh) and 1712 cm^{-1}), consistent with the three slightly different monodentate nitrate groups [112]. The infrared spectrum of **15** above 3100 cm^{-1} is dominated by bands associated with coordinated water (3550 cm^{-1}) and NH_2 groups (3368, 3331, 3287, 3232, 3172 cm^{-1}). The ν_{OH} band at 3409 cm^{-1} in the free ligand PHAAP has disappeared in the complex. The C-O is quite short (1.280 Å), and C(6)-N(2) and N(2)-N(3) are relatively short and similar. Also Cu(1)-N(3) is very short (1.917 Å). This suggests that N(3) might have significant negative charge and that the double bond is delocalized around the O-C-N-N framework. This is consistent with the spectrum indicating significant C=O character. The complexes **16**, **17** have similar bands in the range 4000-500 cm^{-1}. The lattice water band is clearly shown at 3570 cm^{-1} (**16**) and 3574 cm^{-1} (**17**). Rather complex groups of NH_2 bands are observed at 3340-3160 cm^{-1} for **17** and 3350-3161 cm^{-1} for **17**.

All the ligands clearly show strong $\nu_{C=N}$ absorptions: 1608 cm^{-1} for PAHAP, 1613 cm^{-1} for PMHAP, 1618, 1604 cm^{-1} for PHMAP, 1602 for PHAAP and 1606 cm^{-1} for PYPZ. This confirms that all these ligands adopt a *trans*-conformation with an open-chain diazine structure, similar to PAHAP (**Figure 2-1**). If the diazine moiety, together with the NH_2 groups, existed in a triazoline form, all these ligands should have only one $\nu_{C=N}$ band at much higher frequency, as in the case of picolinamide hydrazone (1657 cm^{-1}) and pyrazinamide hydrazone (1643 cm^{-1}). Normally, when the nitrogen in the C=N group is

coordinated to a metal ion, the $\nu_{C=N}$ band will decrease in frequency. The complex **12, 14, 15** of the ligands PMHAP, PHMAP and PHAAP respectively are consistent with this situation. However, the $\nu_{C=N}$ frequency in all PAHAP and PYPZ complexes increases dramatically, since the conjugation in the free ligand is broken when the ligands form binuclear complexes with a twisted conformation about N-N single bond. The deprotonated ligands in the complexes **12, 14, 15** have essentially flat structures, and so the $\nu_{C=N}$ bands decrease as expected, compared with that in the free ligands. The increase of $\nu_{C=N}$ frequencies in the twisted PAHAP and PYPZ dinuclear complexes were mirrored in the structural parameters which show that the bond distances of the C=N bonds in the complexes are somewhat shorter than or essentially the same as those in the free ligands, and not much longer as expected, even though a direct comparison of C=N bond distances in the complexes with those in the free ligands is not reasonable.

One characteristic infrared band for ligands containing 2-pyridyl fragments occurs at about 990 cm^{-1} [117], while for 2,4-pyrazyl fragments it occurs at about 1015 cm^{-1}, and is associated with a pyridine or pyrazine ring breathing mode, which shifts to higher energies on coordination. These bands occur at 997 cm^{-1} for PAHAP, 994 cm^{-1} for PMHAP, 995 cm^{-1} for PHMAP, 996 cm^{-1} for PHAAP, 994 cm^{-1} (2-pyridyl), 1018 cm^{-1} (2,4-pyrazyl) for PYPZ, and are all shifted to higher frequencies on coordination, which are mirrored in the Cu-N bond distances (pyridyl or pyrazyl) in the complexes with the same ligand. The shorter the Cu-N (pyridyl or pyrazyl) distances, the higher the breathing band frequencies.

Table 2-16. UV/Vis spectral data for dicopper(II) complexes **1-17** (nm).

compound	solid	H_2O(ε, $dm^3.mol^{-1}.cm^{-1}$)	DMF(ε, $dm^3.mol^{-1}.cm^{-1}$)
$[Cu_2(PAHAP)Cl_4].H_2O$ (**1**)	730	720(137.8)	780(298.3)
$[Cu_2(PAHAP)Cl_4]$ (**2**)	715	720(164.3)	820(332.6)
$[Cu_2(PAHAP)Br_4].H_2O$ (**3**)	704	720(150.9)	817(455.0)
$[Cu_2(PAHAP)(H_2O)_6](NO_3)_4$ (**4**)	689	715(167.2)	710(300.8)
$[Cu_2(PAHAP\text{-}H)(N_3)_2(NO_3)]$(**5**)	_	_	695(461.4)
$[Cu_2(PAHAP)(NCS)_4(DMF)_2].2DMF$(**6**)	675	_	687(378.3)
$[Cu_2(PAHAP)(NCO)_4].2DMF$(**7**)	620	_	680(435.3)
$[Cu_2(PAHAP)(Bipy)_2(NO_3)_2](NO_3)_2.4H_2O$ (**8**)	725	740(236.8)	722(256.4)
$[Cu_2(PAHAP)(Glyn\text{-}H)_2(NO_3)(H_2O)]$ $(NO3).3H_2O$ (**9**)	630	640(175.1)	600(101.9)
$[Cu_2(PAHAP)(Aln\text{-}H)_2(H_2O)_2](NO_3)_2.$ $3H_2O$ (**10**)	610	640(173.3)	600(170.5)
$[Cu_2(PAHAP)(ACAC\text{-}H)_2(H_2O)_2](NO_3)_2$(**11**)	607	630(165.8)	630(359.0)
$[Cu_2(PMHAP\text{-}H)(NO_3)_3]$(**12**)	680	683(pH=5.5)198.7) 724(pH=4.5)(98.40)	700(289.8)
$[Cu_2(PMHAP)(H_2O)_2(NO_3)_2](NO_3)_2$(**13**)	690	720(100.2)	700(258.5)
$[Cu_2(PHMAP\text{-}H)(NO_3)_3(MeOH)(H_2O)]$ (**14**)	695	710(pH=5.5)(159.7) 752(pH=4.5)(67.41)	710(226.0)
$[Cu_2(PHAAP)(Br)_3(H_2O)]$ (**15**)	870	_	800(298.5)
$[Cu_2(PYPZ)Cl_4].H_2O$ (**16**)	720	715(193.6)	800(286.6)
$[Cu_2(PYPZ)Br_4].H_2O$ (**17**)	712	706(176.3)	820(467.4)

Solid state mull transmittance, aqueous solution and DMF solution electronic spectral data are listed in **Table 2-16**. Solid mull transmittance electronic spectra for **1-17** are quite similar, with one broad visible band in the range 607-870 nm.

Aqueous solutions of **1-4** exhibit essentially identical spectra, with a broad absorption at 720 nm, consistent with the same solution species in each case and solvation of open coordination positions at each copper(II) centre. In DMF solution, however, the spectra are quite different (780 nm (**1**) , 820 nm (**2**), 817 nm (**3**), 710 nm (**4**)), indicating incomplete solvation effects. The longer wavelength absorptions for **1-3** in DMF suggest the persistence of copper-halogen bonds in solution and for **2** a structure somewhat different from that of **1**. The most likely structure to resist solvation effects would be one with intramolecular halogen bridges, and a possible structure for **2** would involve two square-pyramidal copper(II) centers in a pseudo-*cis* conformation with one or even two chlorine bridges. Molecular models suggest these are reasonable structural possibilities, which would create a relatively small angle between the two copper planes and not create any serious steric problems on the part of the two NH_2 groups. Despite the fact that reasonable crystals of **2** were obtained, none have permitted a structural determination. For **3**, the long wavelength band (817 nm) suggests that the weak intramolecular bromine bridging structure may persist in solution. For **4**, the absorption band (710 nm) in DMF is essentially the same as that in solid state, which shows that no solvation takes place in

DMF solution. The electronic spectra of **6** and **7** are quite different (675 nm for **6**, 620 nm for **7**) in solid state, while essentially identical in DMF solution (687 nm for **6**, 680 nm for **7**). In addition, It should be noted that **6** has a similar spectrum in the solid state to that in DMF solution. These electronic spectral data, together with infrared data, indicate that the two DMF molecules in **7** do not coordinate to the copper(II) centers, which indicates that **7** may have a larger torsion angle about the N-N single bond because of less steric problems compared with **6**.

The electronic spectrum of **8** in the solid state and in DMF solution are exactly the same (720 nm), and slightly different from that in aqueous solution (740 nm), suggesting that two weakly bonded NO_3^- ions in the solid state were replaced by water molecules in aqueous solution. Compound **9** has an essentially identical spectrum in the solid state (630 nm) and in aqueous solution (640 nm) because the water molecules are only weakly bonded to the Cu(II) ions in the solid state. However, the spectrum in DMF solution is different (600 nm). The reasonable explanation is that the complex would lose the weakly bonded water molecules in the dried DMF solvent and they would reasonably be replaced by DMF. Compound **10** has a similar spectrum in aqueous and DMF solutions to that of compound **9**, indicative of very similar solvation effects. Complex **11** exhibits an electronic spectrum with a peak at 607 nm in the solid state and 630 nm both in aqueous and DMF solutions because of solvation effects. It is of interest to note that an aqueous solution of **12** has a pH of 5.5 and a visible absorption at 683 nm. However, acidifying the solution

slightly (pH = 4.5) shifts the visible band to 720 nm, the exact position of **13** in aqueous solution, and also consistent with **1-4**, suggesting that the ligand is protonated at its amino group, hence its **Type B** coordination mode in the solid state becomes **Type AB** in aqueous solution. A similar result was observed for complex **14** (**Table 2-16**). Compound **15** exhibits quite a long wavelength absorption at 870 nm in the solid state, and at 800 nm in DMF solution, which suggests a minor coordination environment change in DMF. The spectra of **16** and **17** are quite similar to that of **1** and **3** respectively in the solid state and in solutions, with the same solvation effects.

2.3.3 Magnetism

The room temperature magnetic moments and the best fit data to the Bleaney-Bowers equation (**eqn. 1-4**) for the variable temperature (4-305 K) magnetic data are presented in **Table 2-17**. Room temperature magnetic moments for complexes **5**, **12**, **14**, **15** are subnormal falling in the range of 1.42-1.60 BM, indicating spin coupling between the copper(II) centers and the presence of net antiferromagnetism, while the room temperature magnetic moments for the other complexes are close to the normal values for an uncoupled copper(II) system and might suggest the absence of spin exchange.

A plot of χ_m*T versus temperature for **1** is illustrated in **Figure 1-17** and the rise in χ_m*T values from 0.44 emu.mol^{-1}.K at 296 K to 0.492 emu.mol^{-1}.K at 16 K, clearly indicates the presence of intramolecular ferromagnetic coupling. The drop at lower temperatures suggests the presence also of antiferromagnetism, which only shows up in this temperature range. Fitting of the data to the **eqn. 1-4** was carried out and the

intramolecular ferromagnetic coupling confirmed with $-2J = -24.4(2)$ cm^{-1} ($g = 2.138(5)$, $-2J = -24.4(2)$ cm^{-1}, $N\alpha = 20*10^{-6}$ emu, $\rho = 0$, $\theta = -1.85$ K, $10^2R = 1.3$; $R = [\Sigma(\chi_{obs} - \chi_{calc})^2/\Sigma\chi_{obs}^2]^{1/2}$). The solid line in **Figure 2-17** was calculated using these parameters. The small Curie-Weiss like correction term is negative, as would be expected, and confirms the presence of a very small antiferromagnetic component in the overall exchange, which is clearly intermolecular in nature. This can be assigned to the weak interdimer bridging connection *via* Cl (1), which is the only significant intermolecular contact. A similar bridging arrangement, with long axial copper-bromide contacts (Cu-Br 3.033 Å), in the complex $[Cu(4\text{-}Metz)_2Br_2]_2$ [118], also leads to weak antiferromagnetic coupling ($-2J = 2.4$ cm^{-1}).

Variable temperature magnetism for $[Cu_2(PAHAP)Br_4].H_2O$ (**3**) is very similar to that of **1**, with χ_m*T rising steadily from a value of 0.43 emu.mol^{-1}.K at 295 K to 0.62 emu.mol^{-1}.K at 3.9 K, indicative again of intramolecular ferromagnetic coupling. The data were fitted to **eqn. 1-4** to give $g = 2.067(5)$, $-2J = -22(2)$ cm^{-1}, $\rho = 0.00003$, $N\alpha = 45*10^{-6}$ emu, $\theta = 0.56$ K, $10^2R = 0.9$. No apparent significant intermolecular contacts show up in the structure of **3**, and this is mirrored in the magnetic data.

The variable temperature magnetic properties of $[Cu_2(PAHAP)(H_2O)_6](NO_3)_4$ (**4**) are in sharp contrast to those of **1**. A plot of χ versus temperature is illustrated in **Figure 2-18**, and reveals a maximum in susceptibility at about 25 K. This is clearly indicative of dominant antiferromagnetic exchange. The data were fitted successfully to **eqn. 1-4** with

Table 2-17. Magnetic, structural data and ΔE values of the dicopper(II) complexes.

compound	-2J (cm^{-1})	g	θ (K)	μ_{eff} (RT) (BM)	Cu-Cu (Å)	γ (Deg.)	Δ E (meV)
$[Cu_2(PAHAP)Cl_4].H_2O$ **(1)**	-24.4(2)	2.138(5)	-1.85	1.87	3.845(1)	77.1	29
$[Cu_2(PAHAP)Cl_4]$ **(2)**	44.0(3)	2.101(6)	-7.5	1.77			
$[Cu_2(PAHAP)Br_4].H_2O$ **(3)**	-22(2)	2.067(5)	0.56	1.87	3.826(1)	75.02	46
$[Cu_2(PAHAP)(H_2O)_6](NO_3)_4$ **(4)**	28.3(3)	2.29(1)	-5	1.85	4.389(2)	100.2	153
$[Cu_2(PAHAP\text{-}H)(N_3)_2(NO_3)]$**(5)**	207.4(7)	2.035(3)	-0.4	1.42			
$[Cu_2(PAHAP)(NCS)_4DMF)_2]$.2DMF**(6)**	51.1(3)	2.107(1)	-1.4	1.78	4.453(3)	103.6	155
$[Cu_2(PAHAP)(NCO)_4]$ .2DMF**(7)**	128(4)	2.25(5)	-2.4	1.76			
$[Cu_2(PAHAP)(Bipy)_2(NO_3)_2](NO_3)_2.4H_2O$ **(8)**		no coupling		1.91	4.229	119.8	47
$[Cu_2(PAHAP)(Glyn\text{-}H)_2(NO_3)(H_2O)](NO_3).3H_2O$ **(9)**	1.5(3)	2.09(1)	-0.8	1.86	4.412(4)	85.2	98

Table 2-17. (contd.) Magnetic, structural data and ΔE values of the dicopper(II) complexes

compound	-2J (cm^{-1})	g	θ (K)	μ_{eff} (RT) (BM)	Cu-Cu (Å)	γ (Deg.)	Δ E (meV)
$[Cu_2(PAHAP)(Aln\text{-}H)_2(H_2O)_2].(NO_3)_2 3H_2O$ **(10)**	45.6(4)	2.076(3)	-3.6	1.77	4.392(4) 4.379(4)	86.8(4) (average)	104 (Cu(1)-Cu(2))
$[Cu_2(PAHAP)(ACAC\text{-}H)_2(H_2O)_2](NO_3)_2$ **(11)**				1.78	4.360(2)	82.04	-
$[Cu_2(PMHAP\text{-}H)(NO_3)_3]$ **(12)**	173(3)	2.07(4)	-0.76	1.57	4.778(4)	165.2	453
$[Cu_2(PMHAP)(H_2O)_2(NO_3)_2].(NO_3)_2$**(13)**				1.84			
$[Cu_2(PHMAP\text{-}H)(NO_3)_3(MeOH)(H_2O)]$**(14)**	208(2)	2.09(1)	0	1.53	4.759(1)	168.3	377
$[Cu_2(PHAAP)(Br)_3(H_2O)]$ **(15)**				1.53	4.717(4)	153.2	
$[Cu_2(PYPZ)Cl_4].H_2O$ **(16)**				1.86	3.831(2)	79.68	107
$[Cu_2(PYPZ)Br_4].H_2O$ **(17)**				1.85			

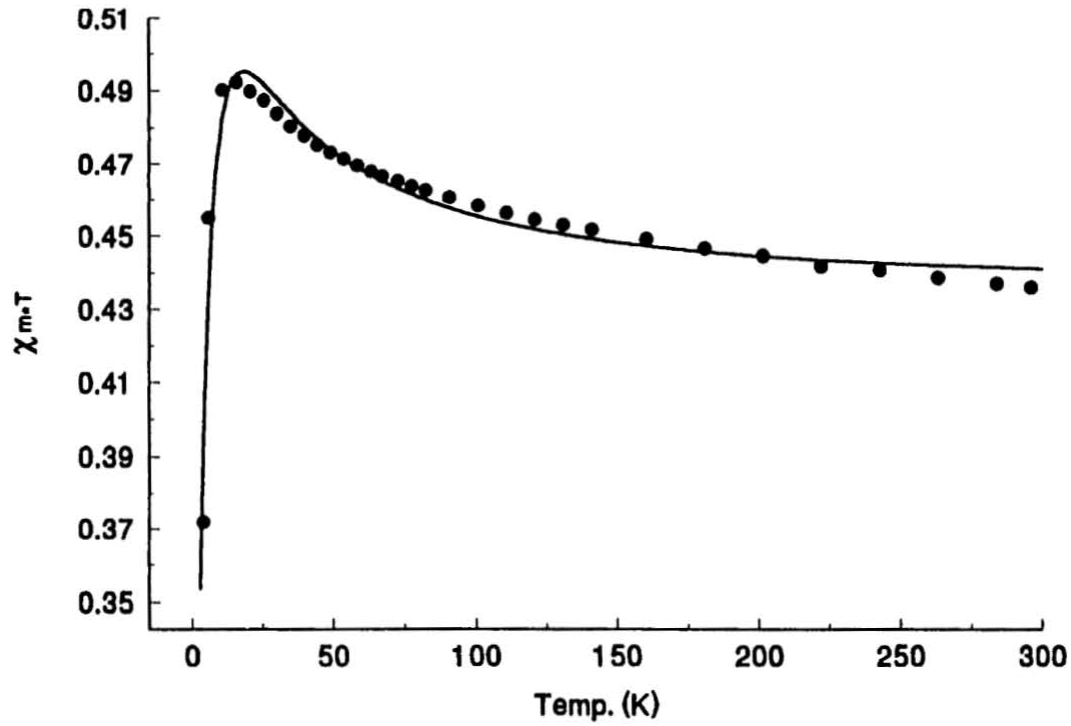

Figure 2-17. Variable temperature magnetic data for complex **1.** The solid line was calculated from **eqn. 1-4** with $g = 2.138(5)$, $-2J = -24.4(2)\ cm^{-1}$, $N\alpha = 20*10^{-6}$ emu, $\rho = 0$, $\theta = -1.85$ K, $10^2R = 1.3$ ($[\Sigma(\chi_{obs}-\chi_{calc})^2/\Sigma\chi_{obs}^2]^{1/2}$).

$g = 2.29(1)$, $-2J = 28.3(7)$ cm^{-1}, $\rho = 0.054$, $N\alpha = 46*10^{-6}$ emu, $\theta = -5$ K, $10^2R = 1.01$. The solid line in **Figure 2-18** was calculated with these parameters. The necessity for the inclusion of a significant Weiss-like correction in the fitting procedure raises the question of the appropriateness of the magnetic model, but it is clear from the structure that the Bleaney-Bowers equation should realistically interpret the exchange situation. Therefore the negative value indicates an intermolecular antiferromagnetic interaction. Although there are many intermolecular hydrogen bonding interactions (*vide infra*), a logical pathway for antiferromagnetic coupling would involve a direct connection between N(3) and Cu(1) (*via* O(2)-O(6)-N(5)-O(8)). This is clearly very long (six bonds and two hydrogen bonds), but is not unreasonable given the small nature of the interaction.

The magnetic properties of $[Cu_2(PAHAP)Cl_4]$ (**2**) are also surprisingly quite different from **1**, even though the only analytical difference between the two compounds is the clearly defined absence of water in **2**. Variable temperature magnetism on **2** shows a maximum in the χ_m versus temperature profile at 45 K, indicative of antiferromagnetic coupling, but stronger than in **4**. A reasonable fit of the data to **eqn. 1-4** was achieved and the best fit gave $g = 2.101(6)$, $-2J = 44.0(3)$ cm^{-1}, $\rho = 0.00005$, $N\alpha = 60*10^{-6}$ emu, $\theta = -7.5$ K, $10^2R = 1.3$. The stronger antiferromagnetism in **2**, comparable with that observed for $[Cu_2(PMK)Cl_4]$, suggests a different structure from **1** with a different angle between the magnetic planes or an additional magnetic bridge. The suggested chlorine bridged

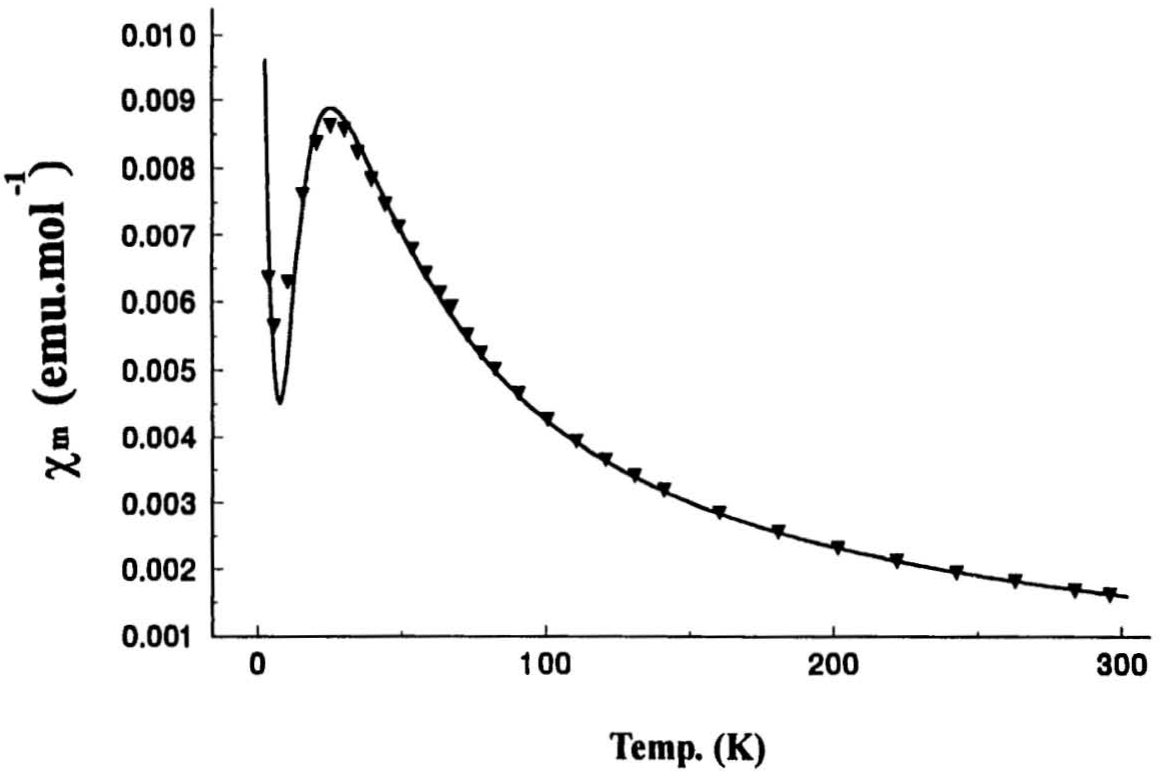

Fure 2-18. Variable temperature magnetic data for complex **4**. The solid line was calculated from **eqn. 1-4** with g = 2.29(1), $-2J = 28.3(7)\ cm^{-1}$, $\rho = 0.054$, $N\alpha = 46*10^{-6}$ emu, $\theta = -5$ K, $10^2R = 1.01(R = [\Sigma(\chi_{obs} - \chi_{calc})^2/\Sigma\chi_{obs}^2]^{1/2})$.

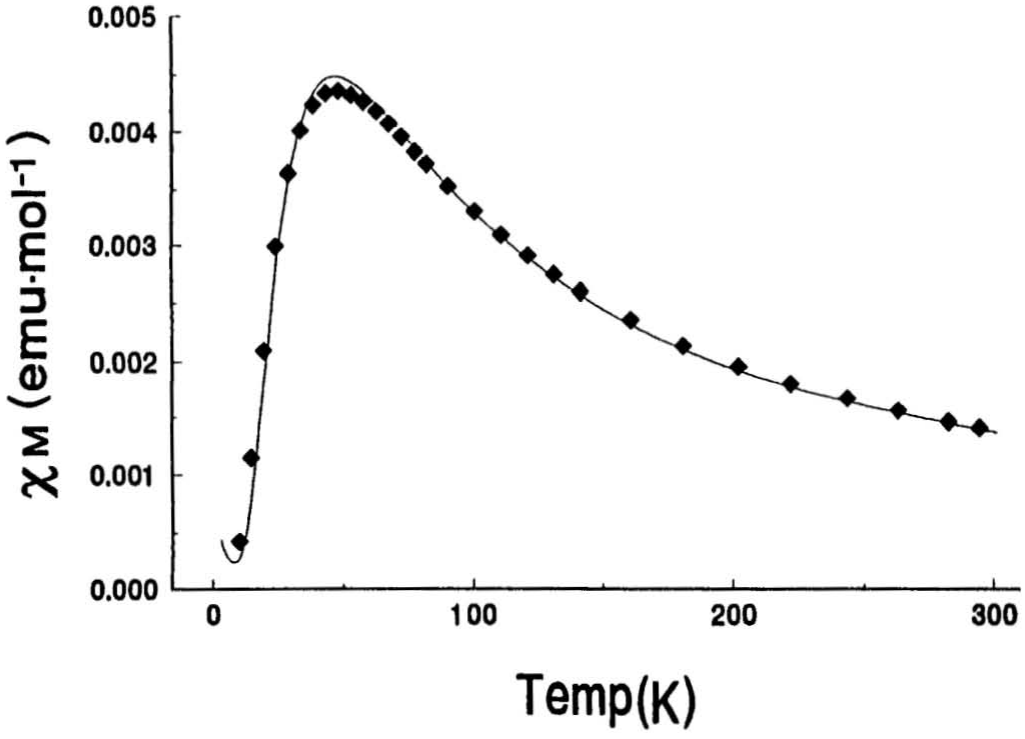

Fure 2-19. Variable temperature magnetic data for complex **6**. The solid line was calculated from **eqn. 1-4** with g = 2.107(1), $-2J = 51.1(3)\ cm^{-1}$, $\rho = 0.006$, $N\alpha = 75*10^{-6}$emu, $\theta = -1.4K$, $10^2R = 1.7$ ($R = [\Sigma(\chi_{obs} - \chi_{calc})^2/\Sigma\chi_{obs}^2]^{1/2}$).

structure for **2** would be consistent with this situation, if the bridge connected the two magnetic orbitals directly. The significant θ value, larger than that in **1**, indicates a stronger intermolecular exchange component, suggesting possible interdimer associations as well.

The azide complex $[Cu_2(PAHAP\text{-}H)(N_3)_2(NO_3)]$ (**5**) has a pronounced maximum in susceptibility at 180 K clearly indicating strong antiferromagnetic exchange. A good fit to **eqn. 1-4** gave g = 2.035(3), -2J = 207.4(7) cm^{-1}, ρ = 0.0013, Nα = 78*10^{-6} emu, θ = -0.4 K, 10^2R = 0.7. The strong antiferromagnetic coupling is consistent with the proposed *trans-trans* (**Type B**) conformation for this compound (*vide infra*).

The compound $[Cu_2(PAHAP)(NCS)_4(DMF)_2]$.2DMF (**6**) has a room temperature magnetic moment 1.78 BM close to the spin-only value for copper(II), but displays a maximum in the χ_m versus temperature profile at 40 K, indicative of weak antiferromagnetic coupling (**Figure 2-19**). A fit to **eqn. 1-4** gave g = 2.107(1), -2J = 51.1(3) cm^{-1}, ρ = 0.006, Nα = 75*10^{-6} emu, θ = -1.4 K, 10^2R = 1.7. Compound $[Cu_2(PAHAP)(NCO)_4]$.2DMF (**7**) has a room temperature magnetic moment of 1.76 BM, close to the spin only value for copper(II). However the χ_m versus temperature profile has a maximum at 100 K indicating significant antiferromagnetic coupling between the copper(II) centers, which are clearly bridged by the N-N diazine group. The data were fitted to **eqn. 1-4** to give g = 2.25(5), -2J = 128(4) cm^{-1}, ρ = 0.012, Nα = 66*10^{-6} emu, θ

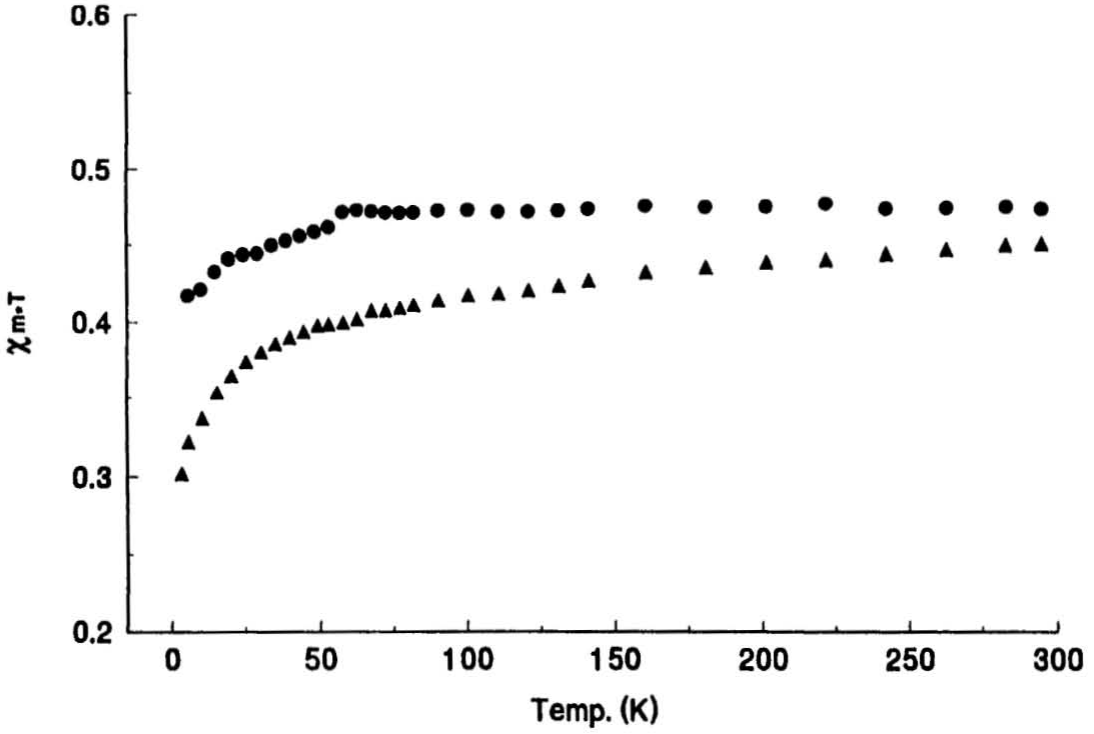

Figure 2-20. χ_m*T *vs* T for compound **8** (●) and compound **9** (▲).

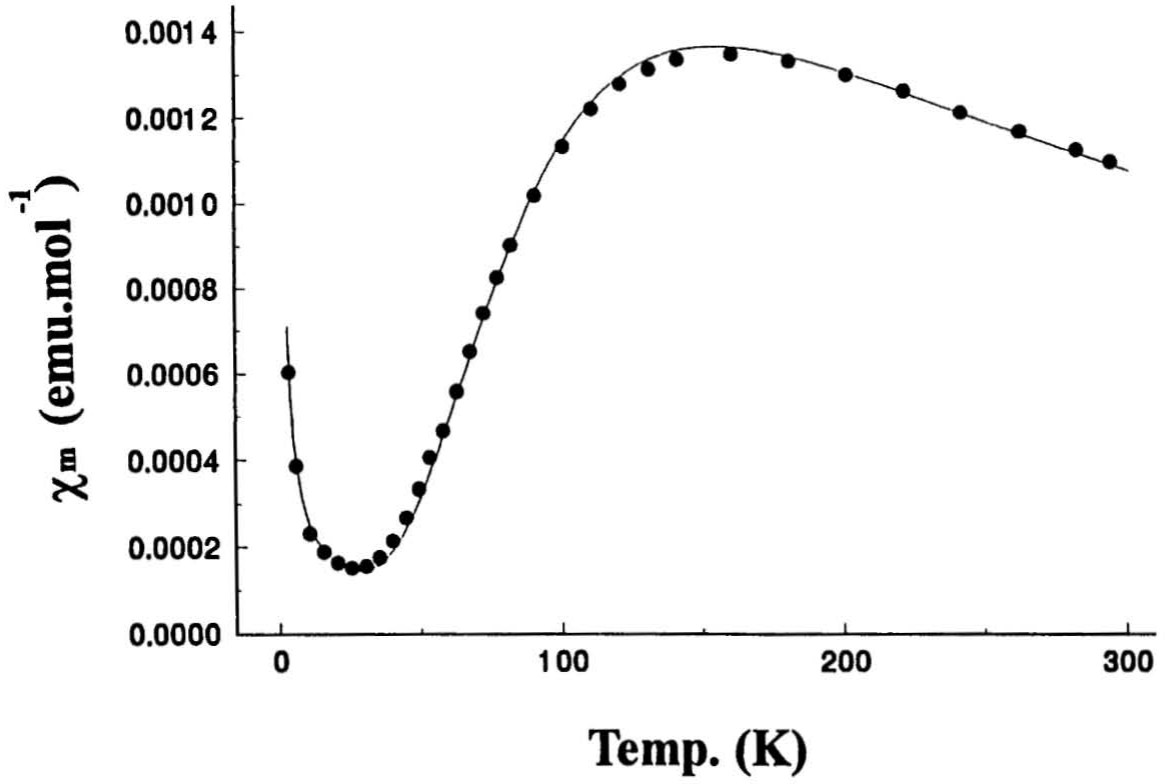

Figure 2-21. Variable temperature magnetic data for complex **12**. The solid line was calculated from **eqn. 1-4** with $g = 2.07(4)$, $-2J = 173(3)\ cm^{-1}$, $\rho = 0.0048$, $N\alpha = 68*10^{-6}$ emu, $\theta = -0.76$ K, $10^2R = 0.85$ ($R = [\Sigma(\chi_{obs} - \chi_{calc.})^2/\Sigma\chi_{obs}^2]^{1/2}$).

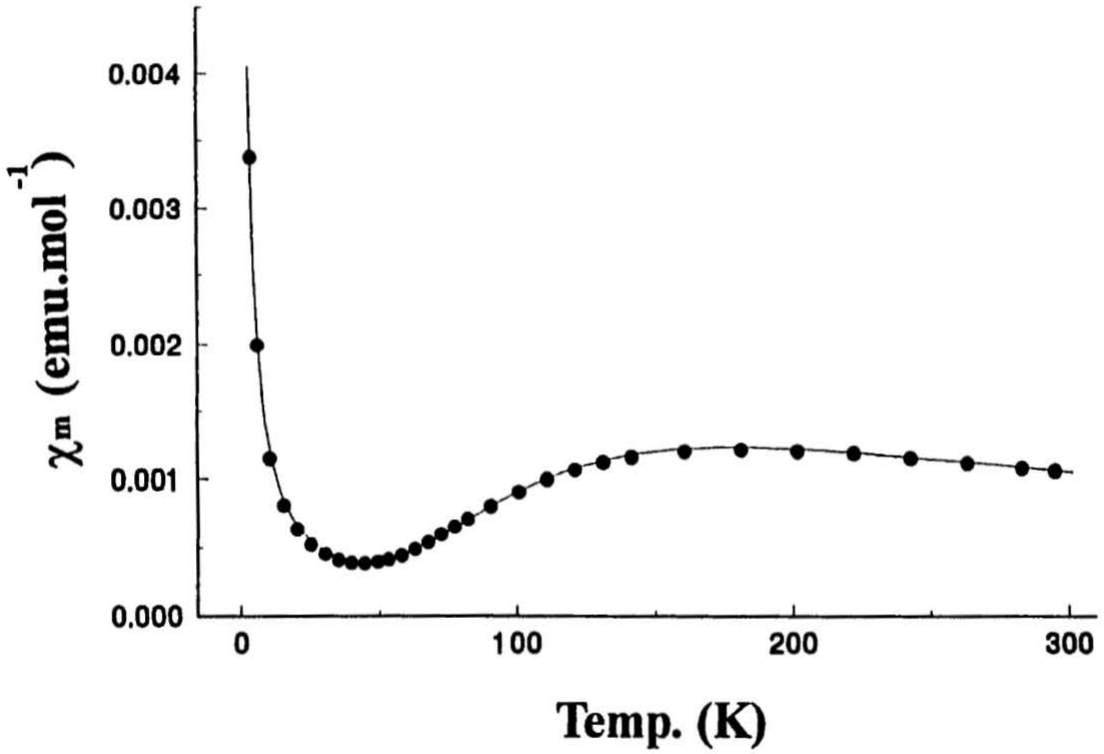

Figure 2-22. Variable temperature magnetic data for complex **14**. The solid line was calculated from **eqn. 1-4** with $g = 2.097(12)$, $-2J = 208(2)\ cm^{-1}$, $\rho = 0.031$, $N\alpha = 66*10^{-6}$ emu, $\theta = 0$ K, $10^2R = 0.64$ ($R = [\Sigma(\chi_{obs} - \chi_{calc})^2/\Sigma\chi_{obs}^2]^{1/2}$).

= -2.4 K (10^2R = 0.64). Compared with **6** the exchange is much larger, suggesting a large dihedral angle between the copper coordination planes. This may well be associated, in part, with the apparent absence of coordinated DMF in this compound, leading to different steric repulsion effects. The significant negative θ value implies a weak intermolecular antiferromagnetic exchange component, but this cannot be evaluated without structural information.

The compound $[Cu_2(PAHAP)(Bipy)_2(NO_3)_2].(NO_3)_2 .4H_2O$ (**8**) has a higher room temperature magnetic moment, 1.91 BM, and the χ_m*T values are larger than 0.41 emu.mol^{-1}.K throughout the 5-300 K temperature range (**Figure 2-20**), indicative of no significant coupling between the copper(II) centers. This is consistent with the distorted trigonal bipyramidal structure of this complex, and the equatorial bonding of the copper centers to the diazine nitrogen bridge.

The compound $[Cu_2(PAHAP)(Glyn\text{-}H)_2(NO_3)_2].4H_2O$ (**9**) has a normal room temperature magnetic moment (1.78 BM), and the χ_m*T values are larger than 0.41 emu.mol^{-1}.K above 75 K. When the temperature is lowered, the χ_m*T values decrease to 0.302 emu.mol^{-1}.K at 4 K (**Figure 2-20**) indicating that there is a very small antiferromagnetic interaction taking place. The data were fitted to **eqn. 1-4** to give g = 2.09(1), -2J = 1.5(3) cm^{-1}, ρ = 0.0007, Nα = 72*10^{-6} emu, θ = -0.8K (10^2R = 3.5). This is not a good fit since the singlet-triplet splitting is very small and comparable with the Zeeman energy ($g\beta H$). The data were also fitted to the magnetization expression (**eqn 2-1- eqn 2-4**) [119, 120] which is considered to be more appropriate for weakly coupled

dinuclear complexes. The presence of an interdimer interaction was considered by using

$$M = Ng\beta(\sinh(g\beta H/kT)) / (\exp(-2J/kT) + 2\cosh(g\beta H/kT) + 1) \quad [2\text{-}1]$$

$$\chi_m = M/H + N\alpha \quad [2\text{-}2]$$

$$\chi'_{Cu} = \chi_{Cu}/(1 - (2zJ'\chi_{Cu}/Ng^2\beta^2)) \quad [2\text{-}3]$$

$$\chi''Cu = \chi'_{Cu}(1 - \rho) + (Ng^2\beta^2\rho)/(4kT) + N\alpha \quad [2\text{-}4]$$

eqn 2-4, where z is the number of nearest neighbour dimers and J' the interdimer exchange parameter. Comparable fitting parameters were obtained by this method, with a slightly improved fit (g = 2.103(7), -2J = 1.4(5) cm^{-1}, zJ' = −1.44 cm^{-1}, $N\alpha = 60*10^{-6}$ emu, ρ = 0.0005), confirming the very weak antiferromagnetic exchange in **9**. The comparable 2J and zJ' values suggests that the hydrogen bonds *via* the water and the weakly coordinated nitrate molecule provide a significant intermolecular antiferromagnetic exchange pathway.

The compound $[Cu_2(PAHAP)(Aln\text{-}H)_2(NO_3)_2].5H_2O$ (**10**) has a room temperature magnetic moment (μ_{eff} = 1.77 BM) close to the spin only value, but a plot of χ_m versus temperature shows a maximum at ≈ 40 K, indicative of intramolecular antiferromagnetic coupling. Fitting of the variable temperature data to **eqn. 1-4** gives g = 2.076(3), -2J = 45.6(4) cm^{-1}, ρ = 0.0382, $N\alpha = 75*10^{-6}$ emu, θ = -3.6 K, 10^2R = 0.93. A somewhat larger than usual Weiss-like correction was applied to give a reasonable data fit, and this implies an intermolecular antiferromagnetic exchange component.

Compound $[Cu_2(PAHAP)(ACAC\text{-}H)_2](NO_3)_2$ (**11**) has a room temperature magnetic moment of 1.78 BM, close to the spin only value for copper (II). No variable

temperature magnetic data on **11** are available. However, from a structural perspective, weak intramolecular antiferromagnetic coupling should be observed in this complex.

The plot of molar susceptibility versus temperature for $[Cu_2(PMHAP\text{-}H)(NO_3)_3]$ **(12)** is illustrated in **Figure 2-21**. The maximum at ≈ 160 K is indicative of fairly strong intramolecular antiferromagnetic coupling, and the solid line corresponds to a good data fit to **eqn. 1-4** for $g = 2.07(4)$, $-2J = 173(3)\ cm^{-1}$, $\rho = 0.0382$, $N\alpha = 68*10^{-6}$ emu, $\theta = -0.76$ K, $10^2R = 0.85$. The strong antiferromagnetic coupling is consistent with the *trans-trans* **(Type B)** structure of this compound, in which there is clearly good overlap of the magnetic copper orbitals and the *p* orbitals of the diazine bridge (*vide supra*).

$[Cu_2(PMHAP)(H_2O)_2(NO_3)_2]$ $(NO_3)_2$ **(13)** gives a room temperature magnetic moment of 1.84 BM, close to the spin only value for copper(II) and may have very similar variable temperature magnetism to that of **4**.

$[Cu_2(PHMAP)(MeOH)(H_2O)(NO_3)_3]$ **(14)** has a room temperature magnetic moment (μ_{eff} = 1.53 BM) well below the spin-only value, indicative of significant antiferromagnetic coupling. The variable temperature susceptibility versus temperature profile **(Figure 2-22)** displays a maximum at about 180 K, and fitting to **eqn. 1-4** gives $g = 2.097(12)$, $-2J = 208(2)\ cm^{-1}$, $\rho = 0.031$, $N\alpha = 66*10^{-6}$ emu, $\theta = 0$ K, $10^2R = 0.64$. The solid line in **Figure 2-22** was calculated with these parameters. The sharp rise in susceptibility at low temperature is indicative of a significant proportion of paramagnetic impurity (3.1%). The extensive hydrogen bonding network in this compound **(Figure**

2-14) does not appear to provide any intermolecular contribution to the exchange situation.

The complex $[Cu_2(PHAAP\text{-}H)Br_3(H_2O)]$(**15**) has a room temperature magnetic moment (μ_{eff} = 1.53 BM) well below the spin-only value, indicating significant antiferromagnetic coupling. We await its variable temperature magnetism.

Complexes **16** and **17** have quite high room temperature magnetic moments (μ_{eff} = 1.86 BM for **16** and 1.85 BM for **17**), and from structural perspectives may have very similar variable temperature magnetism to that of **1** and **3** respectively.

2.3.4 Magnetostructural correlation for dicopper(II) complexes bridged by single N-N bonds

In the previous sections, a series of binuclear copper(II) complexes with open-chain diazine ligands has been described. In all cases, two copper(II) centers are bridged by the N-N single bond of the open-chain diazine ligands. However these complexes exhibit dramatically different magnetic properties. X-ray structures show that in all these complexes, except compound $[Cu_2(PAHAP)(Bipy)_2(NO_3)_2].(NO_3)_2.4H_2O$ (**8**), the unpaired electron of the copper (II) ion occupies a magnetic orbital of $d_{x^2-y^2}$ symmetry, which points towards the co-ordinating diazine nitrogen atoms. Therefore, considerable electron delocalization should take place over these two nitrogen atoms only, and the magnetic superexchange interaction becomes possible via mainly the σ orbitals of the ligands. Changes in the bridging geometry (e.g. the dihedral angle about the N-N single bond) of the ligand are likely to influence directly the efficiency of the exchange pathway.

Before trying to correlate the magnetic and the structural data, two facts should be considered: 1) The terminal co-ligands are different in each complex. 2) The ligands, PMHAP, PHMAP, PHAAP are deprotonated in the complexes **12**, **14**, **15** respectively and have a negative charge. Firstly the electronegativity of the atoms bound to the copper(II) centers will affect the spin exchange by affecting the electron density on the bridging atoms and the copper(II) ions. The antiferromagnetic interaction will decrease when electron density is removed from the bridging atoms and copper(II) ions. However, the effect for terminal atoms is comparatively less important. Secondly, Oshio and Nagashima [121] concluded that in the case of bridging ligands with a negative charge, the energy levels of the nitrogen $p\ \sigma$ orbitals coordinated to the copper(II) ions, are closer in energy to the copper(II) *d* orbitals than those of the neutral bridging ligand. In other words, the bridging ligand with negative charge will result in a stronger antiferromagnetic interaction. However, the variable temperature magnetic property studies on a series of doubly N1,N2-1,2,4-triazole (neutral) bridged copper(II) complexes and doubly N1,N2-1,2,4-triazolate (negative) bridged binuclear copper(II) compounds indicate that the isotropic exchange constants for both series fall in the same range, namely, there is a very close similarity in the superexchange capability of the triazole and the triazolate bridge. Koningsbruggen et al. made a further conclusion that in determining the effectiveness of the magnetic superexchange mechanism, electronic effects are of minor importance [13].

Therefore, obviously, geometrical factors involving the copper(II) ions and the bridging ligands should be invoked to account for the difference in magnitude of the

isotropic exchange constant for the present series of the dicopper(II) complexes. The structural parameters involving the copper(II) atoms and the open-chain diazine network, together with the isotropic exchange constants (-2J) are summarised in **Table 2-17**. With the exception of compound $[Cu_2(PAHAP)(Bipy)_2(NO_3)_2].(NO_3)_2 .4H_2O$ (**8**), all complexes contain two approximately square planar or square pyramidal or distorted six-coordinate copper(II) centers linked by N-N single bonds with different dihedral angle (γ). With the increase of γ values, the Cu-Cu distances increase significantly because of obvious geometric factors. However, the increase of the Cu-Cu distances in different complexes in the present series does not decrease the magnitude of -2J values at all, as would be expected. Hence, the effect of changing the copper-copper distance is also less important to the magnitude of the isotropic exchange constant (-2J).

Consequently, the only factor that significantly affects the isotropic exchange constant is the dihedral angle (torsion angle) between the two copper(II) magnetic planes. Although a handful of compounds have previously been structurally characterized, variable temperature studies, have been limited to $[Cu_2(PMK)Cl_4]$ [79], $[Cu_2(HL)Cl_3(H_2O)].1.5H_2O$ [88] and $[Cu(OPA)]_4(NO_3)_4.8H_2O$ [98] as mentioned in **Chapter 1**. Both $[Cu_2(PMK)Cl_4]$ and $[Cu_2(HL)Cl_3(H_2O)].1.5H_2O$ are antiferromagnetically coupled (-2J = 52(4) cm^{-1} and 213.3 cm^{-1} respectively), but to a dramatically different extent. The variable temperature magnetic property studies on $[Cu(OPA)]_4(NO_3)_4.8H_2O$ indicated no coupling at all between copper(II) centers. This is clearly related to the angle between the magnetic planes in these three complexes. For $[Cu_2(PMK)Cl_4]$, the Cu-N-N-Cu dihedral

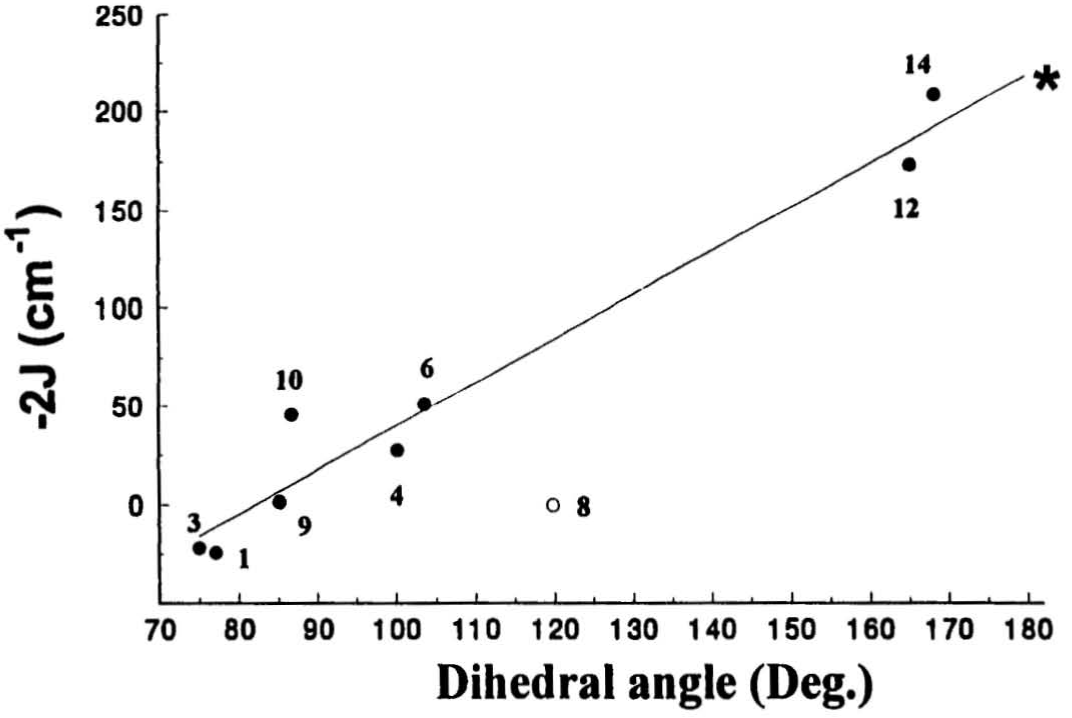

Figure 2-23. plot of -2J (cm^{-1}) *vs* magnetic plane dihedral angle for **1**, **3**, **4**, **6**, **9**, **10**, **12**, **14**(•); **8**(○); ref. [82] (*). The solid line represents the best fit to the (•) data.

angle is 70.8° indicating an acute angle between the magnetic planes. In contrast, the magnetic orbitals in $[Cu_2(HL)Cl_3(H_2O)].1.5H_2O$ are almost coplanar, while the angle in $[Cu(OPA)]_4(NO_3)_4.8H_2O$ is 90°. In these three cases, the magnetic ground state for the copper(II) centers is of the $d_{x^2-y^2}$ type. The present series of dicopper(II) complexes, with the exception of compound **8**, is consistent with this situation, in that the magnetic plane dihedral angles are 77.1° (**1**), 75.02° (**3**), 100.2° (**4**), 103.6° (**6**), 85.2° (**9**), 105° (**10**), 87.48°(**11**), 165.2° (**12**), 168.3° (**14**), 150.5° (**15**) and 79.68° (**16**) respectively. **Figure 2-23** shows that the value of -2J increases from -28.3 cm^{-1} to 208 cm^{-1} as a function of increasing magnetic plane dihedral angles from 75.02° to 168.3°. The solid line in **Figure 2-23** corresponds to a best line fit, leading to the equation [122, 123]:

$$-2J = 2.233\gamma - 183.7(cm^{-1}) \quad \text{.....[2-5]}$$

This fairly good linear relationship in such a large range of angles and -2J values might suggest that any other factors, such as the negative charge of the ligands in the related complexes and the differences of the terminal co-ligands, might have little effect on the isotropic exchange constant. This result represents the first successful magnetostructural correlation between the isotropic exchange constant and structural parameters for copper(II) ions linked by a diatomic bridge. Even though Koningsbruggen et al. [13] worked out a relationship between the isotropic exchange constant and the N-Cu-N angles (the angle of N1-Cu2-N2' or N2-Cu1-N1' see **Figure 1-12**) in a planar

Cu-(N-N)$_2$-Cu framework for the series of doubly N1,N2-1,2,4-triazole bridged copper(II) compounds, it is difficult to say whether the relationship is linear or not .

It should be noted that **eqn. 2-5** was obtained only within the dihedral angle range 75E-180E. It would obviously need to be modified for a very small dihedral angle system or a system which involves a drastically different open-chain ligand, because of steric and electronic effects. In addition, this equation can only be applied for dicopper(II) complexes which have a $d_{x^2-y^2}$ ground state. Using the equation to calculate the -2J value for compound **8** with a dihedral angle 119.8°, the calculated -2J value (83.8 cm^{-1}) is clearly inconsistent with the experimental data (no coupling). However, examination of the copper(II) ion stereochemistry reveals why. The geometry at the copper(II) centers is quite distorted, but is closer to a trigonal bipyramid than a square pyramid (τ = 0.58) [81], with the two coppers bridged through the N-N linkage via the equatorial lobes of their d_{z^2} orbitals. This is mirrored in the Cu-Cu separation (4.229 Å), which is not longer as expected, but significantly shorter than that in complex **4** or **6**. Since this component of the d_{z^2} orbital carries a small proportion of the unpaired electron density, these observed magnetic properties are entirely reasonable, which will be proved by molecular orbital calculations in the next section. The lack of coupling between the copper centers in compound **8** means that effective J_{total} = zero. Such an example should therefore provide an opportunity for a theoretical calculation of the J_F term for this complex ($|J_F| = |J_{AF}|$).

2.3.5 Molecular orbital calculations for the complexes and appropriate models

To test the conclusion that the twist angle between the magnetic planes is the major factor in determining the type and extent of coupling, molecular orbital calculations based on the extended Hückel model turned out to be very useful in providing a more quantitative description of the magnetic exchange interactions which occur in these compounds.

The molecular orbital calculations have been carried out at the extended Hückel [124] level for **1**, **3**, **4**, **6**, **8-12**, **14-16** and also for the complex $[Cu_2(PMK)Cl_4]$ [79], using the exact crystallographic coordinates. The data set for **4** was simplified by the removal of the axial water molecules (O(9)), which did not alter the copper(II) magnetic ground state, or the molecular geometry. The differences in energy between the two triplet state magnetic molecular orbitals for the present compounds are listed in **Table 2-17**.

The two highest antibonding triplet state molecular orbitals (SOMO's, Singly Ocupied Molecular Orbitals) for compound **1**, which are responsible for the magnetic properties, are dominated by *p* orbital components on the diazine nitrogens and the pyridine nitrogens. The molecular twist along the N-N bond (γ = 77.1°) results in misalignment of the adjacent *p* orbitals in the N-N bond, almost amounting to a situation of orthogonality. With very limited overlap between these orbitals, it is no surprise that the energy difference between the symmetric and antisymmetric MO is very small (ΔE = 29

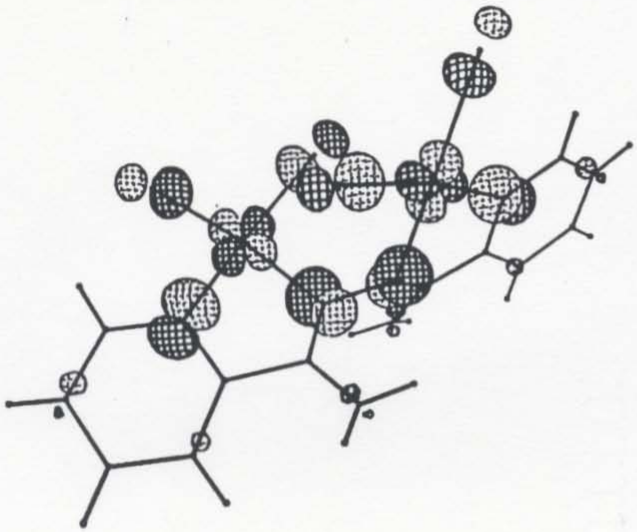

E = -11.422 eV

Symmetric SOMO

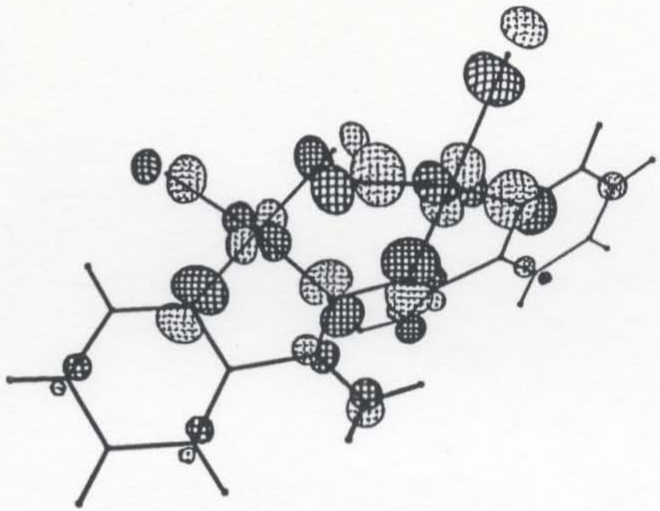

E = -11.451 eV

Antisymmetric SOMO

Figure 2-24. the symmetric and antisymmetric SOMOs for compound **1** .

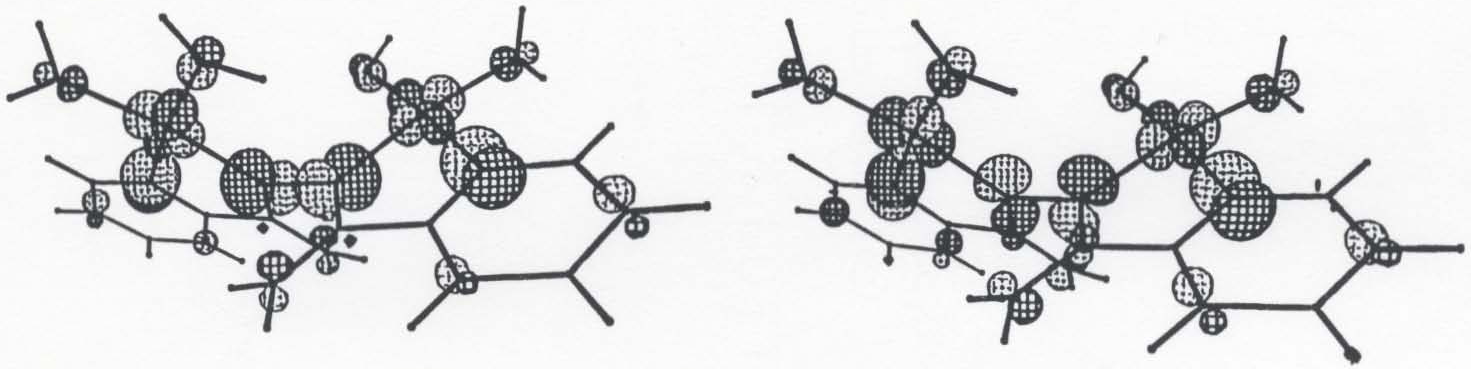

E = -11.569 eV

Symmetric SOMO

E = -11.722 eV

Antisymmetric SOMO

Figure 2-25. The symmetric and antisymmetric SOMOs for compound **4** .

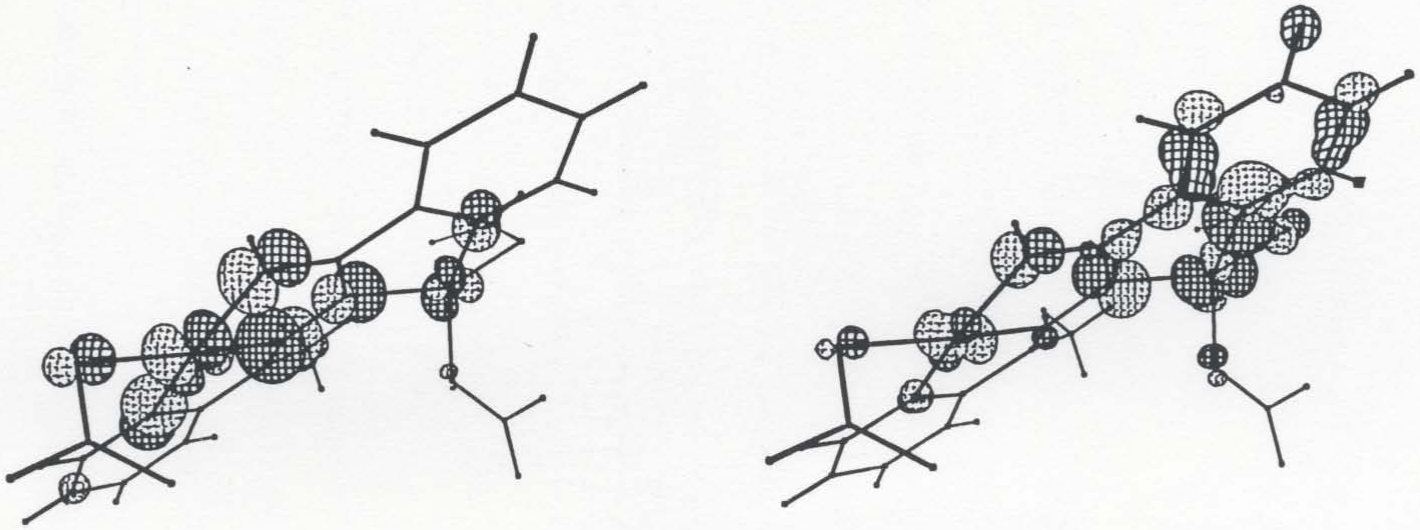

E = -11.341 eV

Symmetric SOMO

E = -11.794 eV

Antisymmetric SOMO

Figure 2-26. The symmetric and antisymmetric SOMOs for compound **12**.

meV). The symmetric and antisymmetric molecular orbital combinations are illustrated in **Figure 2-24**. A similar situation exists for compound **3**, again with a small energy difference between the triplet state SOMO's (46 meV). The two comparable highest energy molecular orbitals for **4** (**Figure 2-25**) and **6** are again dominated by *p* orbital components on the pyridine ring and diazine nitrogens, but because of the flatter nature of the molecule, overlap between the diazine *p* orbitals is enhanced such that the difference in energy between the symmetric and antisymmetric magnetic MOs is substantially larger (ΔE = 153 meV for **4** and 155 meV for **6**). A similar calculation for $[Cu_2(PMK)Cl_4]$ indicates a large energy difference between the symmetric and antisymmetric molecular orbitals (ΔE = 269 meV), consistent with the stronger antiferromagnetic coupling. However a direct comparison of ΔE here cannot be made because of the different ligands.

The difference in energy between the symmetric and antisymmetric magnetic MO's for compounds **9** and **10** is similar and relatively small (98 meV for **9** and 104 meV for **10**), consistent with the weak magnetic coupling in these two compounds .

The molecular orbital picture for compound **12** (**Figure 2-26**) is complicated by the presence of a different ligand and the additional copper-nitrogen bond (Cu(1)-N(3) 1.916(5) Å), which is very short, and the antisymmetric MO shows a significant contribution from the *p* orbitals in the framework Cu(1)-N(3)-C(13)-N(4)-Cu(2). This, combined with the almost flat nature of the molecule, leads to a very large difference in energy between the two magnetic molecular orbitals (453 meV), consistent with the strong

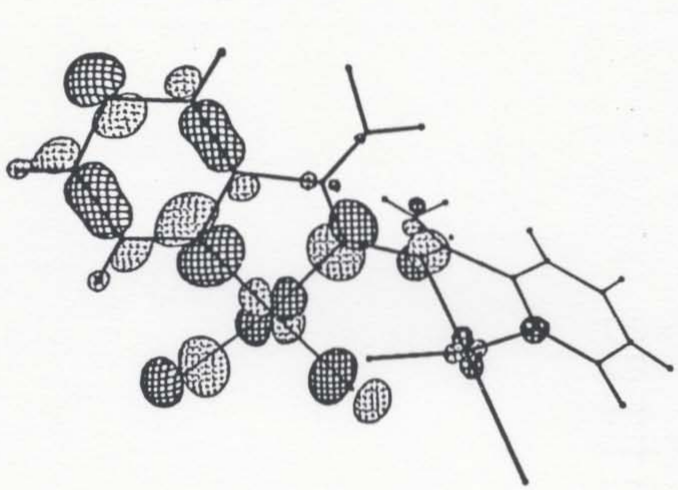

E = -11.337 eV

Symmetric SOMO

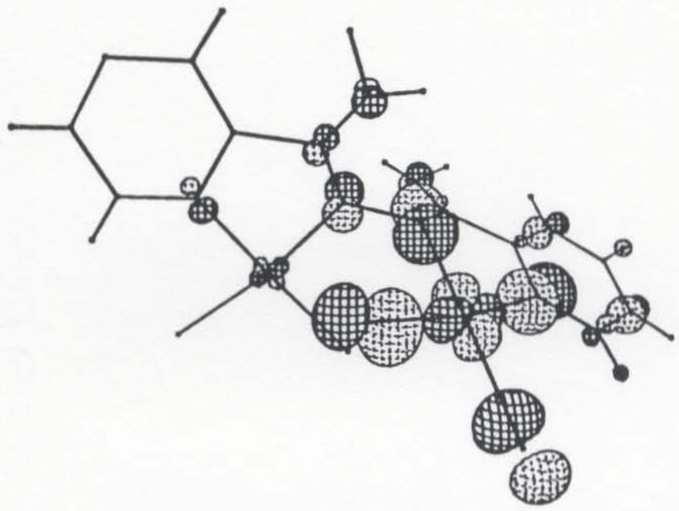

E = -11.444 eV

Antisymmetric SOMO

Figure 2-27. The symmetric and antisymmetric SOMOs for compound **16**.

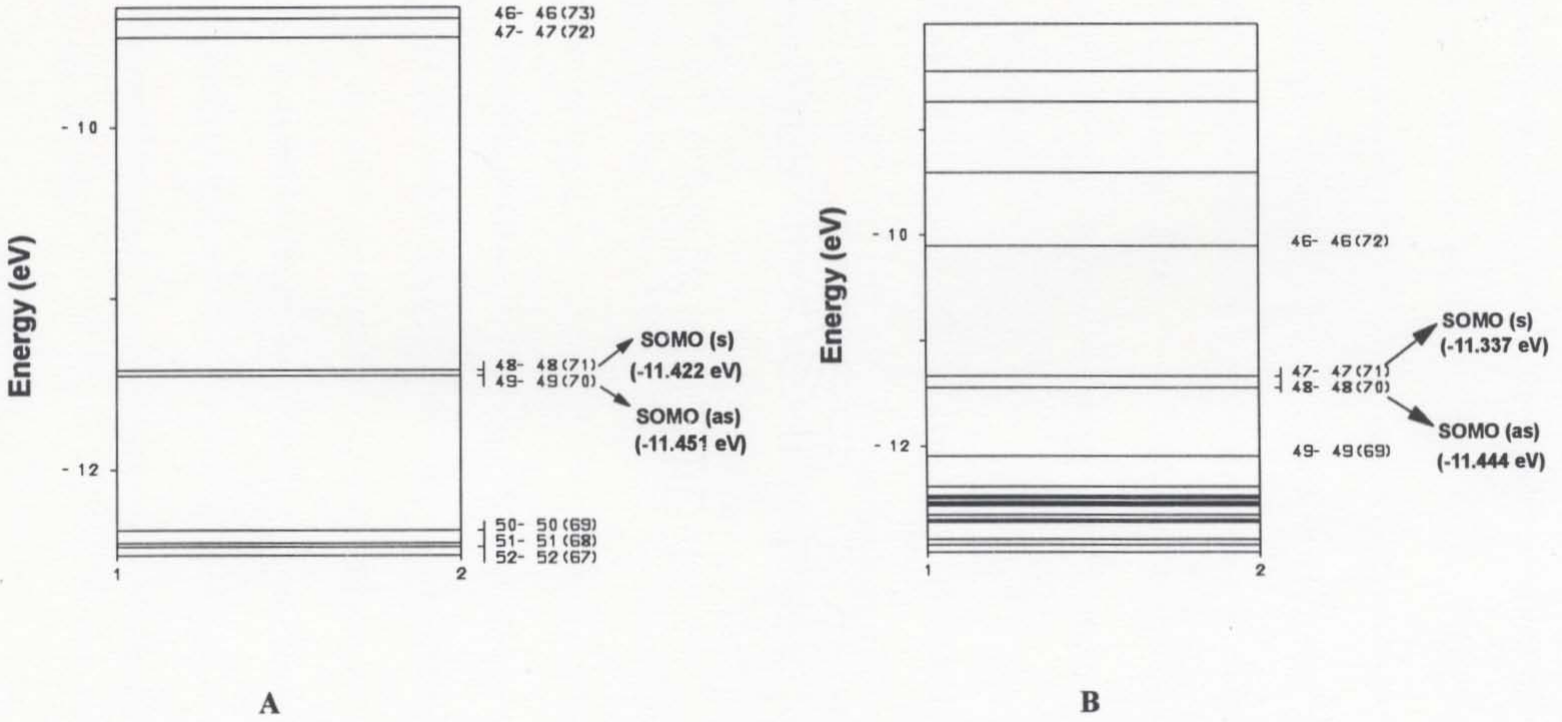

Figure 2-28. Comparision of expanded views of energy levels in complex **1(A)** and **16(B)**.

antiferromagnetic coupling observed for this complex. However the strong exchange in this case appears not to be due entirely to the diazine bridge. Similar results were obtained for compound **14** with ΔE = 377 meV. Even though **16** shows a very similar structure to that of **1**, the energy difference between two SOMOs is much larger (107 meV) than that for **1** (29 meV), which is probably due to the contribution of the free pyrazine nitrogen (**Figure 2-27**). However, the expanded views (**Figure 2-28**) of the energy level scheme for both complexes are very similar, suggesting that **16** might also demonstrate a ferromagnetic coupling.

These calculations may be used in conjunction with the orbital model for the exchange interaction [125-127] (**eqn. 2-6**) between two copper(II) centers, in which the exchange integral J can be correlated with geometric distortions. J can be written as the sum of two terms,

$$J = J_F + J_{AF} = -K_{12} + (\varepsilon_s - \varepsilon_a)^2/(J_{11} - J_{12}) \quad [2\text{-}6]$$

J_F being the term defined by the exchange integral between the two localised molecular orbitals, which is always ferromagnetic, and J_{AF}, which is composed of two components, the square of the difference in energy between the two molecular orbitals (ε_s, ε_a) in the triplet state, and the difference in coulomb integrals between the localised molecular orbitals (J_{11}, J_{12}). In dealing with correlations within a series of related compounds the term that changes most is $(\varepsilon_s - \varepsilon_a)^2$, and the other terms are considered to be largely invariant. The energy difference between the two molecular orbitals calculated above is therefore a major function of the J_{AF} term.

The validity of these observations, within a limited data set, is best examined in the context of a set of molecular models, and appropriate molecular orbital calculations. A simple set of model systems that combines the essential features of the ligand (i.e. the two sp^2 nitrogen centers linked by a single N-N bond), and the copper square planes, is illustrated in **Figure2-29**.

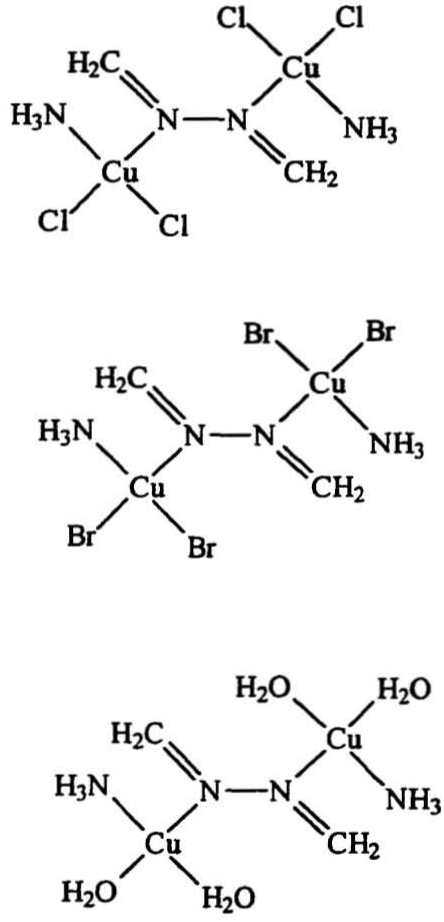

Figure 2-29. Model compounds for MO calculations.

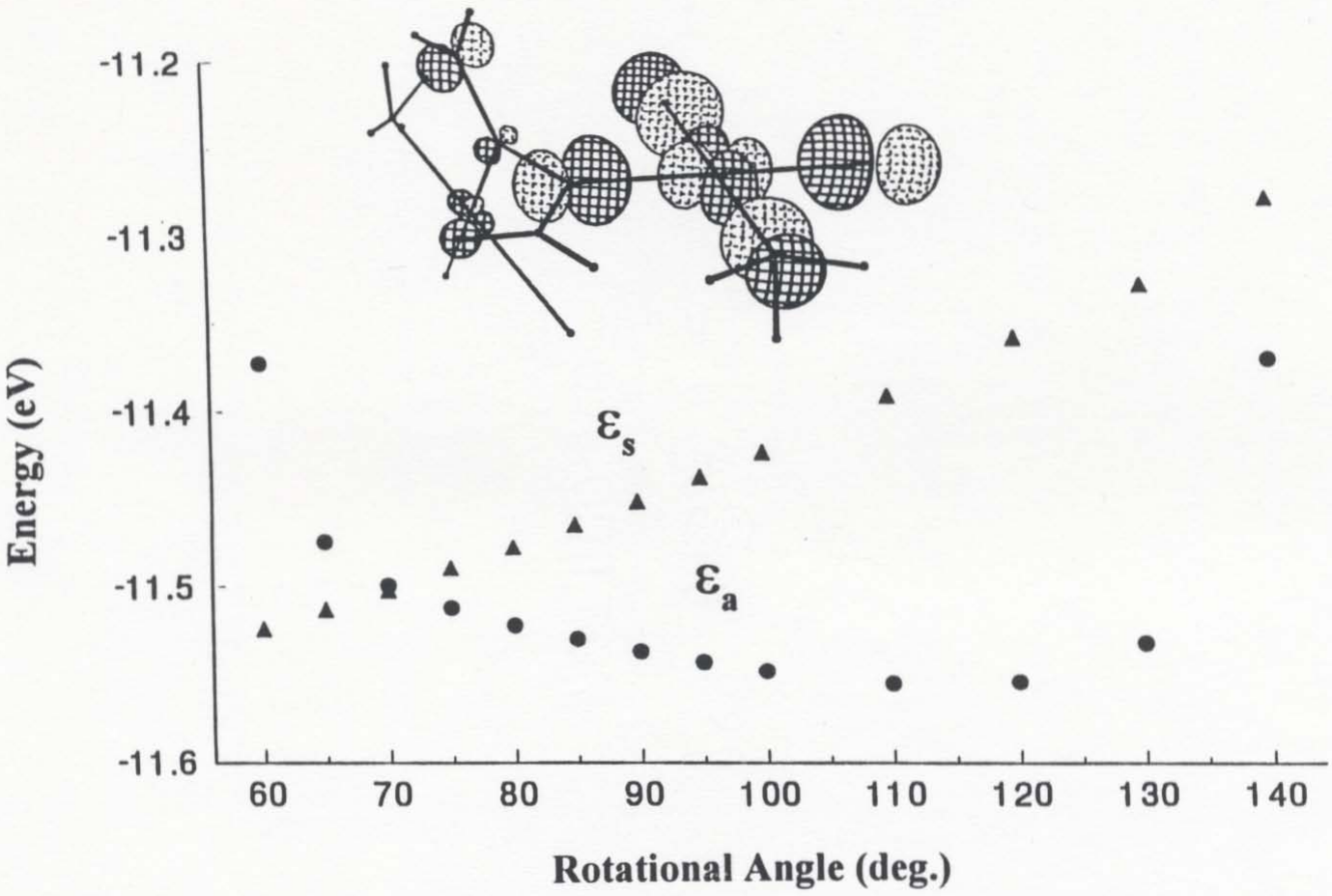

Figure 2-30. Plot of orbital energies (ε_s , ε_a) against the magnetic plane rotational angle for the chloride model.

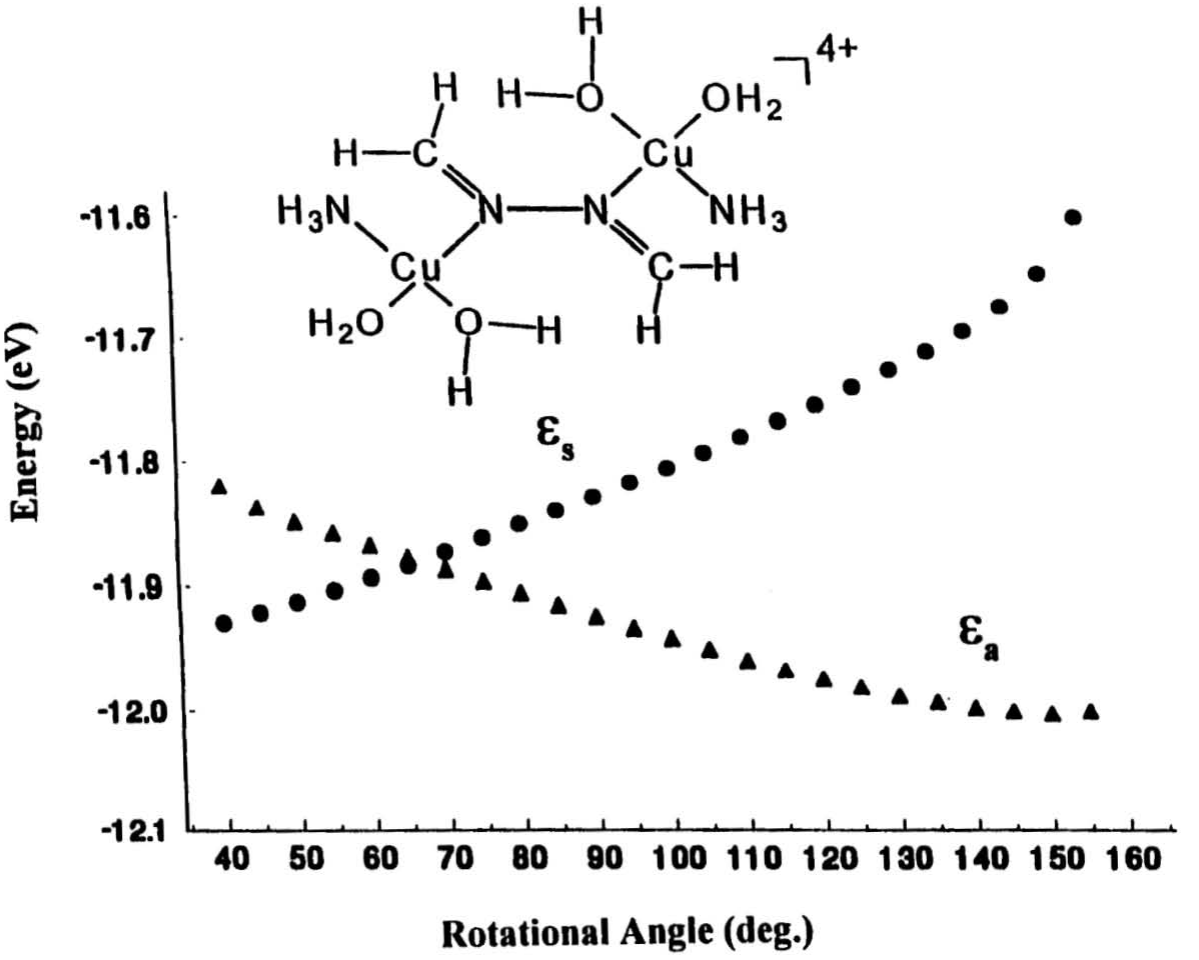

Figure 2-31. Plot of orbital energies (ε_s, ε_a) against the magnetic plane rotational angle for the H_2O model.

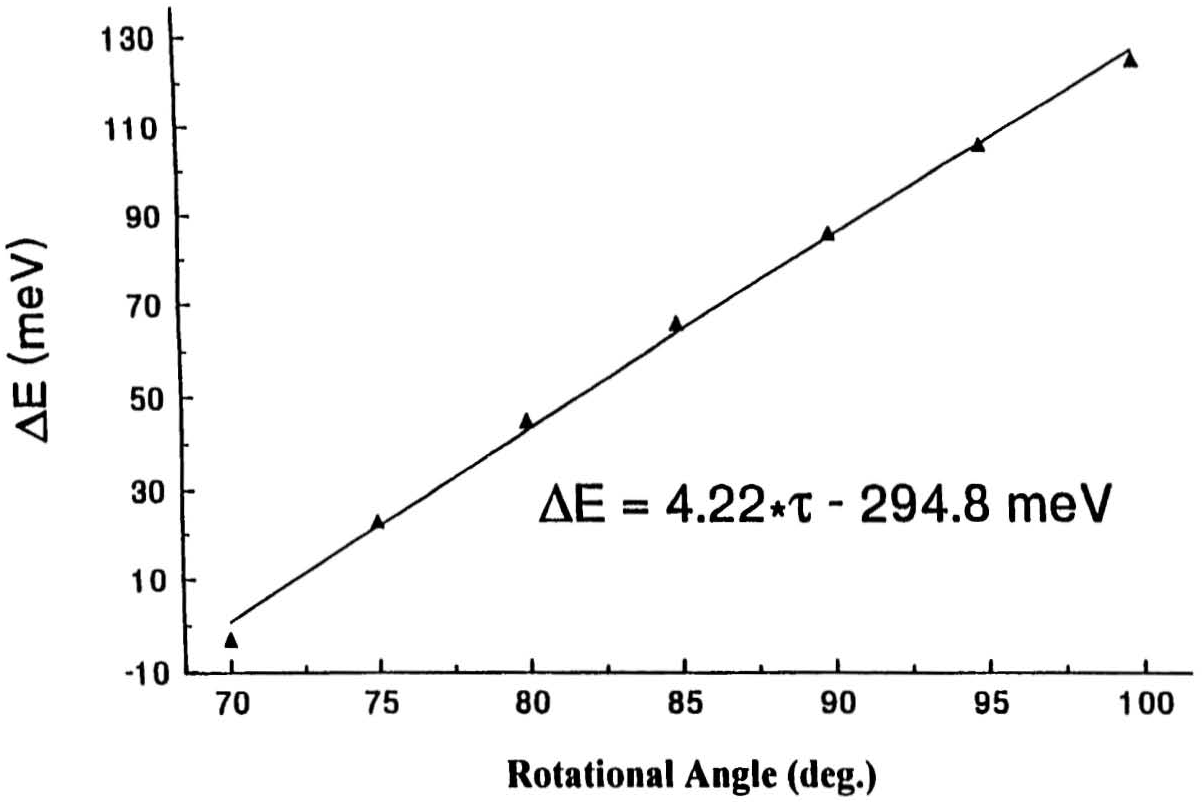

Figure 2-32. Plot of energy difference ($\varepsilon_s - \varepsilon_a$) for the chloride model.

Averaged bond distances have been used from existing and related structures (e.g. C-N 2.00 Å, Cu-Cl 2.25 Å, Cu-Br 2.40 Å, Cu-O 1.95 Å, N-N 1.43 Å, C=N 1.30 Å), and the only molecular geometrical change involves rotation of each copper plane, in conjunction with the CH_2 group, as a fixed unit, around the N-N bond. The energies of the appropriate SOMOs in the triplet state (ε_s and ε_a) are plotted as a function of magnetic plane dihedral angle γ (dihedral angle between the copper planes) in **Figure 2-30** for the neutral chloro model complex. The crossover of the symmetric and antisymmetric molecular orbital energies occurs at 70° for the chloro-model (**Figure 2-30**). This is the point at which the J_{AF} term is effectively zero.

A smooth variation in orbital energies occurs between about 65° and 120°, but outside these limits the antisymmetric molecular orbital energy increases rapidly, consistent with steric interactions between the chlorine and CH_2 groups approaching the *trans*-conformation, and intramolecular chlorine bridging interactions approaching the *cis*-conformation. **Figure 2-30** also illustrates the symmetric molecular orbital for the chloro-model complex with a magnetic plane dihedral angle of 70°. Replacement of the terminal chlorine ligands by bromines creates a similar energy profile with an energy crossover at 70° also, indicating no significant effect on changing the halogen. The model aquo-complex shows a smooth variation in symmetric and antisymmetric molecular orbital energies in the magnetic plane dihedral angle range 40° to 140°, due mainly to the reduced steric constraints approaching the **Type AB** conformation. The energy crossover occurs at 65° (**Figure 2-31**).

A comparison of the exchange situation for **1** and **4** with the model study provides a satisfying rationale for the dramatically different magnetic properties of these two compounds. The positions of the coordination planes in these two complexes are fixed with respect to the two nitrogen donors, as a result of the formation of the two five-membered chelate rings. The net effect is that the copper magnetic planes simply rotate about the N-N bond. This is modelled by fixing the relative positions of the NH_3, and the $N{=}CH_2$ groups, as the metal plane rotates. For **1** the magnetic plane rotational angle, based on the five membered chelate ring , is 77.1° ($\varepsilon_s > \varepsilon_a$; ΔE = 29 meV) with the antisymmetric molecular orbital lower in energy. A plot of ε_s - ε_a for the chloro-model complex is illustrated in **Figure 2-32**, and shows a good straight line relationship in the range 70-100° ($\Delta E = 4.22*\gamma - 294.8$ meV). For a magnetic plane dihedral angle (γ) of 77.1°, the value of ΔE calculated from this line is 30.6 meV, in very close agreement with the value calculated for **1**. This small difference in energy, in the same relative position in the energy profile (i.e. $\varepsilon_s > \varepsilon_a$), clearly indicates that the J_{AF} term for **1** is very small, giving a very reasonable explanation as to why this compound is ferromagnetic.

For **4** the situation is quite different. The calculated energy difference between the symmetric and antisymmetric triplet state molecular orbitals is 153 meV for magnetic plane dihedral angle of 100.2°, while for the model system a linear regression of E_s - E_a as a function of magnetic plane dihedral angle in the range 65-120° (from **Figure 2-31**, $\Delta E = 4.11*\gamma - 275.6$ meV) gives a ΔE value of 137 meV (100.2°), in close agreement. This relatively large energy difference for **4** leads to a large value for J_{AF} , which clearly

dominates the overall exchange situation, leading to net antiferromagnetic coupling. It is very significant that the tetranuclear complex $[Cu(OPA)]_4(NO_3)_4.8H_2O$ has an effective magnetic plane dihedral angle of $\approx$ 90°, and exhibits no coupling. A similar result was found for compound **9** with a magnetic plane rotational angle of 85.2° and ΔE = 98 meV. Clearly J_{AF} and J_F for these two systems are approximately the same.

Optimal alignment of the nitrogen *p* orbitals, and the metal magnetic orbitals, might reasonably be expected at large fold angles, approaching molecular planarity. Compound **12** (as well as compound **14** and **15**) is almost flat and exhibits much stronger antiferromagnetic coupling than observed for **1**, **3** and **4**. This is also consistent with the large energy difference between the triplet state molecular orbitals (453 meV) calculated for this complex. However the possibility of a longer, four-bond secondary exchange route (Cu(1)-N(3)-C(13)-N(4)-Cu(2)) must also be considered in this case. Complex $[Cu_2(HL)Cl_3(H_2O)].1.5H_2O$ [88] has a comparable exchange integral ($-2J$ = 213.3 cm^{-1}), and a similar additional four-bond potential exchange route.

The exchange process must be dominated by σ interactions, because of the hybridisation situation at the diazine nitrogens, and also the extent of exchange will, of necessity, be dependent upon the extent of overlap of the appropriate diazine nitrogen *p* orbitals. The free ligand HOMO is a σ bonding molecular orbital with a comparable energy to the metal *d* orbitals, and involves diazine nitrogen *p* orbital components which point along the C=N bonds. Interaction of the copper d_{xy} type orbitals with these two *p* orbitals leads to the formation of the antisymmetric and symmetric triplet state molecular orbitals,

in which the *p* orbitals align themselves according to the relative orientation of the copper *d* orbitals planes. The extent of overlap between the *p* orbitals along the single N-N bond is therefore dependent upon the dihedral angle between the magnetic copper planes, and so at some angle effective *p* orbital orthogonality is achieved. For the model complexes these angles fall in a narrow range (65-75°), less than 90°, which is reasonable based on the trigonal nitrogen atom geometry. Complexes **1, 3** and **16** have fold angles (77.1°, 75.0° and 77.1° respectively) very close to this situation , whereas for complexes **12, 14** and **15** the much larger twist leads to more effective *p* orbital overlap.

2.4 Conclusion

A spin exchange situation in a dicopper(II) system bridged only by a single N-N bond, in which the exchange mechanism is dominated by σ interaction, was investigated as a function of twist of the copper magnetic planes (dihedral angle) about this bond. At an acute angle approaching orthogonality between the nitrogen p orbitals, ferromagnetic coupling was observed, while at much larger angles significant overlap between the nitrogen p orbitals was seen to lead to net antiferromagnetic coupling. A linear relationship is found between the dihedral angle and the exchange integral over a 105° range. This alignment is controlled mostly by the co-ligands bound to the copper centers, which exert primarily steric effects resulting in rotation of the copper magnetic planes about the N-N bond. Molecular orbital calculations on comparable models successfully reproduced this situation and indicated that, with appropriately chosen co-ligands, which can systematically

influence the molecular twist, the specific synthesis of ferromagnetic dinuclear complexes involving simple N-N bridging ligands is possible.

CHAPTER 3 Dinuclear and Tetranuclear Copper(II) Complexes Containing Two Diazine Ligands

3.1 Introduction

In the last Chapter, seventeen complexes were prepared and characterized. All of these complexes are dinuclear and contain only one diazine ligand. However, as reviewed in Chapter 1, O'Connor et al. reacted PMK with copper(II) nitrate and got a mononuclear complex which was characterized by X-ray crystallography [79]. Stratton et al. reported a copper chloride a mononuclear complex with PAA [73]. Thompson et al. gave another example of mononuclear copper(II) complex of IAMM [80]. All these open-chain diazine ligands are symmetric and coordinated with copper(II) in a *cis-trans* (**Type C**) conformation. However an asymmetric open-chain diazine ligand, HOPA, forms a cyclic tetranuclear copper(II) complex when it reacts with copper(II) nitrate in a 1:1 ratio [98]. It is quite clear that the coordination modes of such ligands to copper(II) are largely dependent on what the R, R', X and X' groups are (see **Figure 1-14**). Therefore, it is quite possible to obtain dinuclear copper(II) complexes containing two open-chain diazine ligands. Even though many dicopper complexes bridged by two diazine linkages in fused aromatic rings have been documented, to our knowledge, there are no reports of any structurally characterized dicopper complexes bridged by two open-chain N-N diazine units. This chapter presents a series of this type of dinuclear copper(II) complex containing two symmetric or asymmetric open-chain diazine ligands (compound **18**, **19**, **20**). This chapter also describes a dinuclear copper(II) complex which contains one open-chain

diazine ligand (PAHAP) and one aromatic heterocyclic diazine ligand DPPN (**21**). In addition, a unique tetranuclear copper(II) complex containing N-N single bond bridges and two kinds of μ_2-1,1-N_3^- bridges (**22**) will be described.

Scheme 3-1

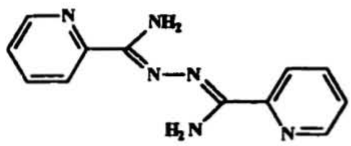

(PAHAP)

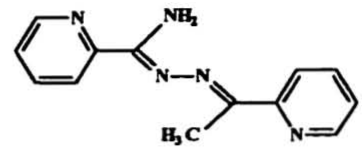

(PMHAP)

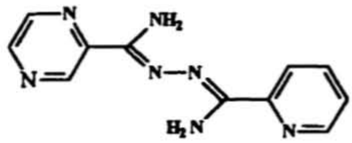

(PYPZ)

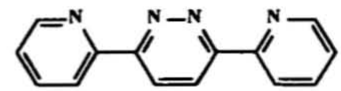

(DPPN)

3.2 Experimental

3.2.1 Material

Commercially available solvents and chemicals were used without further purification.

3.2.2 Measurements

Analysis, spectroscopic and physical measurements (see Chapter 1)

3.2.3 Synthesis of the ligands

PAHAP, PYPZ and PMHAP were prepared by procedures described in Chapter 2. The preparation of DPPN and related information can be found in references [128-133].

3.2.4 Synthesis of the complexes

$[Cu_2(PAHAP)_2(NO_3)(H_2O)_2](NO_3)_3.H_2O$ (**18**)

Method A: 0.24 g (1.0 mmol) PAHAP was added to a solution of complex $[Cu_2(PAHAP)(H_2O)_6](NO_3)_4$ (**4**) (0.72 g, 1.0 mmol dissolved in 20 mL deionized water), forming a clear deep green solution after a few minutes. The solution was filtered and allowed to stand at room temperature for a few days. Deep green crystals, suitable for structure analysis formed which were filtered off and dried in air (Yield, 85 %). Anal. calcd. for $[Cu_2(C_{12}H_{12}N_6)_2(NO_3)(H_2O)_2](NO_3)_3.H_2O$: C, 31.69; H, 3.32; N, 24.64. Found: C, 31.56; H, 3.34; N, 24.50.

Method B: This complex was also synthesized in identical yield by mixing equimolar amounts (2.0 mmol, 0.48 g) of PAHAP and copper(II) nitrate (2.0 mmol, 0.46 g) in 20 mL deionized water.

$[Cu_2(PMHAP)_2(NO_3)_2](NO_3)_2.3H_2O$ (**19**)

This compound was prepared as green crystals in a similar manner (method A or B) to compound **18** in identical yield, using PMHAP. Anal. calcd. for $[Cu_2(C_{13}H_{13}N_5)_2(NO_3)_2](NO_3)_4.3H_2O$: C, 34.75; H, 3.48; N, 21.82. Found: C, 34.82; H, 3.46; N, 21.94.

$[Cu_2(PYPZ)_2(H_2O)_2](NO_3)_4.H_2O$ (**20**)

Compound **20** was prepared as deep green, rod-like crystals in a procedure similar to that for compound **18** in comparable yield, except for the use of PYPZ instead of PAHAP. Anal. calcd. for $[Cu_2(C_{11}H_{11}N_7)_2(H_2O)_2](NO_3)_4.H_2O$: C, 29.00; H, 3.10; N, 27.65. Found: C, 29.04; H, 2.92; N, 27.81.

$[Cu_2(PAHAP)(DPPN)(H_2O)(NO_3)](NO_3)_3$ **(21)**

0.243 g (1.00 mmol) DPPN (3,6-bis(2'-pyridyl)-pyridazine) was added to a solution of the complex $[Cu_2(PAHAP)(H_2O)_6](NO_3)_4$ **(4)** (0.72 g, 1.0 mmol dissolved in 20 mL deionized water) forming a clear green solution immediately. The solution was filtered and allowed to stand at room temperature for a few days. Green crystals, suitable for structure analysis, formed (Yield, 85 %). Anal. calcd. for $[Cu_2(C_{12}H_{12}N_6)(C_{14}H_{10}N_4)(NO_3)(H_2O)](NO_3)_3$: C, 35.99; H, 2.79; N, 22.60. Found: C, 35.80; H, 2.90; N, 22.52.

$[Cu_2(PAHAP)(N_3)_2(MeOH)_2]_2.(NO_3)_4.2H_2O$ **(22)**

A hot solution of PAHAP (0.24 g, 1.0 mmol) in dichloromethane (10 mL) was added to a hot solution of copper(II) nitrate (0.46 g, 2.0 mmol) in methanol (15 ml). A hot methanolic solution (10 mL) of 0.13 g (2.0 mmol) NaN_3 was added dropwise to the solution above and a dark green solution formed. This dark green solution was filtered and allowed to stand at room temperature for 1-2 days, dark green crystals, suitable for structural analysis, formed (Yield 73%). Anal. calcd. for $[Cu_2(C_{12}H_{12}N_6)(N_3)_2(CH_4O)_2]_2(NO_3)_4.2H_2O$: C, 24.96; H, 2.90; N, 31.35. Found: C, 24.95; H, 2.18; N, 31.60.

3.2.5 Crystallographic data collection and refinement of the structures

Crystal data collection and structure refinement for **18,19, 21, 22** were carried out in a similar manner to that for **12**. Abbreviated crystal data for all of these complexes are given **Table 3-1**. Note in **Table 3-1**: * = Siemens Smart data.

$$\mathbf{R} = \Sigma||F_o| - |F_c||/\Sigma|F_o|,\ \mathbf{R_w} = [(\Sigma(|F_o| - |F_c|)^2/\Sigma wF_o^2)]^{1/2}$$

$$\mathbf{R1} = \Sigma||F_o| - |F_c||/\Sigma|F_o|,\ \mathbf{wR_2} = [\Sigma[w(|F_o|^2 - |F_c|^2)^2/\Sigma[w(|F_o|^2)^2]]^{1/2}$$

Table 3-1. Summary of crystallographic data for complexes **18, 19, 21and 22.**

Compound	18*	19*
chemical formula	$C_{12}H_{15}CuN_8O_6$	$C_{13}H_{13.75}CuN_7O_7$
formula wt.	430.86	443.60
space group	$P2_1c$	Cc
a (Å)	11.281(2)	20.938(4)
b(Å)	14.036(3)	14.887(3)
c(Å)	22.853(5)	14.372(3)
α(deg)	90	90
β(deg)	102.92(3)	127.43(3)
γ(deg)	90	90
V ($Å^3$)	3527.1(12)	3557.4(12)
$\rho_{calcd}(gcm^{-3})$	1.623	1.657
Z	8	8
$\mu(mm^{-1})$	1.288	1.282
λ (Å)	0.71073	0.71073
T, K	293(2)	293(2)
R1(R)	0.1029	0.0299
wR2(R_w)	0.2314	0.0374

Table 3-1. (contd.) Summary of crystallographic data for complexes **18, 19, 21and 22.**

Compound	21*	22*
chemical formula	$C_{26}H_{25}Cu_2N_{14}O_{13.5}$	$C_{15}H_{24}Cu_2N_{14}O_9$
formula wt.	876.68	671.56
space group	PI	PI
a (Å)	9.709(1)	8.4920
b(Å)	17.688(2)	11.5573
c(Å)	19.155(2)	15.4597
α(deg)	91.691(4)	70
β(deg)	95.085(3)	83.200
γ(deg)	97.501(3)	69.205
V (Å^3)	3245.7(9)	1337.10
ρ_{calcd}(gcm^{-3})	1.792	1.683
Z	4	2
μ(cm^{-1})	1.402	1.66
λ (Å)	0.71073	0.71073
T, K	150(2)	150(2)
R1(R)	0.0375	0.0369
wR2(R_w)	0.0794	0.1006

3.3 Results and discussion

3.3.1 Structures

$[Cu_2(PAHAP)_2(NO_3)(H_2O)_2](NO_3)_3.H_2O$ (**18**)

The structure of **18** and the expanded view of the coordination core are depicted in **Figure 3-1** and **Figure 3-2** respectively, and relevant bond distances and angles are listed in **Table 3-2**. The two distorted octahedral copper(II) ions are bridged by two ligands in a spiral-like arrangement with diazine nitrogens acting as the bridging groups in the equatorial planes and one bidentate nitrate bridging in axial positions. Each ligand provides one pyridine ring coordinating in the equatorial plane of one copper center (N(6) for Cu(1); N(7) for Cu(2)) and another pyridine ring coordinating in the axial position of another copper center (N(11) for Cu(1); N(1) for Cu(2)). A water molecule is coordinated to each copper(II) center completing the equatorial coordination (O(10) for Cu(1); O(11) for Cu(2)). The two copper equatorial planes are twisted by 63.47° (the angle between the least-squares planes of Cu(1)-N(4)-C(7)-C(8)-N(6) and Cu(2)-N(9)-C(18)-C(17) -N(7)) about the two diazine bond vectors (N(4)-N(3) and N(10)-N(9)) and folded 130.24° by the axially bridging nitrate *via* O(7) and O(8). The Cu(1)-Cu(2) separation is 3.863(5) Å.

Within each ligand, bond distances in the NH_2-C=N framework are very similar to those of the free ligand, indicating single bond character in the N-N diazine bonds (N(3)-N(4) 1.423(8) Å, N(10)-N(9) 1.409(8) Å) and in C-NH_2 bonds (N(2)-C(6) 1.323(10) Å, N(5)-C(7) 1.327(9) Å, N(8)-C(18) 1.315(9) Å, C(19)-N(12) 1.343(10) Å),

Table 3-2. Interatomic distances (Å) and angles (Deg.) relevant to the copper coordination spheres and the ligand in $[Cu_2(PAHAP)_2(NO_3)(H_2O)_2](NO_3)_3.H_2O$(**18**).

Cu(1)-N(6)	1.995(6)	Cu(2)-N(3)	1.987(6)
Cu(1)-N(10)	2.003(6)	Cu(2)-N(7)	1.998(6)
Cu(1)-N(4)	2.016(6)	Cu(2)-N(9)	2.004(6)
Cu(1)-O(10)	2.076(7)	Cu(2)-O(11)	2.033(5)
Cu(1)-N(11)	2.238(9)	Cu(2)-N(1)	2.221(6)
Cu(1)-O(8)	2.434(6)	Cu(2)-O(7)	2.621(5)
Cu(1)-Cu(2)	3.863(5)		
N(10)-C(19)	1.323(9)	N(10)-N(9)	1.409(8)
N(3)-C(6)	1.303(9)	N(3)-N(4)	1.423(8)
N(4)-C(7)	1.300(9)	N(2)-C(6)	1.323(10)
N(5)-C(7)	1.327(9)	N(8)-C(18)	1.315(9)
N(9)-C(18)	1.314(9)	C(19)-N(12)	1.343(10)
N(6)-Cu(1)-N(10)	167.9(2)	N(6)-Cu(1)-N(4)	80.1(3)
N(10)-Cu(1)-N(4)	89.9(2)	N(6)-Cu(1)-O(10)	93.7(3)
N(10)-Cu(1)-O(10)	95.9(3)	N(4)-Cu(1)-O(10)	173.1(3)
N(6)-Cu(1)-N(11)	112.4(3)	N(10)-Cu(1)-N(11)	76.6(3)
N(4)-Cu(1)-N(11)	104.5(3)	O(10)-Cu(1)-N(11)	80.6(3)

contd.

N(6)-Cu(1)-O(8)	84.1(3)	N(10)-Cu(1)-O(8)	90.8(2)
N(4)-Cu(1)-O(8)	98.9(2)	O(10)-Cu(1)-O(8)	77.3(3)
N(11)-Cu(1)-O(8)	153.2(3)	N(3)-Cu(2)-N(7)	169.5(2)
N(3)-Cu(2)-N(9)	89.7(2)	N(7)-Cu(2)-N(9)	79.8(2)
N(3)-Cu(2)-O(11)	97.1(2)	N(7)-Cu(2)-O(11)	93.3(2)
N(9)-Cu(2)-O(11)	163.3(2)	N(3)-Cu(2)-N(1)	77.7(2)
N(7)-Cu(2)-N(1)	104.0(2)	N(9)-Cu(2)-N(1)	105.7(2)
O(11)-Cu(2)-N(1)	90.6(2)	O(7)-Cu(2)-N(1)	161.53(2)
O(7)-Cu(2)-O(11)	78.13(2)	O(7)-Cu(2)-N(7)	91.37(2)
O(7)-Cu(2)-N(9)	86.82(2)	O(7)-Cu(2)-N(3)	89.05(2)

and largely double bond character in the C=N bonds (N(3)-C(6) 1.303(9) Å, N(4)-C(7) 1.300(9) Å, N(9)-C(18) 1.314(9) Å, N(10)-C(19) 1.323(9) Å). The torsion angles around N-N units in both ligands are very close (C(6)-N(3)-N(4)-C(7), 78.32°; C(18)-N(9)-N(10)-C(19), 73.71°).

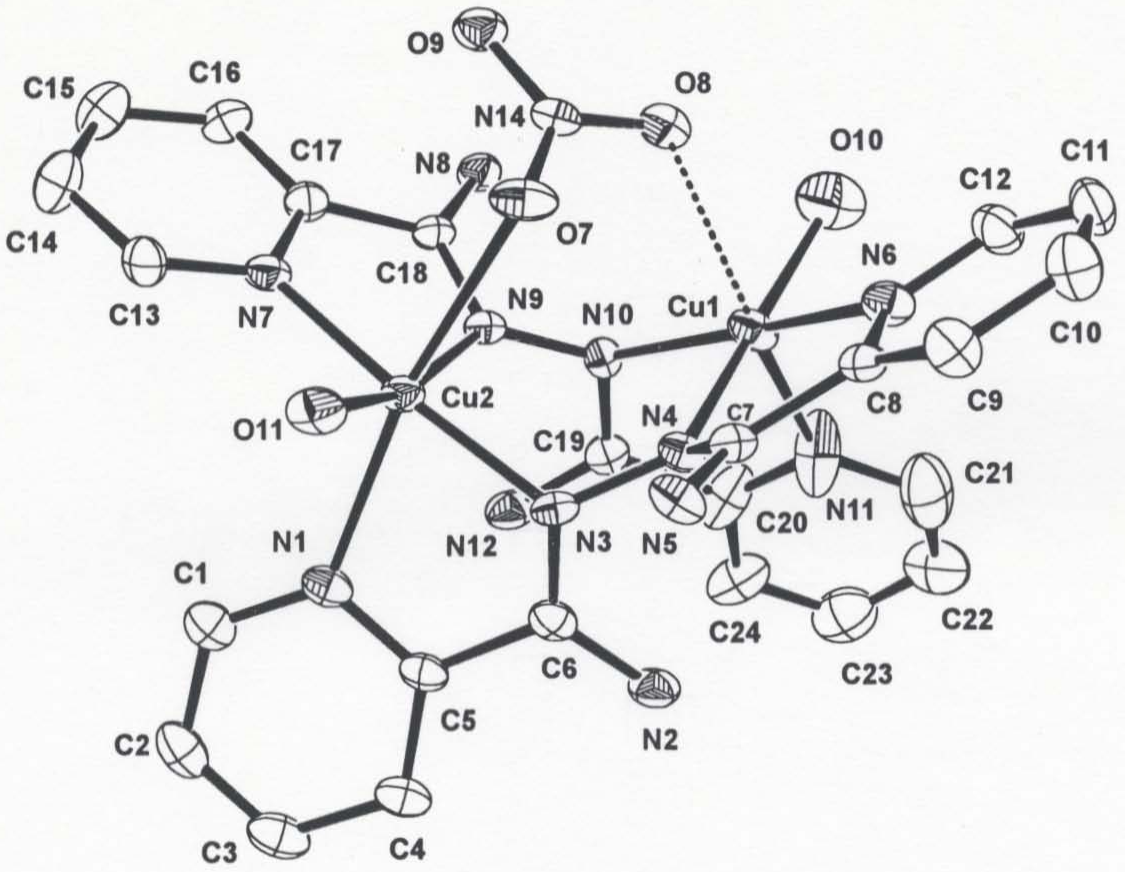

Figure 3-1. Structural representation of $Cu_2(PAHAP)_2(NO_3)(H_2O)_2](NO_3)_3.H_2O$ (**18**) with hydrogen atoms omitted (40% probability thermal ellipsoids).

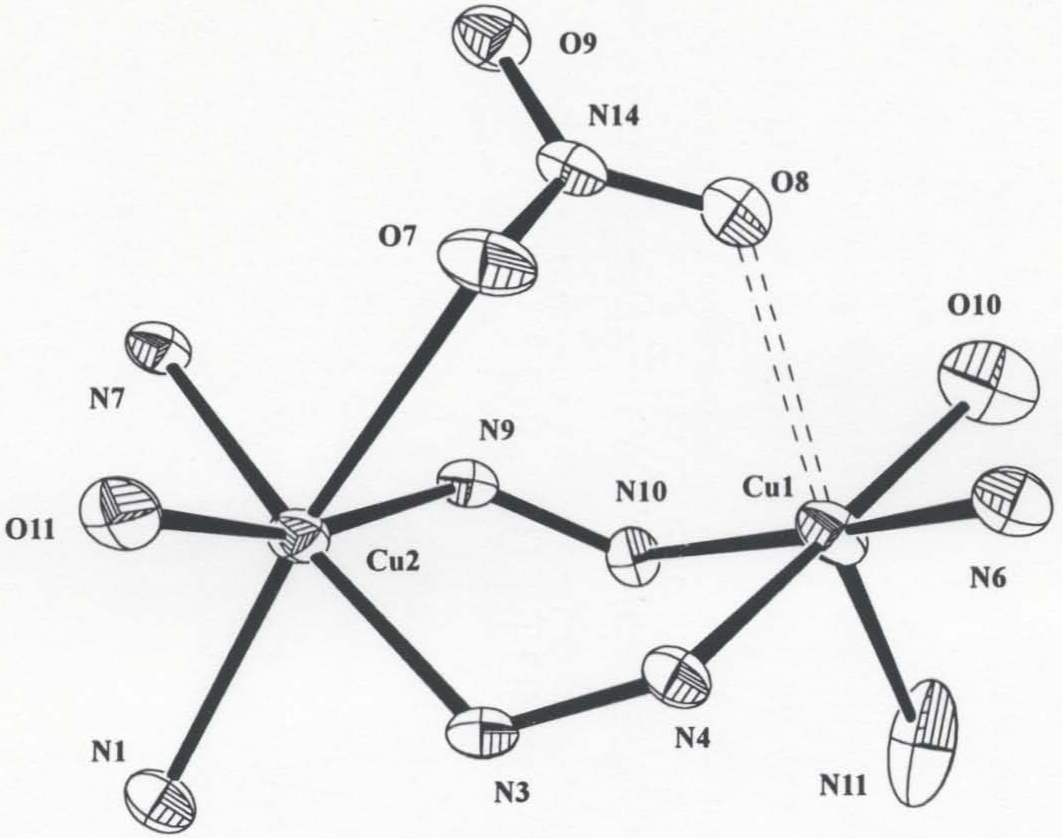

Figure 3-2. Expanded view of the coordination cores in **18** showing the two copper centers twisted by N-N bonds and folded by nitrate bridge.

$[Cu_2(PMHAP)_2(NO_3)_2](NO_3)_2.3H_2O$ **(19)**

The structure of **19** is depicted in **Figure 3-3**, and relevant bond distances and angles are listed in **Table 3-3**. **Figure 3-4** illustrates the expanded view of the coordination cores in **19** with labeling of the relevant bond distances. The dicopper(II) cation consists of two distorted square pyramidal copper(II) centers (the Addison distortion index $\tau = 0.269$ for Cu(1) and 0.319 for Cu(2) [81]) each with two pyridine nitrogens (N(5), N(6) for Cu(1); N((1), N(10) for Cu(2)), one diazine nitrogen (N(3) for Cu(1) and N(8) for Cu(2)) and one nitrate oxygen (O(1) for Cu(1) and O(4) for Cu(2)) in the equatorial plane, and another diazine nitrogen (N(7) for Cu(1) and N(2) for Cu(2)) in the axial position. In each diazine unit, one nitrogen atom (N(3) or N(8)) is in the equatorial plane and the another one (N(2) or N(7)) is in the axial position of the copper(II) polyhedron. Therefore two ligands orthogonally bridge two copper(II) centers in a spiral-like manner, which is the first example of open-chain diazine ligands adopting such a coordination mode. The least-squares planes Cu(2)-N(10)-C(22)-C(21)-N(8) and Cu(1)-N(6)-C(18)-C(19)-N(7) are twisted of 79.76°, and the least-squares plane Cu(2)-N(1)-C(5)-C(6)-N(2) and Cu(1)-N(3)-C(8)-C(9)-N(5) are twisted of 82.43°.

Table 3-3. Interatomic distances (Å) and angles (Deg.) relevant to the copper coordination spheres and the ligand in $[Cu_2(PMHAP)_2(NO_3)_2](NO_3)_2 .3H_2O$ **(19)**.

Cu(1)-N(3)	1.965(3)	Cu(1)-N(6)	1.988(3)
Cu(1)-N(5)	2.022(3)	Cu(1)-O(1)	2.041(3)
Cu(1)-N(7)	2.198(3)	Cu(2)-N(8)	1.967(3)
Cu(2)-N(1)	1.996(3)	Cu(2)-N(10)	2.029(3)
Cu(2)-O(4)	2.084(3)	Cu(2)-N(2)	2.158(3)
Cu(1)-Cu(2)	3.930(2)		
N(3)-Cu(1)-N(6)	168.72(13)	N(3)-Cu(1)-N(5)	80.75(11)
N(6)-Cu(1)-N(5)	104.69(12)	N(3)-Cu(1)-O(1)	89.23(11)
N(6)-Cu(1)-O(1)	89.94(11)	N(5)-Cu(1)-O(1)	152.60(11)
N(3)-Cu(1)-N(7)	92.06(12)	N(6)-Cu(1)-N(7)	77.19(12)
N(5)-Cu(1)-N(7)	102.47(11)	O(1)-Cu(1)-N(7)	103.33(10)
N(8)-Cu(2)-N(1)	171.09(13)	N(8)-Cu(2)-N(10)	80.33(11)
N(1)-Cu(2)-N(10)	103.54(11)	N(8)-Cu(2)-O(4)	91.50(11)
N(1)-Cu(2)-O(4)	88.60(11)	N(10)-Cu(2)-O(4)	151.93(11)
N(8)-Cu(2)-N(2)	93.54(12)	N(1)-Cu(2)-N(2)	77.67(12)
N(10)-Cu(2)-N(2)	107.39(11)	O(4)-Cu(2)-N(2)	99.85(10)

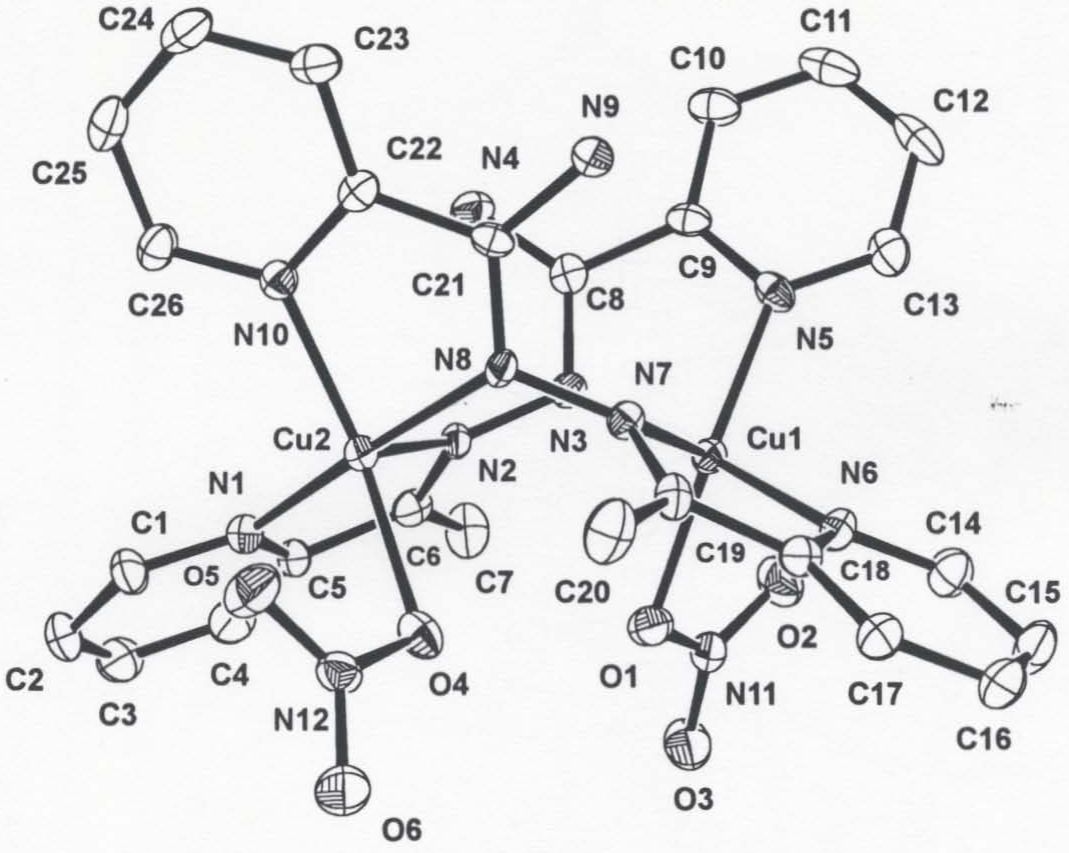

Figure 3-3. Structural representation of $[Cu_2(PMHAP)_2(NO_3)_2](NO_3)_2.3H_2O$ (**19**) with hydrogen atoms omitted (40% probability thermal ellipsoids).

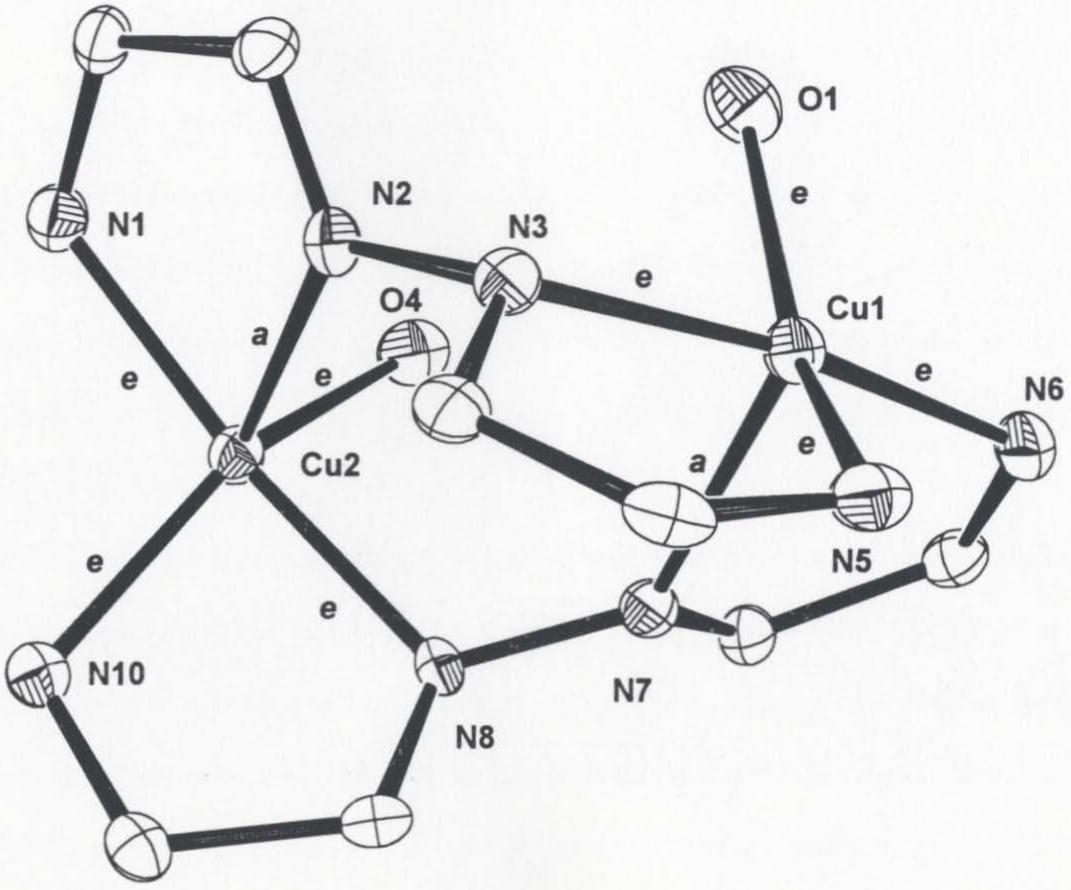

Figure 3-4. Expanded view showing the orthogonality between two copper magnetic planes in **19** *via* N-N single bonds.

$[Cu_2(PAHAP)(DPPN)(H_2O)(NO_3)](NO_3)_3$ **(21)**

Two crystallographically independent, but very similar molecules have been found in **21**. **Figure 3-5** illustrates the structure of one of them and **Figure 3-6** depicts the expanded view of the coordination cores in both molecules. Bond distances and angles relevant to the copper coordination spheres are given in **Table 3-4**. In each molecule, the ligand DPPN adopts a planar structure, as expected, with the same structural features as found in its other complexes [128-133], and the open-chain diazine ligand PAHAP has a twisted conformation as usual.

The coordination geometries for all copper(II) centers are in between a square pyramid and a trigonal bipyramid, and using the distortion index established by Addison [81] ($\tau = (\beta - \alpha)/60$) the values in the range 0.219-0.421 suggest that a distorted square pyramid is the most appropriate stereochemical description for all copper centers with short equatorial contacts to an N_4 in-plane donor set for Cu(1) and Cu(3), and N_3O for Cu(2) and Cu(4). The weak axial coordination positions are occupied by nitrate anions for Cu(1) (O(24)) and Cu(3) (O(15)), whereas diazine nitrogens from DPPN are bonded axially to Cu(2) (N(3)) and Cu(4) (N(13)). Therefore, within each molecule two copper(II) centers are bridged by an open-chain diazine unit in the equatorial plane, and another aromatic diazine unit in an orthogonal manner, to form a boat conformation (boat 1: Cu(1)-N(2)-N(3)-Cu(2)-N(6)-N(7); boat 2: Cu(3)-N(12)-N(13)-Cu(4)-N(16)-N(17)).

Table 3-4. Interatomic distances (Å) and angles (Deg.) relevant to the copper coordination spheres and the ligand in $[Cu_2(PAHAP)(DPPN)(H_2O)(NO_3)](NO_3)_3$ (**21**).

Cu(1)-O(24)	2.536(2)	Cu(3)-O(15)	2.629(2)
Cu(1)-N(1)	1.990(2)	Cu(3)-N(11)	1.977(2)
Cu(1)-N(2)	2.048(2)	Cu(3)-N(12)	2.064(2)
Cu(1)-N(7)	1.935(2)	Cu(3)-N(17)	1.923(2)
Cu(1)-N(8)	2.027(2)	Cu(3)-N(18)	2.024(2)
Cu(2)-O(1)	2.032(2)	Cu(4)-O(2)	2.055(2)
Cu(2)-N(3)	2.228(2)	Cu(4)-N(13)	2.194(2)
Cu(2)-N(4)	1.988(2)	Cu(4)-N(14)	1.980(2)
Cu(2)-N(5)	2.018(2)	Cu(4)-N(15)	2.022(2)
Cu(2)-N(6)	1.940(2)	Cu(4)-N(16)	1.935(2)
Cu(1)-Cu(2)	3.932(2)	Cu(3)-Cu(4)	3.936(2)
N(2)-N(3)	1.334(3)	N(12)-N(13)	1.334(3)
N(6)-N(7)	1.405(3)	N(6)-C(20)	1.311(3)
N(7)-C(21)	1.317(3)	N(8)-C(22)	1.358(3)
N(9)-C(20)	1.322(4)	N(16)-N(17)	1.410(3)

contd.

N(16)-C(46)	1.316(3)	N(17)-C(47)	1.310(3)
N(19)-C(46)	1.321(3)	N(20)-C(47)	1.320(3)
O(24)-Cu(1)-N(1)	78.85(9)	O(24)-Cu(1)-N(2)	118.11(9)
O(24)-Cu(1)-N(7)	91.23(9)	O(24)-Cu(1)-N(8)	98.11(9)
N(1)-Cu(1)-N(2)	80.68(9)	N(1)-Cu(1)-N(7)	168.94(9)
N(1)-Cu(1)-N(8)	105.01(9)	N(2)-Cu(1)-N(7)	100.04(9)
N(2)-Cu(1)-N(8)	143.66(9)	N(7)-Cu(1)-N(8)	81.04(9)
O(1)-Cu(2)-N(3)	92.46(9)	O(1)-Cu(2)-N(4)	87.46(10)
O(1)-Cu(2)-N(5)	154.03(9)	O(1)-Cu(2)-N(6)	96.64(10)
N(3)-Cu(2)-N(4)	78.67(9)	N(3)-Cu(2)-N(5)	113.39(8)
N(3)-Cu(2)-N(6)	92.31(9)	N(4)-Cu(2)-N(5)	99.53(9)
N(4)-Cu(2)-N(6)	170.28(9)	N(5)-Cu(2)-N(6)	80.60(9)
O(15)-Cu(3)-N(11)	92.79(9)	O(15)-Cu(3)-N(12)	77.83(9)
O(15)-Cu(3)-N(17)	101.70(9)	O(15)-Cu(3)-N(18)	74.82(9)
N(11)-Cu(3)-N(12)	80.66(9)	N(11)-Cu(3)-N(17)	165.33(9)
N(11)-Cu(3)-N(18)	105.27(9)	N(12)-Cu(3)-N(17)	100.03(9)
N(12)-Cu(3)-N(18)	152.22(9)	N(17)-Cu(3)-N(18)	81.04(9)
O(2)-Cu(4)-N(13)	92.53(9)	O(2)-Cu(4)-N(14)	92.92(9)

contd.

O(2)-Cu(4)-N(15)	150.19(9)	O(2)-Cu(4)-N(16)	92.00(9)
N(13)-Cu(4)-N(14)	79.13(8)	N(13)-Cu(4)-N(15)	116.67(8)
N(13)-Cu(4)-N(16)	93.81(8)	N(14)-Cu(4)-N(15)	98.14(9)
N(14)-Cu(4)-N(16)	171.56(9)	N(15)-Cu(4)-N(16)	80.79(9)

To our knowledge, this is the first orthogonal bridging mode reported for an aromatic diazine in a dicopper(II) complex. Concerning the boat conformations, the only difference between the two molecules rests with the fact that two oxygens (water O(1) and nitrate O(24)) are located in a *trans* position in boat 1, while another two oxygens (water O(15) and nitrate O(2)) are located in a *cis*-position in boat 2. This results in the dihedral angle between the least squares planes Cu(1)-N(7)-C(21)-C(22)-N(8) and Cu(2)-N(5)-C(19)-C(20)-N(6) (85.91°) being quite different from that between the least squares planes Cu(3)-N(17)-C(47)-C(48)-N(18) and Cu(4)-N(15)-C(45)-C(46)-N(16) (78.79°). The torsion angle around the N(6)-N(7) bond vector in C(20)-N(6)-N(7)-C(21) is 104.72°, while that around the N(16)-N(17) bond vector in C(46)-N(16)-N(17)-C(47) is only 90.60°.

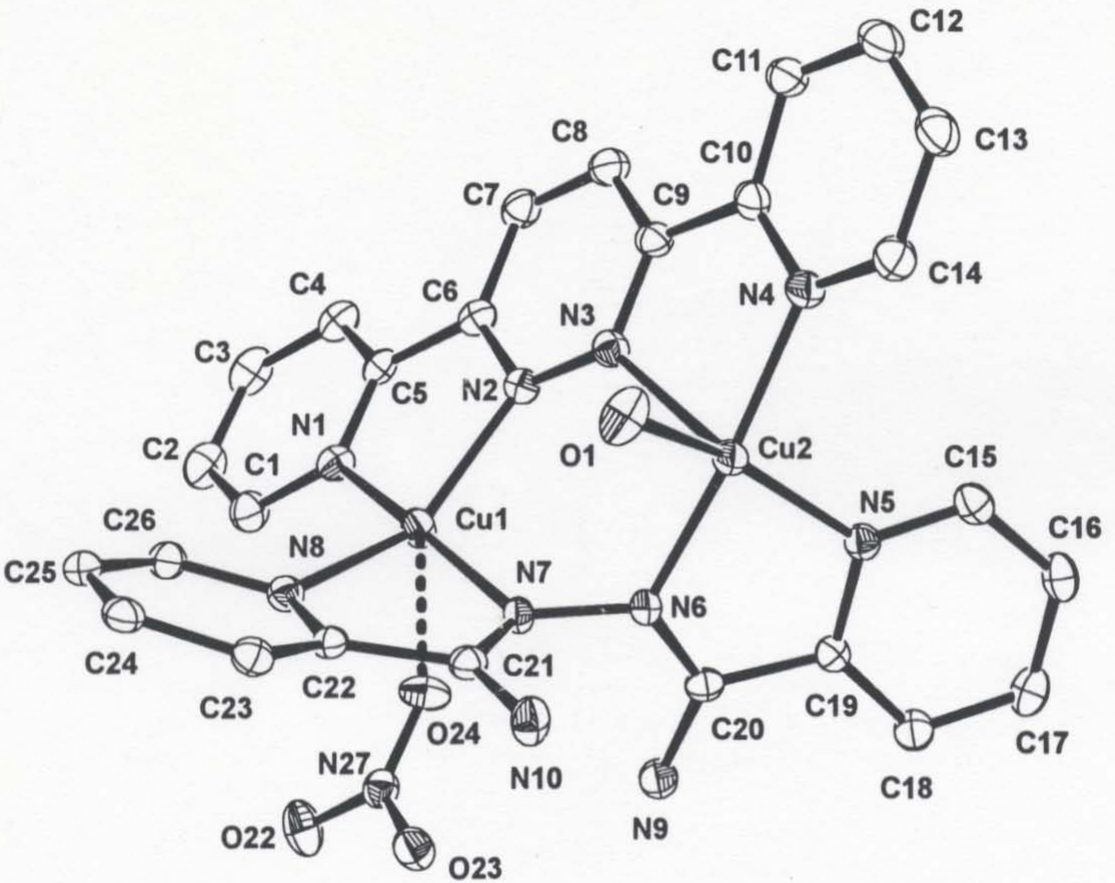

Figure 3-5. Structural representation of one of the two crystallographically independent molecules in $[Cu_2(PAHAP)(DPPN)(NO_3)(H_2O)](NO_3)_3$ (**21**) with hydrogen atoms omitted (40% probability thermal ellipsoids).

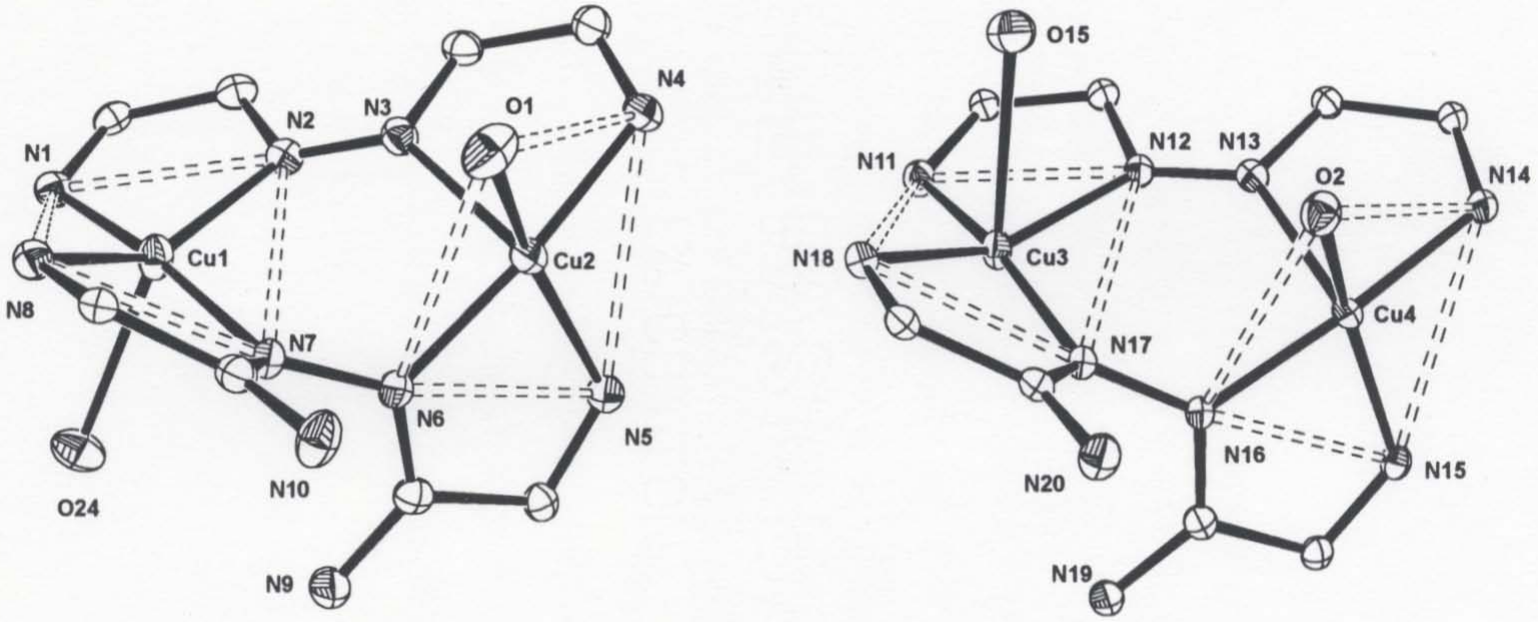

Figure 3-6. Expanded view showing copper coordination conformation difference between two molecules in **21**.

$[Cu_2(PAHAP)(MeOH)_2(N_3)_2]_2.(NO_3)_4.2H_2O$ (22)

The structure of **22** is depicted in **Figure 3-7**, and relevant bond distances and angles are listed in **Table 3-5**. The tetranuclear cation can be described as the combination of two $[Cu_2(PAHAP)(MeOH)_2(N_3)_2]^{2+}$ units bridged orthogonally by two μ_2-1,1-N_3^- anions. In each dinuclear $[Cu_2(PAHAP)(MeOH)_2(N_3)_2]^{2+}$ unit, the copper(II) ion Cu(1) has a distorted square pyramidal coordination environment (τ = 0.589) [81] and is coordinated to two nitrogen atoms (N(1) and N(3)) of the ligand PAHAP. It is also coordinated to another two nitrogen atoms (N(10) and N(7A)) from different μ_2-1,1-N_3^- anions in the basal plane (Cu(1)-N(7A) 1.971(2) Å, Cu(1)-N(3) 1.977(2) Å, Cu(1)-N(1) 2.030(2) Å, Cu(1)-N(10) 2.055(2) Å), and the nitrogen N(7) from another μ_2-1,1-N_3^- in the apical position (Cu(1)-N(7) 2.271(2) Å), while the copper(II) ion, Cu(2) has a typical square pyramidal (τ = 0.124) coordination environment (Cu(2)-N(4) 1.950(2) Å, Cu(2)-N(6) 2.029(2) Å, Cu(2)-N(10) 2.014(2) Å, Cu(2)-O(8) 1.971(2) Å, Cu(2)-O(7) 2.348(2) Å). The two copper(II) centers are bridged by a diazine unit (N(3)-N(4)) and a μ_2-1,1-N_3^- unit at N(10) in their equatorial planes.

The dihedral angle between the least-squares planes Cu(1)-N(1)-C(5)-C(6)-N(3) and Cu(2)-N(4)-C(12)-C(11)-N(6) is quite small (53.86°). This small angle makes it

Table 3-5. Interatomic distances (Å) and angles (Deg.) relevant to the copper coordination spheres and the ligand in $[Cu_2(PAHAP)(N_3)_2(MeOH)_2)]_2 \cdot (NO_3)_4 \cdot 2H_2O$ (**22**).

Cu(1)-N(7)#1	1.971(2)	Cu(1)-N(3)	1.977(2)
Cu(1)-N(1)	2.030(2)	Cu(1)-N(10)	2.055(2)
Cu(1)-N(7)	2.271(2)	Cu(2)-N(4)	1.950(2)
Cu(2)-O(8)	1.971(2)	Cu(2)-N(10)	2.014(2)
Cu(2)-N(6)	2.029(2)	Cu(2)-O(7)	2.348(2)
Cu(1)-Cu(2)	3.497(2)	Cu(1)-Cu(1A)	3.351(2)
N(2)-C(6)	1.327(3)	N(3)-C(6)	1.319(3)
N(3)-N(4)	1.406(2)	N(4)-C(12)	1.313(3)
N(5)-C(12)	1.321(3)	N(10)-N(11)	1.223(3)
N(11)-N(12)	1.135(3)	N(7)-N(8)	1.241(3)
N(8)-N(9)	1.121(5)		

N(7)#1-Cu(1)-N(3)	174.99(8)	N(7)#1-Cu(1)-N(1)	98.75(8)
N(3)-Cu(1)-N(1)	79.98(8)	N(7)#1-Cu(1)-N(10)	97.55(8)
N(3)-Cu(1)-N(10)	86.42(8)	N(1)-Cu(1)-N(10)	139.68(9)
N(7)#1-Cu(1)-N(7)	75.82(8)	N(3)-Cu(1)-N(7)	100.20(8)

contd.

N(1)-Cu(1)-N(7)	113.96(8)	N(10)-Cu(1)-N(7)	105.71(9)
N(4)-Cu(2)-O(8)	171.82(8)	N(4)-Cu(2)-N(10)	88.06(8)
O(8)-Cu(2)-N(10)	99.33(9)	N(4)-Cu(2)-N(6)	79.85(8)
O(8)-Cu(2)-N(6)	92.01(8)	N(10)-Cu(2)-N(6)	157.48(9)
N(4)-Cu(2)-O(7)	91.83(8)	O(8)-Cu(2)-O(7)	90.72(8)
N(10)-Cu(2)-O(7)	97.43(8)	N(6)-Cu(2)-O(7)	101.85(8)
N(7)-N(8)-N(9)	169.7(4)	N(10)-N(11)-N(12)	179.2(4)
Cu(1)-N(10)-Cu(2)	118.48(10)	Cu(1)-N(7)-Cu(1)#1	104.18(8)

possible for the azide (N(10)) to bridge the two copper(II) centers in a μ_2-1,1 fashion, and leads to a relatively short Cu(1)-Cu(2) separation (3.497(2) Å) and a large Cu(1)-N(10)-Cu(2) azide bridge angle (118.48(10)°). However, compared with the Cu-Cu separation found in some dicopper(II) complexes bridged by a μ_2-1,1-N_3^- and an aromatic diazine unit (e.g. pyridazine, phthalazine), the Cu(1)-Cu(2) separation in **22** is still quite large, which is exactly consistent with the large Cu(1)-N(10)-Cu(2) angle.

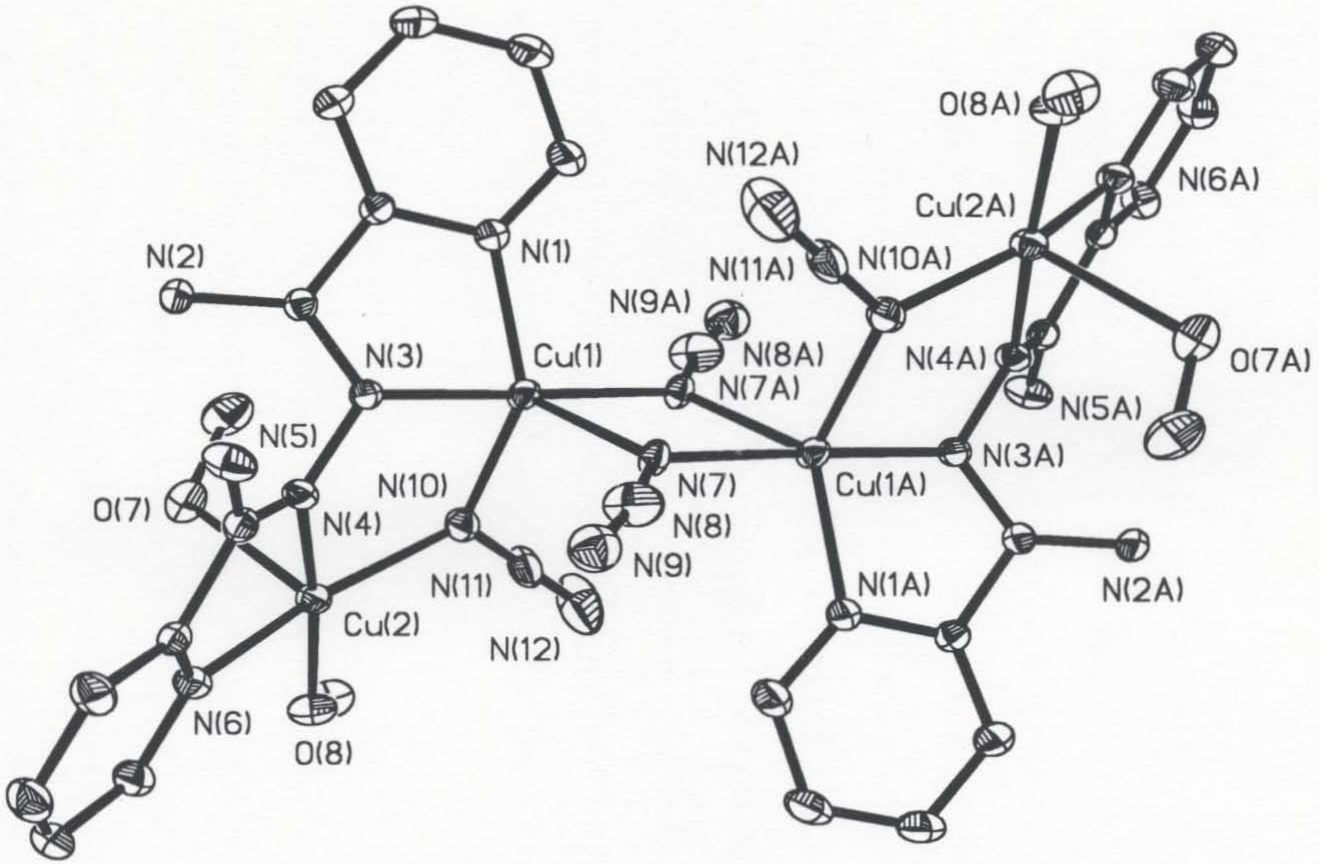

Figure 3-7. Structural representation of $[Cu_2(PAHAP)(N_3)_2(MeOH)_2]_2.(NO_3)_4.2H_2O$ (**22**) with hydrogen atoms omitted (40% probability thermal ellipsoids).

3.3.2 Spectroscopy

The major infrared absorption bands for **18-22** are listed in **Table 3-6**. Complex **18** exhibits two ν_{NH} infrared bands at 3355 and 3165 cm^{-1} associated with the NH_2 groups in PAHAP, and a sharp band at 3510 cm^{-1} due to coordinated water molecules and the lattice water band at ca. 3525 cm^{-1} (sh). Two strong $\nu_{C=N}$ bands at 1644 and 1665 cm^{-1}, which are much higher in energy than those of the free ligand, are in agreement with the fact that the PAHAP ligands in the complex adopt a twisted conformation. A prominent ($\nu_1 + \nu_4$) [112] nitrate band is observed at 1755 cm^{-1}. Based on the structure more nitrate combination bands would be expected, however. The pyridine ring breathing bands occur at 1043, 1033, 1024 and 1013 cm^{-1}, all of which are higher than for the free ligand (997 cm^{-1}) [117], in agreement with the fact that all four pyridine rings from two PAHAP ligands are coordinated. Two of them are strongly bound to the copper(II) centers, which is mirrored by the Cu-N_{py} bond distances (Cu(1)-N(6) 1.995(6) Å, Cu(2)-N(7) 1.998(6) Å, Cu(1)-N(11) 2.238(9) Å, Cu(2)-N(1) 2.221(6) Å).

The infrared spectrum of **19** above 3100 cm^{-1} is dominated by bands associated with water (3500 cm^{-1}) and NH_2 groups (3340 and 3146 cm^{-1}). Nitrate combination bands [112] are observed at 1762 and 1749 cm^{-1}, and their difference (13 cm^{-1}) is in agreement with the presence of monodentate nitrate in the structure. The ionic nitrate band probably coincides with one of three observed bands. A very strong band at 1664 cm^{-1} due to the $\nu_{C=N}$ of the PMHAP ligands agrees with the twisted arrangement of the ligands in this complex. Two pyridine ring breathing bands appearing at totally different positions (1044

and 1017 cm^{-1}) show the asymmetric property of the ligand. The higher energy band (1044 cm^{-1}) is due to the pyridine ring in which the pyridine nitrogen is strongly coordinated to copper(II) (Cu(1)-N(5) 1.997(5) Å), while the lower energy band (1017 cm^{-1}) can be assigned to the pyridine ring in which the pyridine nitrogen is weakly coordinated to copper(II) (Cu(1)-N(2) 2.021(5) Å).

Complex **20** shows very similar infrared absorptions above 3100 cm^{-1} to those of **18**, and exhibits only one prominent ($\nu_1 + \nu_4$) [112] nitrate band at 1763 cm^{-1} associated with free nitrates. A broad and strong band at 1673 cm^{-1} due to $\nu_{C=N}$ suggests a twisted arrangement of the PYPZ ligands like the cases in **18** and **19**. A very strong band at 1034 cm^{-1} is most likely a combination of the strongly coordinated pyridine ring breathing band and the weakly coordinated pyrazine ring breathing band, which is consistent with its preliminary structure which shows one pyrazine nitrogen in the apical position and one pyridine nitrogen in the basal plane of each copper(II) centre.

A broad and strong band due to coordinated water dominates the region above 3100 cm^{-1} in the spectrum of **21**. A complex group of ($\nu_1 + \nu_4$) [112] nitrate bands is observed at 1754, 1744 and 1764 cm^{-1}, consistent with the two slightly different monodentate nitrates and free nitrates. Two well separated $\nu_{C=N}$ bands at 1662 and 1686 cm^{-1} clearly suggest that the PAHAP ligands exist in two different conformations, which is confirmed by its single crystal structure that shows totally different torsion angles around the N-N bond vectors of the PAHAP ligands in each of the two crystallographically independent dicopper molecules. The bands at 1026 and 1036 cm^{-1} due to the pyridine ring

breathing modes are associated with the two different types of pyridine ring found in the complex. Strong ν_{NH} bands at 3335 and 3167 cm^{-1} appear to mask the ν_{OH} bands of the coordinated CH_3OH and lattice water molecules in the spectrum of **22**. Two azide bands were observed at 2086 and 2057 cm^{-1}. The higher energy band is associated with the μ_2-1,1-azide linking Cu(1) and Cu(2) (N(10)), in agreement with other related systems [21,113]. The lower energy band is therefore assigned to the intermolecular μ_2-1,1-azide bridge. Two clearly separated and equally intense $\nu_{C=N}$ bands at 1663 and 1679 cm^{-1} indicate that the ligand is twisted in agreement with the structure data. Pyridine ring breathing bands are observed at 1023 cm^{-1}, with a shoulder peak at 1002 cm^{-1}. One (ν_1 + ν_4) [112] nitrate band at 1764 cm^{-1} is associated with the free nitrates.

Solid state Nujol mull transmittance electronic spectra for **18-22** are quite similar, with one broad visible band observed in each case in the range 644-719 nm, consistent with square or square-pyramidal coordination geometries at the copper(II) centers. Aqueous solution spectra of **18**, **20** and **22** are slightly different from their solid spectra (**Table 3-7**), suggesting minor changes to the coordination environment in solution. The aqueous solution spectra of **19**and **21** are essentially the same as those in the solid state, indicative of no significant solvation in these two cases. The UV/vis absorption data for **18-22** are summarised in **Table 3-7**.

Table 3-6. Infrared spectral data of dicopper(II) complexes **18-22**.

compound	IR (cm^{-1})
$[Cu_2(PAHAP)_2(NO_3)(H_2O)_2](NO_3)_3.H_2O$ **(18)**	3510,3525(H_2O); 3356,3165(ν_{NH2}); 1756(NO_3^-); 1665,1644($\nu_{C=N}$); 1043, 1033, 1024, 1013(Py)
$[Cu_2(PMHAP)_2(NO_3)_2](NO_3)_2.3H_2O$ **(19)**	3500(H_2O); 3340,3146(ν_{NH2}); 1763,1749(NO_3^-) 1664($\nu_{C=N}$) ; 1044,1017(Py)
$[Cu_2(PYPZ)_2(H_2O)_2](NO_3)_4.H_2O$ **(20)**	3510-3100(H_2O and NH_2); 1763(NO_3^-); 1673($\nu_{C=N}$); 1033(Py and Pr)
$[Cu_2(PAHAP)(DPPN)(H_2O)(NO_3)](NO_3)_3$ **(21)**	3310(H_2O and NH_2);1764, 1744, 1754(NO_3^-); 1686,1662($\nu_{C=N}$) ; 1026, 1036(Py)
$\{[Cu_2(PAHAP)(N_3)_2(MeOH)_2)]\}_2$. $(NO_3)_4.2H_2O$ **(22)**	3335, 3167 (ν_{NH2});2086,2057(N_3^-); 1764(NO_3^-); 1678,1663($\nu_{C=N}$); 1023,1003(Py)

Table 3-7. UV/vis spectral data for dicopper(II) complexes **18-22** (nm).

compound	solid	H_2O (ε, $dm^3.mol^{-1}.cm^{-1}$)
$[Cu_2(PAHAP)_2(NO_3)(H_2O)_2](NO_3)_3.H_2O$ **(18)**	705	721(272.4)
$[Cu_2(PMHAP)_2(NO_3)_2](NO_3)_2.3H_2O$ **(19)**	719	712(177.6)
$[Cu_2(PYPZ)_2(H_2O)_2](NO_3)_4.H_2O$ **(20)**	700	710(216.3)
$[Cu_2(PAHAP)(DPPN)(H_2O)(NO_3)](NO_3)_3$ **(21)**	650	657(255.0)
$\{[Cu_2(PAHAP)(N_3)_2(MeOH)_2)]\}_2.(NO_3)_4.2H_2O$ **(22)**	644	695 (324.2)

3.3.3 Magnetism

Variable temperature magnetic susceptibility measurements were carried out for powdered samples of the complexes **18**, **19**, **21** and **22**, taken from the same uniform batches used for structural determinations. The samples were pre-dried under vacuum in order to prevent possible mass loss during sample preparation prior to a variable temperature run. The room temperature magnetic moments and the best fit parameters to the Bleaney-Bowers equation (**eqn. 1-4**) for the variable temperature (4-305 K) magnetic data are summarised in **Table 3-8**.

The room temperature magnetic moment for complex **18** (1.94 BM) is close to the normal value for an uncoupled copper(II) system, and might suggest the absence of spin exchange. A plot of χ_m*T versus temperature for **18** is illustrated in **Figure 3-8**, which shows that the χ_m*T values are larger than 0.40 emu.mol^{-1}.K above 25 K. When the temperature is lowered, the χ_m*T values decrease to 0.322 emu.mol^{-1}.K at 4 K, indicating that there is a very small antiferromagnetic interaction taking place. The data were fitted to **eqn. 1-4** to give g = 2.191(7), -2J = 0.4(3) cm^{-1}, ρ = 0.00046, Nα = 75*10^{-6} emu, θ = -2.1 K (10^2R = 2.2). From the structural point of view, any intramolecular spin coupling between the copper(II) centers will occur *via* the two diazine linkages (e.g. N(9)-N(10) and N(3)-N(4)), and the small dihedral angle (63.47°) of the copper planes about the two diazine bonds might be expected to provide a ferromagnetic coupling pathway based on

Table 3-8. Magnetic, structural data of the dicopper(II) complexes **18-22.**

compound	-2J (cm^{-1})	g	θ (K)	μ_{eff} (RT) (BM)	Cu-Cu (Å)	γ (Deg.)
$[Cu_2(PAHAP)_2(NO_3)(H_2O)_2]$	0.4(3)	2.19(1)	-2.1	1.94	3.863(5)	63.47
$(NO_3)_3.H_2O$(**18**)						
$[Cu_2(PMHAP)_2(NO_3)_2]$		no coupling		1.91	3.932(2)	81.24
$(NO_3)_2.3H_2O$(**19**)						
$[Cu_2(PYPZ)_2(H_2O)_2]$				1.79		
$(NO_3)_4.H_2O$(**20**)						
$[Cu_2(PAHAP)(DPPN)(H_2O)$	40(2)	2.09(1)	0	1.74	3.932(2)(Cu(1)-Cu(2))	85.91
$(NO_3)](NO_3)_3$(**21**)					3.936(2)(Cu(3)-Cu(4))	78.79
$\{[Cu_2(PAHAP)(N_3)_2(MeOH)_2)]\}_2$.	246(7)	2.15(7)	-0.3	1.52	3.497(2)(Cu(1)-Cu(2))	53.86
$(NO_3)_4.2H_2O$(**22**)					3.351(2)(Cu(1)-Cu(1A))	

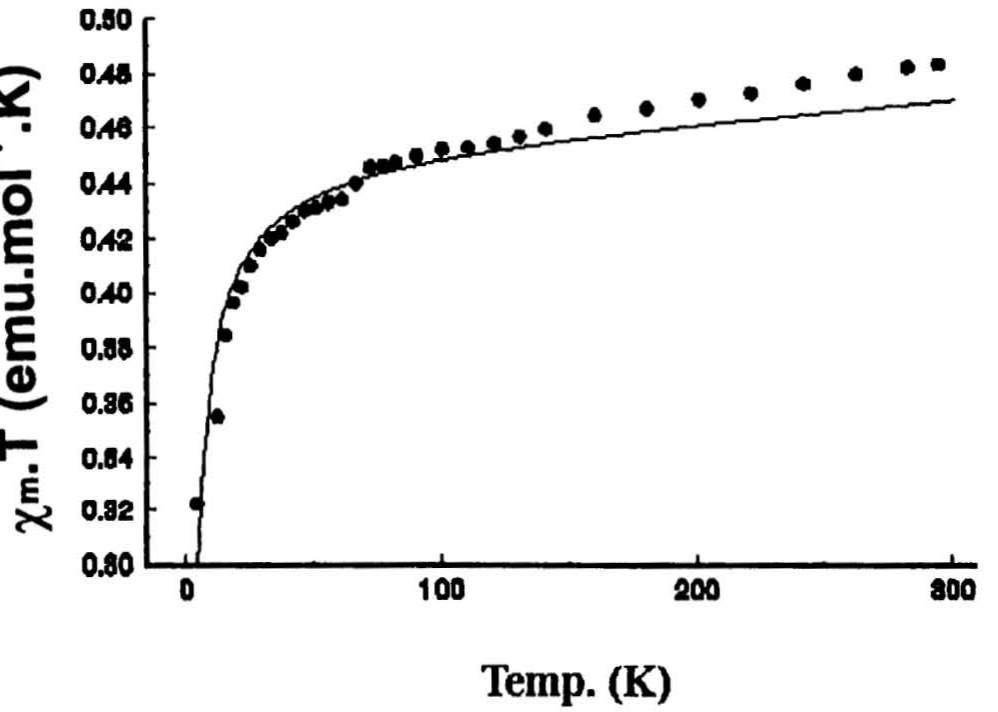

Figure 3-8. Variable temperature magnetic data for complex **18**. The solid line was calculated from **eqn. 1-4** with g = 2.191(7), $-2J = 0.4(3)\ cm^{-1}$, $\rho = 0.00046$, $N\alpha = 75*10^{-6}$ emu, $\theta = -2.1$ K, $10^2R = 2.2$ ($R = [\Sigma(\chi_{obs}-\chi_{calc})^2/\Sigma\chi_{obs}^2]^{1/2}$).

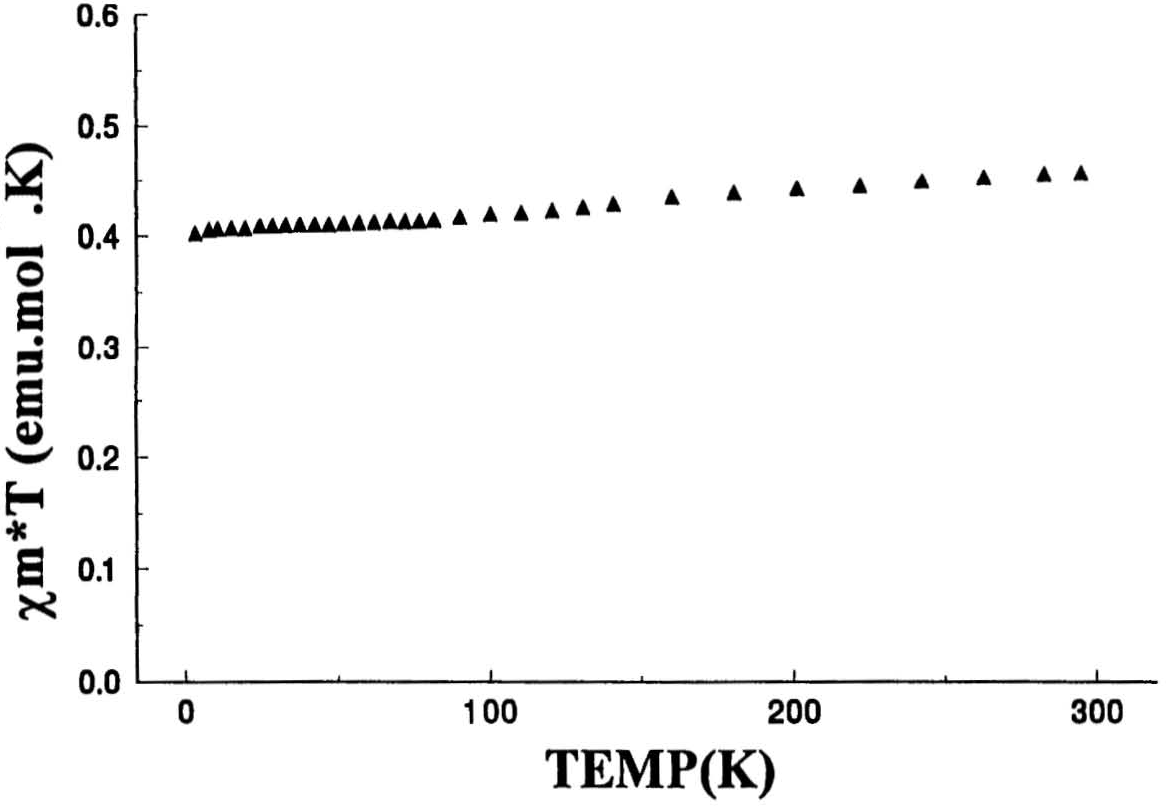

Figure 3-9. χm*T *vs.* T curves for **19**.

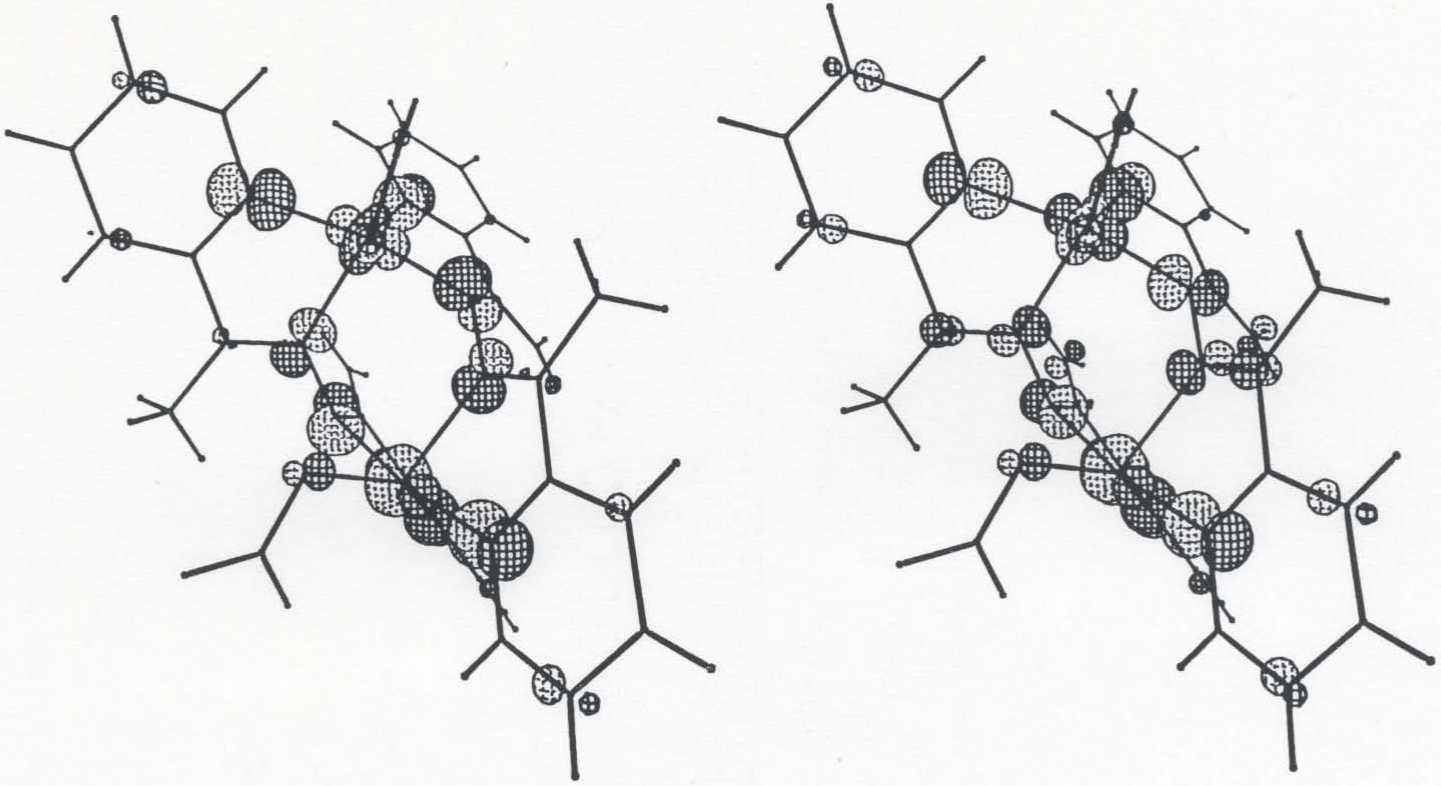

E = -11.572 eV

Symmetric SOMO

E = -11.599 eV

Antisymmetric SOMO

Figure 3-10. The symmetric and antisymmetric SOMOs for compound **19**.

the results of Chapter 2. However, since there are no similar magnetostructural and model studies on dicopper systems bridged by two N-N single bonds, the critical angle of changeover from antiferromagnetic to ferromagnetic behaviour is likely to be different.

The compound $[Cu_2(PMHAP)_2(NO_3)_2](NO_3)_2.3H_2O$ (**19**) also has a high room temperature magnetic moment, 1.91 BM, and the χ_m*T values are larger than 0.40 emu.mol^{-1}.K throughout the 5-300 K temperature range (**Figure 3-9**), indicative of no net coupling between the copper(II) centers. This clearly results because the two square pyramidal copper(II) centers are orthogonally bridged by two N-N single bonds (**Figure 3-4**), which is mirrored by the MO calculation (the energy gap between two SOMOs is only 27 meV; see **Figure 3-10**).

The room temperature magnetic moment for complex **20** (1.79 BM) is close to the normal value for an uncoupled copper (II) system, and might suggest the absence of spin exchange. However, its preliminary structure shows a very similar twist angle to that found in **18**, indicative of very weak antiferromagnetic coupling between two copper (II) centers. We await the variable temperature magnetic data for this complex.

The compound $[Cu_2(PAHAP)(DPPN)(H_2O)(NO_3)](NO_3)_3$ (**21**) has a slightly lower room temperature magnetic moment (1.74 BM) and a plot of χ versus temperature in **Figure 3-11** reveals a maximum in the susceptibility at about 40 K. This is clearly indicative of dominant antiferromagnetic exchange. The data were fitted successfully to **eqn. 1-4** with $g = 2.097(12)$, $-2J = 40(2)$ cm^{-1}, $\rho = 0.031$, $N\alpha = 66*10^{-6}$, $\theta = 0$ K, $10^2R =$

0.64 ($R = [\Sigma(\chi_{obs}-\chi_{calc})^2/\Sigma\chi_{obs}^2]^{1/2}$). The solid line in **Figure 3-11** was calculated with these parameters. This dominant antiferromagnetic exchange obviously arises from the two crystallographically independent dicopper molecules and therefore represents an average of the two structures. This raises the question as to which dicopper molecule dominates the total magnetic coupling. From a structural perspective, the diazine unit in the DPPN ligand contributes very little to the exchange because it bridges two copper centers in an orthogonal manner in both molecules. Based on the observations for the dicopper systems bridged by one N-N single bond in **Chapter 2**, the molecule containing the Cu(1) and Cu(2) centers should be the dominant, because it involves a larger dihedral angle around the N-N single bond in the PAHAP ligand. On the other hand, the extended Hückel MO calculations for both molecules surprisingly show that the energy difference between the symmetric and antisymmetric MO in the molecule containing the Cu(1) and Cu(2) centers is significantly smaller (ΔE = 141 meV) than that in the molecule containing the Cu(3) and Cu(4) centers (ΔE = 177 meV). The expanded views of the energy levels for both dicopper centers in the different molecules are illustrated in **Figure 3-12**, which implies a contradicting conclusion to the above. However, examinations of the copper(II) ion stereochemistries may reveal why. The geometries at all the copper(II) centers are close to square pyramidal, but trigonal bipyramidal distortions for Cu(1) (τ = 0.421) and Cu(2)

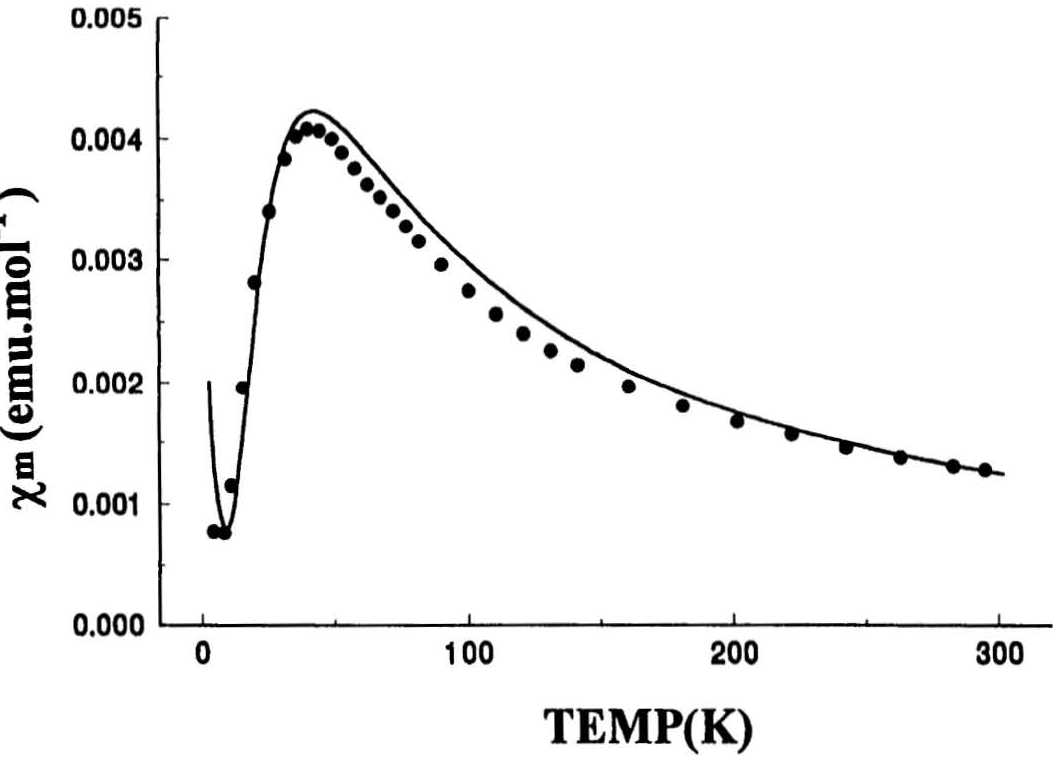

Figure 3-11. Variable temperature magnetic data for complex **21**. The solid line was calculated from **eqn. 1-4** with g = 2.097(12), -2J = 40(2) cm^{-1}, $\rho = 0.031$, $N\alpha = 66*10^{-6}$ emu, $\theta = 0$ K, $10^2R = 0.64$ ($R = [\Sigma(\chi_{obs.}-\chi_{calc.})^2/\Sigma\chi_{obs.}^2]^{1/2}$).

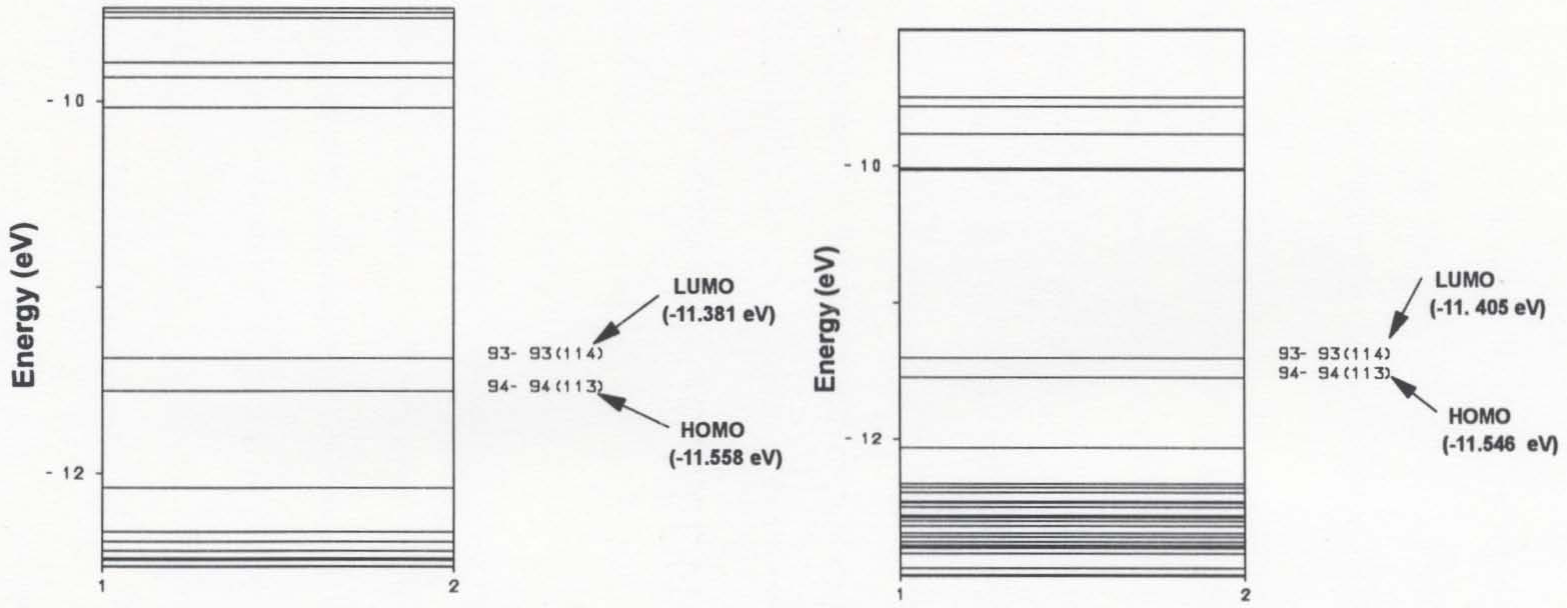

Figure 3-12. Comparision of expanded views of energy levels of two dicopper centers in **21**.

(τ = 0.271) are significantly larger than those for Cu(4) (τ = 0.356) and Cu(3) (τ = 0.219) respectively. These larger geometric distortions in the molecule containing the Cu(1) and Cu(2) centers will reduce the antiferromagnetic contribution to the total magnetic exchange.

The azide complex $[Cu_2(PAHAP)(MeOH)_2)(N_3)_2]_2.(NO_3)_4.2H_2O$ (**22**) has a room temperature magnetic moment as 1.52 BM, and a pronounced maximum in susceptibility at 220 K clearly indicating strong antiferromagnetic exchange (**Figure 3-13**). A good fit to **eqn. 1-4** gave g = 2.15(7), $-2J = 246(7)\ cm^{-1}$, $\rho = 0.0115$, $N\alpha = 59*10^{-6}$ emu, θ = -0.3 K, $10^2R = 1.8$. The structure shows that two μ_2-1,1-N_3^- anions bridge Cu(1) and Cu(1A) in a orthogonal fashion as described before, therefore any magnetic exchange in each dinuclear unit should occur through the N-N single bond (N(3)-N(4)) and the equatorially bridging μ_2-1,1-N_3^- *via* N(10). Since the dihedral angle around the bridging open-chain diazine unit is extremely small (53.86° between the least-squares planes Cu(1)-N(1)-N(3)-C(5)-C(6) and Cu(2)-N(4)-N(6)-C(11)-C(12)), the N-N single bond would not be expected to provide a large antiferromagnetic contribution to the total magnetic exchange, based on the result in Chapter 2, and might, even, be expected to provide a ferromagnetic contribution. Therefore, the equatorially bridging μ_2-1,1-N_3^- *via* N(10) seems to be the only factor likely to be responsible for the net strong antiferromagnetic coupling. This result is exactly consistent with the conclusion made by Thompson et al. [49-51], that when the μ_2-1,1-azide bridge angle exceeds a value of approximately 106°, the azide

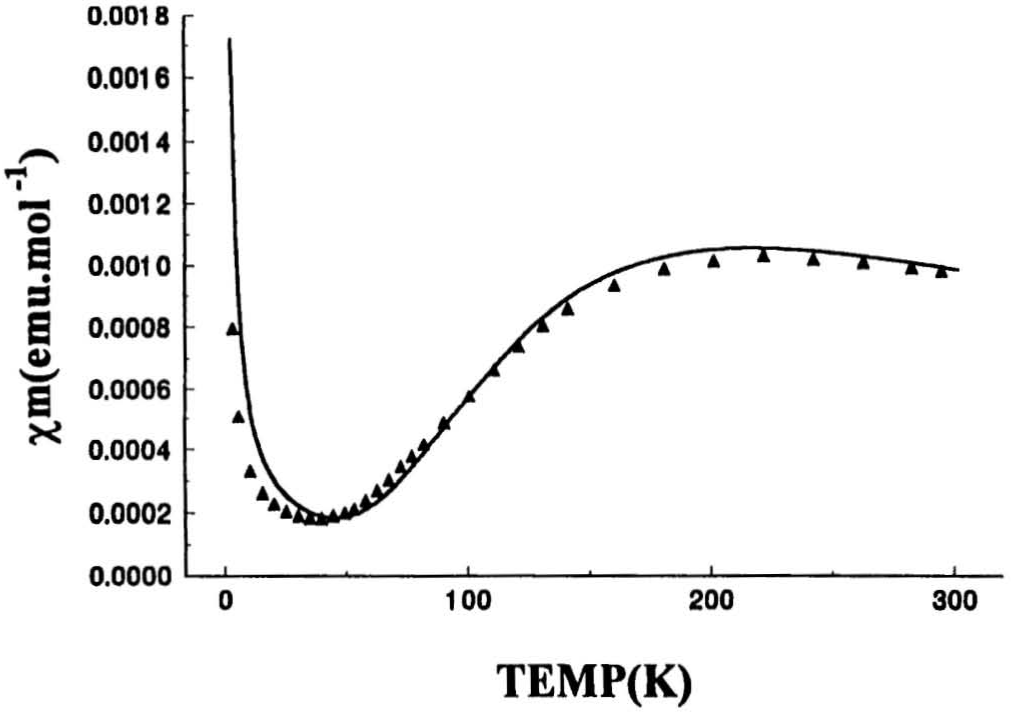

Figure 3-13. Variable temperature magnetic data for complex **22**. The solid line was calculated from **eqn. 1-4** with $g = 2.15(7)$, $-2J = 246(7)\ cm^{-1}$, $\rho = 0.0115$, $N\alpha = 59*10^{-6}$ emu, $\theta = -0.3$ K, $10^2R = 1.8$ ($R = [\Sigma(\chi_{obs} - \chi_{calc.})^2/\Sigma\chi_{obs}^2]^{1/2}$).

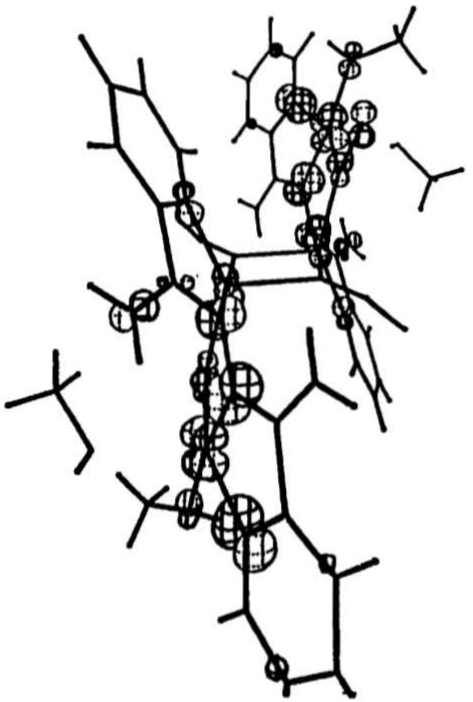

E = -11.622 eV

Symmetric SOMO

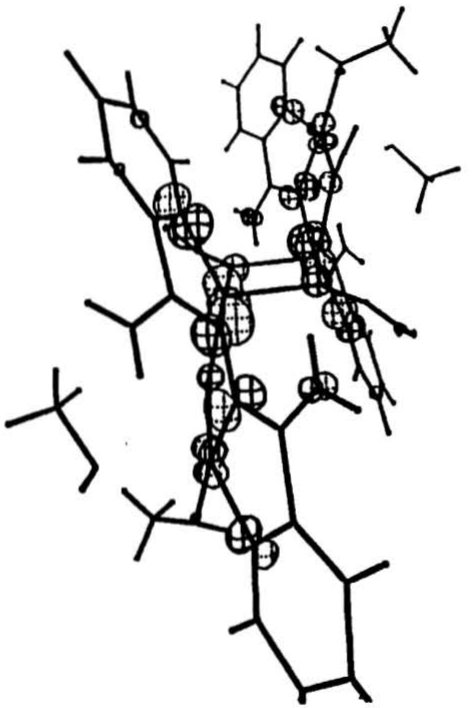

E = -11.693 eV

Antisymmetric SOMO

Figure 3-14. The symmetric and antisymmetric SOMOs for compound **22** .

bridge is responsible for antiferromagnetic coupling. The azide bridge angle in **22** (118.5°) is very large, and entirely consistent with the strong antiferromagnetic coupling in this compound. To our knowledge, complex **22** might be the first real example which contradicts the spin polarization mechanism [45-47] proposed 15 years ago to account for the magnetic properties of azide bridged dicopper complexes. The extended Hückel MO calculation for this complex was carried out by using exact structural data with two weakly apically bound CH_3OH molecules included. The energy difference between the symmetric and antisymmetric MO (orbital 132 and 133 respectively, see **Figure 3-14**) is 71 meV,

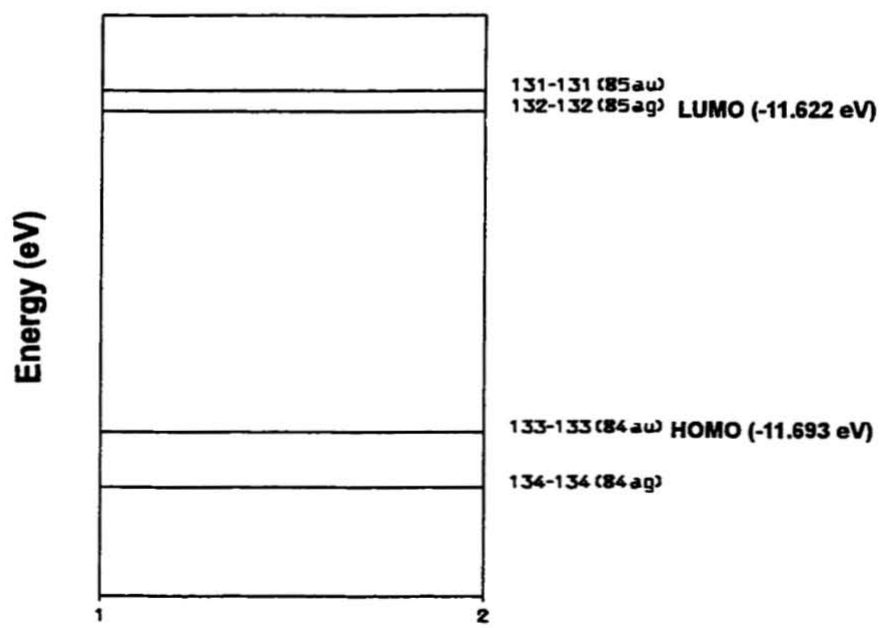

Figure 3-15. Expanded view of the energy levels for **22**.

which is fairly large and consistent with the magnetic behaviour. The fact that ΔE in this case is significantly smaller than e.g. in **21** (ΔE = 141, 177 meV), and that antiferromagnetic coupling in this compound is very much weaker, has little relevance because MO calculations at the extended Hückel level can only be safely compared in a closely related series of compounds.

3.4 Conclusion

Three dicopper complexes doubly bridged by open-chain N-N units show no or weak antiferromagnetic interactions. There is no coupling in **19** because of simple orbital orthogonality ($d_{x^2-y^2}$ (Cu(1))⊥ d_{z^2} (Cu(1)a). The very weak coupling in **18** may result from the twist of the two copper magnetic planes about two N-N single bonds which has not reached the ferromagnetic realm for this type of compound. The stronger coupling in the mixed diazine bridged dicopper complex **21** occurs through the open-chain N-N diazine bridge and is consistent with the much larger dihedral angles (85.9°, 78.8°). The aromatic diazine ligand DPPN does not contribute to the coupling because it acts as an orthogonal bridge. Strong antiferromagnetic coupling has been found in the μ_2-1,1-N_3^- and open-chain diazine mixed bridged complex (**22**). Since the dihedral angle between the two copper magnetic planes about N-N single bond is very small, the N-N single bond would be expected to contribute very little to the total magnetic interaction. Therefore, the μ_2-1,1-N_3^- is the only factor responsible for the strong antiferromagnetic exchange in **22**, which presents the first genuine example contradicting the spin-polarization mechanism for coupling in azide bridged complexes.

Chapter 4. Spiral Dinuclear Complexes of Tetradentate N_4 Open-chain Diazine Ligands with Mn(II), Fe(II), Fe(III), Co(II), Co(III) and Ni(II) Salts.

4.1 Introduction

A number of Ni(II) and Co(II) dinuclear complexes bridged by a diazine group incorporated in a heterocyclic aromatic ring, e.g. pyridazine, phthalazine, have been documented. X-ray structures showed that coordination occurs with one ligand or two ligands (e.g. pyridazine or phthalazine) together with attached co-donors like imine or carboxylic acid. The variable temperature magnetic susceptibility studies indicated antiferromagnetic interactions between the Ni(II) centers ($-2J = 25\text{-}47\ cm^{-1}$) and cobalt(II) centers ($-2J = 8\text{-}15\ cm^{-1}$) [134-144].

Open-chain diazine ligands have variable coordination modes to copper ions and lead to very interesting magnetic coupling phenomena as presented in Chapter 2, as well as Chapter 3. Early investigations in the 1950's and 1960's showed that such ligands could form variable types of coordination compounds with Co(II), Ni(II) and Fe(II) salts, including species with ML_2, M_2L_3 and ML_3 stoichiometries [73-76]. Among them the type M_2L_3 systems turned out to be the most interesting and received more attention. Studies by Busch et al. [73-75] on pyridine aldazine (PAA) suggested that the Fe(II), Co(II), Ni(II) dinuclear complexes contain the cation $[M_2(PAA)_3]^{4+}$ (M = Fe(II), Co(II), Ni(II)) with a spiral structure, but no X-ray structures were reported. Magnetic property studies indicated that the Fe(II) centres were low spin; the cobalt(II) centres were high spin but no

variable temperature magnetic susceptibility studies were reported and the Ni(II) centres were coupled weakly (-J/k = 8.3 - 13.7 K) [139]. Similar complexes of the related ligand 2-pyridyl-methyl-ketazine (PMK) $[M_2(PMK)_3]^{4+}$ (M = Fe(II), Co(II), Ni(II)) were also reported later on with similar magnetic properties, namely the Fe(II) centres were low spin and the Ni(II) centres were weakly coupled (-J = 11.8 cm^{-1}) [142]. The Co(II) complexes showed no coupling at all, which is mirrored by NMR studies reported by Dei et al. [143]. A recent magnetic property study on dinuclear cobalt(II) complexes of an open-chain diazine ligand, 4,5-dimethyl-3-pyrazolyl aldazine, indicated a weak antiferro- magnetic interaction between two cobalt(II) centres (-J = 6.88-7.36 cm^{-1}) in the complexes $[Co_2X_4L_2].H_2O$ (X= Cl or Br) [144]. However no X-ray structures were reported.

The first X-ray structure of a spiral complex in this class was reported for $[Co_2(PMK)_3].ZnCl_4.[ZnCl_3(H_2O)]_2.4H_2O$ in 1974 by Boyd et al. [145a], and showed that the three tetradentate ligands around the two distorted octahedral Co(II) centres form a spiral dinuclear structural arrangement with the diazine nitrogens forming a triple bridge in a **Type AB** conformation. The Co-Co distance is 3.81(1) Å, and the average Co-N-N-Co torsion angle is 44°, indicating a very pronounced twist of the three ligands about the Co-Co vector. A very recent paper gave another example of such spiral-like structure in a dinuclear Fe(III) complex [145b].

In order to further investigate the coordination chemistry of open-chain diazine ligands to the other first row transition metal ions in general and target new approaches to supramolecular architecture which is currently a very active field [146-160], this chapter

presents a series of spiral homodinuclear Mn(II), Fe(II), Fe(III), Co(II), Co(III) and Ni(II) complexes of the ligands PAHAP and PZHPZ (**Scheme 4-1**). The studies on these complexes focus on the structures and spectral, variable temperature magnetic susceptibility and electrochemical properties.

Scheme 4-1

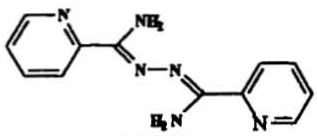

(PAHAP)

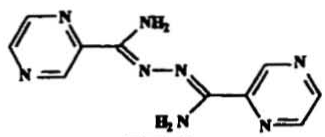

(PZHPZ)

4.2 Experimental

4.2.1 Materials

Commercially available solvents and chemicals were used without further purification.

4.2.2 Measurements

Analysis, spectroscopic and physical measurements (see Chapter 1)

4.2.3 Synthesis of the ligands

PZHPZ was synthesized in a similar manner to PAHAP (see Chapter 2) using 2-cyanopyrazine instead of 2-cyanopyridine with a yield of 81% (mp. 306-308°C, decompose) and was recrystalized from ethanol.

4.2.4 Synthesis of the complexes

$[Mn_2(PAHAP)_3](ClO_4)_4.5H_2O$ (**23**), $[Fe_2(PAHAP)_3](ClO_4)_4.4H_2O$ (**24**), $[Ni_2(PAHAP)_3(ClO_4)_4.5H_2O$ (**25**)

PAHAP (0.36 g, 1.5 mmol) was added to a hot aqueous methanol (80/20) solution

(40 mL) of 1.0 mmol $M(ClO_4)_2.xH_2O$ ($M = Mn^{2+}$, Fe^{2+}, Ni^{2+}), and the mixture stirred at room temperature for several minutes, until the ligand dissolved. The clear solution was filtered and the filtrate allowed to stand at room temperature overnight. Well formed crystals were produced in each case, which were filtered off, washed quickly with cold water, and dried in air (Yields 80-85%). Anal Calcd. for $[Mn_2(C_{12}H_{12}N_6)_3](ClO_4)_4.5H_2O$ (yellow) (**23**): C, 33.25; H, 3.40; N, 19.38. Found: C, 33.21; H, 2.97; N, 19.26. Anal Calcd. for $[Fe_2(C_{12}H_{12}N_6)_3](ClO_4)_4.4H_2O$ (dark red-brown) (**24**): C, 28.63; H, 3.00; N, 16.69. Found: C, 28.63; H, 3.27; N, 16.71. Anal Calcd. for $[Ni_2(C_{12}H_{12}N_6)_3](ClO_4)_4.5H_2O$ (orange brown) (**25**): C, 32.61; H, 3.50; N, 19.01. Found: C, 32.63; H, 3.31; N, 19.07.

$[Fe_2(PAHAP)_3](NO_3)_4.3H_2O$ (**26**), $[Fe_2(PZHPZ)_3](NO_3)_4.5H_2O$ (**27**), $[Co_2(PAHAP)_3](NO_3)_6.3H_2O$ (**28**), $[Ni_2(PAHAP)_3][Ni(H_2O)_6](NO_3)_6.4.5H_2O$ (**29**), $[Fe(PHAAP)(H_2O)_2(NO_3)](NO_3)_2$ (**30**)

PAHAP (0.48 g, 0.20 mmol) was added to a warm aqueous solution (40 mL) of $M(NO_3)_x.yH_2O$ (M = Fe; x =3, y = 9: M = Co, Ni; x = 2, y = 6) (2.0 mmol). The mixture was stirred in air at room temperature for a few minutes until a clear solution formed, which was filtered and allowed to stand at room temperature for several days. After this time, well formed crystals appeared, which were filtered off, washed quickly with a small amount of cold water, and air dried (Yields 30-40% for **26** and **28**; 80% for **29**). Close examination of the product in **26** revealed that it was a mixture, containing a small amount (≈20 mg) of dark, almost black rectangular prisms (**30**), which were separated by hand. Complex **30** has been shown to be a mononuclear derivative of a hydrolysed ligand

PHAAP, derived from PAHAP (*vide supra*). PHAAP was synthesized independently according to a procedure described in Chapter 2 and **30** prepared independently by reaction of PHAAP with $Fe(NO_3)_3.9H_2O$ in water. PHAAP (0.24 g, 1.0 mmol) was added to an aqueous solution (20 mL) of $Fe(NO_3)_3.9H_2O$ (0.40 g, 1.0 mmol) with stirring at room temperature. Methanol (5 mL) was added to aid solution of the ligand. Within a few minutes a dark greenish-black clear solution formed, which was filtered and the filtrate allowed to stand at room temperature overnight. Black prismatic crystals formed, which were filtered off, washed with a small amount of cold water, and air dried (Yields 80%). Complex **27** was prepared in a similar manner to **24** by adding PZHPZ (0.36 g, 1.5 mmol) to an aqueous methanol (75/25) solution of $Fe(NO_3)_3.9H_2O$ (0.40 g, 1.0 mmol). The resulting dark colored solution was filtered and allowed to stand at room temperature for several days. Dark brown crystals suitable for structural determination formed, which were filtered off, washed quickly with a small quantity of cold water, and allowed to dry in air (Yield 30%). No mononuclear derivative has been isolated from this reaction, but the low yield of **27** suggests that a similar hydrolysis reaction is occurring. Anal Calcd. for $[Fe_2(C_{12}H_{12}N_6)_3]$ $(NO_3)_4.3H_2O$ (**26**): C, 38.11; H, 3.73; N, 27.16. Found: C, 38.14; H, 3.61; N, 27.37. Anal Calcd. for $[Fe_2(C_{10}H_{10}N_8)_3](NO_3)_4.5H_2O$ (**27**): C, 30.63; H, 3.43; N, 33.32. Found: C, 30.90; H, 3.21; N, 33.20. Anal Calcd. for $[Co_2(C_{12}H_{12}N_6)_3](NO_3)_6.3H_2O$ (**28**): C, 34.19; H, 3.35; N, 26.57. Found: C, 34.19; H, 3.40; N, 25.92. Anal Calcd. for $[Ni_2(C_{12}H_{12}N_6)_3][Ni(H_2O)_6](NO_3)_6.4.5H_2O$ (**29**): C, 29.66; H, 3.94; N, 23.05 Found: C,

29.64; H, 4.02; N, 23.04. Anal Calcd. for $[Fe(C_{12}H_{11}N_5O)(H_2O)_2(NO_3)](NO_3)_2$ **(30)**: C, 27.76; H, 2.91; N, 21.58 . Found: C, 27.96; H, 2.97; N, 21.53.

$[Fe_2(PAHAP)_3](ClO_4)_6.4.5H_2O$ **(31)**

PAHAP (0.24 g, 1.0 mmol) was added to an aqueous solution (20 mL) of $Fe(ClO_4)_3.6H_2O$ (0.36 g, 1.0 mmol) at room temperature, and complex **31** was obtained as brown colored crystals within a few minutes (Yield 70%). The product was filtered off, washed with a small amount of cold water and dried in air. Anal Calcd. for $[Fe_2(C_{12}H_{12}N_6)_3](ClO_4)_6.4.5H_2O$ **(31)**: C, 28.63; H, 3.00; N, 16.69. Found: C, 28.63, H, 3.27; N, 16.71.

$[Co_2(PAHAP)_3](ClO_4)_4.5.5H_2O$ **(32)**

PAHAP (0.36 g, 1.5 mmol) was added to a hot aqueous solution (20 mL) of $Co(ClO_4)_2.6H_2O$, and the mixture was stirred under a nitrogen atmosphere until the mixture became a clear solution. The clear solution was filtered under a nitrogen atmosphere, and the filtrate allowed to stand in a refrigerator overnight. Well formed orange crystals were produced , which were filtered off, washed quickly with cold water, and dried in air (Yield 78%). Anal Calcd. for $[Co_2(C_{12}H_{12}N_6)_3](ClO_4)_4.5.5H_2O$ **(32)**: C, 33.38; H, 3.55, N, 18.88. Found: C, 33.78; H, 3.24; N, 18.64.

4.2.5 Crystallographic data collection and refinement of the structures

Crystals of $[Mn_2(PAHAP)_3](ClO_4)_4.5H_2O$ **(23)** are yellow in appearance. A single crystal of **23** of dimensions 0.10 × 0.10 × 0.10 mm was attached to a quartz fibre and transferred to a Siemens Smart three-circle diffractometer with graphite-monochromatized

Mo-Kα X-radiation and a CCD area detector was used for data collection [108]. ω -scans were used in such a way that an initial 180° scan range consisting of 0.3° intervals was followed by three further 120°, 180° and 120°scans with ϕ offsets of 88°, 180° and 268°, respectively. This strategy samples the sphere of reciprocal space up to 2θ = 50.04°. Cell parameters were refined using the centroid values of 300 reflections with 2θ angles up to 50.04°. Raw frame data were integrated using the SAINT program [109]. The structure was solved by direct methods [110]. An empirical absorption correction was applied to the data using the programme SADABS [111]. Abbreviated crystal data are listed in **Table 4-1**. Crystal data collection and structure refinement for **26**, **29**, **30** were carried out in a similar manner to that for **23**. Abbreviated crystal data for all of these complexes are also given **Table 4-1.**

The crystals of $[Co_2(PAHAP)_3](NO_3)_6.3H_2O$ (**28**) are deep blood red in appearance. The diffraction intensities of a crystal of approximate dimensions 0.40 × 0.20 × 0.40 mm were collected with graphite-monochromatized Mo-Kα X-radiation using a Rigaku AFC6S diffractometer at 299(1) K and the ω–2θ scan technique to a $2\theta_{max}$ value of 50.1°. A total of 3549 reflections was measured, of which 1839 were considered unique (R_{int} = 0.024) and 1218 were considered significant with $I_{net} > 2.0\ \sigma\ (I_{net})$. The intensities of three representative reflections, which were measured after every 150 reflections, remained constant through the data collection, indicating crystal and electronic stability (no decay correction was applied). An empirical absorption correction, based on azimuthal scans of several reflections, was applied and resulted in transmission factors

ranging from 0.97 to 1.00. The data were corrected for Lorentz and polarisation effects. The cell parameters were obtained from the least-squares refinement of the setting angles of 24 carefully centred reflections with 2 θ in the range 32.1-35.1°.

The structure was solved by direct methods [102, 103]. All atoms except hydrogens were refined anisotropically. Hydrogen atoms were optimized by positional refinement with isotropic thermal parameters set 20% greater than those of their bonded partners at the time of their inclusion. However, they were fixed for the final round of refinement. The final cycle of full-matrix least-squares refinement was based on 1218 observed reflections ($I > 2.00\sigma(I)$) and 139 variable parameters and converged with unweighted and weighted agreement factors of $R=\Sigma||F_o|-|Fc||/\Sigma|F_o| = 0.050$ and $R_w = [(\Sigma w(|F_o|-|F_c|)^2/ \Sigma wF_o^2]^{1/2} = 0.054$. The maximum and minimum peaks on the final difference Fourier map correspond to 0.52 and -0.45 electron $Å^{-3}$, respectively. Neutral atom scattering factors [104] and anomalous-dispersion terms [105, 106], were taken from the usual sources. All calculations were performed with the TEXSAN [107] crystallographic software package using a VAX3100 work station. The structural data for **27** were collected and treated in a similar manner. Abbreviated crystal data for **27** and **28** are given in **Table 4-1**

Note in **Table 4-1**, # = Rigaku data; * = Siemens Smart data

$$\mathbf{R} = \Sigma||F_o| - |F_c||/\Sigma|F_o|, \quad \mathbf{R_w} = [(\Sigma(|F_o| - |F_c|)^2/\Sigma wF_o^2)]^{1/2}$$

$$\mathbf{R1} = \Sigma||F_o| - |F_c||/\Sigma|F_o|, \quad \mathbf{wR_2} = [\Sigma[w(|F_o|^2 - |F_c|^2)^2/\Sigma[w(|F_o|^2)^2]]^{1/2}$$

Table 4-1. Summary of crystallographic data for complexes **23, 26, 27, 28, 29** and **30**.

Compound	**23***	**26***	**27#**
chemical formula	$C_{36}H_{46}Cl_4Mn_2N_{18}O_{21}$	$C_{39}H_{45}Fe_2N_{22}O_{15}$	$C_{60}H_{80}N_{56}Fe_4O_{34}$
formula wt.	1318.59	1173.67	2353.2
space group	C2/c	$Pa\bar{3}$	P2/n
a (Å)	13.4086(2)	21.0024(1)	14.039(3)
b(Å)	32.0249(1)	21.0024(1)	11.335(6)
c(Å)	14.3132(2)	21.0024(1)	14.6517(15)
α(deg)	90	90	90
β(deg)	115.635(1)	90	96.852(11)
γ(deg)	90	90	90
V ($Å^3$)	5541.2(1)	9264.18(8)	2314.9(13)
$\rho_{calcd}(gcm^{-3})$	1.581	1.683	1.688
Z	4	8	1
$\mu(cm^{-1})$	0.738	0.723	0.7330
λ	0.71073	0.71073	0.71069
T, K	298(2)	298(2)	299(2)
R1(R)	0.0664	0.0615	0.0448
wR2(R_w)	0.1524	0.1640	0.1154

Table 4-1. (contd.) Summary of crystallographic data for **23, 26, 27, 28, 29** and **30**.

Compound	**28#**	**29***	**30***
chemical formula	$C_{36}H_{54}N_{24}O_{27}Co_2$	$C_{8.33}H_{10.67}C_{10.67}N_{5.33}Ni_{0.67}O_{5.33}$	$C_{12}H_{15}N_8O_{12}Fe$
formula wt.	686.42	337.67	519.17
space group	$R\bar{3}c$(h) (#197)	$R\bar{3}c$	$P2_1/c$
a (Å)	17.38(6)	17.373(3)	8.4517(3)
b(Å)	17.38(6)	17.373(3)	19.6456(6)
c(Å)	32.15(2)	33.235(6)	12.6511(4)
α(deg)	90	90	90
β(deg)	90	90	109.400(1)
γ(deg)	90	120	90
V (Å^3)	8415(5)	8685(5)	1981.31(11)
ρ_{calcd}(gcm^{-3})	1.625	1.743	1.740
Z	12	27	4
μ(cm^{-1})	0.692	1.207	0.845
λ	0.71069	0.71073	0.71073
T, K	299(1)	150(2)	150(2)
R1(R)	0.050(R)	0.0488	0.0462
wR2(R_w)	0.054(Rw)	0.1133	0.0754

4.3 Results and discussion

4.3.1 Structures

$[Mn_2(PAHAP)_3](ClO_4)_4.5H_2O$ (**23**)

The structure of **23** is illustrated in **Figure 4-1**, and relevant bond distances and angles are listed in **Table 4-2**. The dimanganese cation consists of two distorted octahedral manganese(II) centres bridged by three ligands in a spiral-like arrangement, with the diazine nitrogens acting as the bridging groups and the pyridine rings occupying the remaining coordination positions. A second projection of the structure (**Figure 4-2**), viewed approximately down the Mn-Mn axis, shows the parts of the molecule related by the two-fold rotational axis. Mn-N distances are all very similar, falling in the range 2.22-2.26 Å. The Mn-Mn separation is 3.946(4) Å, and the least squares planes of the two five membered chelate rings of each ligand (e.g. Mn(a)-N(30)-C(11)-C(12)-N(9)) are twisted by 67.8°. On the outside of the complex ion pairs of NH_2 groups are arranged in three groups, with a separation of 3.735 Å between adjacent pairs (e.g. N(7)-N(8)).

Within each ligand the bond distances in the N=C-NH_2 framework are very similar to those of the free ligand (e.g. N(2)-N(4) 1.425(6) Å, N(2)-C(6) 1.309(6) Å, C(6)-N(7) 1.331(7) Å, C(5)-C(6) 1.492(7) Å), indicating single bond character in the N-N diazine bonds, and C-NH_2 bonds, and largely double bond character in the C=N bonds. The large dihedral angle between the chelate rings within the same ligand indicates flexibility about the N-N bond, an attribute which allows the spiral wrapping of the three ligands around

the two metals centres, and the geometric variability apparent in the copper complexes of this ligand.

Table 4-2. Interatomic distances (Å) and angles (Deg.) relevant to the Mn coordination spheres and the ligand in $[Mn_2(PAHAP)_3](ClO_4)_4.5H_2O$ (**23**).

Mn-N(4)#1	2.221(4)	Mn-N(6)	2.235(4)
Mn-N(3)#1	2.240(4)	Mn-N(1)	2.244(4)
Mn-N(5)	2.252(4)	Mn-N(2)	2.259(4)
N(2)-C(6)	1.309(6)	N(2)-N(4)	1.425(6)
N(4)-C(12)	1.298(6)	N(6)-C(18)	1.298(6)
N(6)-N(6)#1	1.437(8)	N(7)-C(6)	1.331(7)
N(8)-C(12)	1.324(6	N(9)-C(18)	1.334(6)
Mn-Mna	3.946(4)		
N(4)#1-Mn-N(6)	90.3(2)	N(4)#1-Mn-N(3)#1	72.3(2)
N(6)-Mn-N(3)#1	161.3(2)	N(4)#1-Mn-N(1)	158.2(2)
N(6)-Mn-N(1)	96.9(2)	N(3)#1-Mn-N(1)	101.8(2)
N(4)#1-Mn-N(5)	95.3(2)	N(6)-Mn-N(5)	71.7(2)
N(3)#1-Mn-N(5)	102.5(2)	N(1)-Mn-N(5)	106.5(2)
N(4)#1-Mn-N(2)	86.9(2)	N(6)-Mn-N(2)	90.4(2)
N(3)#1-Mn-N(2)	95.2(2)	N(1)-Mn-N(2)	72.5(2)
N(5)-Mn-N(2)	162.0(2)		

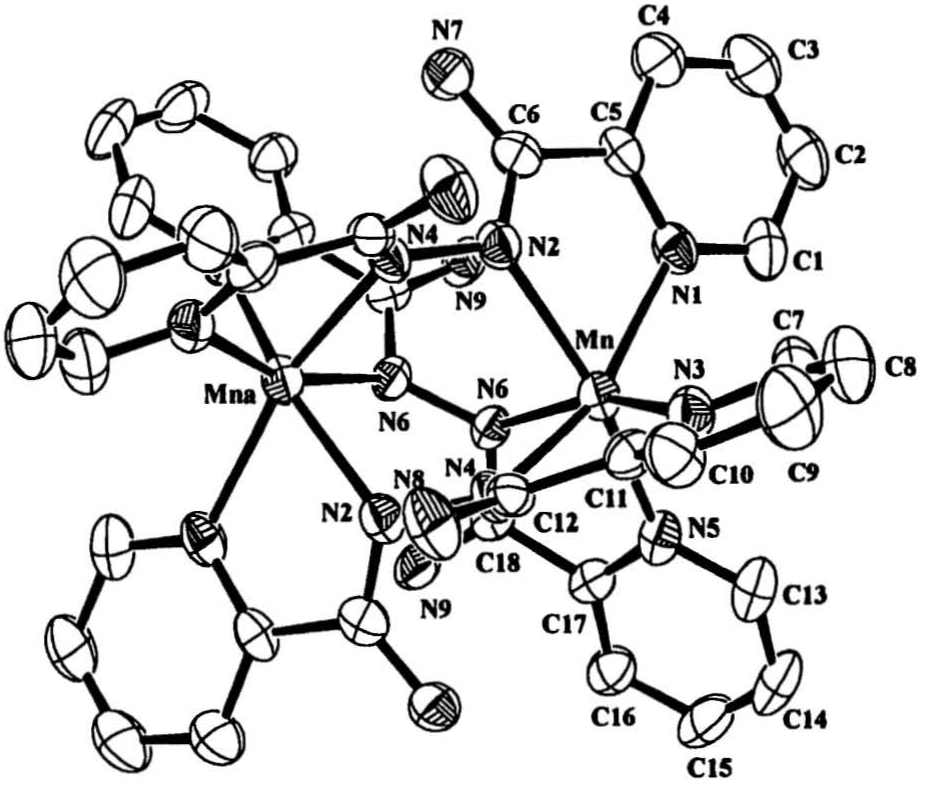

Figure 4-1. Structural representation of $[Mn_2(PAHAP)_3](ClO_4)_4.5H_2O$ **(23)** with hydrogen atoms omitted (50% probability thermal ellipsoids).

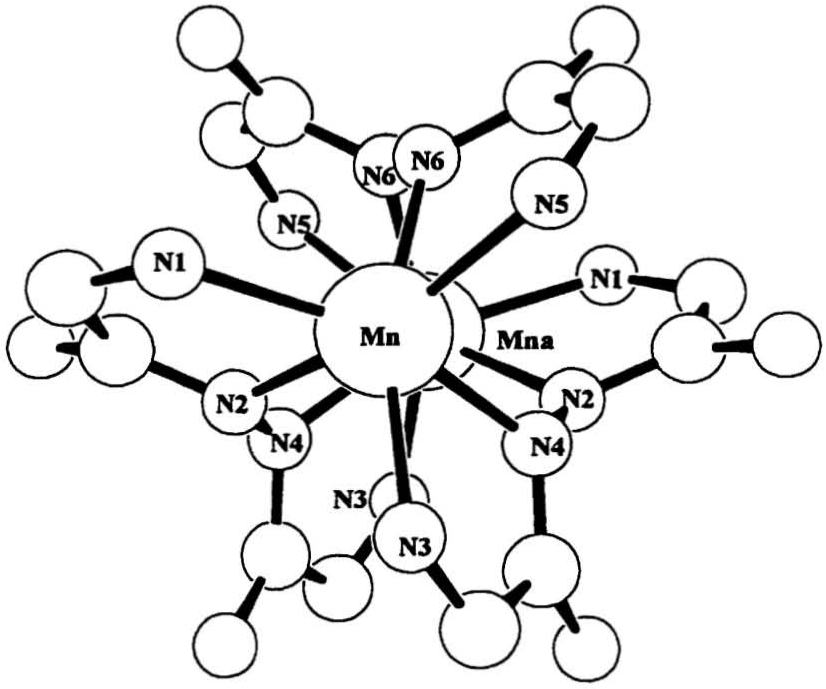

Figure 4-2. Expanded view approximately down the Mn-Mn axis with some carbon atoms in the pyridyl rings removed for clarity.

$[Fe_2(PAHAP)_3](NO_3)_4.3H_2O$ (**26**)

The structure of **26** is very similar to **23.** The labelled asymmetric unit and a molecular projection down the Fe-Fe axis are illustrated in **Figure 4-3**. Important bond distances and angles are listed in **Table 4-3**. Metal ligand bond distances are substantially shorter than those in **23**, with Fe-N distances falling in the range 1.95-2.0 Å, and a distance of 3.552(4) Å between the two iron centres. Angles around the iron centres are in the range 79.2-93° indicating some distortion from an idealized octahedron. The ligands exhibit a marked spiral twist around the dinuclear iron centre, with a dihedral angle of 67.5° between the five-membered iron chelate rings belonging to the same ligand. Despite the shorter metal nitrogen distances in this complex compared with **23**, the ligand twist is very similar. Within each ligand the bond distances in the NH_2-C=N framework (e.g. N(2)-N(5) 1.409(6) Å, N(2)-C(6) 1.309(7) Å) C(6)-N(3) 1.323(7) Å) are very similar to those in **23** and in the free ligand, although in this case the similarity in C-N distances suggests some double bound delocalization into the C-NH_2 bond.

Table 4-3. Interatomic distances (Å) and angles (Deg.) relevant to the iron coordination spheres and the ligand in $[Fe_2(PAHAP)_3](NO_3)_4.3H_2O$ (**26**).

Fe(1)-N(2)	1.960(4)	Fe(1)-N(2)#1	1.960(4)
Fe(1)-N(2)#2	1.960(4)	Fe(1)-N(1)	1.989(4)
Fe(1)-N(1)#1	1.989(4)	Fe(1)-N(1)#2	1.989(4)
Fe(2)-N(5)#1	1.951(4)	Fe(2)-N(5)#2	1.951(4)
Fe(2)-N(5)	1.951(4)	Fe(2)-N(4)	1.996(4)

contd.

Fe(2)-N(4)#2	1.996(4)	Fe(2)-N(4)#1	1.996(4)
N(1)-C(5)	1.369(7)	N(2)-C(6)	1.309(7)
N(2)-N(5)	1.409(6)	N(3)-C(6)	1.323(7)
N(5)-C(12)	1.321(7)	N(6)-C(12)	1.318(7)
C(5)-C(6)	1.486(8)	Fe(1)-Fe(2)	3.552(4)
N(2)-Fe(1)-N(2)#1	89.9(2)	N(2)-Fe(1)-N(2)#2	89.9(2)
N(2)#1-Fe(1)-N(2)#2	89.9(2)	N(2)-Fe(1)-N(1)	79.2(2)
N(2)#1-Fe(1)-N(1)	93.5(2)	N(2)#2-Fe(1)-N(1)	168.6(2)
N(2)-Fe(1)-N(1)#1	168.6(2)	N(2)#1-Fe(1)-N(1)#1	79.2(2)
N(2)#2-Fe(1)-N(1)#1	93.5(2)	N(1)-Fe(1)-N(1)#1	97.8(2)
N(2)-Fe(1)-N(1)#2	93.5(2)	N(2)#1-Fe(1)-N(1)#2	168.6(2)
N(2)#2-Fe(1)-N(1)#2	79.2(2)	N(1)-Fe(1)-N(1)#2	97.8(2)
N(1)#1-Fe(1)-N(1)#2	97.8(2)	N(5)#1-Fe(2)-N(5)#2	90.5(2)
N(5)#1-Fe(2)-N(5)	90.5(2)	N(5)#2-Fe(2)-N(5)	90.5(2)
N(5)#1-Fe(2)-N(4)	169.9(2)	N(5)#2-Fe(2)-N(4)	93.2(2)
N(5)-Fe(2)-N(4)	80.1(2)	N(5)#1-Fe(2)-N(4)#2	93.2(2)
N(5)#2-Fe(2)-N(4)#2	80.1(2)	N(5)-Fe(2)-N(4)#2	169.9(2)
N(4)-Fe(2)-N(4)#2	96.7(2)	N(5)#1-Fe(2)-N(4)#1	80.1(2)
N(5)#2-Fe(2)-N(4)#1	169.9(2)	N(5)-Fe(2)-N(4)#1	93.2(2)
N(4)-Fe(2)-N(4)#1	96.7(2)	N(4)#2-Fe(2)-N(4)#1	96.7(2)

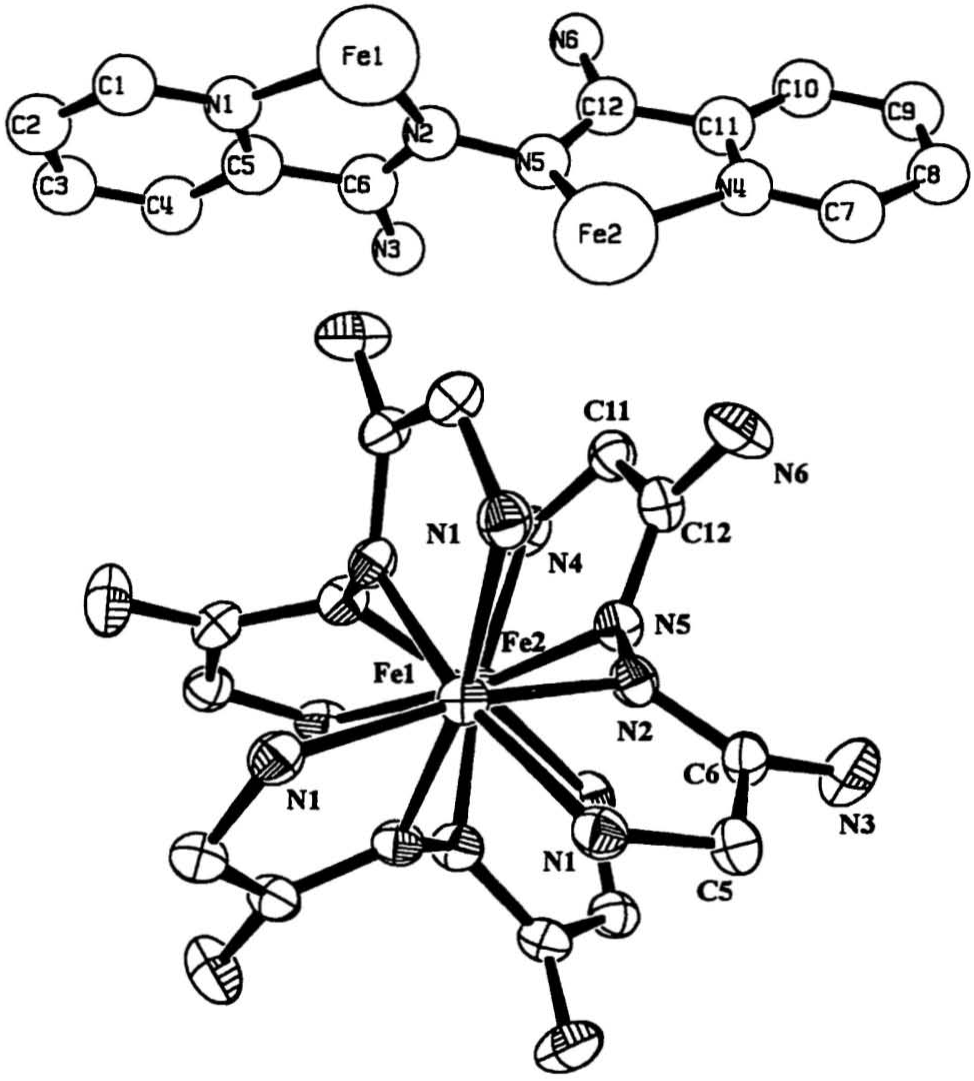

Figure 4-3. Up: Asymmetrical view of **26** with labelling of the ligand; Down: Expanded view approximately down the Fe-Fe axis with removal of some carbon atoms in the pyridyl rings for clarity and with hydrogen atoms omitted (40% probability thermal ellipsoids).

$[Fe_2(PZHPZ)_3](NO_3)_4.5H_2O$ (27)

The labelled asymmetric unit and the structure of the molecular cation in **27** is illustrated in **Figure 4-4**, projected slightly off the Fe-Fe axis, and shows the groups related by the two-fold rotational axis. Important bond distances and angles are listed in **Table 4-4**. The structure is essentially identical with those in **23** and **26** with a distance of 3.570(3) Å between the iron(II) centres. The Fe-N distances lie in the range 1.94-1.97 Å, very similar to those in **26**. There is no evidence for further interactions between the dinuclear units that would involve any additional coordination of the external pyrazine nitrogens. The N-N distances (e.g. N(2)-N(12) 1.4133 Å, N(22)-N(22)a 1.4183 Å) indicate single N-N bonds within each ligand, and the distances within the $N{=}C{-}NH_2$ ligand framework are very close to those in the free ligand PAHAP, which is very similar to the current ligand PZHPZ, as expected. The spiral twist of the ligand around the two iron centres is very similar to that found in **23** and **26**, with e.g. a 66.3° angle between the least-squares planes Fe(1)-N(2)- C(6)-C(5)-N(1) and Fe(1)a-N(11)-N(12)-C(15)-C(16).

Table 4-4 . Interatomic distances (Å) and angles (deg.) relevant to the iron coordination spheres in $[Fe_2(PZHPZ)_3](NO_3)_4.5H_2O$ (27).

Fe1-N1	1.951(3)	Fe1-N2	1.943(3)
Fe1-N21	1.954(3)	Fe1-N22	1.963(3)
Fe1-N11a	1.959(3)	Fe1-N12a	1.951(3)
N2-N12	1.4133	N23-C26	1.3202
C2-C6	1.3023	C5-C6	1.4736
N3-C6	1.3309	C11-C12	1.3855
N12-C16	1.3083	C14-C15	1.3779
N13-C16	1.3155	C15-C16	1.4773
N22-C26	1.3046	C21-C22	1.3770
N22-N22a	1.418(5)	C24-C25	1.3777
N1-Fe1-N2	79.90	N1-Fe1-N21	95.03
N1-Fe1-N22	168.99	N1-Fe1-N11a	97.30
N1-Fe1-N12a	95.72	N2-Fe1-N21	94.31
N2-Fe1-N22	90.60	N2-Fe1-N11a	169.17
N2-Fe1-N12a	89.70	N21-Fe1-N22	80.06
N1a-Fe1-N21	96.36	N12a-Fe1-N21	169.04
N11a-Fe1-N22	93.05	N12a-Fe1-N22	89.72
N1a-Fe1-N12a	80.13		

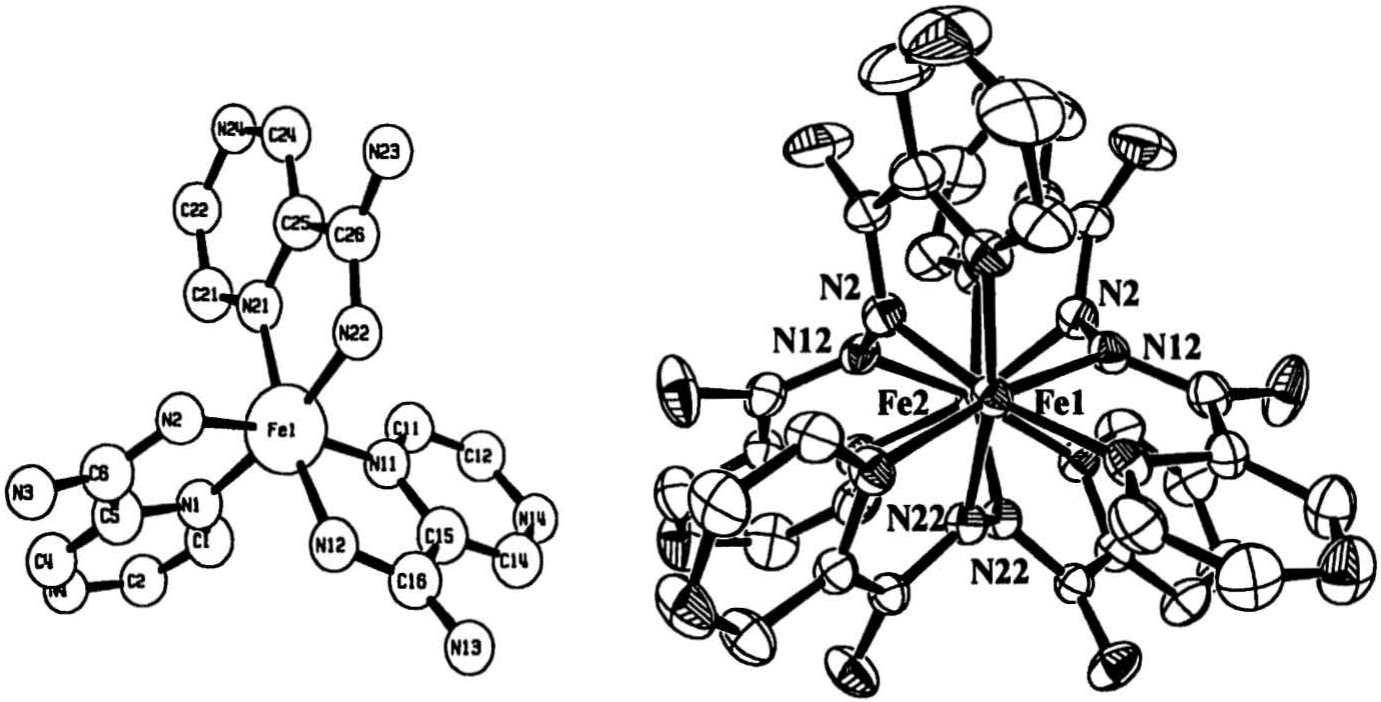

Figure 4-4. Right: Structural representation of $[Fe_2(PZHPZ)_3](NO_3)_4.5H_2O$ (27) with hydrogen atoms omitted (40% probability thermal ellipsoids)

Left: Asymmetrical view with labelling of the atoms.

$[Co_2(PAHAP)_3](NO_3)_6.3H_2O$ (**28**)

The structure of **28** is the same as the spiral structures reported for **23**, **26** and **27** and illustrated in **Figure 4-5**. Important distances and angles are listed in **Table 4-5**. Bond distances to the nitrogen donor atoms are very short (Co(1)-N(1) 1.915(4) Å, Co(1)-N(3) 1.942(4) Å, in keeping with the 3+ oxidation state of the cobalt centres. The cobalt octahedra are somewhat distorted with N-Co-N angles ranging from 82.0-95.9°. The Co-Co separation is 3.508(3) Å. Within the N-C-N-N framework of the ligand the N-N distance is quite short (1.397(7) Å), in keeping with very short Co-N contacts.

The N-C (e.g. N(1)-C(1) 1.324(5) Å) distance is somewhat longer, and the C-NH_2 distance (C(1)-N(2) 1.305(5) Å) somewhat shorter than in **23**, **26** and **27**, resulting in more double bond character in the C-NH_2 bond. A comparison with the $[Co_2(PMK)_3]^{4+}$ structure reveals much longer Co-N distances (2.07-2.18 Å), and very much longer Co-Co separation (3.81(1) Å) in keeping with the lower oxidation state of the metal [145]. The dihedral angle Co-N-N-Co for this compound is small (44°), but perhaps a direct comparison with **28** is unwise because of the differences in the ligands. For **28** the dihedral angle between the mean planes of the cobalt chelate rings associated with the same ligand (50.8°) is in keeping with the general spiral geometry of the dimetal cation, but is substantially smaller than those in the other complexes, and may be associated with short metal-nitrogen contacts, and average N-Co-N angles closer to 90°.

Table 4-5. Interatomic distances (Å) and angles (Deg.) relevant to the cobalt coordination spheres and the ligand in $[Co_2(PAHAP)_3](NO_3)_6 \cdot 9H_2O$ (**28**).

Co(1)-N(1)	1.915(4)	Co(1)-N(1)	1.915(4)
Co(1)-N(1)	1.915(4)	Co(1)-N(3)	1.942(4)
Co(1)-N(3)	1.942(4)	Co(1)-N(3)	1.942(4)
N(1)-N(1)	1.397(7)	N(1)-C(1)	1.324(5)
N(1)-N(1)	1.305(5)	Co(1)-Co(1)'	3.508(3)
N(1)-Co(1)-N(1)	90.1(1)	N(1)-Co(1)-N(3)	171.8(2)
N(1)-Co(1)-N(3)	92.2(2)	N(1)-Co(1)-N(3)	82.0(2)
N(3)-Co(1)-N(3)	95.9(1)		

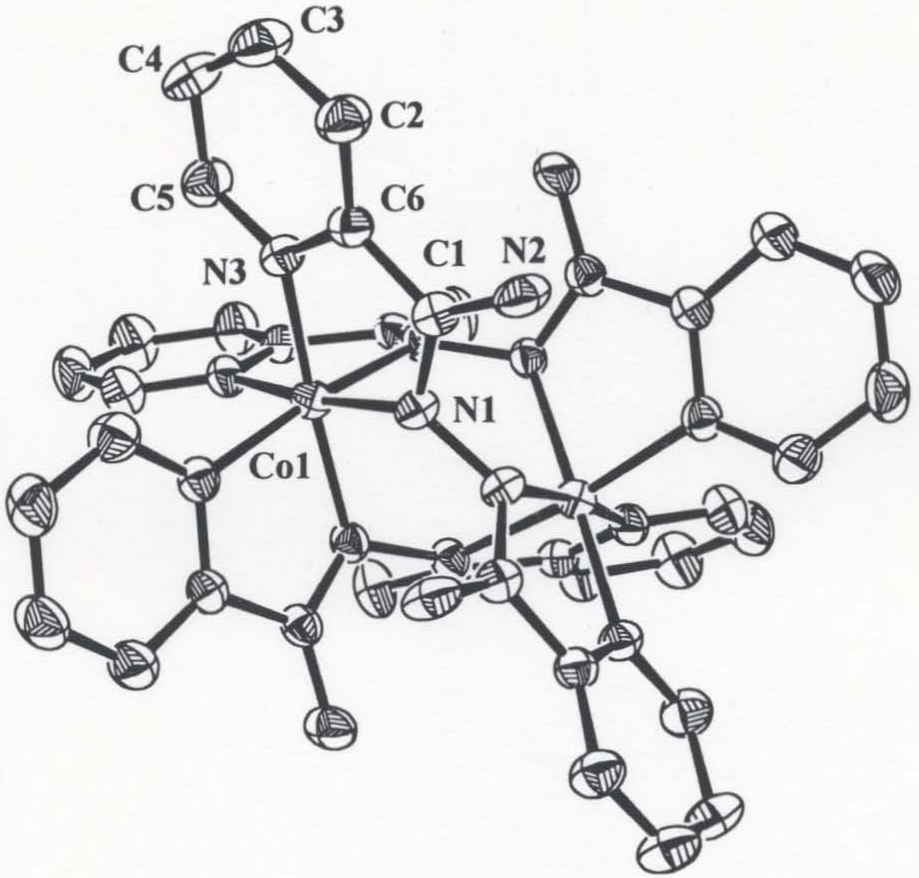

Figure 4-5. Structural representation of the dinuclear unit in $[Co_2(PAHAP)_3](NO_3)_6.3H_2O$ **(28)** (40% probability thermal ellipsoids).

$[Ni_2(PAHAP)_3][Ni(H_2O)_6](NO_3)_6.4.5H_2O$ (**29**)

Complex **29** consists of two metal fragments, a dinuclear cation, with a similar spiral twist to the other complexes, and the mononuclear cation $[Ni(H_2O)_6]^{2+}$. A structural representation for the cations is illustrated in **Figure 4-6**. Important bond distances and angles are listed in **Table 4-6.** Nickel-nitrogen bond angles in the dinuclear cation fall in the range 78.8-97.1°, indicating significant distortion of the nickel octahedra. The mononuclear cation $[Ni(H_2O)_6]^{2+}$ has an almost regular octahedral geometry (Ni-O 2.056(3) Å, O-Ni-O 89.24-90.75°). The Ni-Ni distance is 3.691(5) Å. The N-N distance (N(3)-N(3)') is 1.428(5) Å, and the C-N distances in the ligand framework (N(3)-C(6) 1.307(4) Å, N(2)-C(6) 1.325(4) Å) are very close to those in the free ligand, indicating single N-N bond character in the ligand bridge. The dihedral angles between the mean planes of the nickel chelate rings (70.1°) are close to those reported for the other complexes, in keeping with the relatively long Ni-N bonds and large range of angles at the nickel centres.

Table 4-6. Interatomic distances (Å) and angles (Deg.) relevant to the nickel coordination spheres and the ligand in $[Ni_2(PAHAP)_3][Ni(H_2O)_6](NO_3)_6.4.5H_2O$ (**29**).

Ni1-N1#1	2.063(3)	Ni1-N1	2.063(3)
Ni1-N1#2	2.063(3)	Ni1-N3	2.078(3)
Ni1-N3#1	2.078(3)	Ni1-N3#2	2.078(3)

contd.

Ni2-O1#3	2.056(3)	Ni2-O1#3	2.056(3)
Ni2-O1#4	2.056(3)	Ni2-O1#5	2.056(3)
Ni2-O1	2.056(3)	Ni2-O1#6	2.056(3)
Ni2-O1#7	2.056(3)	C5-C6	1.494(4)
C6-N3	1.307(4)	C6-N2	1.325(4)
N3-N3#8	1.418(5)		
N1#1-Ni1-N1	97.04(10)	N1#1-Ni1-N1#2	97.04(10)
N1-Ni1-N1#2	97.04(10)	N1-Ni1-N3	78.81(10)
N#2-Ni1-N3	168.76(10)	N1#1-Ni1-N3	93.85(10)
N1#1-Ni1-N3#1	78.81(10)	N1-Ni1-N3#1	168.76(10)
N1#2-Ni1-N3#1	93.85(10)	N1#3-Ni1-N3#1	90.98(10)
N1#1-Ni1-N3#2	168.76(10)	N1-Ni1-N3#2	93.85(10)
N1#2-Ni1-N3#2	78.81(10)	N3-Ni1-N3#2	90.98(10)
N3#1-Ni1- N3#2	90.98(10)	O1-Ni2-O1	89.26(10)
O1-Ni2-O1	90.74(10)	O1-Ni2-O1	180.0 19
N1-C5-C6	114.6(3)	C4-C5-C6	123.7(3)
N3-C6-N2	125.4(3)	N3-C6-C5	115.2(3)
N2-C6-C5	119.4(3)	C-N1-Ni1	127.2(2)
C5-N1-Ni1	113.9(2)	C6-N3-N3	116.7(3)
C6-N3-Ni1	113.9(2)	N3-N3-Ni1	119.56(11)

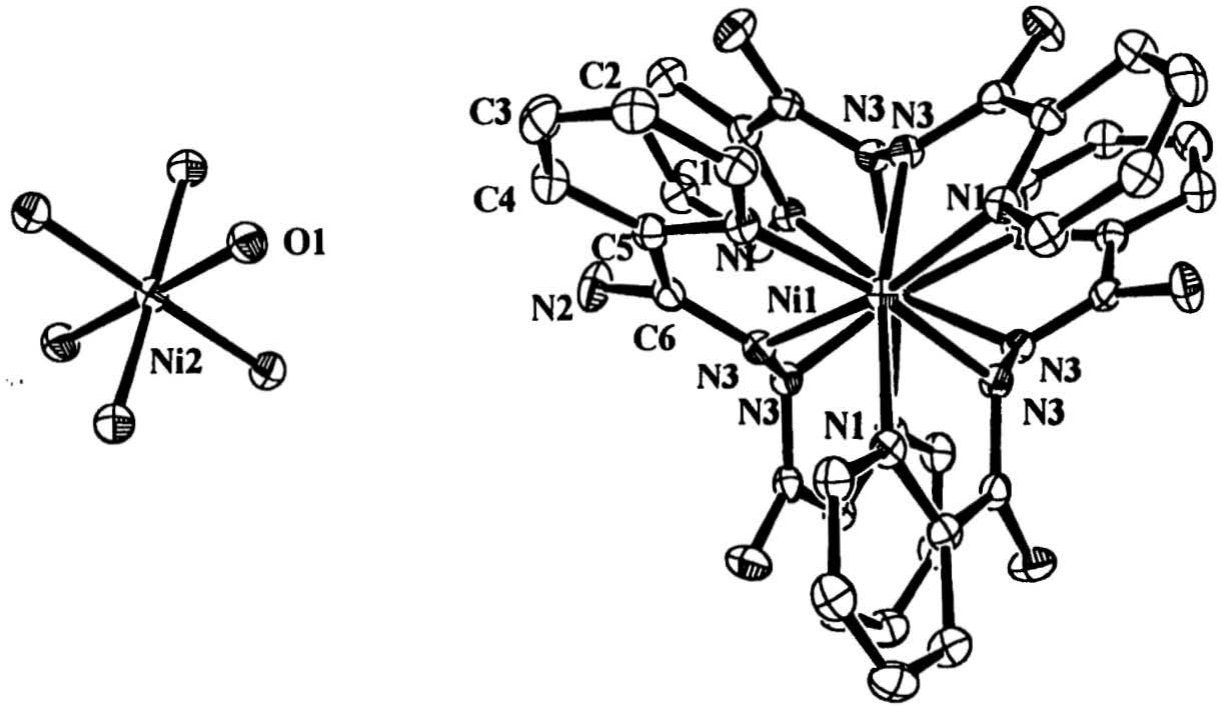

Figure 4-6. Structural representation of the dinuclear unit in $[Ni_2(PAHAP)_3][Ni(H_2O)_6](NO_3)_6.4.5H_2O$ (**29**) (40% probability thermal ellipsoids).

$[Fe(PHAAP)(H_2O)_2(NO_3)](NO_3)_2$ (**30**)

The structure of the mononuclear cation in **30** is illustrated in **Figure 4-7**, and important bond distances and angles are listed in **Table 4-7**. The ligand PHAAP has an OH group in place of one of the NH_2 groups present in PAHAP. The iron(III) center is seven-coordinate with the ligand acting as an N_2O donor. Oxygen O(1) is deprotonated. The presence of two 5-membered chelate rings provides a quite distorted environment in the equatorial plane of the iron(III) center (N(1)-Fe(1)-N(3) 72.24(7)°; N(3)-Fe(1)-O(1) 75.04(7)°), such that the chelating bidentate nitrate (N(6)) can be accommodated easily within this plane. The O(5)-Fe(1)-O(4) angle (58.30(6)°) is quite small, as would be expected, with the other two angles being comparable with those associated with PHAAP. Axial positions in the pentagonal bipyramid are occupied by two water molecules with quite short contacts (< 2.014 Å). A similar situation exists with other Fe(III) complexes of chelating ligands with adjacent five-membered chelate rings [161,162]. The five equatorial donors and the iron center are almost coplanar with < 0.08 Å displacement of any atom from the FeN_2O_3 least-squares plane. The ligand itself is almost flat, and adopts a pseudo-*trans* conformation with the uncoordinated pyridine ring pointing away from the iron center. The pyridine ring has a protonated nitrogen (N(5)), and this takes part in a hydrogen bonding interaction to nitrate oxygen O(12) (H(5N)-O(12) 2.04 Å; N(5)-H(5N)-O(12) 164°), which also is weakly hydrogen bonded to another hydrogen bonded to nitrogen N(2) (H(22N)-O(12) 2.38 Å; N(2)-H(22N)-O(12) 175°). This combination of hydrogen bonds effectively locks the pyridine in place creating the

trans-conformation (torsion angles N(4)-C(7)-C(8)-N(5) -2.9°, N(4)-C(7)-C(8)-C(12) 178°). Further hydrogen bonding contacts involving lattice nitrates and an axial water (O(2)) effectively dimerize the structure (**Figure 4-8**), and an additional hydrogen bonding contact via water O(3) links the dimers in a chain in the *a* direction (**Figure 4-9** and **Table 4-8**).

The presence of uncoordinated nitrogen donor sites, and an alkoxo-oxygen provide the potential for additional coordination capacity, and this has been used to advantage in a most unusual reaction of **30** with copper perchlorate to produce a tetranuclear complex (see **Chapter 5**) with a roughly rectangular arrangement of three copper(II) centres and one iron(III) center linked by alkoxide bridges (*vide supra*).

Table 4-7. Interatomic distances (Å) and angles (Deg.) relevant to the iron coordination spheres and the ligand in $[Fe(PHAAP)(H_2O)_2(NO_3)](NO_3)_2$ (**30**).

Fe(1)-O(2)	2.009(2)	Fe(1)-O(3)	2.013(2)
Fe(1)-O(1)	2.018(2)	Fe(1)-N(3)	2.052(2)
Fe(1)-O(5)	2.163(2)	Fe(1)-O(4)	2.228(2)
Fe(1)-N(1)	2.250(2)	C(6)-N(3)	1.306(3)
C(6)-N(2)	1.323(3)	C(7)-O(1)	1.293(3)

contd.

C(7)-N(4)	1.303(3)	C(7)-C(8)	1.482(3)
N(2)-H(21N)	0.82(3)	N(2)-H(22N)	0.86(3)
N(3)-N(4))	1.395(3)	N(5)-H(5N)	0.82(3)

O(2)-Fe(1)-O(3)	172.97(9)	O(2)-Fe(1)-O(1)	91.17(8)
O(3)-Fe(1)-O(1)	93.69(8)	O(2)-Fe(1)-N(3)	95.44(8)
O(3)-Fe(1)-N(3)	90.71(9)	O(1)-Fe(1)-N(3)	75.04(7)
O(2)-Fe(1)-O(5)	88.44(8)	O(3)-Fe(1)-O(5)	84.53(8)
O(1)-Fe(1)-O(5)	133.65(7)	N(3)-Fe(1)-O(5)	151.09(7)
O(2)-Fe(1)-O(4)	88.93(8)	O(3)-Fe(1)-O(4)	87.40(8)
O(1)-Fe(1)-O(4)	75.34(7)	N(3)-Fe(1)-O(4)	150.13(7)
O(5)-Fe(1)-O(4)	58.30(6)	O(2)-Fe(1)-N(1)	88.86(8)
O(3)-Fe(1)-N(1)	89.80(8)	O(1)-Fe(1)-N(1)	147.13(7)
N(3)-Fe(1)-N(1)	72.24(7)	O(5)-Fe(1)-N(1)	79.22(7)
O(4)-Fe(1)-N(1)	137.51(7)		

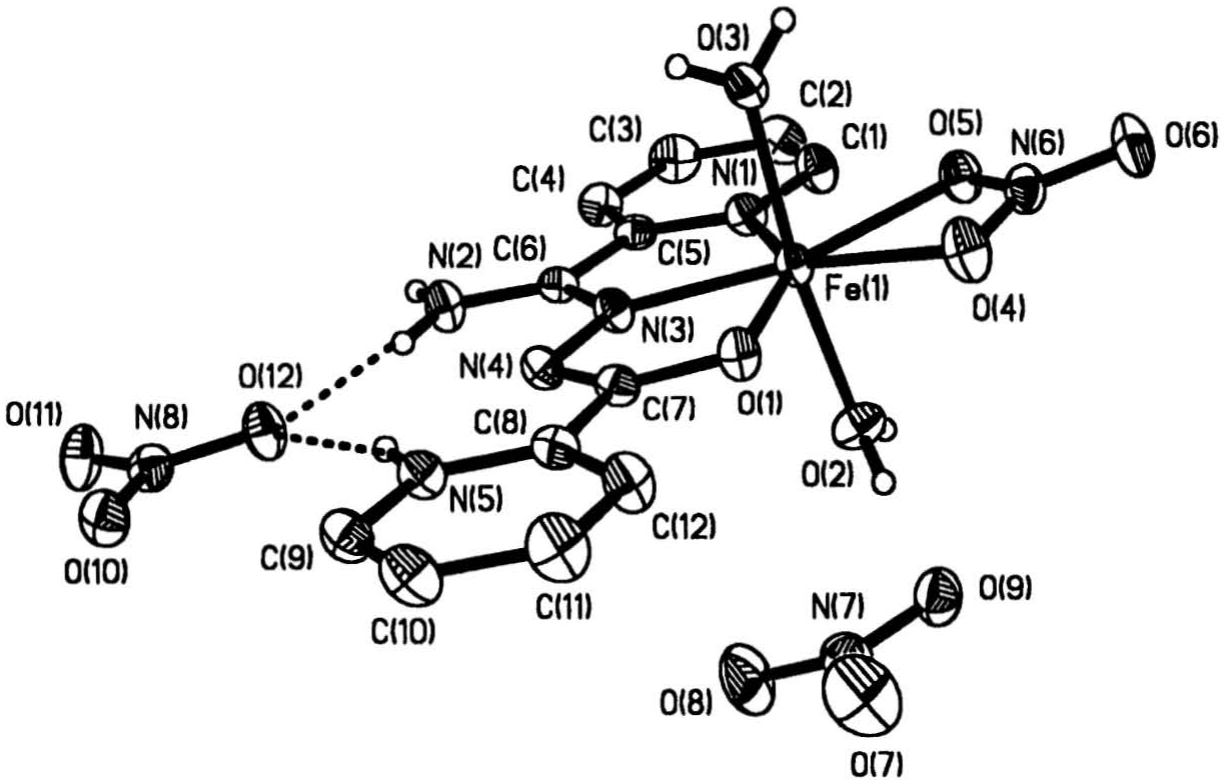

Figure 4-7. Structural representation of $[Fe(PHAAP)(H_2O)_2(NO_3)](NO_3)_2$ **(30)** (40% probability thermal ellipsoids).

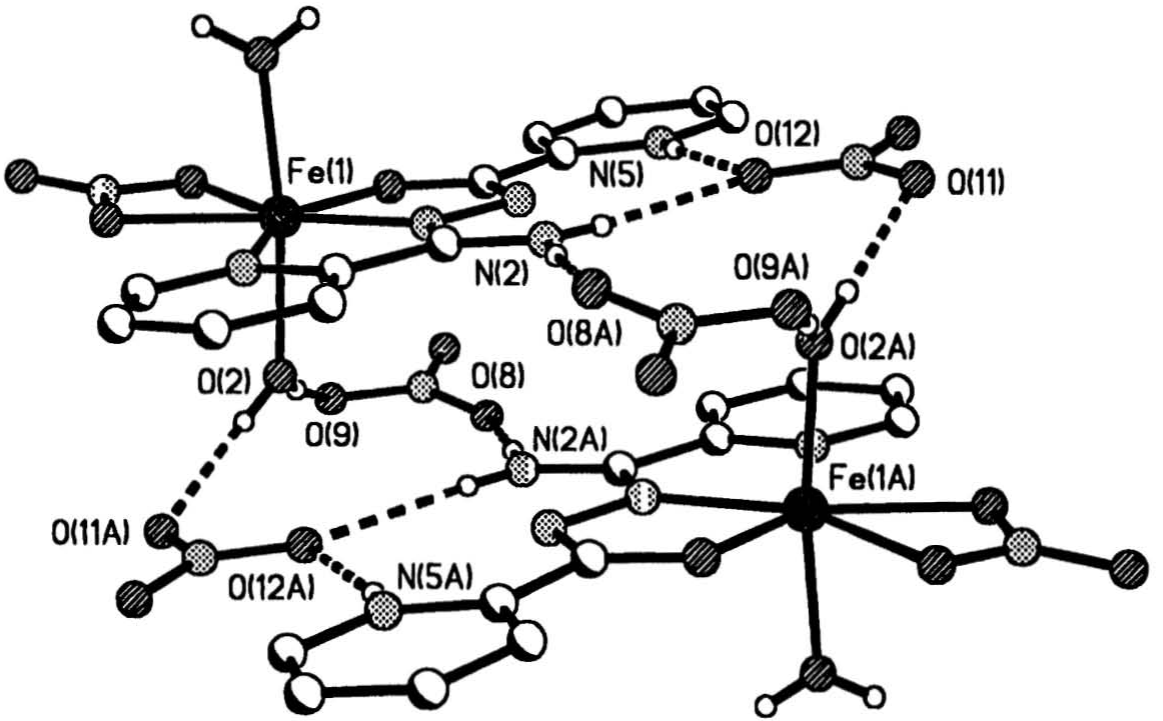

Figure 4-8. Hydrogen bonding network in $[Fe(PHAAP)(H_2O)_2(NO_3)](NO_3)_2$ **(30)**.

Table 4-8. Hydrogen bonding distances (Å) and angles (Deg.) in $[Fe(PHAAP)(H_2O)_2(NO_3)](NO_3)_2$ **(30)**.

N(5)-O(12)	2.836(3)	H(5N)-O(12)	2.042(29)
N(2)-O(12)	3.242(3)	H(22N)-O(12)	2.380(29)
N(2)-O(8A)	2.953(3)	H(21N)-O(8A)	2.133(30)
O(2)-O(9)	2.630(3)	H(21W)-O(9)	1.816(33)
O(2)-O(11A)	2.671(3)	H(22W)-O(11A)	1.869(37)
O(3)-O(10B)	2.762(3)	H(32W)-O(10B)	2.015(37)
O(3)-O(9C)	2.686(3)	H(31W)-O(9C)	1.870(36)
N(5)-H(5N)-O(12)	163.64(2.75)	N(2)-H(22N)-O(12)	174.72(2.44)
N(2)-H(21N)-O(8A)	176.52(2.65)	O(2)-H(21W)-O(9)	171.72(3.12)
O(2)-H(22W)-O(11A)	178.02(3.33)	O(3)-H(32W)-O(10B)	164.02(3.58)
O(3)-H(31W)-O(9C)	170.96(3.16)		

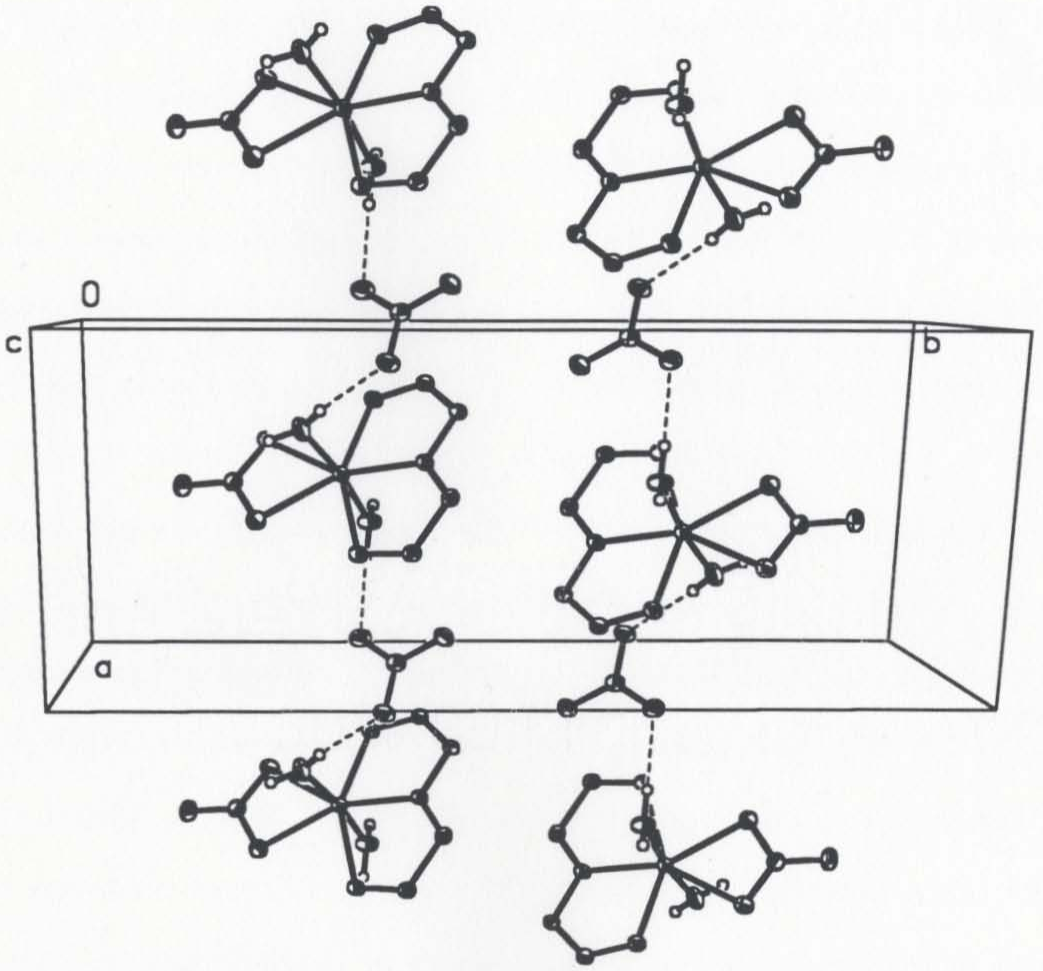

Figure 4-9. Chain structure of [Fe(PHAAP)$(H_2O)_2(NO_3)$] $(NO_3)_2$ **(30)** in the *a* direction.

4.3.2 Synthesis

PAHAP closely resembles PAA and PMK in terms of its coordinating ability, and the spiral dinuclear complexes of PAHAP are very similar in structure to the only previously reported example which contains the cation $[Co_2(PMK)_3]^{4+}$. It is reasonable to assume that other related complexes of PMK and PAA have similar spiral structures. Previous reports on iron and cobalt complexes of PAA and PMK involve reactions of Fe(II) only, and in the case of Co(II) air was excluded in the syntheses, preventing any oxidation to Co(III). In the present study all reactions were conducted in air, with the exception that PAHAP reacted with $Co(ClO_4)_2.6H_2O$ under nitrogen, and in the case of iron both Fe(II) and Fe(III) salts were used in the syntheses.

Reaction of iron(III) nitrate with both PAHAP and PZHPZ in aqueous solution led to spontaneous reduction over several days with the formation of low yields of $[Fe_2(L)_3]^{4+}$ (L = PAHAP, PZHPZ). This suggests that a reducing medium is formed through hydrolysis of the ligand. The discovery of the mononuclear Fe(III) complex **30**, which contains the ligand PHAAP, indicates that in addition a small proportion of the ligand PAHAP itself undergoes a different hydrolytic process. Fe(II) complexes of PAA, e.g. $[Fe_2(PAA)_3]^{4+}$, are unstable in aqueous solution, and have been shown to decompose rapidly with the formation of the species $[Fe(PAH)_3]^{2+}$ (PAH = 2-pyridinalhydrazone) and 2-pyridinealdehyde. In fact the complex cation $[Fe_2(PAA)_3]^{4+}$ could only be stabilized as a solid by rapid addition of excess iodide to the aqueous solution. Further evidence for the

solution decomposition of $[Fe_2(PAA)_3]^{4+}$ was obtained from magnetic measurements, which showed that the low spin dinuclear complex was transformed into a high spin Fe(II) solution species [77].

The spontaneous reduction of Fe(III)/PAHAP and Fe(III)/PZHPZ solutions can be understood in terms of a simple hydrolysis of the coordinated ligand e.g. PAHAP, to produce picolinamide hydrazone (starting material for the synthesis of PAHAP), which would have significant reducing ability. Preliminary coordination of Fe(III) to a diazine nitrogen would enhance such attack by water by making the adjacent carbon more electrophilic. The low yields of **26** and **27** suggest that some ligand is sacrificed to reduce Fe(III) to Fe(II) and produce the dinuclear Fe(II) complex of the remaining PAHAP and PZHPZ. The explanation for the formation of the mononuclear Fe(III) complex **30** and dinuclear Fe(III) **31** can be made as follows (**Figure 4-10**): In the preliminary complex $[Fe(III)(PAHAP)_3]^{3+}$, Fe(III) acts as a Lewis acid to catalyze the hydrolysis process. The bond breaking could happen either by route A-B, or A-C. In the presence of nitrate, the A-B route leads to the formation of **30,** while the A-C route generates an intermediate Fe(III) picolinamide hydrazone complex, which will be reduced to an Fe(II) species quickly, due to the strong reducing property of picolinamide hydrazone. These Fe(II) species then react with free PAHAP to produce **26**. If the Fe(III) perchlorate salt is used, a reasonably stable dinuclear Fe(III) complex (**31**) is obtained which has much lower solubility in aqueous solution, and so it precipitates before any significant hydrolysis and reduction can occur.

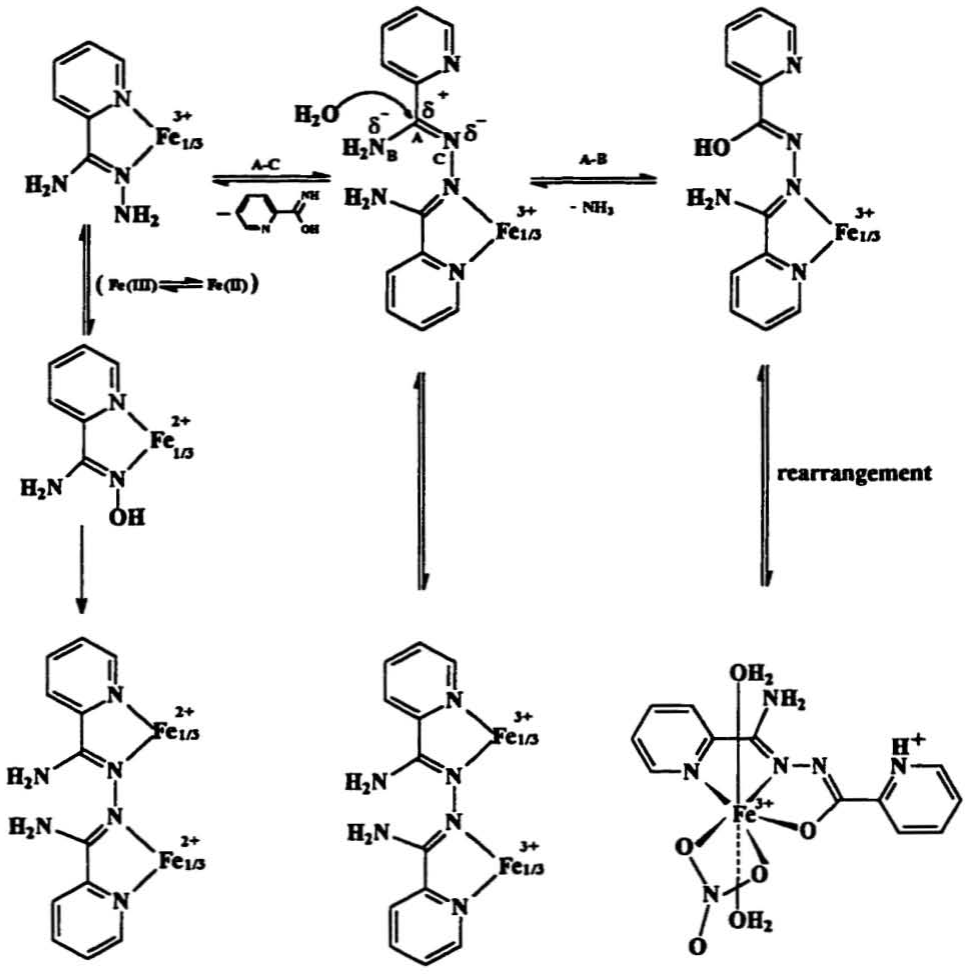

Figure 4-10. Schematic representation of the reaction of PAHAP with $Fe(NO_3)_3.9H_2O$ in water.

The formation of the Co(III) complex **28** under similar conditions in rather low yield indicates the instability of Co(II) PAHAP systems to oxidation (cobalt(II) derivatives of PAA and PMK were prepared under a nitrogen atmosphere), but thus far there is no evidence for ligand hydrolysis. It seems reasonable to assume in this case that the oxidation step, common in cobalt(II) chemistry, occurs through the prior formation of a 1:2 or 2:2 (ligand:metal) intermediate complex leaving vacant coordination sites for interaction with O_2, with the subsequent formation of the stable spiral complex.

To test this, the Co(II) spiral dinuclear complex **32** was prepared by the reaction of PAHAP with $Co(ClO_4)_2.6H_2O$ in aqueous solution under a nitrogen atmosphere. This complex is stable both in the solid state (checked with room temperature magnetic moment and UV/vis) and in aqueous solution (UV/vis) indicating that the spiral dinuclear Co(II) complex cannot be easily oxidized by air. In other words, the formation of the dinuclear Co(III) complex may occur only from the initial reaction of the ligand and metal salt. The formation of a Co(III) dinuclear complex also implies that the ligand PAHAP has less reducing ability than PAA or PMK.

4.3.3 Spectroscopy electrochemistry and magnetism

Infrared and UV/vis spectral, and room temperature magnetic moment data of complexes **23-32** are quoted in **Table 4-9**.

The infrared spectra of all the compounds show high energy absorptions (> 3200 cm^{-1}) associated with lattice and coordinated water, and the NH_2 groups. ν_3 perchlorate

Table 4-9. Infrared and UV/vis spectral and room temperature magnetic moment data of complexes **23-32**.

compound	IR (cm^{-1})	UV/vis (nm)	μ_{RT} (BM)
$[Mn_2(PAHAP)_3](ClO_4)_4.5H_2O$ **(23)**	3600(H_2O), 3360,3280,3180(NH_2),1657(C=N), 1078(ClO_4^-), 1014(Py)	-	6.0
$[Fe_2(PAHAP)_3](ClO_4)_4.4H_2O$ **(24)**	3580(H_2O), 3340,3202(NH_2), 1657(C=N), 1164(ClO_4^-)	641(solid) 532(ε, 5200), 374(ε, 3600)[a]	0.93
$[Ni_2(PAHAP)_3](ClO_4)_4.5H_2O$ **(25)**	3550(H_2O), 3370,3300,3210(NH_2), 1659(C=N), 1087(ClO_4^-), 1021(Py)	820, 890(sh), 546 (solid) 823(ε, 222.8), 890(sh), 545(ε, 172.4)[a]	3.07
$[Fe_2(PAHAP)_3](NO_3)_4.3H_2O$ **(26)**	3550(sh, H_2O), 3362,3331,3193(NH_2), 1656(C=N), 1753(NO_3^-), 1027(Py)	570(solid) 532(ε, 5000), 550(sh), 380(ε, 3560), 420(sh)[a]	0.71
$[Fe_2(PZHPZ)_3](NO_3)_4.5H_2O$ **(27)**	3500(sh. H_2O), 3375,3317,3178(NH_2), 1659(C=N), 1764(NO_3^-), 1040(Pyr)	635(solid) 411, 581[a]	0.69
$[Co_2(PAHAP)_3](NO_3)_6.3H_2O$ **(28)**	3600(sh, H_2O), 3375,3250,3180(NH_2), 1667(C=N), 1032(Py)	550(solid and aqueous solution)	0.71
$[Ni_2(PAHAP)_3][Ni(H_2O)_6](NO_3)_6.$ $4.5H_2O$ **(29)**	3530(sh, H_2O), 3367,3175(NH_2), 1649(C=N), 1764(NO_3^-), 1020(Py)	814, 890(sh), 550 (solid) 815(ε,106),545(ε, 69)[a]	3.10
$[Fe(PHAAP)(H_2O)_2(NO_3)]$ $(NO_3)_2$ **(30)**	3480(H_2O), 3380,3250,3180(NH_2), 1664(C=O), 1794,1774,1763,1703(NO_3^-), 1035,1009(Py)	630(solid) 634(ε, 900)[a]	6.0
$[Fe_2(PAHAP)_3](ClO_4)_6.4.5H_2O$ **(31)** 1089(ClO_4^-), 1013(Py)	3558(H_2O), 3355,3178(NH_2), 1658(C=N), b	645, 540(sh)	4.70
$[Co_2(PAHAP)_3](ClO_4)_4.5.5H_2O$ **(32)**	3583(H_2O), 3336,3200,3120(NH_2), 1658(C=N) 1092(ClO_4^-), 1018(Py)	962 (solid) 960 (ε, 25.93)[a]	4.35

Note: [a], measured in aqueous solution, ε, $dm^3.mol^{-1}.cm^{-1}$; [b], essentially the same as those for **26**.

absorptions associated with ClO_4^{-1} are found at 1078 cm^{-1} in **23**, 1164 cm^{-1} in **24**, 1089 cm^{-1} in **31**, 1090 cm^{-1} in **25**, 1088 cm^{-1} in **32**, and $\nu_1 + \nu_4$ nitrate combination bands associated with free nitrate are found at 1753 cm^{-1} (**26**), 1765 cm^{-1} (**27**), and 1764 cm^{-1} (**28**), while for **30** three prominent bands are found at 1794, 1774 and 1703 cm^{-1} associated with bidentate and ionic nitrate [112].

Solid state electronic spectra for the iron(II) complexes are dominated by intense low energy charge transfer absorptions in the range 560-650 nm (570 nm (**26**), 565 nm (**24**), 641 nm (**27**)). The iron(III) complex (**31**) has a slightly longer wavelength absorption than **26** and **24** (645, 540 (sh) nm). In aqueous solution **26** and **24** have identical spectra, with major absorptions at 532 nm (ε = 5200 $dm^3.mol^{-1}.cm^{-1}$), 580 nm, (sh), 374 nm (3600 $dm^3.mol^{-1}.cm^{-1}$) and 420 nm (sh) (comparable spectra are obtained in DMF). The general similarity in the solid state and solution spectra for **26** and **24** suggests that the spiral dinuclear cation retains its integrity in solution. The aqueous solution spectra remain essentially unchanged over an extended period of time (days), suggesting that the hydrolytic instability which characterizes the comparable PAA systems does not occur significantly with the Fe(II) PAHAP complexes.The longer wavelength charge transfer absorption for **27** in the solid state indicates the effect of replacing pendant pyridine with pyrazines, consistent with metal to ligand charge transfer as the origin of this absorption. In aqueous solution similar shifts to lower energy are observed (580 nm, 411 nm).

Complex **31** dissolves in water to give a brown solution, which gradually becomes purple on standing over a period of several days. Initial broad bands at $\approx$ 550 nm and 360

nm in aqueous solution change in relative intensity with the 550 nm band increasing and the 360 nm band decreasing to be replaced exactly by the characteristic bands associated with the iron(II) complex. The suggested mechanism (**Figure 4-10**) for reduction involves ligand hydrolysis presumably to form mononuclear Fe(II) intermediates, but the intense charge transfer bands of both the Fe(III) and Fe(II) dinuclear complexes precludes the observation of such species which are likely to be weaker absorbers in this spectral region. **28** has a broad shoulder absorption in the solid state at ≈ 550 nm , associated with a spin allowed transition in low spin Co(III) ($^1A_{1g} \rightarrow {}^1T_{1g}$), which appears essentially unchanged in aqueous solution. Complex **29** shows two solid state *d-d* absorption

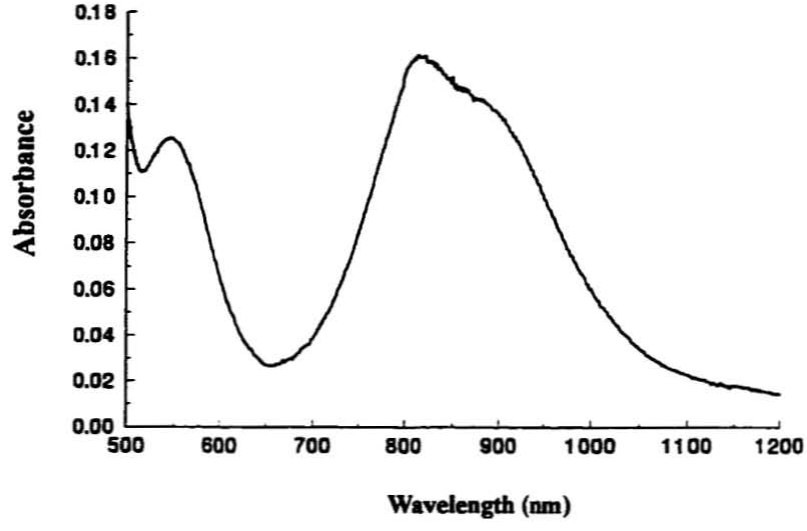

Figure 4-11. UV-visible spectrum of $1.74*10^{-3}$ mol.L^{-1} solution of **29** in H_2O

envelopes centred at 852 nm, and 550 (sh) nm (or $11.8*10^3$ cm^{-1} and $18.4*10^3$ cm^{-1}). Using an octahedral model these absorptions can be associated with the ν_1 ($^3A_{2g} \rightarrow {}^3T_{2g}$) and ν_2

($^3A_{2g} \rightarrow {}^3T_{1g}$) transitions respectively. The splitting of ν_1 may be associated with a lowering of the octahedral symmetry, or a spin forbidden transition. These band positions compare closely with those for $[Ni(dipy)_3]^{2+}$ [163]. The aqueous solution spectrum is essentially identical, with quite high extinction coefficients (900 nm (ε = 75 $dm^3.mol^{-1}.cm^{-1}$); 815 nm (ε = 106 $dm^3.mol^{-1}.cm^{-1}$); 545 nm (ε = 69 $dm^3.mol^{-1}.cm^{-1}$)), indicating that the weakly absorbing $[Ni(H_2O)_6]^{2+}$ cation would not appear significantly in the spectrum. A strong charge transfer band is also found at 305 nm ($\varepsilon = 2.4*10^4$ $dm^3.mol^{-1}.cm^{-1}$), which covers the ν_3 ($^3A_{2g} \rightarrow {}^3T_{1g}$) transition band at 345.2 nm calculated from **eqn. 4-1** to **4-3** [164] .

$$\nu_1 = \Delta_0 = 11.8*10^3 \ (cm^{-1}) \quad \text{.....[4-1]}$$

$$\nu_2 \ B = 18.4*10^3 \ (cm^{-1}) = 3/2\Delta_0 + 15/2B - 1/2[(15B)^2 - 18\Delta_0 B + \Delta_0^2]^{1/2} \quad \text{.....[4-2]}$$

$$\nu_3 \ B = 3/2\Delta_0 + 15/2B + 1/2[(15B)^2 - 18\Delta_0 B + \Delta_0^2]^{1/2} \quad \text{.....[4-3]}$$

The calculations based on the **eqn. 4-1** to **4-3** also give B as 800 cm^{-1} for complex **28**, which implies that PAHAP produces a very strong ligand field for Ni(II). **25** has an identical spectrum, both in the solid state and in solution, except that the aqueous solution absorption intensities are higher, as would be expected.

Complex **30** has a strong absorption at 630 nm in the solid state, and a dark green colored aqueous solution of the complex has an intense single band at 634 nm (ε = 990 $dm^3.mol^{-1}.cm^{-1}$), which is clearly charge transfer in nature. This complex shows no tendency to reduce, unlike its parental counterpart.

The fact that **31** is reduced slowly in aqueous solution to a more stable dinuclear Fe(II) species, with no tendency for spontaneous re-oxidation prompted us to examine the

redox properties of complex **26** (**Figure 4-12**). Cyclic voltammetry for an aqueous solution of **26** (Pt counter electrode, glassy carbon working electrode, SCE reference electrode, 0.1 M $NaNO_3$, 10^{-3} M complex) reveals two well separated waves ($E_{1/2}(1)$ = 0.16 V [ΔE_p = 70 mV (25 mVs^{-1})]; $E_{1/2}$ (2) = 0.38 V [ΔE_p = 70 mV (25 mVs^{-1})], which show very little change as a function of scan rate. The redox processes are associated with two one-electron oxidation steps, with the formation of Fe(II)-Fe(III) and Fe(III)-Fe(III) species by what are essentially reversible processes. This clearly indicates the stability of the spiral dinuclear cation in aqueous solution in two oxidation states, during the lifetime of the experiment. Current heights for the anodic and cathodic components of these waves are equal.

The low spin Co(III) complex **28** was examined electrochemically under the same conditions as for **26**, and exhibits two sets of waves around 0 V associated with Co(II) and Co(III) species (**Figure 4-13**). A weak quasi-reversible wave (some variation of ΔE_p with scan rate) at $E_{1/2}$ = 0.1 V (ΔE_p = 100 mV at 25 mVs^{-1}) is associated with the formation of a Co(II)-Co(III) species, while a similar wave at $E_{1/2}$ = -0.050 V (ΔE_p = 100 mV) corresponds to the formation of the fully reduced Co(II)-Co(II) species. Current heights for the anodic and cathodic components of the second wave are equal. It is reasonable to assume that the integrity of the dinuclear cation is maintained during the redox process. Electrochemical investigations of the dimanganese(II) and dinickel(II) species were unsuccessful, and at the high potentials necessary to see electrochemical activity ligand oxidation was beginning to occur.

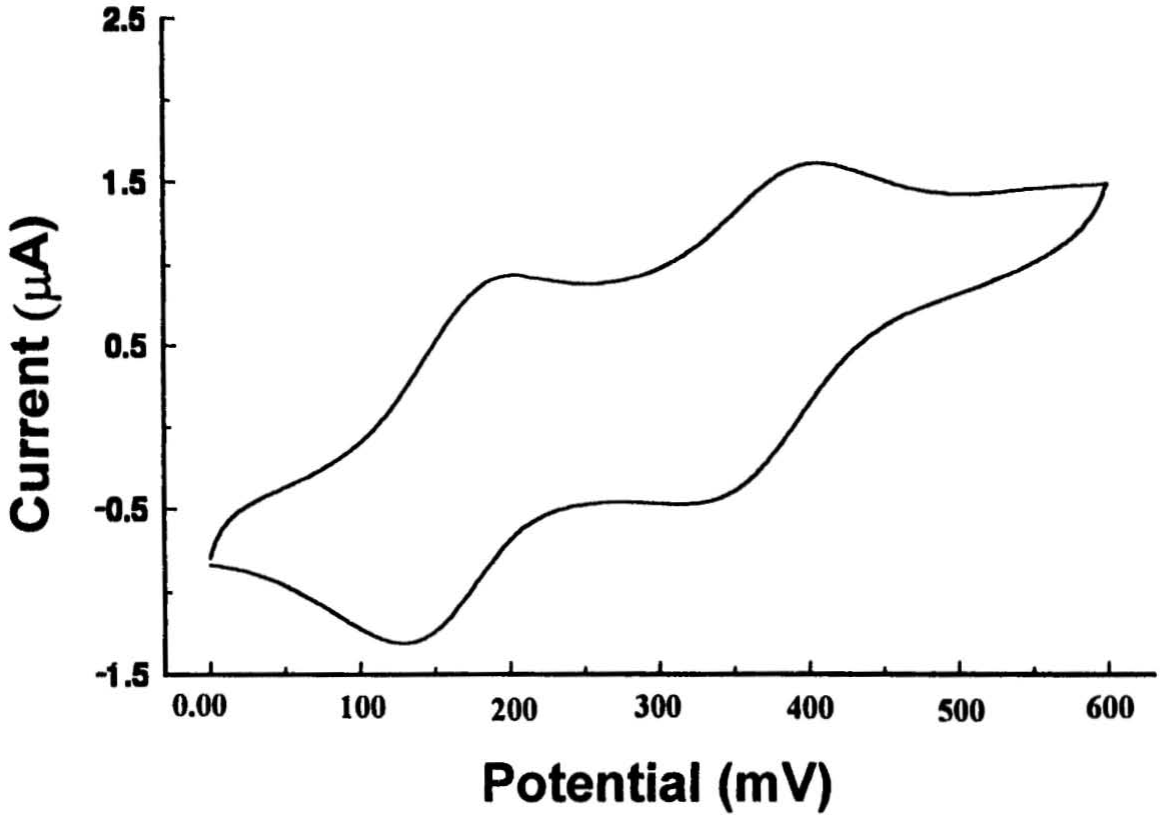

Figure 4-12. Cyclic voltammograms for complex **26** ($GC/H_2O/Pt/NaNO_3$.

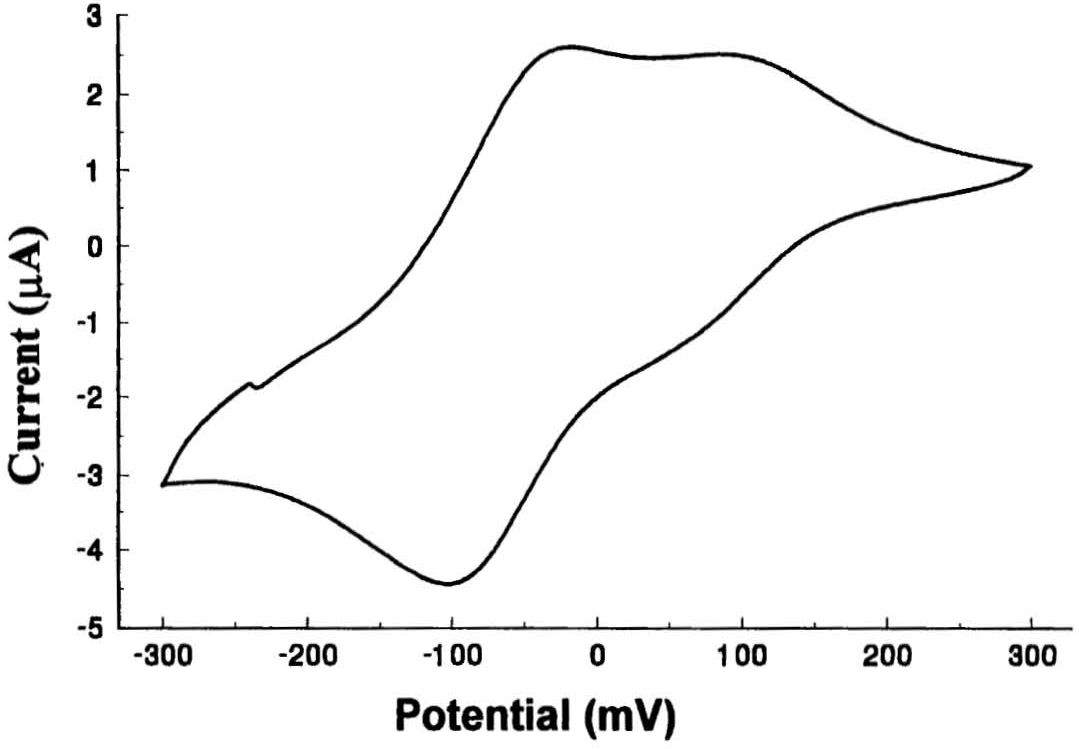

Figure 4-13. Cyclic voltammograms for complex **28** ($GC/H_2O/Pt/NaNO_3$).

Room temperature magnetic moments were determined for all compounds. A high value (μ_{RT} = 6.0 BM) consistent with the presence of high spin manganese(II) centers was found for **23**. The iron(II) complexes are all low spin (μ_{RT} = 0.71 BM (**26**), 0.93 BM (**24**), 0.69 BM (**27**)), while the iron(III) complex **31** has a high value (μ_{RT} = 4.70 BM). This value is smaller than the spin only value for five unpaired electrons and may indicate the presence of antiferromagnetic coupling or a spin transition phenomenon. However, what is more likely is that, since the Fe(III)/PAHAP system is inherently unstable (*vide infra*), the complex is somewhat unstable, even in the solid state, and contains a small amount of a low spin Fe(II) complex, either as a Fe(II)-Fe(II) species or possibly a Fe(II)-Fe(III) species. The low value for **28** (μ_{RT} = 0.71 BM) is consistent with low spin cobalt(III). The nickel(II) complexes have magnetic moments close to the expected values for uncoupled Ni(II) centers (μ_{RT}= 3.05 BM (**25**), μ_{RT} =3.10 BM (**29**)).

Variable temperature magnetic studies were carried out on powdered samples of **23** (13-300K) and **29** (4-300K). The χ_m*T profile for **23** shows an unusual temperature dependence (**Figure 4-14**) with χ_m*T rising from 4.66 emu.mol^{-1}.K at 296 K to a maximum at 40 K of 5.1 emu.mol^{-1}.K, and then falling rapidly to 4.25 emu.mol^{-1}.K at 13 K. This behavior is typical of a ferromagnetically coupled system, but the drop in χ_m*T at low temperature suggests the presence of an antiferromagnetic component in the total spin exchange. The data were fitted to an isotropic exchange expression for two S =5/2 spin

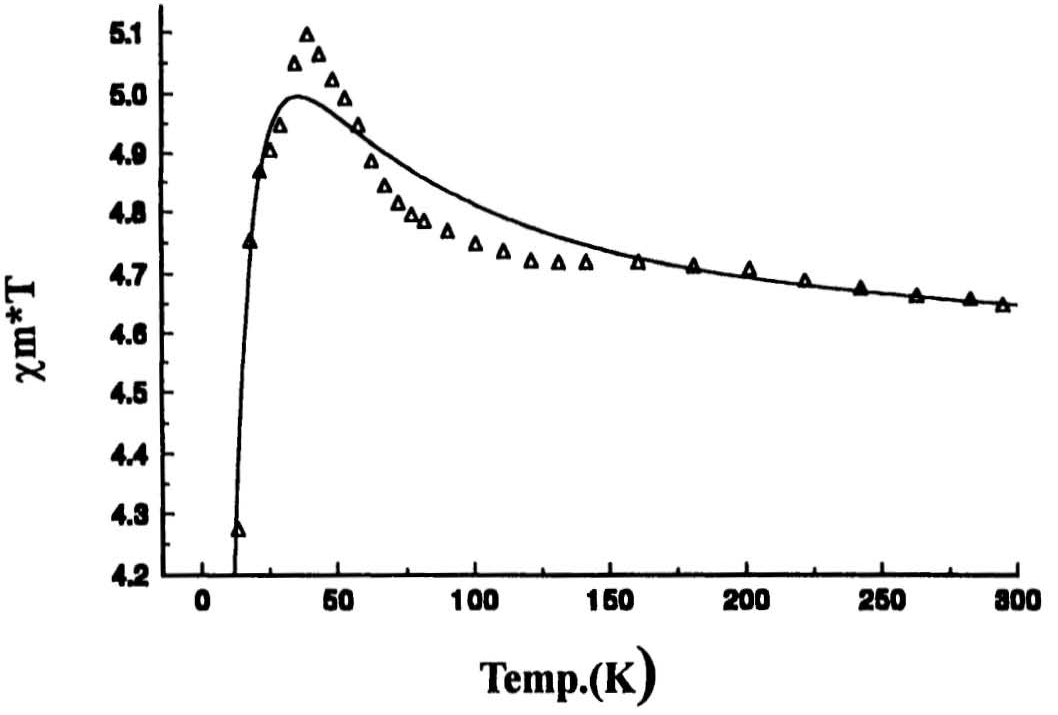

Figure 4-14. Variable temperature magnetic susceptibility data for $[Mn_2(PAHAP)_3](ClO_4)_4.5H_2O$ (**23**). The best fit solid line was obtained from **eqn. 4-4**, with g = 2.029(6), 2J = 2.08(8) cm^{-1}, $N\alpha = 18*10^{-6}$ emu, $\rho = 0.0116$, θ = -9.6 K, $10^2R = 0.95$ ($R = [\Sigma(\chi_{obs}-\chi_{calc})^2/ \Sigma \chi_{obs}]^{1/2}$).

states [7] derived from the exchange Hamiltonian:

$$\mathbf{H = -2JS_1.S_2}$$

$$\chi_m = [\frac{Ng^2\beta^2}{k(T-\theta)} * \frac{A}{B}] * (1-\rho) + \frac{\rho * 1.094 * g^2}{T} + N\alpha \quad \text{.....[4-4]}$$

$A = x^{28} + 5x^{24} + 14x^{18} + 30x^{10} + 55$; $B = x^{30} + 3x^{28} + 5x^{24} + 7x^{18} + 9x^{10} + 11$;

$x = -J/kT$

χ_m is the magnetic susceptibility per metal center and other terms have their usual meaning (ρ = fraction of mononuclear impurity). The best data fit (**Figure 4-14**) was obtained for g = 2.029(6), 2J = 2.08(8) cm^{-1} , $N\alpha = 18*10^{-6}$ emu, $\rho = 0.0116$, $\theta = -9.6$K, $10^2R = 0.95$ ($R = [\Sigma(\chi_{obs}-\chi_{calc})^2/\Sigma\ \chi_{obs}^2]^{1/2}$). Variable temperature magnetic data for **25** indicate no significant magnetic interaction between the nickel(II) centers. The χ_m*T values are temperature invariant (1.2 $emu.mol^{-1}.K$) from 296-10 K, with a very slight increase at lower temperature, suggesting a possible weak intermolecular interaction. No fitting of these data was attempted.

From a structural perspective any intramolecular spin interaction between the metal centers would be dependent on magnetic orbital overlap via the bridging N_2 diazine linkage. This is clearly inconsequential for the low spin systems, but for **23** and **25** interactions via t_{2g} and e_g orbitals are magnetically active (assuming an octahedral model). In a previous study (**Chapter 1** and **2**) the twist angle around the bridging N-N group was found to be a critical factor in exchange propagation between the copper(II) magnetic orbitals and ferromagnetic coupling was achieved at twist angles around 70°, which was

directly related to effective orthogonality between the nitrogen *p* orbitals involved. The average twist angle between the manganese chelate rings (Mn-$N_{diazine}$-C-C-N_{pyr}) for the same ligand was found to be 67.8°, very close to the orthogonal limit found in the dicopper(II) case, and clearly reasonable in terms of the weak ferromagnetism observed for **23**. The significant negative θ value indicates a weak intermolecular antiferromagnetic interaction. The only way that such an interaction could take place is *via* the NH_2 groups of the ligand, which are poised appropriately with respect to the Mn orbitals via a flat ligand portion (N=C-NH_2). Significant hydrogen bonding contacts are found linking N(7) and N(8) in neighboring molecules to water molecules O(91) and N(7) and N(9) to perchlorate oxygens O(6) and O(7). The connection N(7)-O(7)-C1(2)-O(6)-N(9) provides a rather long, but potentially viable route for such an interaction.

Although no structural data are available for **25** it is reasonable to assume that the dinuclear center dimensions are similar to those of the same cation in **29**. In this complex the dihedral angles between the Ni-$N_{diazine}$-C-C-N_{pyr} mean planes are 70.1°, clearly indicating an exchange situation close to the point of orthogonality for the nitrogen *p* orbitals in the N-N bridge. The apparent lack of coupling in **25** is entirely consistent with this structural extrapolation.

^{1}H NMR studies on **26** and **28** were carried out either in d_6-DMSO or in D_2O with the same results. The room temperature ^{1}H NMR spectrum of the free ligand PAHAP in d_6-DMSO is illustrated in **Figure 4-15**, and those of the complexes **26** and **28** in D_2O are

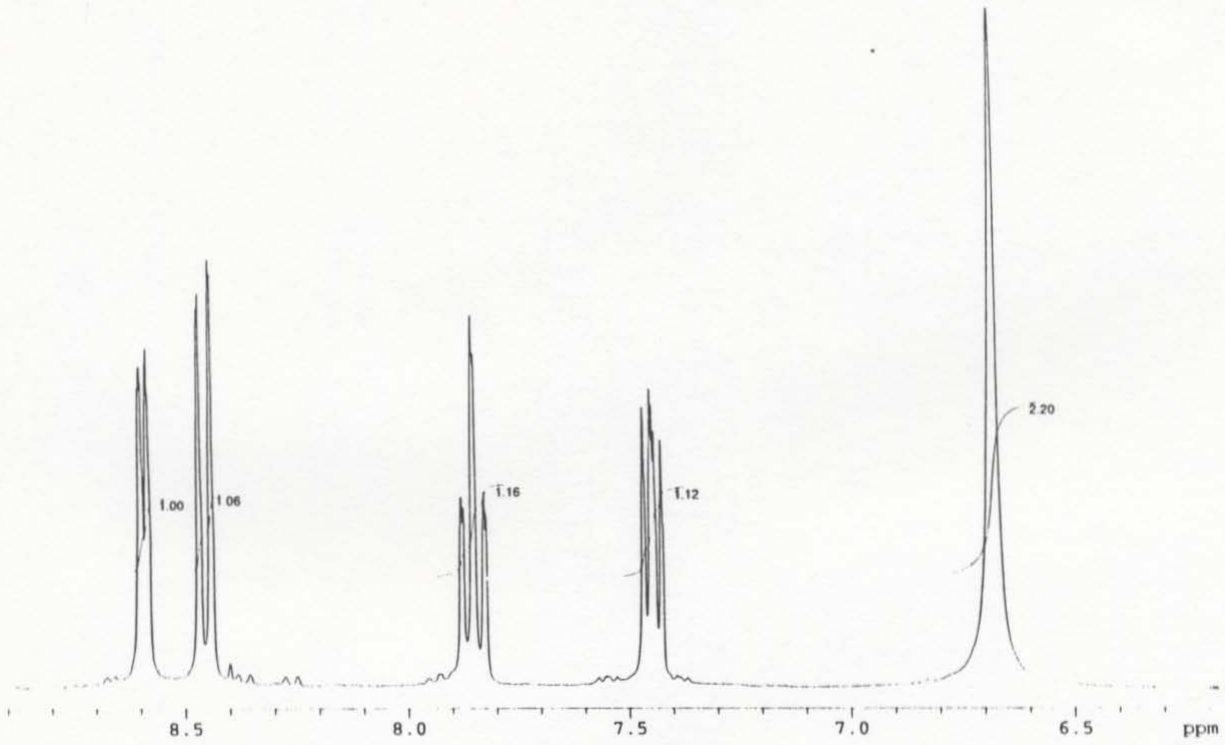

Figure 4-15. Room temperature ^{1}HNMR spectrum of PAHAP in d_6-DMSO.

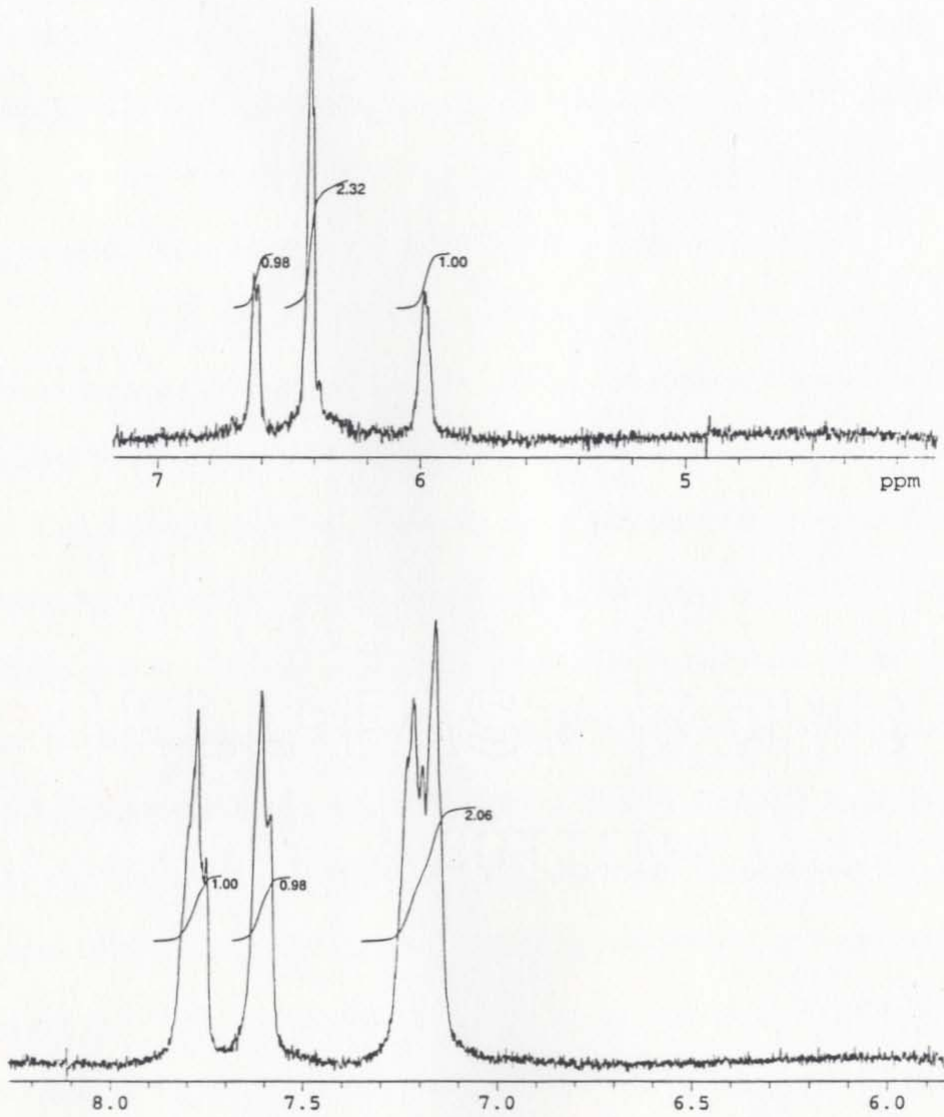

Figure 4-16. Room temperature ^{1}H NMR spectrum of complex **26** (up) and **28** (down) in D_2O.

depicted in **Figure 4-16**. The signal due to the free amino NH_2 groups does not show up because of H-D exchange between NH_2 and D_2O, while the pyridyl multiplets in both complexes can be clearly observed. It should be noted that there are three possible factors which could affect the chemical shifts of the protons in the pyridyl rings:

First of all, the coordination of the ligands to the metal ions can reduce the electron density in the pyridyl rings, which would lead to a shift of the pyridyl multiplets downfield, in other words, having larger chemical shifts compared with those of the free ligand. This is called the electronic effect. Secondly, due to the twisted structures in the complexes about the diazine N-N units, the delocalization in the free ligand will be broken after the formation of the complexes, which could increase the electron density in the pyridyl rings, hence reduce the chemical shifts of the protons in the pyridyl rings. However, the C=N and N-N distances of the complexes are very similar to those of the free ligand, which implies that this factor is less important. The last one, which probably is the most important one, is the so-called shielding effect. Because of the particular spiral-like arrangement of the three ligands in such dinuclear complexes, the three pyridyl rings bound at each metal center are so close to one another that the protons in one pyridyl ring could be located in the π-cloud of another pyridyl ring, thus producing lower chemical shifts (**Figure 4-17**, which was generated by ORTEP3 by using X-ray data of **26**, exactly shows such a situation). This factor is sensitively depended on how close the three pyridyl rings are, in other words, it is largely depended on the $M\text{-}N_{py}$ bond distances. The shorter the $M\text{-}N_{py}$ bond distances, the larger the shielding effect. However, shorter $M\text{-}N_{py}$ bond distances also

means stronger coordination, thereby leading to a larger electronic effect which results in larger chemical shifts.

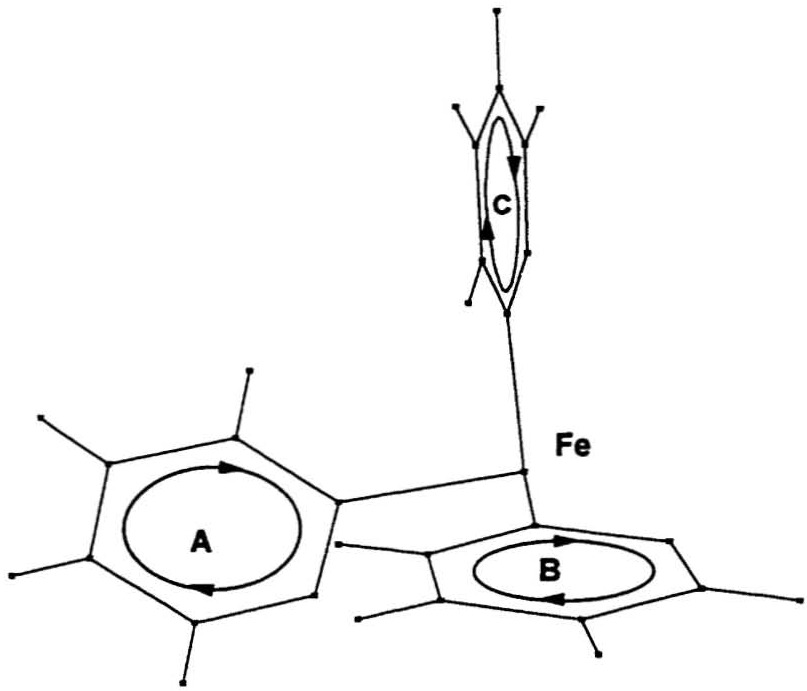

Figure 4-17. Shielding effect in the spiral-like complex **26** with labeling of the current circle.

M-N_{py} bond distances in both of these diamagnetic (low spin) dinuclear complexes are quite short (e.g. Co(1)-N(3) 1.942(4) Å in **28**, and Fe(1)-N(1) 1.989(4) Å, Fe(2)-N(4) 1.996(4) Å in **26**), which suggests that both the electronic effect and shielding effect are significant. The observation that the pyridyl multiplets in the spectra of both complexes are observed at lower chemical shifts compared with those in the spectra of the free ligand

indicates that the shielding effect is the dominant one in both complexes. However, the electronic effect is also a major factor which clearly explains that the set of pyridyl multiplets of **28** appears in a higher chemical shift position than that of **26** (Co-N_{py} bond distances in **28** are significantly shorter than those of Fe-N_{py} in **26**).

The shielding effect will disappear if the pyridyl rings are not close enough in a complex molecule, but the electronic effect will still exist. Examples will be given in **Chapter 5**.

4.4 Conclusion

Although one structural report on the elusive spiral dinuclear complexes of this class of tetradentate diazine ligand (e.g. PMK) appeared in 1974, the structural details of this class of compounds has remained somewhat of a mystery since the original discovery by Busch in 1958. Five complexes in this class are presented in this chapter, all showing the same spiral structure with three canted ligands wrapped around the dinuclear metallic core and three diazine N_2 groups acting as bridges between the manganese, iron, cobalt and nickel centers. The Fe(II) and Co(III) complexes are low spin, while the Fe(III), Co(II), Mn(II) and Ni(II) complexes are high spin. The magnetic properties of the $Mn(II)_2$ derivative imply the presence of weak ferromagnetic coupling, associated with the twisted nature of the PAHAP ligands. The shielding effect has been found to be a dominant factor influencing the chemical shifts related to the pyridyl mutiplets in the ^1H NMR of both **26** and **28**.

Chapter 5 Coordination Chemistry and Magnetochemistry of Open-chain Diazine Ligands in Other Coordination Modes

5.1 Introduction

Chapter 2 and 3 presented a series of **Type AB** as well as quasi-**Type B** copper(II) dinuclear complexes which show very interesting magnetic properties. Chapter 4 described a series of spiral-like dinuclear complexes of Mn(II), Fe(II), Fe(III), Co(II), Co(III), Ni(II) with **Type AB** coordination mode for the ligands, together with an unusual seven-coordinate Fe(III) complex in which the deprotonated ligand PHAAP adopts a new coordination mode. In this chapter, to more thoroughly investigate the coordination chemistry of open-chain diazine ligands and the magnetic properties of their complexes, and to search for new approaches to generate homo-polynuclear metal complexes [165-167], a series of mononuclear and polynuclear (homo- and hetero-) complexes of the first row transition metal ions have been prepared with one symmetric ligand (PAHAP), one pseudosymmetric ligand (PHAAP) and two asymmetric ligands (PAHOX and PTS).

The X-ray structures and magnetic properties of some complexes, together with their spectral properties are presented.

Scheme 5-1

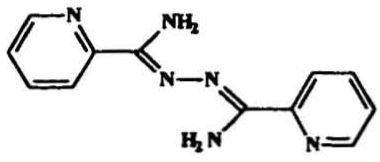

(PAHAP)

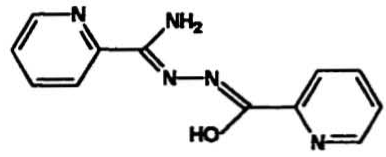

(PHAAP)

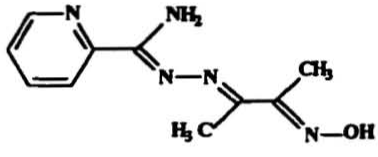

(PAHOX)

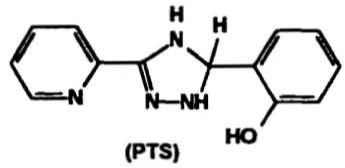

(PTS)

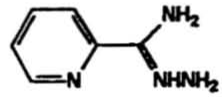

(PAH)

5.2 Experimental

5.2.1 Materials

Commercially available solvents and chemicals were used without further purification.

5.2.2 Measurements

Analysis, spectroscopic and physical measurements (see Chapter 1)

5.2.3 Synthesis of the ligands

PAHAP and PHAAP were prepared by procedures described in Chapter 2.

PTS was prepared by the reaction of picolinamide hydrazone with salicylaldehyde in absolute ethanol according to a published procedure [100, 101].

PAHOX

2,3-butanedione monoxime (10.1 g, 0.100 mol) was dissolved in absolute ethanol (30 mL) and added slowly to a boiling solution of picolinamide hydrazone (13.6 g, 0.100 mol) in absolute ethanol (40 mL). The resulting solution was refluxed for 4 hours. Yellow crystals were obtained on cooling (yield 20 g, 92%). The product was recrystallized in high yield from hot ethanol (mp. 153-155°). Mass spectrum (major mass peaks; m/z); 219 (M), 202, 161, 105, 98, 79, 78. IR, ν_{OH} 3470 cm^{-1}, ν_{NH} 3362 cm^{-1} $\nu_{C=N}$ 1610 cm^{-1}. Anal. Calcd. for $C_{10}H_{13}N_5O$: C, 54.78; H, 5.98; N, 31.94. Found: C, 54.63; H, 5.98; N, 32.55.

5.2.4 Synthesis of the complexes

$[Cu_2(PAHOX\text{-}H)_2](ClO_4)_2.H_2O$ **(33)**

PAHOX (0.22g, 1.00 mmol) was suspended in a solution of $Cu(ClO_4)_2.6H_2O$ (0.74 g, 2.0 mmol) in deionized water (40 mL) and the mixture heated to about 60°C for a few minutes. A clear solution formed which was filtered and allowed to stand at room temperature for a few days. Dark, almost black crystals, suitable for structural analysis, formed, which were filtered off and dried in air (yield, 0.35 g). Anal. Calcd. for $[Cu_2(C_{10}H_{12}N_5O)_2](ClO_4)_2.H_2O$ **(33)**; C, 30.78; H, 3.36; N, 17.95. Found: C, 30.86; H, 3.25; N, 17.89. The analytical sample contains a water molecule that was not revealed in the X-ray structure.

$[Cu(PAHOX)(SO_4)]_2.2H_2O$ (**34**)

Complex **34** was prepared in a similar manner using $CuSO_4.5H_2O$ and obtained as dark green crystals. Anal. Calcd. for $[Cu(C_{10}H_{13}N_5O)(SO_4)]_2.2H_2O$ (**34**); C, 30.26; H, 3.81; N, 17.65. Found: C, 30.39; H, 3.86; N, 17.80.

$[Co(PAHOX)_2](NO_3)_3.2H_2O$ (**35**)

PAHOX (0.22g, 1.0 mmol) was suspended in a solution of $Co(NO_3)_2.6H_2O$ (0.58 g, 2.0 mmol) in deionized water (20 mL) and the mixture heated to about 60°C for a few minutes. A clear solution formed which was filtered and allowed to stand at room temperature for a few days. Orange-red crystals, suitable for structural analysis formed which were filtered off and dried in air (yield, 0.15 g). The composition of the complex was confirmed by X-ray crystallography.

$[VO_2(PAHAP\text{-}H)]$ (**36**)

A hot solution of PAHAP (0.24 g, 1.0 mmol) in dichloromethane (10 mL) was added to a hot solution $VO(acac)_2$ (0.27 g, 1.0 mmol) in methanol (20 mL), then 0.17g NH_4NO_3 (2.0 mmol) was added to the solution. The resulting solution was filtered and the filtrate was allowed to stand at room temperature overnight. Red crystals formed, which were suitable for X-ray structure determination (yield 0.26 g, 81%). Anal. Calcd. for $[VO_2(C_{12}H_{11}N_6)]$: C, 44.73; H, 3.44; N, 26.08. Found: C, 44.51; H, 3.49; N, 26.22.

$[Cd_2(PAHAP)_2(NO_3)_2(H_2O)_2](NO_3)_2.6H_2O$ (**37**)

PAHAP (0.24 g, 1.0 mmol) was added to an aqueous solution (30 mL) of $Cd(NO_3)_2.6H_2O$ (0.69 g, 2.0 mmol), and the mixture was stirred for several minutes at

room temperature until the ligand dissolved. The colorless solution was filtered, and the filtrate was allowed to stand at room temperature for several days. Very slight yellow (almost colorless) crystals, suitable for an X-ray structural determination, formed; these were filtered off, washed quickly with water and air-dried (yield 90%). The composition of the complex was confirmed by X-ray crystallography.

$[Cu_4(PHAAP\text{-}H)_4](ClO_4)_4.4H_2O$ (**38**), $[Ni_4(PHAAP\text{-}H)_4(H_2O)_4](NO_3)_4.2.5H_2O$ (**39**)

PHAAP (0.24 g, 1.0 mmol) was added to a hot aqueous methanol (80/20) solution (40 mL) of 1.0 mmol metal salt ($Cu(ClO_4)_2.6H_2O$ or $Ni(NO_3)_2.6H_2O$) and the mixture stirred at room temperature for several minutes, until the ligand dissolved. The clear solution was filtered and the filtrate allowed to stand at room temperature overnight. Well formed crystals (black-green for **38** and orange-red for **39**) were produced in each case, which were filtered off, washed quickly with cold water, and dried in air (yields 80-85%). Anal. Calcd. for $[Cu_4(C_{12}H_{10}N_5O)_4](ClO_4)_4.4H_2O$ (**38**): C, 34.21; H, 2.87; N, 16.62. Found: C, 34.25; H, 2.49; N, 16.68. The composition of **39** was confirmed by X-ray crystallography.

$[Cu_3Fe(PHAAP\text{-}H)_4(H_2O)_2](ClO_4)_5$ (**40**)

To a hot solution of the complex $[Fe(PHAAP)(H_2O)_2(NO_3)](NO_3)_2$ (**30**) (0.52 g, 1.0 mmol) in methanol (20 mL), 1 mmol triethylamine was added. A few minutes later, a hot solution of $Cu(ClO_4)_2.6H_2O$ (1.0 mmol in 10 mL methanol) was added to the solution. The resulting solution was filtered and the filtrate was allowed to stand at room temperature overnight. Black crystals formed, which were suitable for X-ray structure

determination (yield 0.46 g). Anal. Calcd. for $[Cu_3Fe(C_{12}H_{10}N_5O)_4(H_2O)_2](ClO_4)_5$ (**40**): C, 33.18; H, 2.55; N, 16.13. Found: C, 33.44; H, 2.66; N, 16.13.

$[Cu(II)_4Cu(I)_2(PAH)_4Br_{10}]$ (**41**)

PTS (0.24 g, 1.0 mmol) was dissolved in acetonitrile (10 mL) and added to a hot solution of $CuBr_2$ (0.45 g, 2.0 mmol) in methanol (20 mL). The resulting dark brown solution was filtered and the filtrate allowed to stand at room temperature overnight. Dark brown crystals formed, which were filtered off, washed with methanol and dried in air (yield 0.10 g). The composition of the complex was confirmed by X-ray crystallography.

5.2.5 Crystallographic data collection and refinement of the structures

$[Cu_2(PAHOX\text{-}H)_2](ClO_4)_2.H_2O$ (**33**)

Crystals of $[Cu_2(PAHOX\text{-}H)_2](ClO_4)_2.H_2O$ (**33**) are dark green, almost black in appearance. A single crystal of **33** of dimensions 0.40 × 0.12 × 0.10 mm was attached to a quartz fiber and transferred to a Siemens Smart three-circle diffractometer with graphite-monochromatized Mo-Kα X-radiation and a CCD area detector was used for data collection [108]. ω-scans were used in such a way that an initial 180° scan range consisting of 0.3° intervals was followed by three further 88°, 180° and 268° respectively. This strategy samples the sphere of reciprocal space up to 2 θ = 50.04°. Cell parameters were refined using the centroid values of 300 reflections with 2θ angles up to 50.04°. Raw frame data were integrated using the SAINT [109] program. The structure was solved by direct methods [110]. An empirical absorption correction was applied to the data using the program SADABS [111]. Abbreviated crystal data are listed in **Table 5-1**.

$[Co(PAHOX)_2](NO_3)_3.2H_2O$ (**35**), $[Ni_4(PHAAP\text{-}H)_4(H_2O)_3](ClO_4)_4.2.5H_2O$ (**39**)

Crystal data collection and structure refinement for these crystals were carried out in a similar manner to that for **33**. Abbreviated crystal data for all of these complexes are given in **Table 5-1**.

$[Cu(PAHOX)(SO_4)]_2.2H_2O$ (**34**)

The crystals of $[Cu(PAHOX)(SO_4)]_2.2H_2O$ (**34**) are green yellow in appearance. The diffraction intensities of an approximately 0.20 × 0.20 × 0.40 mm crystal were collected with graphite-monochromatized Mo-Kα X-radiation using a Rigaku AFC6S diffractometer at 26±1°C and the ω-2θ scan technique to a $2\theta_{max}$ value of 50.1°. A total of 2917 reflections was measured and 1986 were considered significant with $I_{net} > 2.0\ \sigma(I_{net})$. The intensities of three representative reflections, which were measured after every 150 reflections, remained constant through the data collection, indicating crystal and electronic stability (no decay correction was applied). Azimuthal scans of several reflections indicated no need for an absorption correction. The data were corrected for Lorentz and polarization effects. The cell parameters were obtained from the least-squares refinement of the setting angles of 20 carefully centered reflections with 2θ in the range 34.31-40.51°.

The structure was solved by direct methods [102, 103]. All atoms except hydrogens were refined anisotropically. Hydrogen atoms were optimized by positional refinement, with isotropic thermal parameters set 20% greater than those of their bonded partners at the time of their inclusion. However, they were fixed for the final round of

refinement. The final cycle of full-matrix least-squares refinement was based on 1986 observed reflections ($I > 2.00\sigma(I)$) and 209 variable parameters and converged with unweighted and weighted agreement factors of $R = \Sigma||F_o| - |Fc||/\Sigma|F_o| = 0.035$ and $R_w = [(\Sigma w(|F_o| - |F_c|)^2/ \Sigma wF_o^2]^{1/2} = 0.033$. The maximum and minimum peaks on the final difference Fourier map correspond to 0.39 and -0.45 electrons $Å^{-3}$ respectively. Neutral atom scattering factors [104] and anomalous-dispersion terms [105, 106], were taken from the usual sources. All calculations were performed with the TEXSAN [107] crystallographic software package using a VAX3100 work station. Abbreviated crystal data are given in **Table 5-1**.

$[VO_2(PAHAP\text{-}H)]$ **(36)**, $[Cd_2(PAHAP)_2(NO_3)_2(H_2O)_2](NO_3)_2.6H_2O$ **(37)**, $[Cu_3Fe(PHAAP\text{-}H)_4(H_2O)_2](ClO_4)_5$ **(40)**, $[Cu(II)_4Cu(I)_2(PAH)_4Br_{10}]$ **(41)**.

The data collections and structure solutions for these crystals were carried out in a manner similar to that for $[Cu(PAHOX)(SO_4)]_2.2H_2O$ **(34)**. Abbreviated crystal data for those crystals are also given in **Table 5-1.**

Note in **Table 5-1**:

= Rigaku data; ***** = Siemens Smart data

$\mathbf{R} = \Sigma||F_o| - |F_c||/\Sigma|F_o|$, $\mathbf{R_w} = [(\Sigma(|F_o| - |F_c|)^2/\Sigma wF_o^2)]^{1/2}$

$\mathbf{R1} = \Sigma||F_o| - |F_c||/\Sigma|F_o|$, $\mathbf{wR_2} = [\Sigma[w(|F_o|^2 - |F_c|^2)^2/\Sigma[w(|F_o|^2)^2]]^{1/2}$

Table 5-1. Summary of crystallographic data for complexes **33-37, 39-41.**

Compound	33*	34#	35*
chemical formula	$C_{20}H_{24}Cl_2Cu_2N_{10}O_{10}$	$C_{10}H_{15}CuN_5O_6S$	$C_{20}H_{32}CoN_{13}O_{13}$
formula wt.	762.47	396.86	721.52
space group	C2/c	$P2_1/n$(#14)	PI
a (Å)	33.5849(6)	9.866(2)	9.6852(3)
b(Å)	7.6016(1)	10.128(2)	10.4377(4)
c(Å)	22.6654(3)	15.418(1)	14.3896(5)
α(deg)	90	90	78.313(1)
β(deg)	106.949(1)	108.051(8)	84.565(1)
γ(deg)	90	90	83.748(1)
V ($Å^3$)	5535.1(1)	1464.7(3)	1412.08(9)
$\rho_{calcd}(gcm^{-3})$	1.830	1.800	1.697
Z	8	4	2
$\mu(mm^{-1})$	1.804	1.668	0.699
λ	0.71073	0.71069	0.71073
T, K	150(2)	299(1)	298 (2)
R1(R)	0.0465	0.035(R)	0.0730
wR2(R_w)	0.0991	0.033(R_w)	0.2180

Table 5-1. (contd.) Summary of crystallographic data for complexes **33-37, 39-41.**

Compound	**36#**	**37#**	**39***
chemical formula	$C_{12}H_{11}N_6O_2V$	$C_{24}H_{40}N_{16}O_{19}Cd_2$	$C_{48}H_{53}N_{23.5}Ni_4O_{24.5}$
formula wt.	322.21	1081.50	1585.98
space group	Cc	C2/c(#15)	PI
a (Å)	8.973(9)	23.870(3)	12.0509(6)
b(Å)	11.2792(18)	13.418(8)	12.7498(6)
c(Å)	13.2184(9)	14.721(5)	23.1208(11)
α (deg)	90	90	93.1050(10)
β(deg)	96.170(7)	119.90(1)	100.1500(10)
γ(deg)	90	90	108.5050(10)
V (Å^3)	1330.1(14)	4087(2)	3292.9(3)
ρ_{calcd}(gcm^{-3})	1.609	1.757	1.600
Z	4	4	2
μ(mm^{-1})	0.6385	1.136	1.222
λ	1.54178	0.71069	0.71073
T, K	293(2)	299(1)	193(2)
R1(R)	0.0383	0.034(R)	0.0659
wR2(R_w)	0.0991	0.040(R_w)	0.1992

Table 5-1. (contd.) Summary of crystallographic data for complexes **33- 37, 39-41.**

Compound	**40#**	**41#**
chemical formula	$C_{48}H_{52}O_{30}N_{20}Cu_3FeCl_5$	$C_{12}H_{16}Br_5Cu_3N_8$
formula wt.	1812.80	862.47
space group	PI(#2)	PI(#2)
a (Å)	14.639(2)	9.253(3)
b(Å)	17.707(2)	18.159(3)
c(Å)	14.448(2)	7.199(4)
α (deg)	103.65(1)	91.31(3)
β(deg)	108.674(9)	107.35(4)
γ(deg)	86.17	104.22(2)
V ($Å^3$)	3447.4(9)	1113(2)
$\rho_{calcd}(gcm^{-3})$	1.746	2.573
Z	2	2
$\mu(mm^{-1})$	5.371	11.76
λ	1.54178	0.71069
T, K	299(1)	299(1)
R1(R)	0.089(R)	0.037(R)
wR2(R_w)	0.072(R_w)	0.032(R_w)

5.3 Results and discussion

5.3.1 Structures

$[Cu_2(PAHOX\text{-}H)_2](ClO_4)_2$ (33)

The structure of **33** is illustrated in **Figure 5-1**, and bond distances and bond angles relevant to the copper coordination spheres are listed in **Table 5-2**. The dinuclear structural arrangement in **33** involving NO bridging is the result of a compromise in the coordinating abilities of two very different portions of the same ligands. The well-documented ability of this class of N_4 dinucleating ligand to bind two metals does not prevail, and the resulting mode of coordination is dominated by the oxime group. A similar coordination mode occurs in the complex $[Cu(HdoxN_2)]_2^{2+}$ (H_2doxN_2 = 4,4-diaza-3,6-dimethyl-3,5-octadiene-2,7-dione-2,7-dioxime) [84]. However, with a similar N_4 ligand (pyridazine-3,6-dicarbaldehyde dioxime) involving two terminal oxime groups bound to a pyridazine, the dinucleating ability of the N_4 fragment prevails and the oxime oxygens remain uncoordinated [63].

The copper centers are quite distorted, with four short in-plane contacts to the nitrogen and oxygen atoms. The Cu-O contacts are very short (< 1.92 Å), consistent with proton loss from the ligand OH group. Longer axial contacts between the copper centers and one perchlorate create an infinite chain structure along the b axis (Cu(1)-O(6) 2.458(3) Å, Cu(2)-O(4) 2.733(3) Å, Cu(1)-O(5A) 3.124(3) Å), suggesting that each copper probably should be considered as having a distorted square-pyramidal structure

Table 5-2. Interatomic distances (Å) and angles (Deg.) relevant to the copper coordination spheres in $[Cu_2(PAHOX\text{-}H)_2](ClO_4)_2.H_2O$ **(33)**.

Cu(1)-O(2)	1.916(2)	Cu(1)-N(3)	1.934(3)
Cu(1)-N(5)	1.937(3)	Cu(1)-N(1)	2.024(3)
Cu(2)-O(1)	1.891(2)	Cu(2)-N(10)	1.930(3)
Cu(2)-N(8)	1.934(2)	Cu(2)-N(6)	2.018(3)
Cu(1)-Cu(2)	3.491(1)	N(5)-O(1)	1.344(3)
N(10)-O(2)	1.331(3)	N(3)-N(4)	1.386(3)
N(8)-N(9)	1.386(4)		
O(2)-Cu(1)-N(3)	156.71(10)	O(2)-Cu(1)-N(5)	102.81(10)
N(3)-Cu(1)-N(5)	90.59(11)	O(2)-Cu(1)-N(1)	87.64(10)
N(3)-Cu(1)-N(1)	80.76(10)	N(5)-Cu(1)-N(1)	168.98(11)
O(1)-Cu(2)-N(10)	103.12(10)	O(1)-Cu(2)-N(8)	149.93(11)
N(10)-Cu(2)-N(8)	90.96(11)	O(1)-Cu(2)-N(6)	88.96(10)
N(10)-Cu(2)-N(6)	166.65(11)	N(8)-Cu(2)-N(6)	80.97(11)

(**Figure 5-2**). The Cu(1)-O(5A) contact, despite being long, clearly is responsible for the chain ordering. The result of the axial perchlorate coordination is to fold the molecule and create a boat conformation in the six-membered $Cu_2N_2O_2$ ring, with an angle of 129.3° between the CuNO planes. As a result the copper-copper separation (3.491(1) Å) is fairly short for a system of this sort. An additional contact involving a hydrogen bond between amino hydrogen H(71N) and perchlorate oxygen O(4B) (H(71N)-O(4B) 2.20(4) Å, N(7)-O(4B) 2.958(4) Å, N(7)-H(71N)-O(4B) 158(4)°) links the chains in pairs with a double strand arrangement (**Figure 5-3**).

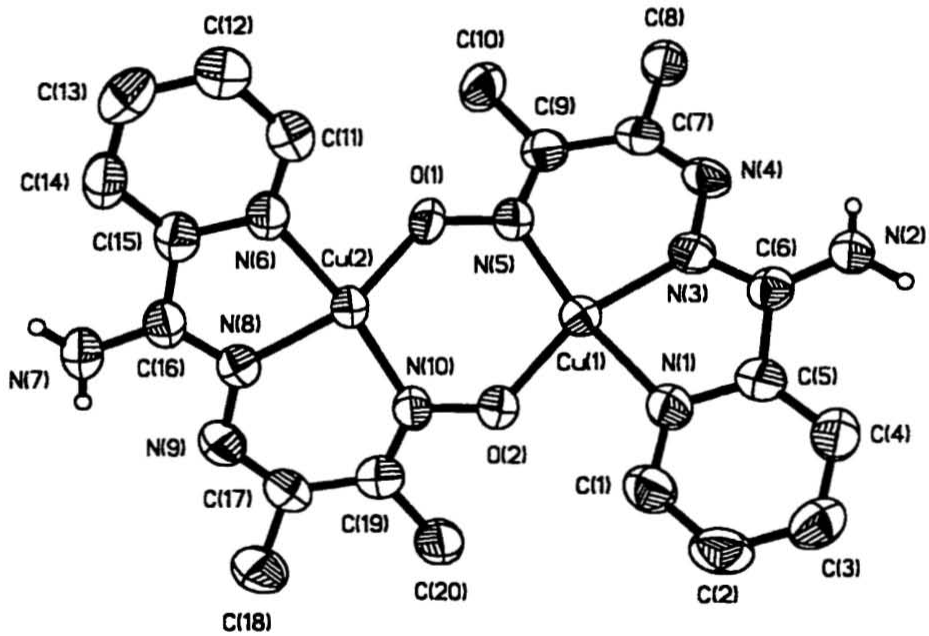

Figure 5-1. Structural representation of $[Cu_2(PAHOX\text{-}H)_2](ClO_4)_2$ (**33**) with hydrogen atoms omitted (50% probability thermal ellipsoids).

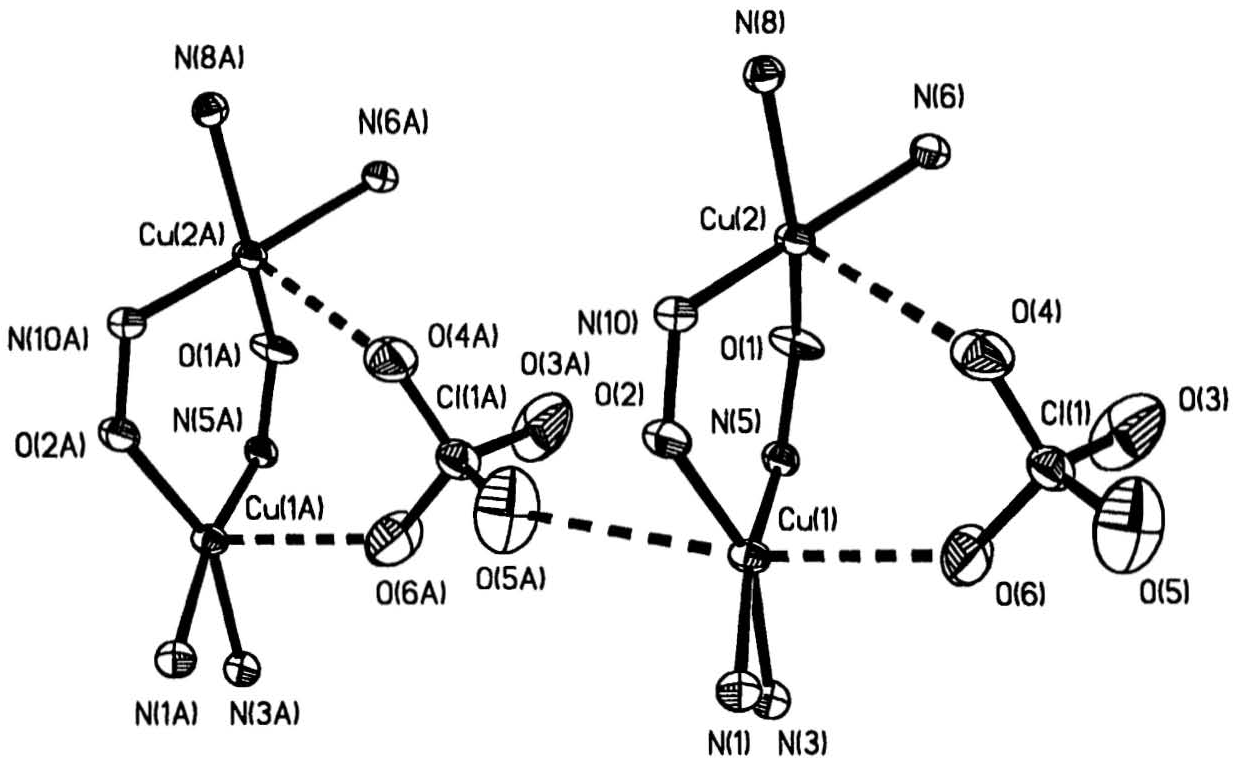

Figure 5-2. Chain structure in **33** associated with axial perchlorate bridging interaction.

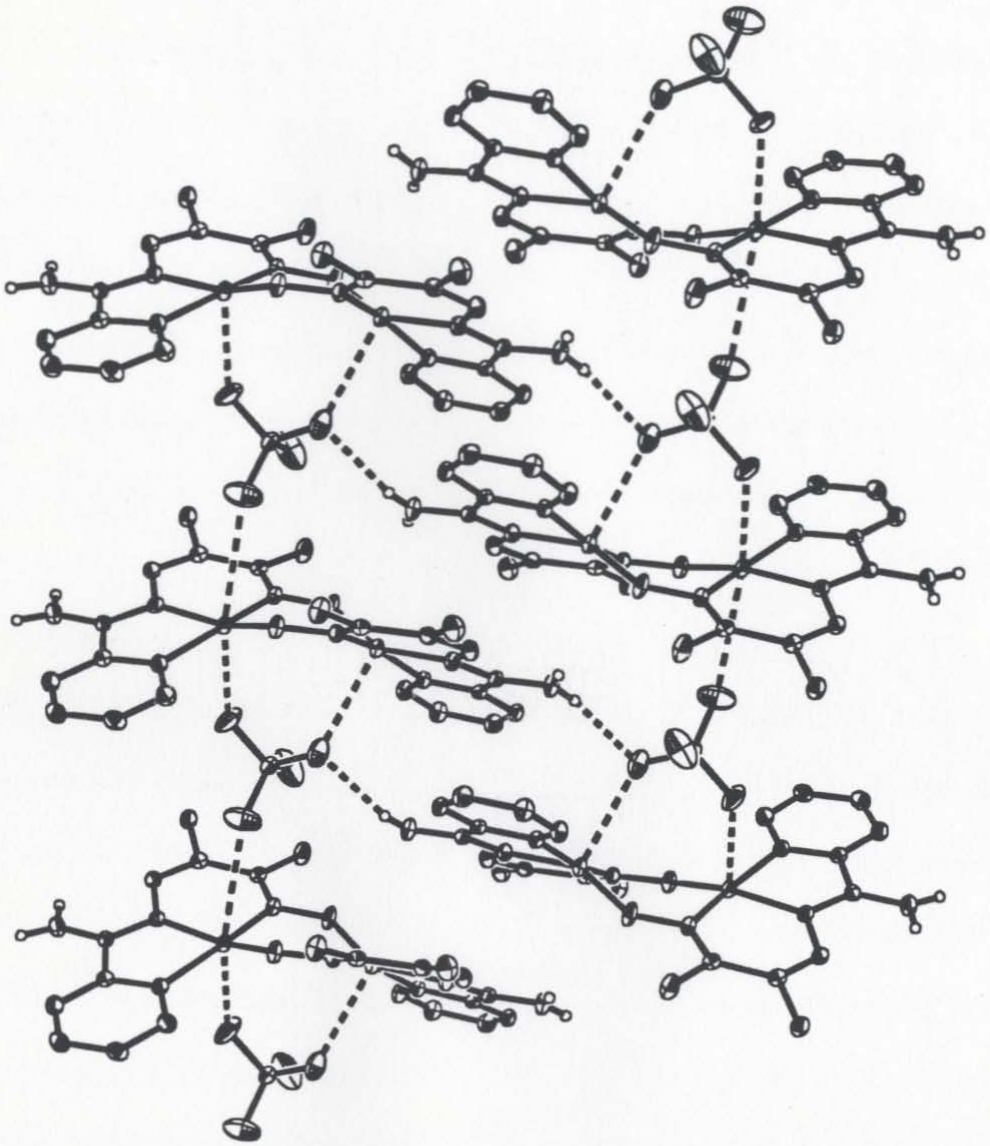

Figure 5-3. Double stranded chain structure in **33**.

$[Cu(PAHOX)(SO_4)]_2.2H_2O$ (34)

The molecular structure of **34** is illustrated in **Figure 5-4**, and bond distances and bond angles relevant to the copper coordination spheres are listed in **Table 5-3**. The bonding mode of the ligand PAHOX is similar to that in **33** (**Type C**), creating five- and six-membered chelate rings, but the oxygen of the N-OH group is not bonded to an adjacent copper. This equivalent basal position in **34** is occupied by an oxygen of a μ_2-SO_4, which bridges the two square-pyramidal copper centers with another oxygen occupying the axial site in the adjacent copper. The basal copper-nitrogen and copper-oxygen distances are short (< 2.01 Å), with a somewhat longer axial contact to a sulfate oxygen (Cu(1)-O(5) 2.199(3) Å). The ligand bonding arrangement resembles that in $[Cu(PMK)(NO_3)_2]$, which is a mononuclear complex with an axial and equatorial monodentate nitrate. The copper atom in **34** is displaced from the mean basal ligand plane towards the sulfate oxygen by 0.338 Å. The two sulfate bridges form an unusual chair-like eight-membered chelate ring bridging the two copper atoms in an orthogonal manner with a Cu-Cu distance of 4.992(1) Å. This is a most unusual sulfate bridging arrangement, and while μ_2-SO_4 groups can bridge two metal centers in a chelating intramolecular fashion [168, 169], and in bidentate chain bridging arrangement [170, 171], the current inter-molecular bridging mode appears to be only the second example of this kind of coordination mode for sulfate [172]. A comparable non-sulfate structural analogue involves two μ_2-PO_4 bridges linking two square-pyramidal copper(II) centers with the

formation of an eight-membered chelate ring [173]. However in this case each phosphate bridges the two copper(II) centers *via* equatorial coordination sites.

Table 5-3. Interatomic distances (Å) and angles (Deg.) relevant to the copper coordination spheres in $[Cu(PAHOX)(SO_4)]_2.2H_2O$ (**34**).

Cu(1)-O(2)	1.972(3)	S(1)-O(2)	1.491(3)
Cu(1)-O(5)	2.199(3)	S(1)-O(5)	1.464(3)
Cu(1)-N(1)	1.995(3)	N(2)-N(3)	1.376(4)
Cu(1)-N(2)	1.934(3)	N(2)-C(6)	1.319(5)
Cu(1)-N(4)	2.009(3)	N(3)-C(7)	1.284(1)
Cu(1)- Cu(1)a	4.992(1)		
O(2)-Cu(1)-O(5)	100.0(1)	O(2)-Cu(1)-N(1)	89.9(1)
O(2)-Cu(1)-N(2)	150.9(1)	O(2)-Cu(1)-N(4)	96.4(1)
O(5)-Cu(1)-N(1)	101.9(1)	O(5)-Cu(1)-N(2)	109.0(1)
O(5)-Cu(2)-N(4)	87.3(1)	N(1)-Cu(1)-N(2)	81.5(1)
N(1)-Cu(1)-N(4)	167.8(1)	N(2)-Cu(1)-N(4)	88.0(1)
O(2)-S(1)-O(5)	109.6(2)	Cu(1)-O(2)-S(1)	135.1(2)
Cu(1)-O(5)-S(1)	135.9(2)		

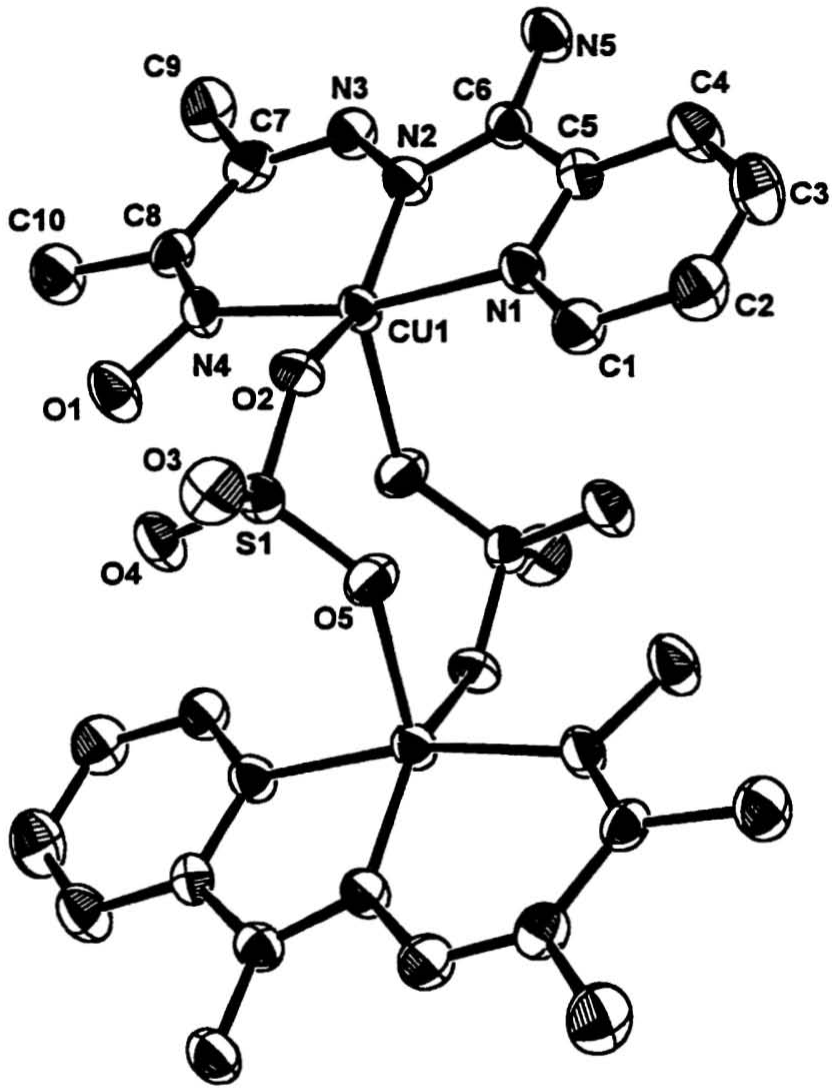

Figure 5-4. Structural representation of $[Cu_2(PAHOX)_2(SO_4)_2]$ **(34)** with hydrogen atoms omitted (50% probability thermal ellipsoids).

$[Co(PAHOX)_2](NO_3)_3.2H_2O$ (35)

The structure of the mononuclear cation in **35** is illustrated in **Figure 5-5**, and relevant bond distances and angles are listed in **Table 5-4**. The complex molecule contains two identical PAHOX ligands. The Co(III) center has a slightly distorted octahedral coordination environment with each ligand acting as an N_3 tridentate donor in a **Type C** manner, and with six comparable bonds in the range 1.890(4)-1.976(5) Å. The angles between two neighboring bonds fall in the range 81.8(2)-94.7(2)° and the axial angles are almost the same (172.1(2)-172.7(2)°). The oxime oxygens (O(1) and O(1)') are not deprotonated and do not coordinate to the Co(III) center, and provide potential additional coordination capacity to form polynuclear complexes [174-176].

Table 5-4. Interatomic distances (Å) and angles (Deg.) relevant to the cobalt coordination spheres in $[Co(PAHOX)_2](NO_3)_3.2H_2O$ (**35**).

Co-N(2)	1.890(4)	Co-N(2')	1.893(4)
Co-N(5')	1.923(5)	Co-N(5)	1.931(5)
Co-N(1')	1.961(5)	Co-N(1)	1.976(5)
N(2)-N(4)	1.390(6)	N(2')-N(4')	1.371(6)
N(2)-Co-N(2')	172.7(2)	N(2)-Co-N(5')	94.7(2)
N(2')-Co-N(5')	90.5(2)	N(2)-Co-N(5)	90.7(2)
N(2')-Co-N(5)	94.6(2)	N(5')-Co-N(5)	87.0(2)
N(2)-Co-N(1')	92.7(2)	N(2')-Co-N(1')	82.2(2)

contd.

N(5')-Co-N(1')	172.4(2)	N(5)-Co-N(1')	91.4(2)
N(2)-Co-N(1)	81.8(2)	N(2')-Co-N(1)	93.1(2)
N(5')-Co-N(1)	90.8(2)	N(5)-Co-N(1)	172.1(2)
N(1')-Co-N(1)	91.7(2)		

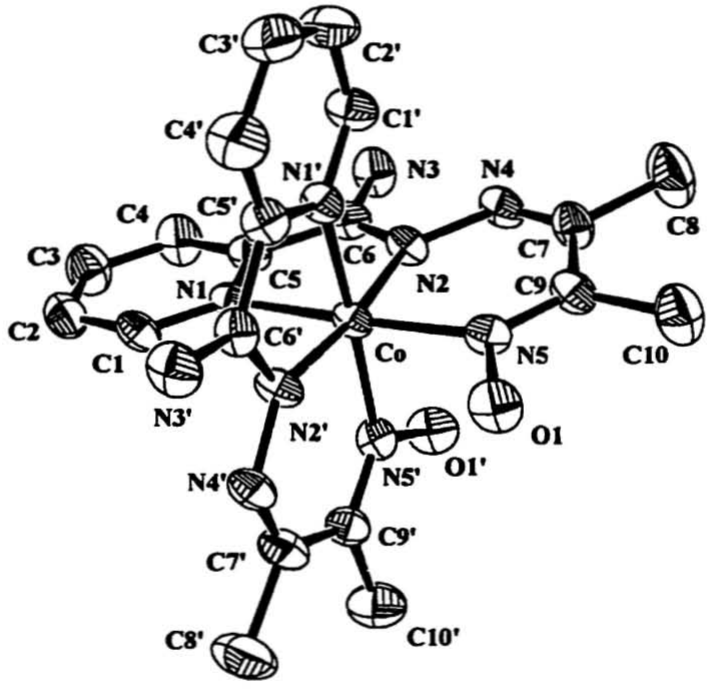

Figure 5-5. Structural representation of $[Co(PAHOX)_2](NO_3)_3.2H_2O$ **(35)** with hydrogen atoms omitted (50% probability thermal ellipsoids).

$[VO_2(PAHAP\text{-}H)]$ **(36)**

The structure of **36** is depicted in **Figure 5-6**, and relevant bond distances and angles are listed in **Table 5-5**. The ligand PAHAP binds the VO_2^+ cation in a tridentate fashion with V(1) coordinated to pyridine (N(1)), diazine (N(2)), and amino (N(4)) nitrogens. The complex is neutral indicating that the ligand has become deprotonated at N(4), which shows the presence of just one proton. The effect of this arrangement is to lock the ligand into an almost planar configuration because of the coordination of N(4), which leads to C=N bonds which are somewhat longer (C(7)-N(5) 1.306(10) Å, C(6)-N(2) 1.299(9).Å) and an N-N bond (N(2)-N(5) 1.396(9) Å) which is somewhat shorter than those in free ligand. The bond distances of V(1) to N(1), N(2) and N(4) are fairly long and similar (V(1)-N(4) 1.993(8) Å, V(1)-N(1) 2.119(7) Å, V(1)-N(2) 2.066(6) Å), while the bond distances of V(1) to O(1) and O(2) are quite short, but normal for VO_2^+ species [177-179] (V(1)-O(1) 1.631(6) Å, V(1)-O(2) 1.635(5) Å), indicating V=O double bond character.

VO_2^+ is one of the four well-defined cation species (V(II), V(III), VO^{2+} and VO_2^+) [180]. Even though the other V(V) species can have variable coordination geometries such as trigonal bipyramidal, square pyramidal, octahedral, pentagonal bipyramidal etc., VO_2^+ usually is six-coordinated with a *cis*-arrangement because this allows better $Op\pi \rightarrow Md\pi$ bonding than a linear arrangement would allow [180].

Table 5-5. Interatomic distances (Å) and angles (Deg.) relevant to the vanadium coordination spheres in $[VO_2(PAHAP\text{-}H)]$ (**36**).

V(1)-O(1)	1.631(6)	V(1)-O(2)	1.635(5)
V(1)-N(4)	1.993(8)	V(1)-N(2)	2.066(6)
V(1)-N(1)	2.119(7)	N(2)-C(6)	1.299(9)
N(2)-N(5)	1.396(9)	N(3)-C(6)	1.312(9)
N(4)-C(7)	1.321(10)	N(5)-C(7)	1.306(10)
O(1)-V(1)-O(2)	110.3(3)	O(1)-V(1)-N(4)	102.3(4)
O(2)-V(1)-N(4)	104.3(3)	O(1)-V(1)-N(2)	128.5(3)
O(2)-V(1)-N(2)	120.6(3)	N(4)-V(1)-N(2)	72.8(3)
O(1)-V(1)-N(1)	96.4(3)	O(2)-V(1)-N(1)	95.6(3)
N(4)-V(1)-N(1)	145.8(2)	N(2)-C(6)-N(3)	124.6(7)
N(2)-C(6)-C(5)	112.9(6)	N(3)-C(6)-C(5)	122.4(7)
N(5)-C(7)-N(4)	122.1(7)	N(5)-C(7)-C(8)	117.4(7)
N(4)-C(7)-C(8)	120.4(7)		

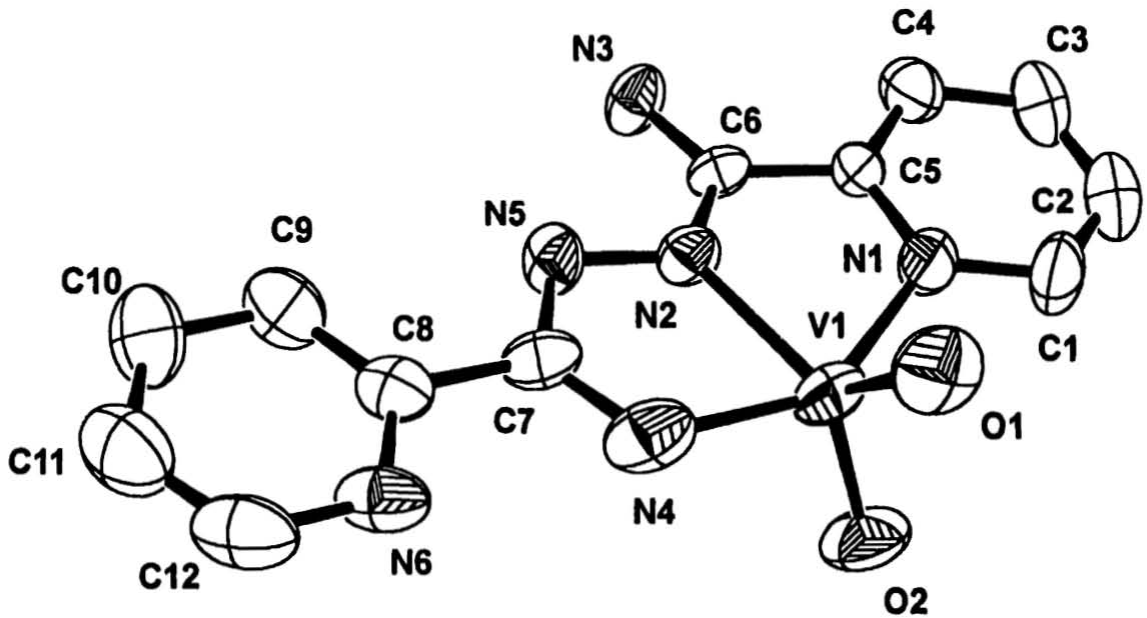

Figure 5-6. Structural representation of $[VO_2(PAHAP\text{-}H)]$ (**36**) with hydrogen atoms omitted (50% probability thermal ellipsoids).

$[Cd_2(PAHAP)_2(NO_3)_2(H_2O)_2](NO_3)_2.6H_2O$ (37)

The structure of **37** is depicted in **Figure 5-7**, and relevant bond length and bond angle information is given in **Table 5-6**. The dinuclear Cd(II) cation consists of two identical octahedral cadmium(II) centers, bridged by two ligands *via* their N-N diazine units in a spiral-like arrangement, with pyridine rings, H_2O molecules and nitrates coordinating to the remaining coordination positions to form a boat conformation through Cd(1)-N(4)-N(3)-Cd(1)'-N(3)'-N(4)'. The expanded view of the coordination cores is illustrated in **Fugure 5-8**. The Cd-donor distances are very similar, falling in the range 2.313(2)-2.403(2) Å. The Cd-Cd separation is 4.783(2) Å, and the least-squares planes of the two five membered chelate rings of each ligand (e.g. Cd(1)-N(1)-C(5)-C(6)-N(3) and Cd(1a)-N(6)-C(8)-C(7)-N(4)) are twisted by 70.38°.

Within each ligand for the NH_2-C=N framework, the C=N bond distances are somewhat shorter (e.g. C(7)-N(4) 1.289(3) Å, C(6)-N(3) 1.265(3) Å) and the N-N bond distances (N(3)-N(4) 1.440(3) Å) somewhat longer than those of the free ligand, also indicative of twisting of the ligands in this complex.

Table 5-6. Interatomic distances (Å) and angles (Deg.) relevant to the cadmium coordination spheres in $[Cd_2(PAHAP)_2(NO_3)_2(H_2O)_2](NO_3)_2.6H_2O$ (**37**).

Cd(1)-O(1)	2.359(2)	Cd(1)-O(2)	2.403(2)
Cd(1)-N(1)	2.313(2)	Cd(1)-N(3)	2.363(2)
Cd(1)-N(4)	2.369(2)	Cd(1)-N(6)	2.314(2)
Cd(1)-Cd(1)a	4.783(2)	N(3)-N(4)	1.440(3)
N(3)-C(6)	1.265(3)	N(4)-C(7)	1.289(3)
C(7)-N(5)	1.331(4)	C(6)-N(2)	1.331(3)
O(1)-Cd(1)-O(2)	82.98(7)	O(1)-Cd(1)-N(1)	92.30(7)
O(1)-Cd(1)-N(3)	146.78(7)	O(1)-Cd(1)-N(4)	83.65(7)
O(1)-Cd(1)-N(6)	88.40(6)	O(2)-Cd(1)-N(1)	82.85(8)
O(2)-Cd(1)-N(3)	120.23(7)	O(2)-Cd(1)-N(4)	157.23(6)
O(2)-Cd(1)-N(6)	90.37(8)	N(1)-Cd(1)-N(3)	69.69(6)
N(1)-Cd(1)-N(4)	116.06(8)	N(1)-Cd(1)-N(6)	173.03(9)
N(3)-Cd(1)-N(4)	80.09(7)	N(3)-Cd(1)-N(6)	112.88(6)
N(4)-Cd(1)-N(6)	70.91(8)		

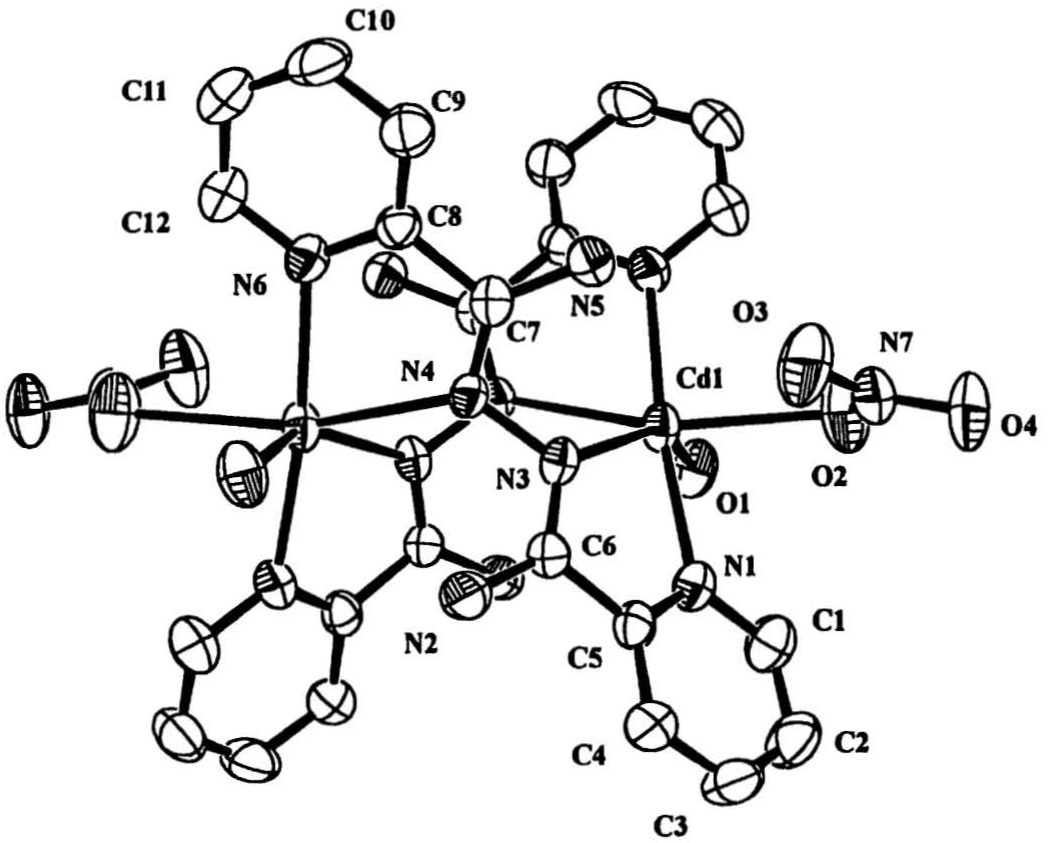

Figure 5-7. Structural representation of $[Cd_2(PAHAP)_2(NO_3)_2(H_2O)_2](NO_3)_2.6H_2O$ **(37)** with hydrogen atoms omitted (50% probability thermal ellipsoids).

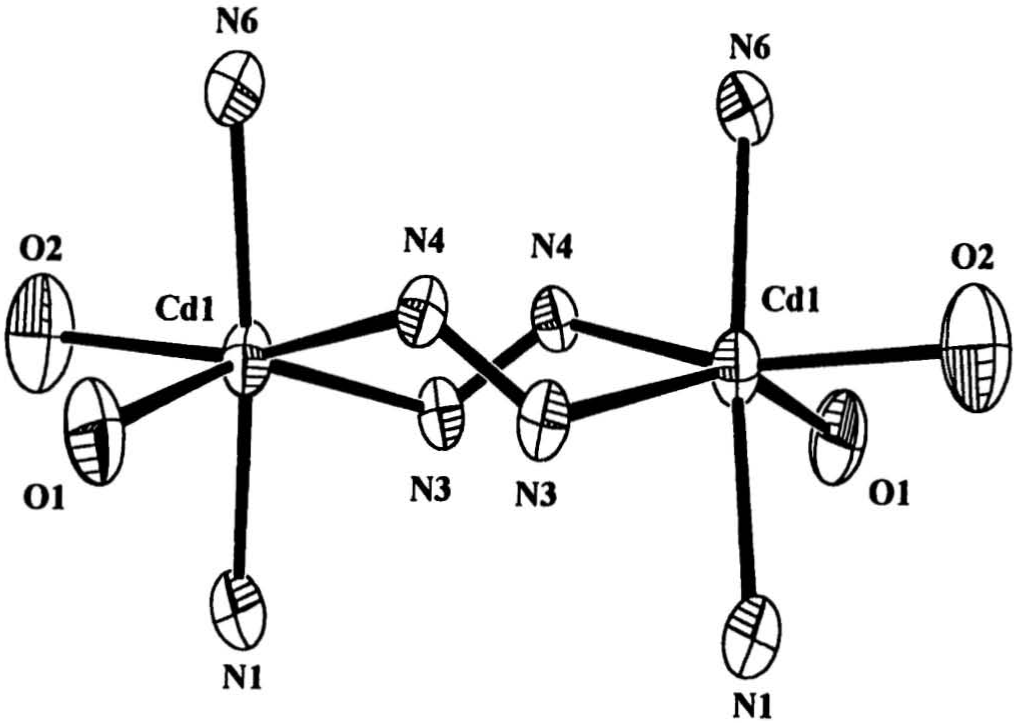

Figure 5-8. Expanded view of the coordination cores in **37**.

$[Ni_4(PHAAP\text{-}H)_4(H_2O)_4](NO_3)_4.2.5H_2O$ **(39)**

The structure of the tetranuclear unit is depicted in **Figure 5-9**, and relevant bond length and bond angle information is given in **Table 5-7**. The expanded view of the coordination cores is illustrated in **Figure 5-10**. The cluster consists of four Ni(II) centers bridged by four alkoxo groups of the four deprotonated ligands (O(1A), O(1B), O(1C) and O(1D)) to form a Ni_4O_4 eight-membered ring with an almost square planar set of four Ni atoms (the deviations from the Ni(1)Ni(2)Ni(3)Ni(4) least squares plane for Ni(1)-Ni(4) are -0.144(2), 0.145(2), -0.145(1) and 0.144(2) Å respectively; Ni(1)-Ni(2) 3.969(2) Å, Ni(2)-Ni(3) 3.954(2) Å, Ni(3)-Ni(4) 3.966(2) Å, Ni(4)-Ni(1) 3.977(2) Å; Ni(1)-Ni(3) 5.684(2) Å, Ni(2)-Ni(4) 5.503(2) Å; Ni(1)-Ni(2)-Ni(3) 91.69°, Ni(2)-Ni(3)-Ni(4) 88.02°, Ni(3)-Ni(4)-Ni(1) 91.40° and Ni(4)-Ni(1)-Ni(2) 87.66°) and a bisphenoid of oxygen atoms. The alkoxo bridging angles (Ni-O(alkoxo)-Ni) are all quite large, falling in the range 136.2(2)-140.1(2)°. This peculiar Ni_4O_4 structure shows some similarities to that of tetrasulfurtetranitride (S_4N_4) [181].

All the Ni(II) centers have distorted octahedral coordination environments. Both Ni(2) and Ni(4) centers have N_3O_3 donor sets from two pyridine nitrogens, one diazine nitrogen, two alkoxo oxygens and one water. The coordination polyhedron for Ni(1) is formed by two pyridine nitrogens, two diazine nitrogens and two alkoxo oxygens, thereby forming an N_4O_2 chromophore. The Ni(3) coordination sphere (NiN_2O_4) is comprised of two pyridine nitrogens, two alkoxo oxygens and two water oxygens.

Each deprotonated ligand is approximately planar (the deviations from the least squares plane formed by the four coordination donors for each of them are in the range -0.00234 to +0.10216 Å), and bond distances are in accordance with the structural data for the relevant groups: the diazine N-N bond distances are very similar in each different

Table 5-7. Interatomic distances (Å) and angles (Deg.) relevant to the nickel coordination spheres in $[Ni_4(PHAAP\text{-}H)_4(H_2O)_3](NO_3)_4.2.5H_2O$ (**39**).

Ni(1)-N(3A)	1.972(5)	Ni(3)-N(1C)	2.053(5)
Ni(1)-N(2D)	1.979(5)	Ni(3)-N(4B)	2.059(6)
Ni(1)-N(1D)	2.132(5)	Ni(3)-O(1C)	2.061(4)
Ni(1)-N(4A)	2.156(5)	Ni(3)-O(1E)	2.072(6)
Ni(1)-O(1A)	2.176(4)	Ni(3)-O(1B)	2.096(4)
Ni(1)-O(1D)	2.177(4)	Ni(3)-O(1G)	2.097(6)
Ni(2)-N(2B)	1.966(5)	Ni(4)-N(3C)	1.966(5)
Ni(2)-N(1A)	2.044(5)	Ni(4)-N(4D)	2.053(5)
Ni(2)-O(1A)	2.075(4)	Ni(4)-O(1D)	2.091(4)
Ni(2)-O(1H)	2.080(6)	Ni(4)-O(4E)	2.107(5)
Ni(2)-N(1B)	2.115(6)	Ni(4)-N(4C)	2.107(5)

contd.

Ni(2)-O(1B)	2.165(4)	Ni(4)-O(1C)	2.158(4)
O(1A)-C(6A)	1.299(7)	N(2A)-N(3A)	1.385(7)
O(1B)-C(7B)	1.288(7)	N(2B)-N(3B)	1.392(8)
O(1C)-C(6C)	1.308(7)	N(2C)-N(3C)	1.387(7)
O(1D)-C(7D)	1.305(7)	N(2D)-N(3D)	1.397(7)
Ni(1)-Ni(2)	3.969(2)	Ni(2)-Ni(3)	3.954(2)
Ni(3)-Ni(4)	3.966(2)	Ni(1)-Ni(4)	3.977(2)
N(3A)-Ni(1)-N(2D)	170.2(2)	N(3A)-Ni(1)-N(1D)	98.0(2)
N(2D)-Ni(1)-N(1D)	77.3(2)	N(3A)-Ni(1)-N(4A)	76.5(2)
N(2D)-Ni(1)-N(4A)	94.8(2)	N(1D)-Ni(1)-N(4A)	90.8(2)
N(3A)-Ni(1)-O(1A)	75.3(2)	N(2D)-Ni(1)-O(1A)	113.6(2)
N(1D)-Ni(1)-O(1A)	97.3(2)	N(4A)-Ni(1)-O(1A)	151.5(2)
N(3A)-Ni(1)-O(1D)	110.1(2)	N(2D)-Ni(1)-O(1D)	75.1(2)
N(1D)-Ni(1)-O(1D)	151.9(2)	N(4A)-Ni(1)-O(1D)	96.0(2)
O(1A)-Ni(1)-O(1D)	89.6(2)	N(2B)-Ni(2)-N(1A)	171.9(2)
N(2B)-Ni(2)-O(1A)	93.2(2)	N(1A)-Ni(2)-O(1A)	80.5(2)
N(2B)-Ni(2)-O(1H)	93.0(3)	N(1A)-Ni(2)-O(1H)	93.5(3)
O(1A)-Ni(2)-O(1H)	173.6(2)	N(2B)-Ni(2)-N(1B)	77.7(2)
N(1A)-Ni(2)-N(1B)	97.1(2)	O(1A)-Ni(2)-N(1B)	90.0(2)
O(1H)-Ni(2)-N(1B)	92.9(3)	N(2B)-Ni(2)-O(1B)	76.0(2)

contd.

N(1A)-Ni(2)-O(1B)	109.1(2)	O(1A)-Ni(2)-O(1B)	92.7(2)
O(1H)-Ni(2)-O(1B)	87.3(2)	N(1B)-Ni(2)-O(1B)	153.8(2)
N(1C)-Ni(3)-N(4B)	177.7(2)	N(1C)-Ni(3)-O(1C)	81.3(2)
N(4B)-Ni(3)-O(1C)	96.9(2)	N(1C)-Ni(3)-O(1E)	90.0(2)
N(4B)-Ni(3)-O(1E)	91.4(2)	O(1C)-Ni(3)-O(1E)	92.3(3)
N(1C)-Ni(3)-O(1B)	99.6(2)	N(4B)-Ni(3)-O(1B)	79.0(2)
O(1C)-Ni(3)-O(1B)	91.7(2)	O(1E)-Ni(3)-O(1B)	170.0(2)
N(1C)-Ni(3)-O(1G)	94.1(2)	N(4B)-Ni(3)-O(1G)	87.8(2)
O(1C)-Ni(3)-O(1G)	175.2(2)	O(1E)-Ni(3)-O(1G)	86.3(3)
O(1B)-Ni(3)-O(1G)	90.4(2)	N(3C)-Ni(4)-N(4D)	174.2(2)
N(3C)-Ni(4)-O(1D)	97.5(2)	N(4D)-Ni(4)-O(1D)	79.7(2)
N(3C)-Ni(4)-O(4E)	91.2(2)	N(4D)-Ni(4)-O(4E)	91.5(2)
O(1D)-Ni(4)-O(4E)	171.1(2)	N(3C)-Ni(4)-N(4C)	78.4(2)
N(4D)-Ni(4)-N(4C)	96.4(2)	O(1D)-Ni(4)-N(4C)	89.4(2)
O(4E)-Ni(4)-N(4C)	90.3(2)	N(3C)-Ni(4)-O(1C)	76.1(2)
N(4D)-Ni(4)-O(1C)	109.1(2)	O(1D)-Ni(4)-O(1C)	94.7(2)
O(4E)-Ni(4)-O(1C)	89.4(2)	N(4C)-Ni(4)-O(1C)	154.5(2)
Ni(2)-O(1A)-Ni(1)	138.0(2)	Ni(3)-O(1B)-Ni(2)	136.2(2)
Ni(3)-O(1C)-Ni(4)	140.1(2)	Ni(4)-O(1D)-Ni(1)	137.5(2)

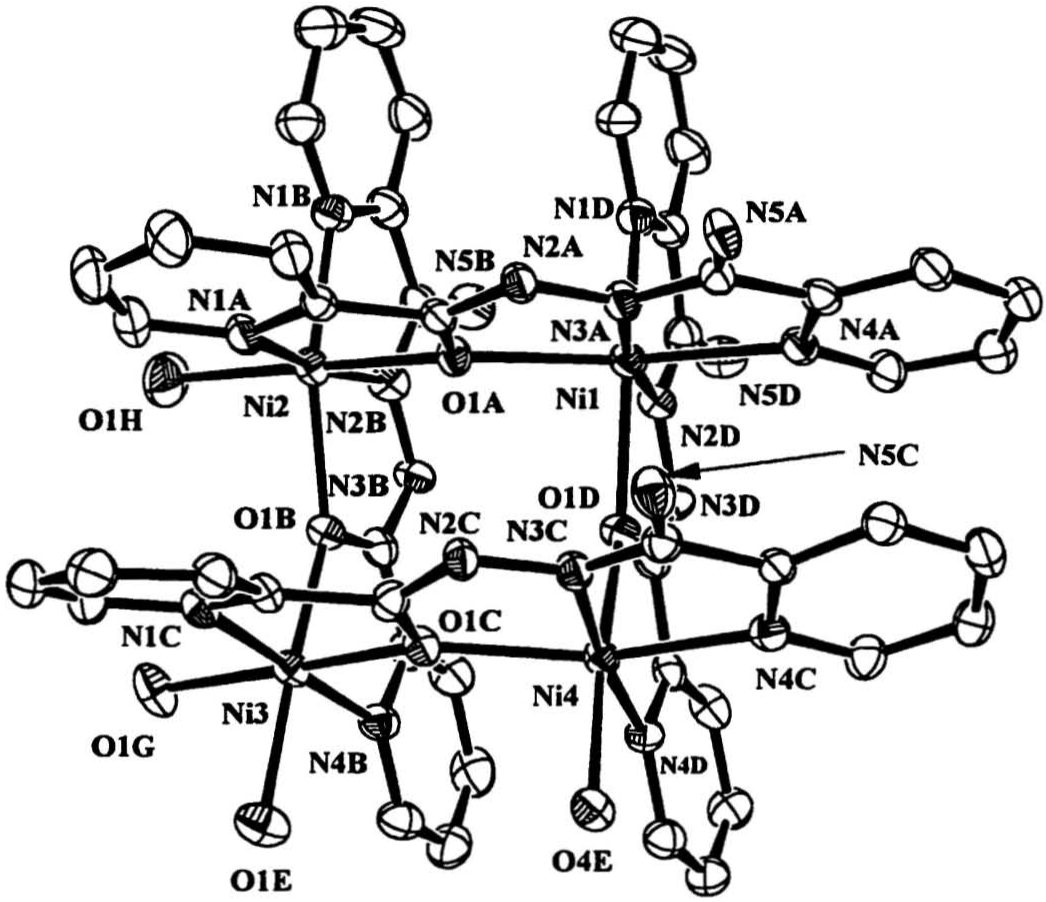

Figure 5-9. Structural representation of $Ni_4(PHAAP\text{-}H)_4(H_2O)_4](NO_3)_4.2.5H_2O$ (39) with hydrogen atoms omitted (50% probability thermal ellipsoids).

ligand, falling in the range 1.385(7)-1.397(7) Å), and slightly shorter than those in the spiral-like dinuclear Ni(II) complex (**29**) with the comparable ligand PAHAP; the C=N double bond distances in the NH_2-C=N framework are somewhat longer (1.292(2) -1.306(2) Å) than those in free ligand PAHAP and its polynuclear complexes, and the C=N and C-O bond distances in the O-C=N framework are comparable to those in $[Cu_4(OPA)](NO_3)_4.8H_2O$ [98] and the other relevant complexes [182, 183], indicating the sp^2 hybridization for N(2A-D) in the NCO (amide) fragments and the electron delocalization over N(2A-D) and O(1A-D).

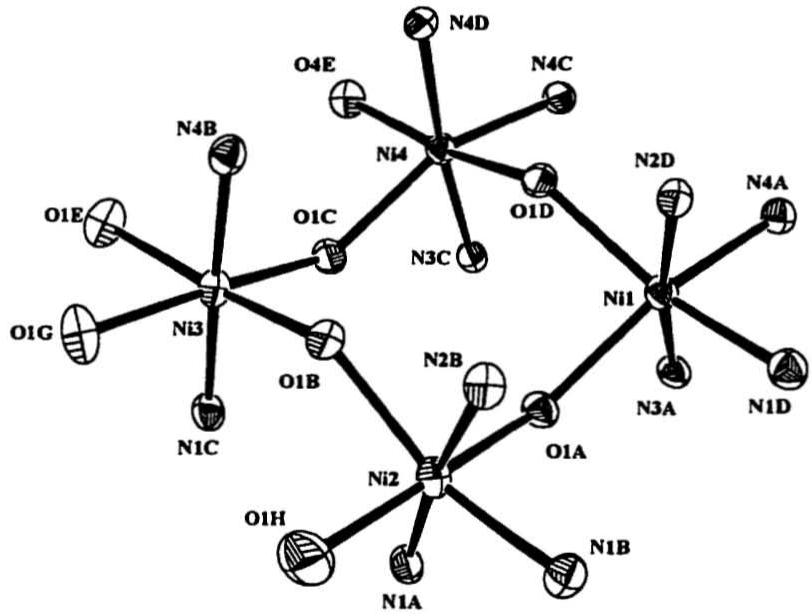

Figure 5-10. Expanded view of the coordination cores in **39**.

$[Cu_3Fe(PHAAP\text{-}H)_4(H_2O)_2](ClO_4)_5$ **(40)**

The structure of this most unusual $FeCu_3$ heterotetranuclear complex cation is depicted in **Figure 5-11**, and relevant bond length and bond angle information is given in **Table 5-8**. The expanded view of the coordination spheres of the metal ions in **40** along with the atom labeling scheme is illustrated in **Figure 5-12**. The four metal ions form a geometry between a trapezium and flattened tetrahedron (Fe(1)-Cu(1) 3.944(2) Å, Cu(1)-Cu(2) 3.960(2) Å, Cu(2)-Cu(3) 3.950(2) Å, Cu(3)-Fe(1) 3.892(2) Å), and the deviations from the least squares plane (Fe(1), Cu(1), Cu(2), Cu(3)) are quite small (-0.313(2), 0.308(2), -0.307(2), 0.313(2) Å respectively) suggesting that a trapezium is the most appropriate stereochemical description.

All four deprotonated PHAAP ligands adopt the same coordination mode as in the tetranuclear nickel (II) complex (**39**), with comparable relevant bond angles and bond distances, and bridge the four metal ions (Fe(1), Cu(1), Cu(2), Cu(3)) *via* their alkoxo groups (O(1), O(2), O(3), O(4)) that project above and below the trapezium plane (the deviations for O(1), O(2), O(3), O(4) from O(1)O(2)O(3)O(4) least squares plane are -0.719(2), 0.705(3), -0.798(2) and 0.812(2) Å respectively). The bridging angles (M-O(oxo)-M(or M')) are very close, falling in the range 133.6(2)-141.7(2)°.

The coordination sphere around Fe(1) is highly distorted octahedral (O(3)-Fe(1)-N(11) 149.7(1)°, O(4)-Fe(1)-N(16) 150.2(1)°, N(13)-Fe(1)-N(18) 171.4(2)°), consisting of two pyridine nitrogens (Fe(1)-N(16) 2.151(5) Å, Fe(1)-N(11) 2.140(4) Å), two diazine nitrogens (Fe(1)-N(13) 2.037(4) Å, Fe(1)-N(18) 2.022(4) Å) and two alkoxo oxygens

(Fe(1)-O(3) 1.996(3) Å, Fe(1)-O(4) 2.009(4) Å). Cu(1) is in a tetragonally distorted octahedron formed by two pyridine nitrogens (Cu(1)-N(1) 2.093(4) Å, Cu(1)-N(20) 1.970(4) Å), one diazine nitrogen (Cu(1)-N(3) 1.903(4) Å) and one alkoxo oxygen (Cu(1)- O(1) 2.201(3) Å) in the equatorial plane. Two additional oxygen atoms from alkoxo (O(4)) and water (O(5)) coordinate axially (Cu(1)-O(4) 2.248(4) Å, Cu(1)-O(5) 2.370(5) Å). The geometries around Cu(2) and Cu(3) centres are very similar, each with a significantly distorted square pyramid. The basal plane for Cu(2) is made up of N(5), O(6), N(10) and O(1) atoms with contacts in the range 1.967(4)-2.034(3) Å, while the one for Cu(3) involves N(15), N(6), N(8) and O(2) atoms with comparable distances (1.898(4)- 2.027(6) Å). O(2) and O(3) coordinate axially to Cu(2) and Cu(3) respectively (Cu(2)-O(2) 2.219(4) Å, Cu(3)-O(3) 2.236(3) Å). Therefore, the structure clearly indicates that the O(2), O(3) and O(4) atoms bridge the Fe(1), Cu(1), Cu(3) centers orthogonally, while O(1) atom bridges Cu(1) and Cu(2) in the equatorial planes.

Even though a number of Fe(III)Cu(II) mixed polynuclear complexes have been reported [184-187], this Fe(III)$Cu(II)_3$ tetranuclear cluster is unique.

Table 5-8. Interatomic distances (Å) and angles (Deg.) relevant to the copper and iron coordination spheres in $[Cu_3Fe(PHAAP\text{-}H)_4(H_2O)_2](ClO_4)_5$ **(40)**.

Cu(1)-O(1)	2.201(3)	Cu(2)-O(1)	1.990(3)
Cu(1)-O(4)	2.248(4)	Cu(2)-O(2)	2.219(4)
Cu(1)-O(5)	2.370(5)	Cu(2)-O(6)	2.034(3)
Cu(1)-N(1)	2.093(4)	Cu(2)-N(5)	1.967(4)
Cu(1)-N(3)	1.903(4)	Cu(2)-N(10)	1.975(5)

contd.

Cu(1)-N(20)	1.970(4)	Fe(1)-O(3)	1.996(3)
Cu(3)-O(2)	2.005(4)	Fe(1)-O(4)	2.009(4)
Cu(3)-O(3)	2.236(3)	Fe(1)-N(11)	2.140(4)
Cu(3)-N(6)	2.027(6)	Fe(1)-N(13)	2.037(4)
Cu(3)-N(8)	1.898(4)	Fe(1)-N(16)	2.151(5)
Cu(3)-N(15)	1.989(4)	Fe(1)-N(18)	2.022(4)
O(1)-C(7)	1.322(6)	N(3)-N(4)	1.369(6)
O(2)-C(19)	1.296(6)	N(8)-N(9)	1.381(8)
O(3)-C(31)	1.309(6)	N(13)-N(14)	1.385(6)
O(4)-C(43)	1.318(6)	N(18)-N(19)	1.397(7)
Fe(1)-Cu(1)	3.944(2)	Cu(1)-Cu(2)	3.960(2)
Cu(2)-Cu(3)	3.950(2)	Cu(3)-Fe(1)	3.892(2)
O(1)-Cu(1)-O(4)	88.4(1)	O(1)-Cu(2)-O(2)	96.2(1)
O(2)-Cu(3)-N(6)	159.7(2)	O(1)-Cu(1)-O(5)	82.7(1)
O(1)-Cu(2)-O(6)	175.5(1)	O(2)-Cu(3)-N(8)	79.1(2)
O(1)-Cu(1)-N(1)	155.3(1)	O(1)-Cu(2)-N(5)	83.7(1)
O(2)-Cu(3)-N(15)	99.4(2)	O(1)-Cu(1)-N(3)	75.4(1)
O(1)-Cu(2)-N(10)	93.5(2)	O(3)-Cu(3)-N(6)	92.2(2)
O(1)-Cu(1)-N(20)	109.6(1)	O(2)-Cu(2)-O(6)	86.8(1)
O(3)-Cu(3)-N(8)	106.7(1)	O(4)-Cu(1)-O(5)	166.0(1)

contd.

O(2)-Cu(2)-N(5)	111.4(2)	O(3)-Cu(3)-N(15)	77.3(1)
O(4)-Cu(1)-N(1)	96.7(2)	O(2)-Cu(2)-N(10)	79.1(2)
N(6)-Cu(3)-N(8)	80.7(2)	O(4)-Cu(1)-N(3)	98.1(2)
O(6)-Cu(2)-N(5)	92.2(2)	N(6)-Cu(3)-N(15)	100.7(2)
O(4)-Cu(1)-N(20)	78.2(2)	O(6)-Cu(2)-N(10)	90.3(2)
N(8)-Cu(3)-N(15)	175.8(2)	O(5)-Cu(1)-N(1)	95.9(2)
N(5)-Cu(2)-N(10)	169.4(2)	O(2)-Cu(3)-O(3)	95.3(1)
O(5)-Cu(1)-N(3)	90.0(2)	O(5)-Cu(1)-N(20)	94.6(2)
Cu(1)-O(1)-Cu(2)	141.7(2)	N(1)-Cu(1)-N(3)	80.0(2)
Cu(2)-O(2)-Cu(3)	138.5(2)	N(1)-Cu(1)-N(20)	95.0(2)
Cu(3)-O(3)-Fe(1)	133.6(2)	N(3)-Cu(1)-N(20)	173.5(2)
Cu(1)-O(4)-Fe(1)	135.7(1)	O(3)-Fe(1)-O(4)	94.9(1)
O(3)-Fe(1)-N(11)	149.7(1)	O(3)-Fe(1)-N(13)	74.3(1)
O(3)-Fe(1)-N(16)	92.0(2)	O(3)-Fe(1)-N(18)	109.3(1)
O(4)-Fe(1)-N(11)	93.6(2)	O(4)-Fe(1)-N(13)	112.6(2)
O(4)-Fe(1)-N(16)	150.2(1)	O(4)-Fe(1)-N(18)	75.3(2)
N(11)-Fe(1)-N(13)	75.6(2)	N(11)-Fe(1)-N(16)	94.9(2)
N(11)-Fe(1)-N(18)	101.0(2)	N(13)-Fe(1)-N(16)	97.2(2)
N(13)-Fe(1)-N(18)	171.4(2)	N(16)-Fe(1)-N(18)	75.1(2)

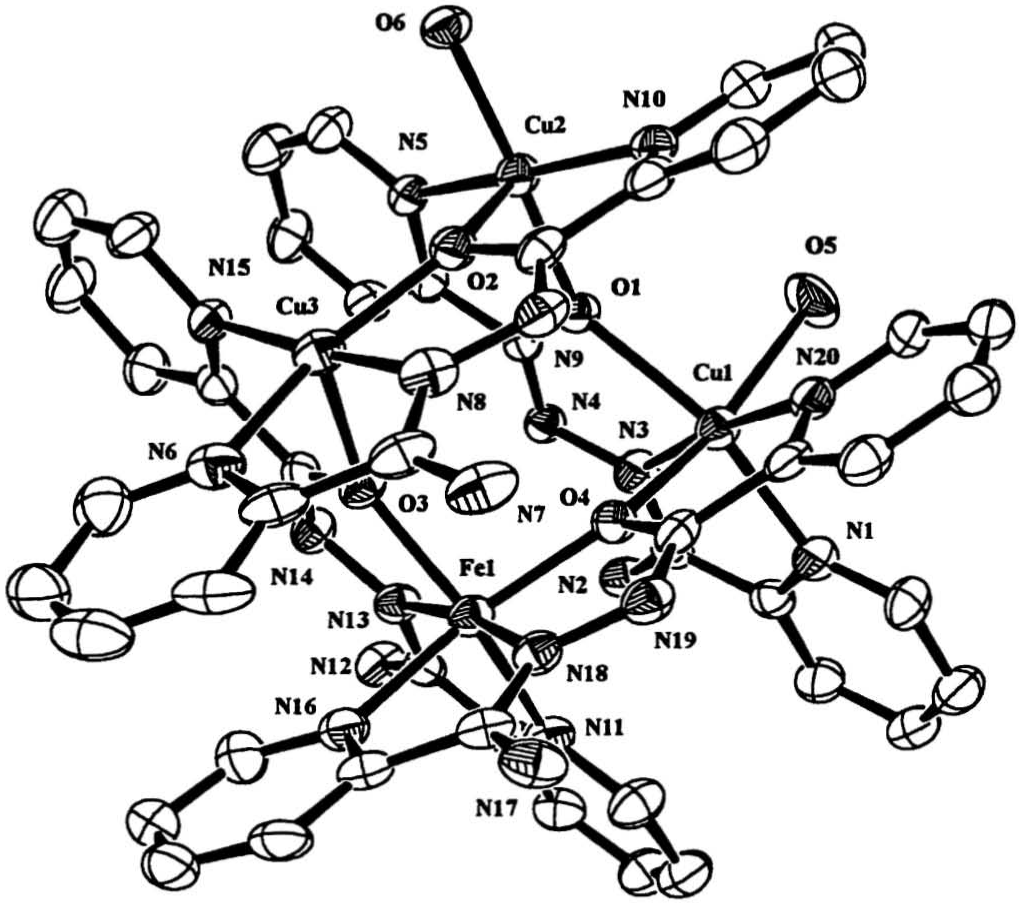

Figure 5-11. Structural representation of $[Cu_3Fe(PHAAP\text{-}H)_4(H_2O)_2](ClO_4)_5$ (40) with hydrogen atoms omitted (30% probability thermal ellipsoids).

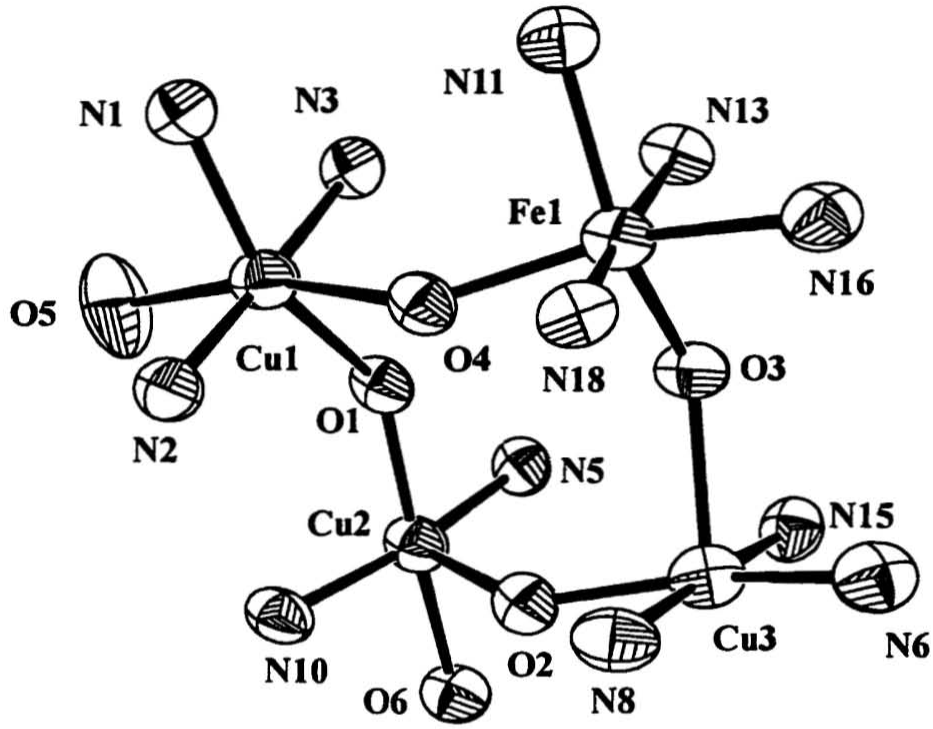

Figure 5-12. Expanded view of the coordination cores in **40**.

$[Cu(II)_4Cu(I)_2(PAH)_4Br_{10}]$ **(41)**

The structure of **41** is illustrated in **Figure 5-13**, and relevant bond distances and angles are listed in **Table 5-9**. This peculiar six-centered mixed valence [188-202] copper complex formed through a partially reducing process of Cu(II) by the hydrolyzed product PAH of PTS **(Scheme 5-2)** and can be described as the combination of four copper (II)

Scheme 5-2

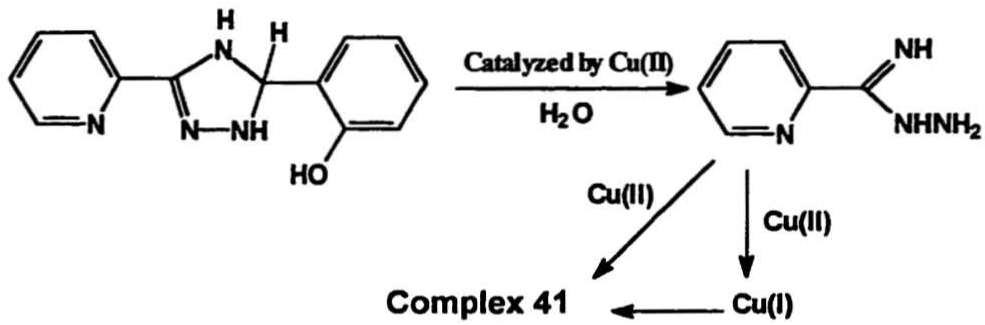

centers bridged by a dinuclear copper(I) anion $[Cu(I)_2Br_6]^{4-}$ *via* Br(1), Br(4), Br(1)a and Br(4)a. All copper (II) centers have a square planner coordination environment. Each of them has normal bond distances and angles e.g. for Cu(1) or Cu(2), the Cu-N_{py} distances fall in the range 1.969(7)-2.047(6) Å and Cu-Br distances in the range 2.366(2)-2.477(1) Å. The neighboring angles around each copper(II) center fall in the range 79.8(3)-95.2(2)° and the angles between two none-adjacent bonds fall in the range 171.3(2)-163.6(2)°. The sum of the angles at the copper(II) centers in each copper plane is 358.68 for Cu(1) and 360.75° for

Cu(2). In the dinuclear copper(I) anion $[Cu(I)_2Br_6]^{4-}$, two identical Cu(I) centers are bridged by Br(5) and Br(5)a to form a typical planar rhombohedral geometry (Cu(3)-Br(5)-Cu(3)a-Br(5)a) and each has a slightly distorted tetrahedral coordination geometry with normal Cu(I)-Br bond distances in the range 2.460(2)-2.572(2) Å and angles in the range 97.88(6)-117.60(7)°. There are no significant interactions between Cu(1) and Br(3), and between Cu(2) and Br(1) (Cu(1)-Br(3) (4.797(3)Å), Cu(2)-Br(1) (4.327(3)Å). The copper-copper separations are 3.081(2), 3.269(2), 4.164(2) and 3.671(3) Å for Cu(3)-Cu(3)a, Cu(3)-Cu(1), Cu(3)-Cu(2) and Cu(1)-Cu(2) respectively.

Within the neutral PAH ligands, the structural data show the existence of a $N{=}C{-}NH{-}NH_2$ framework for PAH (C(6)-N(2) 1.27(1) Å, C(12)-N(6) 1.27(1) Å; C(6)-N(3) 1.30(1) Å, C(12)-N(7) 1.309(9) Å), not the proposed resonance structure HN=C-NH-NH2 $\leftrightarrow$ $HN{=}C{-}NH{-}NH_2$ for the free ligand [100, 101]. This is due to the coordination of the ligand to Cu(II) centers *via* N(2) or N(6) which fixes the double bond characters in the N-C-N framework.

It is interesting to note that even though the free [203-207] or bridging [13, 208, 209] $[Cu(I)Cl_3]^{2-}$ and $[Cu(I)Br_3]^{2-}$ species are known, the bridging arrangement in $[Cu(I)_2Br_6]^{4-}$ is unique.

Table 5-9. Interatomic distances (Å) and angles (Deg.) relevant to the copper coordination spheres in $[Cu(II)_4Cu(I)_2(PAH)_4Br_{10}]$ (**41**).

Cu(1)-Br(2)	2.366(2)	Cu(2)-Br(4)	2.442(2)
Cu(1)-N(1)	2.047(6)	Cu(2)-Br(3)	2.388(1)
Cu(1)-N(2)	1.969(7)	Cu(2)-N(5)	2.044(6)
Cu(1)-Br(1)	2.477(1)	Cu(2)-N(6)	1.972(6)
Cu(1)-Br(3)	4.797(3)	Cu(2)-Br(1)	4.327(3)
Cu(3)-Br(5)	2.467(2)	N(3)-N(4)	1.429(9)
Cu(3)-Br(5)	2.460(2)	N(7)-N(8)	1.424(9)
Cu(3)-Br(1)	2.572(2)	C(6)-N(2)	1.27(1)
Cu(3)-Br(4)	2.503(2)	C(12)-N(6)	1.27(1)
Cu(1)-Cu(2)	3.671(3)	C(6)-N(3)	1.30(1)
Cu(1)-Cu(3)	3.269(2)	C(12)-N(7)	1.309(9)
Cu(2)-Cu(3)	4.163(2)	Cu(3)-Cu(3)a	3.081(2)

Cu(1)-Br(1)-Cu(3)	111.10(5)	Cu(2)-Br(4)-Cu(3)	82.76(6)	Cu(3)-Br(5)-Cu(3)	77.42(5)
Br(1)-Cu(1)-Br(2)	93.28(5)	Br(1)-Cu(1)-N(1)	170.3(2)	Br(1)-Cu(1)-N(2)	91.3(2)
Br(2)-Cu(1)-N(1)	94.3(2)	Br(2)-Cu(1)-N(2)	163.6(2)	N(1)-Cu(1)-N(2)	79.8(3)
Br(3)-Cu(2)-Br(4)	93.25(5)	Br(3)-Cu(2)-N(5)	95.2(2)	Br(3)-Cu(2)-N(6)	163.9(2)
Br(4)-Cu(2)-N(5)	171.3(2)	Br(4)-Cu(2)-N(6)	91.8(2)	N(5)-Cu(2)-N(6)	80.5(3)
Br(1)-Cu(3)-Br(4)	97.88(6)	Br(1)-Cu(3)-Br(5)	109.15(6)	Br(1)-Cu(3)-Br(5)	115.80(6)
Br(4)-Cu(3)-Br(5)	17.60(7)	Br(4)-Cu(3)-Br(5)	114.41(6)	Br(5)-Cu(3)-Br(5)	102.58(5)

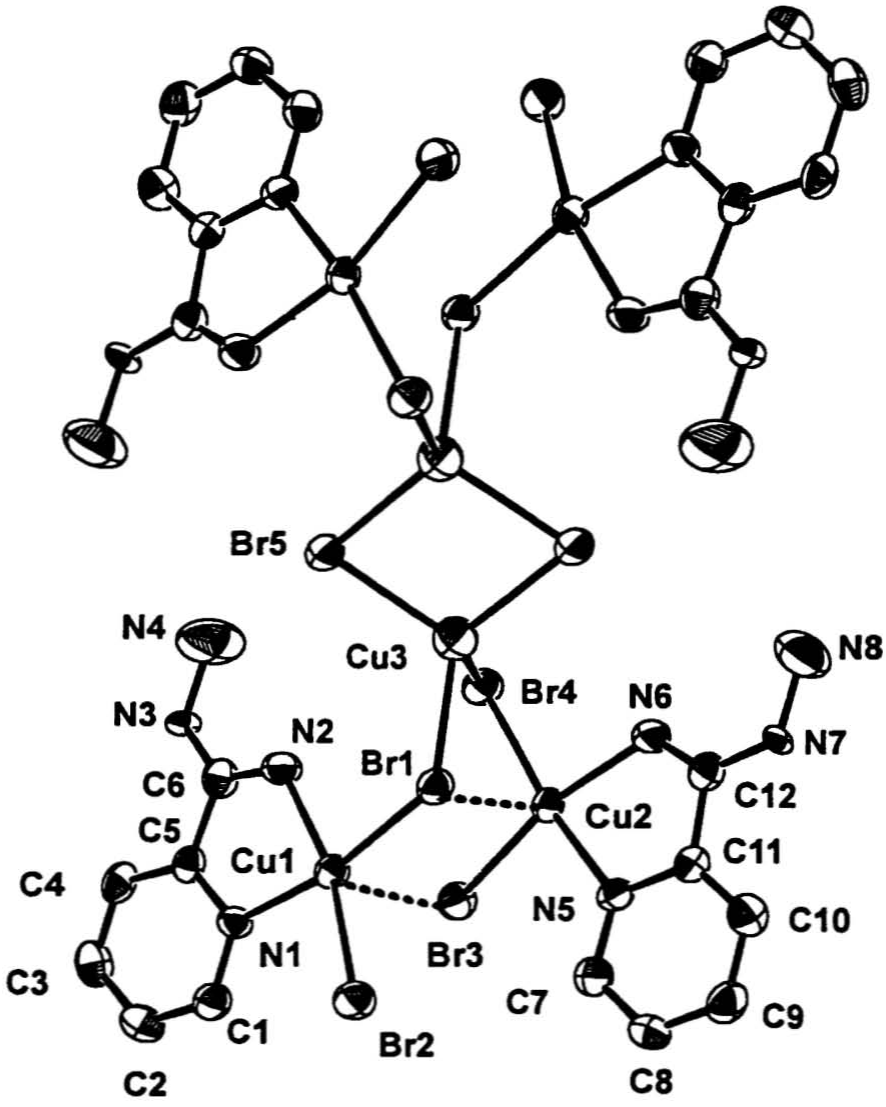

Figure 5-13. Structural representation of $[Cu(II)_4Cu(I)_2(PAH)_4Br_{10}]$ (41) with hydrogen atoms omitted (50% probability thermal ellipsoids).

5.3.2 Spectroscopy

Several ν_{NH} bands are observed in the infrared spectrum of **33** (3387, 3297, 3235 cm^{-1}), confirming the existence of a free NH_2 group, and there is no higher energy band due to ν_{OH}. In the ν_3 Cl-O stretching region three dominant perchlorate bands are observed at 1109, 1050 and 1011 cm^{-1}, but expansion of this region reveals further fine structure and a total of seven bands. The three main bands are sensibly assigned to the bridging perchlorate connecting the two copper centers in an intramolecular fashion, associated with nominal C_{2v} local site symmetry. The additional bands are possibly due to the asymmetric nature of this bridge, and the additional bridging interactions (**Figure 5-2**). The pyridine ring breathing band was found at 1026 cm^{-1}. Visible absorptions for **33** are difficult to resolve, with a broad shoulder occurring at about 600 nm in both solid and solution.

The high energy region of the infrared spectrum of **34** is dominated by a strong, sharp band at 3620 cm^{-1} (ν_{OH}; NO-H), and ν_{NH} bands at 3440 and 3247 cm^{-1} due to the free NH_2 group. A very complex absorption envelope is observed in the range 989-1172 cm^{-1}, with a total of eleven resolvable bands. These are clearly associated with the ν_3 sulfate vibration, split as a result of reduced symmetry in the unusual bridging mode. The band at 1024 cm^{-1} is due to the pyridine ring breathing mode. This complex exhibits a broad visible band in the solid state at 660 nm, which shifts to higher energy (595 nm) in water, but to lower energy (715 nm) in DMF, indicative of a significant structural change in solution.

The infrared spectrum of **35** shows similar bands above 3100 cm^{-1} to those of **34**, indicative that both NH_2 and OH groups in the ligand are not coordinated to the Co(III) ion. The pyridine ring breathing band appears at 1035 cm^{-1} suggesting a strong coordination of the pyridine nitrogen to the Co(III) centre. Only one prominent ($\nu_1 + \nu_4$) [112] nitrate band located at 1755 cm^{-1} indicates that the nitrates in the complex are uncoordinated.

Very complex ν_{NH} bands located in the range 3380-3165cm^{-1} (five bands) are observed in the infrared spectrum of **36**, supporting the presence of two different amino groups. Two pyridine ring breathing bands were observed at 995 cm^{-1}, which is identical to that of the free ligand, and at 1043 cm^{-1}, corroborating the structural evidence that only one pyridine ring is coordinated to the V(V) centre. The strong band at 923 cm^{-1} can be assigned to $\nu_{V=O}$ stretch in the cis-VO_2^+ group [177-179].

Complex **37** exhibits two ν_{NH} infrared bands at 3360 and 3185 cm^{-1} due to the free NH_2 groups in PAHAP, and a sharp band at 3520 cm^{-1} due to coordinated water molecules and the lattice water band at ca. 3550 cm^{-1} (br). The strong $\nu_{C=N}$ band at 1665 cm^{-1} is in agreement with the fact that the PAHAP ligands in the complex adopt a twisted conformation. The prominent ($\nu_1 + \nu_4$) [112] nitrate bands are observed at 1765 and 1755 cm^{-1}, suggesting the presence of monodentate nitrates. Only one pyridine ring breathing band was observed at 1020 cm^{-1}, suggesting that both pyridine nitrogens in each ligand are in the same coordination environment.

Several bands above 3100 cm^{-1} were found in the infrared spectrum of **38**, and the broad bands at ca. 3600 and 3437 cm^{-1} are associated with the lattice water and coordinated molecules respectively, while the bands at 3326 and 3207 cm^{-1} can be assigned to N-H stretch of the free NH_2 groups. The strong band at 1664 cm^{-1} could result from a C=O incorporated in a conjugated system or C=N in a twisted open-chain diazine unit. However the absence of a ν_{OH} band at 3409 cm^{-1} in the free ligand PHAAP suggests the deprotonation of the ligand in this complex. Therefore, it is more reasonable to assign the 1664 cm^{-1} peak to the stretching band of the C-O group with some double bond character in a conjugated O-C-N-N framework. If both pyridine rings are assumed to be coordinated in this compound because there is no free pyridine ring breathing band observed, and considering the normal room temperature magnetic moment (1.83 BM see next section) for this compound, a situation in which the alkoxo group in the deprotonated ligand is bound orthogonally, with a large Cu-alkoxo-Cu angle between adjacent copper centers to form a cyclic structure is most plausible (see the schematic representation, **Scheme 5-4**, of **38** in the next section). The singlet ν_3 Cl-O stretching band of free ClO_4^- at 1074 cm^{-1} is so strong that the pyridine ring breathing bands, expected to be at this region, cannot be observed. **38** exhibits a broad visible band in the solid state at 658 nm, which is essentially unchanged in aqueous solution (665 nm, ε = 550 $dm^3.mol^{-1}.cm^{-1}$), indicative of very little structural change in solution.

The bands above 3100 cm^{-1} in the infrared spectrum of compound **39** are very similar to those of **38** with very little position differences. The C=O (in the O-C-N-N

conjugated framework) stretch band was observed at 1658 cm^{-1} and coordinated pyridine ring breathing bands were found at 1034, 1022 cm^{-1}. Only one prominent ($\nu_1 + \nu_4$) [112] nitrate band located at 1765 cm^{-1} indicates that all nitrates in **39** are uncoordinated. These infrared data are in agreement with its cyclic tetranuclear structure. The solid state Nujol mull transmittance and aqueous solution electronic spectra of **39** give very similar bands at 955 nm (broad, $\varepsilon = 86.26\ dm^3.mol^{-1}.cm^{-1}$) and 565 nm (shoulder, $\varepsilon = 50.97\ dm^3.mol^{-1}.cm^{-1}$) due to ν_1 ($^3A_{2g} \rightarrow {}^3T_{2g}$) and ν_2 ($^3A_{2g} \rightarrow {}^3T_{1g}$) respectively, suggesting that all Ni(II) centers have distorted octahedral coordination environments and the coordination differences among the nickel(II) centers cannot significantly change the positions of the UV/vis bands, and that there is no significant solvation occurring in water.

The infrared spectrum of **40** is very similar to that of **38**, which is as expected. However, the position for each group in the spectrum of **40** is slightly different from that for the corresponding group of **38**, e.g. 3556 cm^{-1} (lattice water), 3437-3173 cm^{-1} (NH_2), 1092 cm^{-1} (ν_3 stretching band of free ClO_4^-). A broad visible band was observed at 615 nm in the solid state and the same value (616 nm) was found in aqueous solution ($\varepsilon = 1834\ dm^3.mol^{-1}.cm^{-1}$), indicative of no significant solvation occurring in water. The large ε value suggests that this band results from the CT absorption of L→Fe(III) or together with *d-d* absorptions in the copper centers.

Two weak but sharp ν_{NH} bands are observed in the infrared spectrum of **41** (3315 and 3286 cm^{-1}), consistent with the presence of NH_2 groups, but a detailed assignment cannot be made. The pyridine ring breathing band occurs at 1021 cm^{-1}, indicative of the

coordination of pyridine nitrogens. The $\nu_{C=N}$ band appears at a slightly higher energy than that of the free PAH (1644 cm^{-1}), which is not as expected. The reason for this is that the C=N bond is delocalized in PAH, which is mirrored by its ^1H NMR spectrum, but in the complex the C-N bond has significant double bond character (C(6)-N(2) (1.27(1) Å). A visible band was observed as a shoulder at 680 nm in the solid state Nujol mull transmittance electronic spectrum of **41**, which is basically dominated by a Br→Cu CT band at 465 nm.

5.3.3 Magnetism

Variable temperature magnetic susceptibility data were collected for powdered samples of the complexes **33**, **34** and **40**, and taken from the same uniform batches used for structural determination. The samples were pre-dried under vacuum in order to prevent possible mass loss during sample preparation prior to a variable temperature run. In those cases where obvious desolvation occurred elemental analyses were repeated.

Compound **33** has a very low room temperature magnetic moment (μ_{eff} = 0.88 BM), indicating spin coupling between the copper(II) centers and the presence of net strong antiferromagnetism. The susceptibility versus temperature profile (**Figure 5-14**) shows a rise in χ_m approaching 300 K, but no maximum, and a sharp rise in χ_m at low temperature indicating significant paramagnetic impurity. Analysis of the data using **eqn. 1-4** gives g = 2.069(22), 2J = -549(6) cm^{-1}, Nα = 49*10^{-6} emu, ρ = 0.035, θ = -1.0 K,

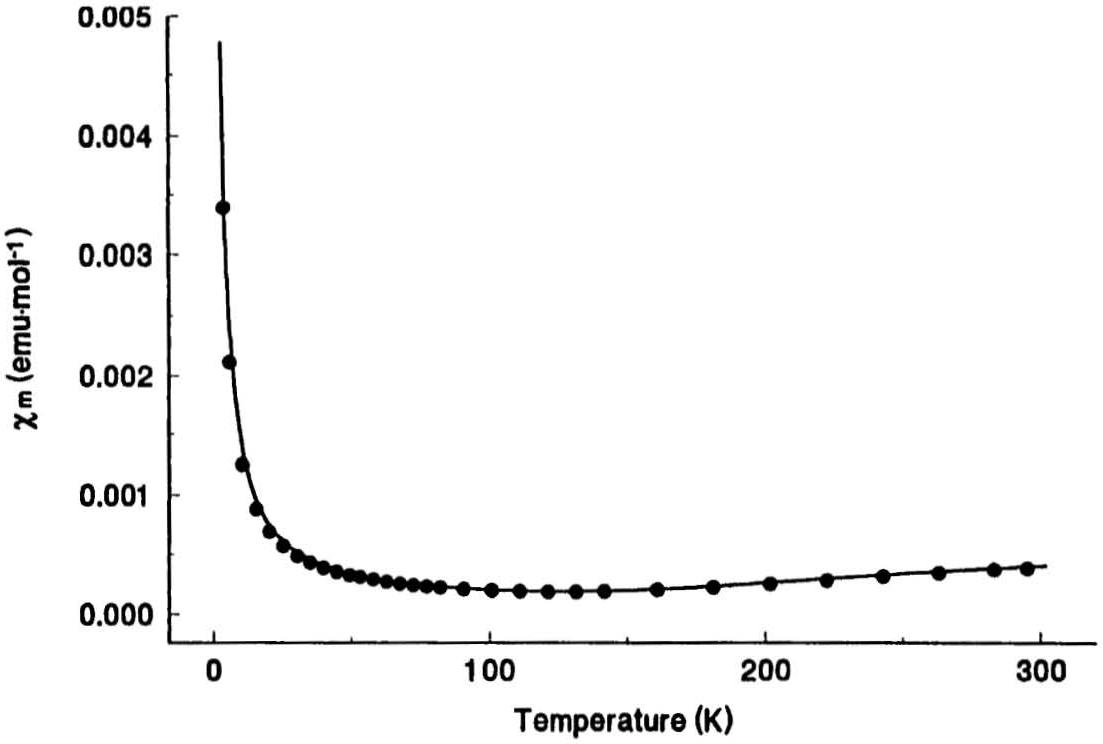

Figure 5-14. Variable temperature magnetic data for complex **33**. The solid line was calculated from **eqn. 1-4** with g = 2.069(22), $-2J = 549(6)\ cm^{-1}$, $\rho = 0.035$, $N\alpha = 49*10^{-6}$emu, $\theta = -1.0K$, $10^2R = 1.7$ ($R = [\Sigma(\chi_{obs} - \chi_{calc})^2/\Sigma\chi_{obs}^2]^{1/2}$).

$10^2R = 1.7$; $R = [\Sigma(\chi_{obs} - \chi_{calc})^2/\Sigma\chi_{obs}^2]^{1/2}$ for the best fit line (**Figure 5-14**). The small negative θ value suggests the presence of a weak intermolecular antiferromagnetic component. This could be associated with the perchlorate bridges and the hydrogen bonding bridging interactions, but these are nominally orthogonal in nature.

Reports of magnetic studies on such dicopper(II) systems symmetrically bridged by a bis-μ_2-NO unit are limited, but strong antiferromagnetic coupling is typical. The symmetrically N-O bridged complex ion $[Cu(DAPDH)]_2^{2+}$ (Cu(NO)(ON)Cu) has a room temperature magnetic moment of 0.6 BM indicative of strong antiferromagnetic coupling [210], while the asymmetrically bridged iodo-complex $[LCu(PyA)_2Cu(I)]ClO_4.CH_3CN$ ($Cu(NO)_2Cu$) (L = 1,4,7-trimethyl-1,4,7-triazacyclononane; PyA = monoanion of pyridine-2-aldoxime) [176] exhibits very strong antiferromagnetic coupling ($-2J > 1000$ cm^{-1}). The copper-copper separation in this complex (3.45 Å) is comparable with that in **33**, and it exhibits a similar boat shaped structure, with an angle of 120° between the copper mean planes. It is not immediately obvious why the exchange situation for these two complexes is so different, but from a structural perspective it appears that the asymmetric $(NO)_2$ bridging arrangement provides the stronger coupling. Extended Hückel calculations on **37** show two triplet state molecular orbitals with a high degree of alignment of the copper *d* orbitals and the nitrogen and oxygen *p* orbitals in the dicopper chelate ring. A ΔE value of 82 meV is large enough to corroborate the antiferromagnetic exchange situation, but no comparison can be made with complexes in Chapters 2 and 3.

Compound **34** has a room temperature magnetic moment of (μ_{eff}) 1.85 BM, suggesting no coupling, and this is confirmed by the χ_m*T versus temperature profile, which shows a constant χ_m*T value of 0.42 throughout the 4-300 K temperature range. The two copper(II) centers in **34** are completely uncoupled, consistent with the axial/equatorial arrangement of bonds to the sulfate bridges, leading to effective orthogonality between the copper magnetic orbitals. This contrasts with the magnetic behaviour of the complex $[Cu(5'\text{-UMP})(dpa)(H_2O)]_2.5H_2O$ [173] (5'-UMP = Uridine-5'-monophosphate; dpa = dipyridyl-amine), which exhibits weak antiferromagnetic exchange ($-2J = 10.8\ cm^{-1}$), associated with the equatorial/equatorial phosphate bridging arrangement. The weak coupling in this case can reasonably be explained by the bridging mode of phosphate, which connects the copper magnetic orbitals directly.

Compound **38** has a room temperature magnetic moment of 1.83 BM (per Cu(II)), suggesting no coupling. Because of their relative ease of synthesis, and of the design of many new polynucleating ligands for use in bioinorganic model and magnetochemical studies, there are many examples of $Cu(II)_4$ complexes reported. The geometries of these tetracopper(II) complexes can be classified into many types [167] e.g. rhomboidal, parallelogram, distorted cubane, tetrahedral, linear, planar cyclic, and pair-of-dimers. The partially finished single crystal structure of **38** shows that the four five-coordinate copper(II) centers (square pyramidal) are arranged approximately in a square and are

bridged orthogonally *via* four alkoxo oxygens from four deprotonated ligands, which are arranged in a very similar manner in the complex **39** and **40** (see **Figure 5-9** and **Figure 5-11**. **Scheme 5-4** represents part of the structure of **38**). Thus complex **38** belongs to one of the planar cyclic $Cu(II)_4$ types. Because of the orthogonality between the copper(II) magnetic orbitals, the four copper(II) centers in **38** should not have significant magnetic coupling, which is consistent with the room temperature magnetic moment measurement. We await a variable temperature magnetic study on this compound.

Scheme 5-4

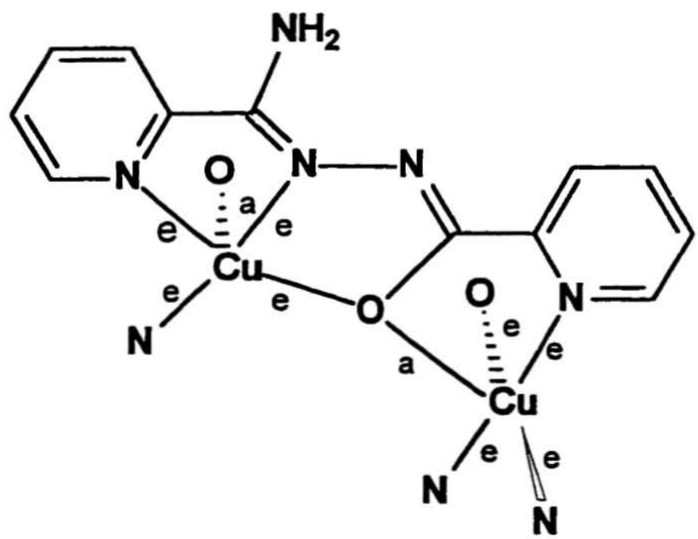

Complex **39** has a room temperature magnetic moment of 3.10 BM (per Ni(II)). The Ni-O-Ni angles are large and fall in the range 136.2-140.1°, which would be expected to propagate some antiferromagnetic coupling between the nickel(II) centres. A comparable tetranickel(II) complex with Ni-O-Ni angles around 141° was shown to be antiferromagnetically coupled, although no fitting of the variable temperature susceptibility data was attempted [211].

Compound **40** has a room temperature magnetic moment of 5.02 BM (per mole). A plot of μ_{mol} versus temperature for **40** is illustrated in **Figure 5-15**, indicating a very complicated magnetic coupling process: the decrees in μ_{mol} value from 5.02 BM at 295.2 K to 4.79 BM at 63 K suggests the presence of intramolecular antiferromagnetic coupling or a high-low spin transition for Fe(III) or both, while the rise in μ_{mol} value from 4.79 BM at 63 K to 5.59 BM at 4 K, evidently demonstrates the presence of intramolecular ferromagnetic coupling. The spin-only magnetic moment for a $Fe(III)Cu(II)_3$ cluster assuming Fe(III) in a high-spin or a low-spin state is estimated on the basis of the expression:

$$\mu_{mol}^2 = \mu_{Cu(1)}^2 + \mu_{Cu(2)}^2 + \mu_{Cu(3)}^2 + \mu_{Fe(1)}^2$$

and using μ_{Cu} = 1.73 BM and μ_{Fe} = 5.92 BM for high spin Fe(III) and μ_{Fe} = 1.73 BM for low spin Fe(III). The calculated values are 6.64 and 3.46 BM respectively, both of which are far away from the experimental value (5.02 BM). From a structural perspective, any intramolecular antiferromagnetic coupling should occur only between Cu(1) and Cu(2) *via*

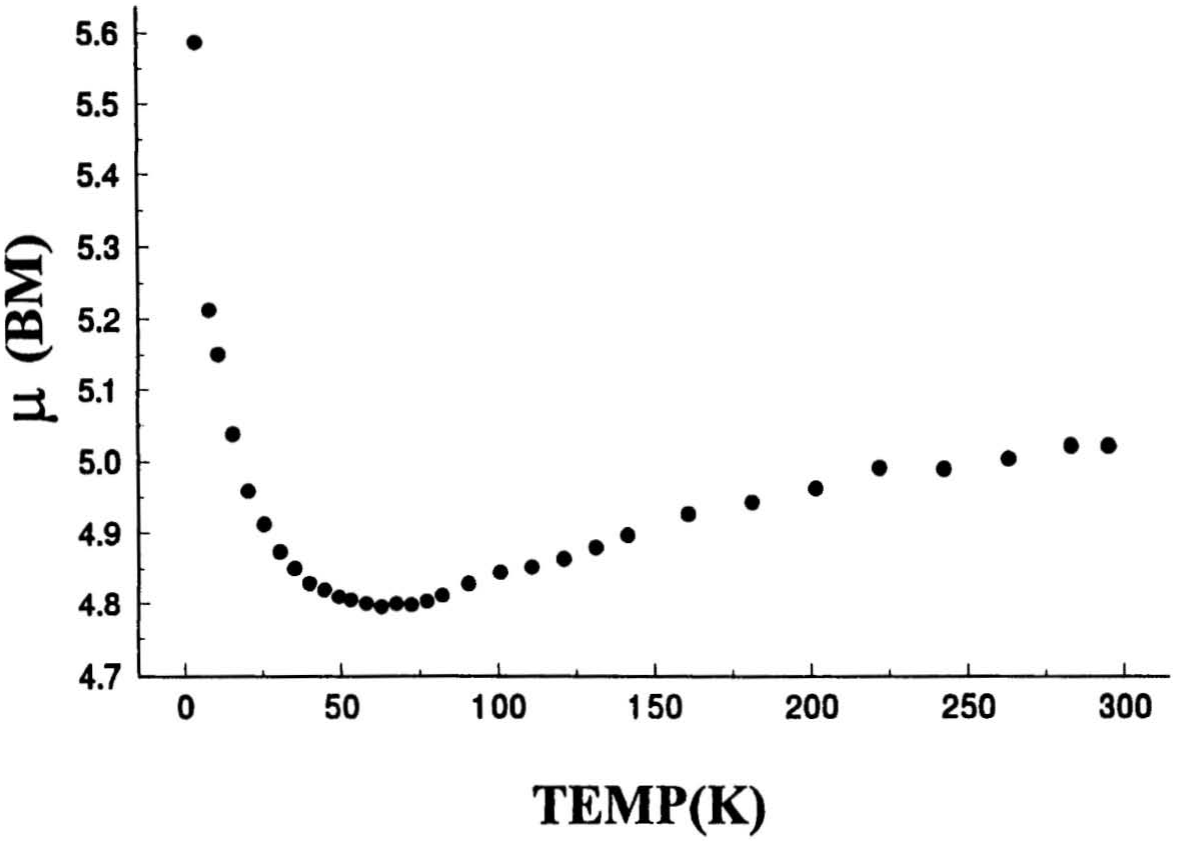

Figure 1-15. Variable temperature magnetic moment for **40**.

O(1). All other bridge connections are effectively orthogonal. Assuming that the antiferromagnetic coupling between Cu(1) and Cu(2) is very strong, because of the very large Cu(1)-O(1)- Cu(2) angle (141.7°) [39] (e.g. $\mu_{Cu(1)} = \mu_{Cu(2)} = 0.5$ BM), and using μ_{Fe} = 5.92 BM for high-spin Fe(III) and μ_{Fe} = 1.73 BM for low-spin Fe(III), the estimated room temperature magnetic moments of 6.28 BM and 2.54 BM for the high-spin or low-spin extremes in **40** are still too far away from the experimental value (5.02 BM). Therefore it is reasonable to assume that the Fe(III) centre in **40** exhibits a LS (S = 1/2) ↔ HS (S = 5/2) transition in the solid state.

The spin transition phenomenon for Fe(III) was observed for the first time by Cambi in the 1930s in some tris(dithiocarbamato) iron(III) complexes [212-214]. The dithiocarbamato ligands are of the type shown in **Scheme 5-3a**, and the complexes have a FeS_6 core. In the family of tris(dithiocarbamato) iron(III) complexes, if there is a spin transition in the solid state, it is always very smooth, without detectable hysteresis.

Scheme 5-3

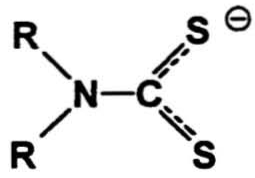

dithiocarbamato⁻(a)

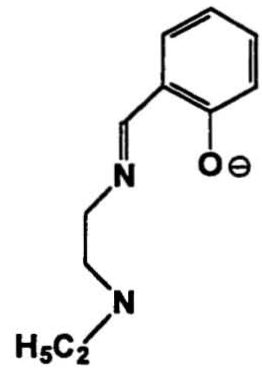

X-saleten⁻ (b)

Other interesting examples of spin transitions in iron(III) chemistry have been reported by Hendrickson et al. [215-217] in the series of complexes with a general formula $[Fe(X\text{-saleten})_2]Y$ (X-saleten$^-$ is shown in **Scheme 5-3b**. Y is a counteranion like NO_3^-, PF_6^- or BPh_4^-). These complexes have a pseudo-octahedral geometry with a FeN_4O_2 core, and exhibit a LS (S = 1/2) $\leftrightarrow$ HS (S = 5/2) transition without an intermediate spin state S = 3/2 being observed. For most of them, the transition is gradual, and often incomplete at low temperature. Compared with these complexes, the Fe(III) centre in complex **40** also has a FeN_4O_2 core, and with a very similar coordination environment. Therefore, assuming that Fe(III)(1) in **40** has an incomplete LS (S = 1/2) $\leftrightarrow$ HS (S = 5/2) transition either at room temperature (e.g. $\mu_{Fe(1)}$ = 4.65 BM at 295.2 K) or at low temperature (e.g. $\mu_{Fe(1)}$ = 4.41BM at 63 K), and there is a weak intramolecular ferromagnetic coupling between Fe(1) and Cu(1) or Cu(3) because of their orthogonalities, the complicated magnetic behaviour for **40** is reasonable, even though its detailed interpretation cannot be made at this time.

Compound **41** has a room temperature magnetic moment of 1.84 BM (per Cu(II)), which suggests no coupling between the four Cu(II) centers. There is no variable temperature magnetic study on this complex. However, from a structural perspective, any intramolecular magnetic interaction should only take place *via* the four Br-Cu(I)-Br linkages of the $[Cu(I)_2Br_6]^{4-}$ unit, which are obviously too long to generate any significant coupling.

Compound **35** has a room temperature magnetic moment of 0.50 BM, indicating that Co(III) is diamagnetic and in a low-spin state, which is consistent with its structure.

Compound **36** is diamagnetic (μ = 0.41 BM at room temperature) and gives a very interesting ^{1}H NMR spectrum. The room temperature ^{1}H NMR spectrum of **36** in d_6-DMSO (illustrated in **Figure 5-16**) shows one set of multiplets (4H) at 8.39-8.89 ppm due to the coordinated pyridyl ring, which is further downfield than those in the free ligand because of an electronic effect, and another set of multiplets (4H) at 7.44-8.35 ppm which is essentially the same as those of the free ligand (**Figure 4-15**). There is only one singlet showing up in the spectrum, which may result from the proton in the coordinated NH^- or a half deuterated free amino group. However, what is more likely is that, since the coordinated amino group has already been deprotonated, further H-D exchange between this amino group with D_2O (d_6-DMSO usually contains trace amounts of D_2O) is not favourable. Thus, the singlet is best assigned to the proton in the coordinated amino group (NH^-) and the singlet due to the free amino group does not appear because of the H-D exchange which is favoured by the coordination of the ligand to the metal ion.

Compared with those in the ^{1}H NMR of the free ligand, the pyridyl multiplets (4H) in the ^{1}H NMR spectrum of **37** in D_2O (**Figure 5-17**) appear at slightly lower field (higher chemical shifts) due to a weak electronic effect, since the coordination of the ligand to the Cd(II) ion is comparatively weak (Cd(1)-N(1) 2.313(2) Å; Cd(1)-N(6) 2.314(2) Å). In addition, each Cd(II) centre only contains two pyridyl rings (not three as in the cases of **26**

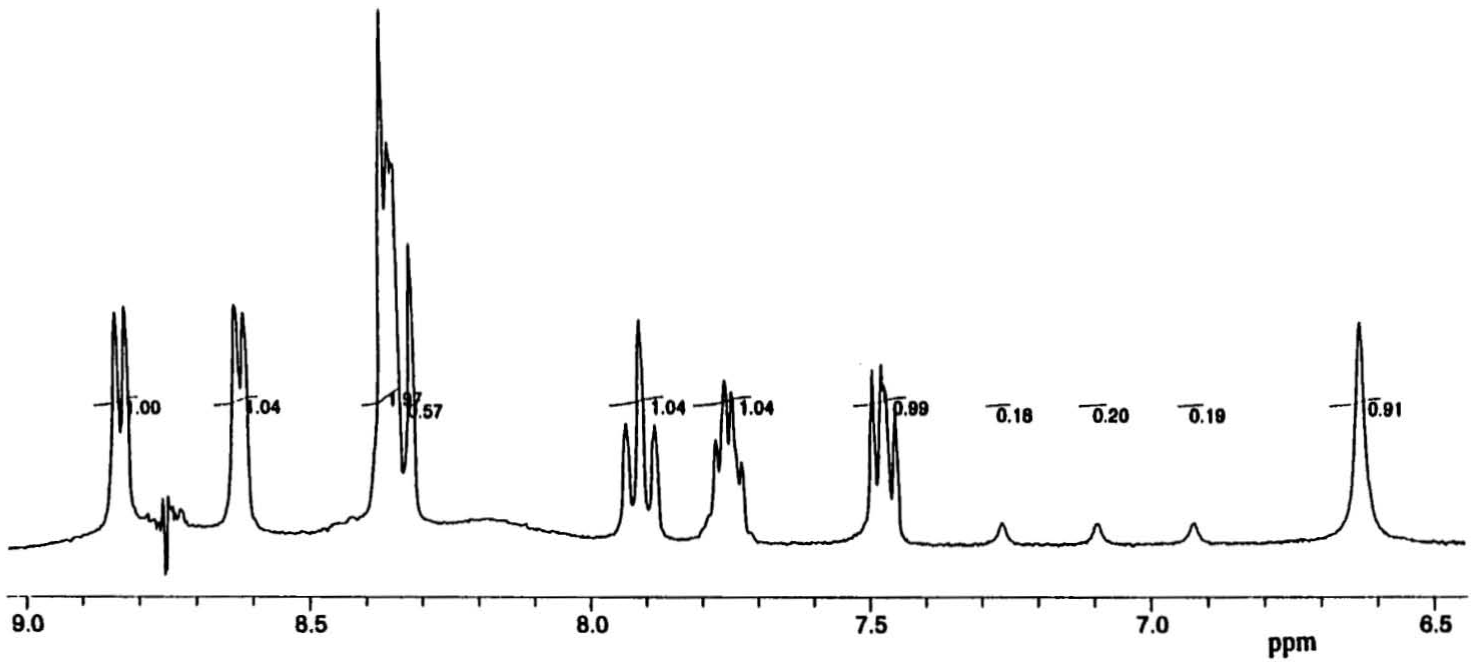

Figure 5-16. Room temperature ^{1}H NMR spectrum of complex **36** in d_6-DMSO.

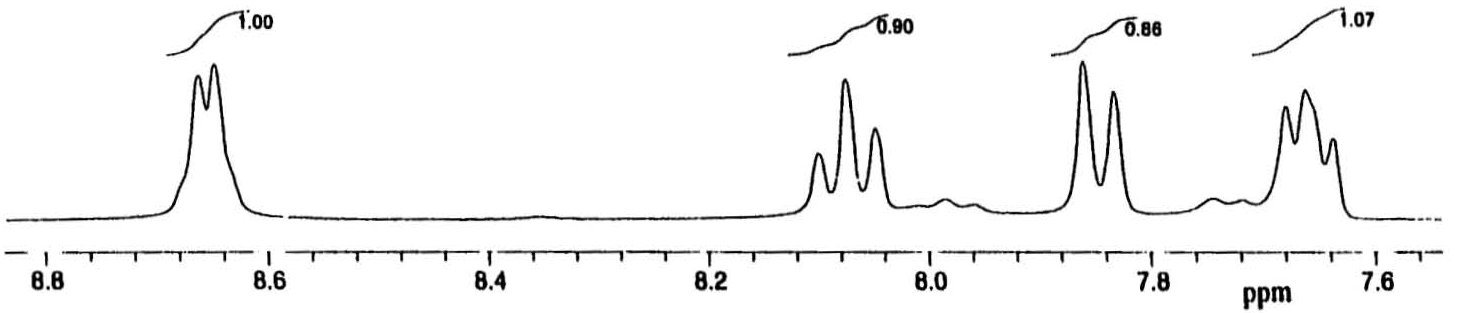

Figure 5-17. Room temperature ^1H NMR spectrum of complex **37** in D_2O.

and **28**), which are quite well separated so that a shielding effect does not exist in this case. The order of the chemical shifts of H(10) and H(11) is reversed in this dicadmium(II) complex compared to the situation of the free ligand. The reason for this is that the electronic effect, which reduces electron density in the pyridyl ring *via* N(6), does not take place for each proton in an average manner.

5.4 Conclusion

Unlike tetradentate N_4 diazine ligands with the diazine unit incorporated in aromatic rings, open-chain N_4 diazine ligands have variable coordination modes depending on the properties of R, R', X and X' (**Figure 1-14**) and the central metal ions. PAHAP has a dominant mode as a **Type AB** ligand as shown by the dicadmium complex **37**, as well as the complexes in HoChapter 2-4. wever, a new mode (**Scheme 1-1a**), which is similar to that of the deprotonated PHAAP in complex **30**, has been found in the novel 5-coordinate VO_2^+ complex **35**. A new N_3O coordination mode (**Scheme 1-2**) for PHAAP with O (alkoxo) acting as a bridging donor has been found in a series of cyclic tetranuclear complexes. The tetranuclear copper(II) complex **38** may not show magnetic coupling because of the orthogonal geometry at each copper centre, while the tetranuclear nickel(II) complex **39** would be expected to have a magnetic interaction, since the Ni-O-Ni angles are quite large. The hetero-tetranuclear $Fe(III)Cu(II)_3$ complex **40** shows a very complicated magnetic behaviour for which a reasonable explanation includes very strong antiferromagnetic coupling between Cu(1) and Cu(2), weak ferromagnetic coupling between Fe(1) and Cu(1) and Cu(3), and an incomplete LS($S = 1/2$) $\leftrightarrow$ HS ($S = 5/2$)

process for Fe(1). In all the PAHOX complexes in which the oxime group of PAHOX acts as a N-O bridge providing a very strong antiferromagnetic pathway (**33**) or is free (**34** and **35**), the ligand PAHOX only demonstrates a **Type C** mode of bonding.

^{1}H NMR spectra of the mononuclear V(V) complex (**36**) and the spiral-like dinuclear cadmium complex (**37**) clearly indicate that chemical shifts of the multiplets (4H) due to the coordinated pyridyl rings are significantly higher than those in the spectrum of the free ligand, which simply results from an electronic effect.

Chapter 6 General Conclusions and Final Remarks

6.1 Synthesis of the ligands

The ligands studied in this thesis have been listed in **Figure 1-15**, and the synthesis routes for some of ligands are shown in **Scheme 2-1**. PAHAP and PZHZP are symmetrical ligands like PAA and PMK [93-96]. Usually, symmetrical organic compounds are synthesized by symmetrical methods, which have been adopted for the synthesis of PAA and PMK. However, there is no similar available method for the preparations of PAHAP and PZHZP. F. H. Case [97] reacted picolinamide hydrazone with some esters and obtained PAHAP. The reaction however occurs in a low yield, and the mechanism for the reaction was not proposed. We repeated the reaction using picolinamide hydrazone and the oxalate ester and separated three major compounds with very low yield (5-10%) for PAHAP as shown in **Scheme 6-1**.

Scheme 6-1

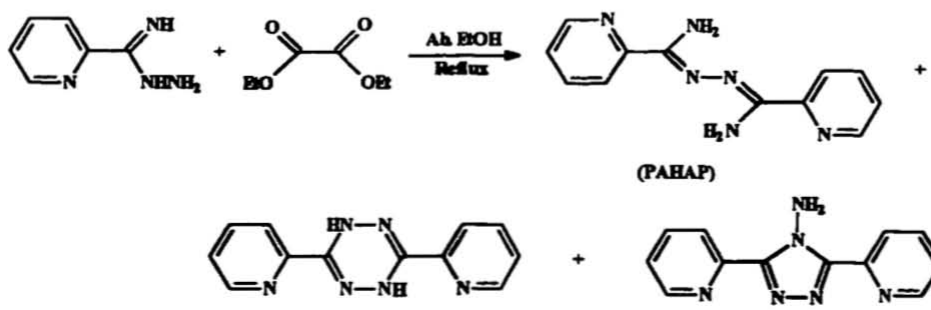

Our procedures for making PAHAP turned out to be more straightforward with a clear mechanism, a high yield and without any detectable side reactions, and has been further used for making another symmetrical ligand PZHPZ, as well as for quasi-symmetrical ligands PYPZ and PHAAP. It should be noted that PHAAP cannot be made by reacting ethyl picolinate with picolinamide hydrazone, which lead to the same compounds as shown in **Scheme 6-1**.

PMHAP and PHMAP were made by known procedures [109], which were adopted to make the new ligand PAHOX. The relevant literature references suggested that such compounds are triazoline species as shown in **Scheme 6-2**:

Scheme 6-2

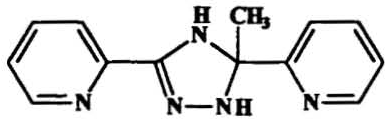

Proposed structure for PMHAP

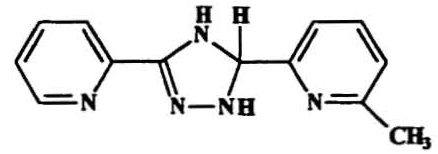

Proposed structure for PHMAP

However, our X-ray structural analyses for the complexes of these ligands showed that the ligands adopt open-chain structures and are not cyclized. We are confident that the free ligands also have an open ring structure, because the IR spectra of the free ligands show two C=N bands in each case. We await a structural determination of these ligands.

6.2 Coordination chemistry

Due to the their large flexibility of coordination originating from the rotation around the N-N bond and the additional donors e.g. NH_2 and OH, these ligands are extremely interesting and present an unusual arrangement of potential donor sites, with many possible mononucleating, dinucleating and polynucleating coordination modes as discussed in Chapter 1. However, the real coordination modes for these open-chain diazine ligands are closely connected to the nature of metal ions and the ligands, anions, organic co-ligands, the presence of hydrogen bonding or stacking interactions and solvent etc.

The ligand PAHAP has a dominant **Type AB** mode of bonding as demonstrated by a series of dicopper (II) complexes in Chapters 2 and 3, the spiral-like complexes in Chapter 4 and the dicadmium (II) complex in Chapter 5, even though a new coordination type for open-chain diazine ligands has been found in its mononuclear VO_2^+ complex (**Scheme 6-3**, New Type 1). The coordination modes for PYPZ and PZHZP relevant to the diazine units may also be dominated by **Type AB** as shown by complexes **16**, **17**, **20** and **27**. The coordination modes for PMHAP and PHMAP are largely dependent on the solvent properties. In weakly polar solvents, **Type B** is preferred (**12**, **14**), otherwise **Type AB** (**13**). PAHOX seems to only have a **Type C** mode either in the complex (**37**), in which oxime acts as a bridge, or in the complexes (**38** and **39**), in which the oxime group only provides a nitrogen atom as a donor. Even though there are many potential coordination modes for PHAAP, three structurally confirmed modes have been found for PHAAP so far. A quasi-**Type B** mode was adopted in its dinuclear $CuBr_2$ complex (**15**) in which the

diazine unit bridges two copper(II) centers with the deprotonated alkoxo group acting as monodentate donor. A new coordination type, which is very similar to that for PAHAP in the mononuclear VO_2^+ complex, has been found in its unusual seven-coordinate mononuclear Fe(III) complex. The most popular mode for PHAAP is as shown in **Scheme 6-3** (New Type 2), which is presented in a series of hetero-tetranuclear (**40**), homo-tetranuclear (**38**,**39**) complexes.

Scheme 6-3

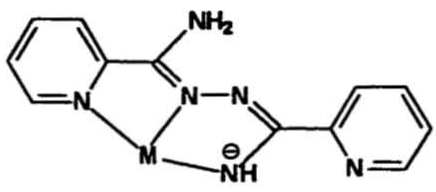

New Type 1

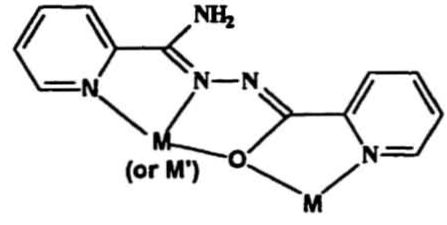

New Type 2

The ligand PTS, belonging to the triazoline family, also contains a N-N single bond, and its paramagnetic dimetal complexes would also be expected to have twisted structures around this diazine linkage. We failed to get any crystals of PTS complexes, but obtained a mixed valence six-centered $Cu(II)_4Cu(I)_2$ complex (**41**) of its hydrolyzed ligand PAH which is responsible for the partial reduction of Cu(II). Some modified ligands have been prepared (see **Figure 6-1**), but no attempts have been made to produce crystals of their complexes.

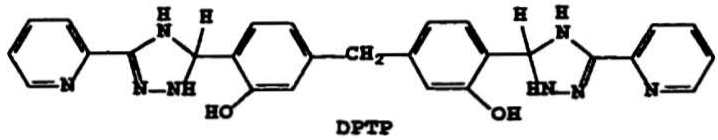

DPTP

IR 1628 $cm^{-1}(\nu_{C=N})$
^{1}HNMR, 8.505-7.382 (4H, multiplet, py); 7.156-6.946 (6H, multiplet, Ph);
8.591 (2H, s, NH); 6.973 (2H, s &br, NNH); 11.571 (2H, s, OH);
2.001 (2H, s, CH_2)
MS, M^+, 492, 2.51%.

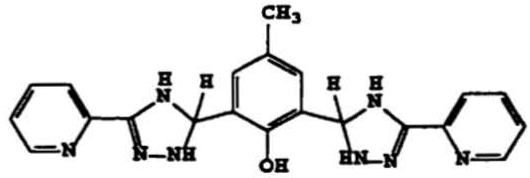

DPTMeP

IR 1618 $cm^{-1}(\nu_{C=N})$
^{1}HNMR, 8.614-7.356 (8H, multiplet, py); 7.651(2H, s, Ph);
8.831(2H, s, NH); 6.370(2H, s &br, NNH); 12.024(1H, s, OH);
2.356(3H, s, CH_3)
MS, M^+, 400, 23.43%.

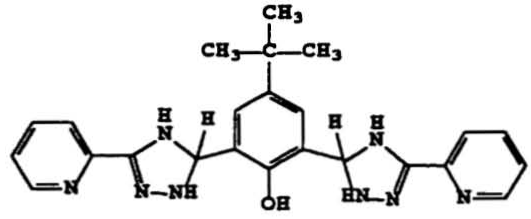

DPTTbP

IR 1613 $cm^{-1}(\nu_{C=N})$
^{1}HNMR, 8.620-7.367(8H, multiplet, py); 7.773(2H, s, Ph);
8.874(2H, s, NH); 1.379(9H, s, CH_3)
MS, M^+, 442, 14.95%.

Figure 6-1. Schematic representation of some triazoline ligands with spectral data included

6.3 Magnetism

6.3.1 Magneto-structural correlations for dicopper(II) complexes containing one N-N single bond

The analysis of the magnetic and structural data for a series of dicopper (II) complexes in Chapter 1, in which the metal ions are linked in the equatorial coordination plane by only one N-N single bond, showed that the singlet-triplet splittings vary as a function of the torsion angle between two magnetic planes about the N-N single bonds. Experimentally, the larger the torsion angle, the more the singlet-triplet molecular orbitals split hence the larger magnetic exchange integral (-2J). Systematic studies on this system by the modification of the open-chain diazine ligands and changing the co-ligands to generate variable torsion angles gave a very good linear relationship between -2J values in the range -24.4 to +208 cm^{-1} and the torsion angles in the range 75-168.3°. The reason for this is that the extent of the overlap, which dominates the magnetic exchange in the system, between the *p* orbitals along the single N-N bond dependent upon the torsion angle between the magnetic copper planes. The observations have been supported by a series of MO calculations for relevant model compounds.

6.3.2 Magnetic properties of the dicopper(II) complexes containing two N-N single bonds or one N-N single bond along with the other bridging species

Attempts to establish a magnetostructural correlation for the dicopper(II) system containing two N-N single bonds have been made. However because of their particular

twisted structures, the distortion of the coordination geometries and the existence of the additional bridge (e.g. μ_2-NO_3^- in **18**), the torsion angles between two copper magnetic planes about these two N-N bonds in **18** and most likely in **20** are very small and close to the angle which is required for effective N-N *p* orbital orthogonality. Therefore no significant magnetic interactions were observed in such system. Complex **19** shows no coupling by a different mechanism, in which two copper(II) centers are bridged by two N-N single bonds in a strictly orthogonal manner.

The magnetic exchange in a mixed diazine bridged dicopper(II) complex occurs principally through the open-chain diazine linkage, since the pyridazine diazine unit bridges two copper centers in a orthogonal way, and the observed coupling in this complex is quite weak because of the geometric distortions and the small torsion angle between the two copper magnetic planes about the N-N single bond.

The first genuine example contradicting the spin polarization mechanism in azide bridged complexes has been achieved in the tetranuclear copper(II) complex **22**, which shows a strong antiferromagnetic interaction ($-2J = 246$ cm^{-1}). The complex contains two dicopper(II) units orthogonally bridged by two μ_2-1,1-azides and each unit bridged by a N-N single bond and a μ_2-1,1-azide in the copper equatorial planes. Since the angle between the two copper magnetic planes about the N-N single bond is particularly small, this bond does not provide any significant contribution to the total antiferromagnetic coupling based on the result in Chapter 1. The strong antiferromagnetic coupling therefore occurs mainly through the equatorially bridging μ_2-1,1-azide because of the very

large Cu-μ_2-1,1-N_3^--Cu angle. The net antiferromagnetic exchange has been further corroborated on the basis of MO calculations.

6.3.3 Magnetism of the other dinuclear and polynuclear complexes

Weak ferromagnetic coupling was observed in the spiral-like dimanganese(II) complex (**23**), while no significant magnetic exchange was observed in the dinickel(II) case (**25**) with the same spiral-like structure. In both complexes the torsion angles around the three N-N single bonds are extremely small, but close to the angle required for the effective orthogonality established for the dicopper(II) systems containing one N-N single bond.

The dicopper complexes of PAHOX demonstrate no coupling e.g. in **34** in which two copper(II) centers are orthogonally bridged by two bidentate SO_4^{2-} groups, or very strong antiferromagnetic coupling e.g. in **33** in which two copper(II) centers are equatorially bridged by two symmetrical N-O groups of the ligands.

The cyclic hetero-tetranuclear $Cu(II)_3Fe(III)$ complex exhibits very complicated magnetic behaviour, and based on the structural data, the complicated magnetism may result from the combination of the very strong antiferromagnetic interaction between two copper centers (Cu(1) and Cu(2)) *via* the alkoxo bridge (O(1)) in their equatorial planes, and the incomplete high-low spin transition of Fe(III), and weak ferromagnetic exchange between Fe(III) and Cu(1) and Cu(3).

6.4 Spectral and electrochemical properties

It is very interesting to note that the $\nu_{C=N}$ bands in all complexes with twisted structures around the N-N bond (**Type AB**) appear in higher energy positions compared with those for the free relevant ligands, which seems to be in contradiction to the observations for some complexes containing imine (C=N) ligands. It is evident that the twisting of the ligand in those complexes increases the $\nu_{C=N}$ frequency significantly through breaking the conjugation *via* the N-N single bond in the free ligand, even though the coordination reduces the $\nu_{C=N}$ frequency to some extent.

Another interesting spectral result was obtained through studies on the ^{1}H NMR spectra of a series of spiral-like diamagnetic complexes either containing three N-N linkages (**26** and **28**) or two N-N linkages (**37**), and the mononuclear V(V) complex (**36**). The result indicates that in the spiral-like diamagnetic complexes (**26** and **28**) containing three N-N linkages, the chemical shifts of the multiplets (4H) due to the coordinated pyridyl rings are much lower than that for the free ligand, while those in the spectra of the spiral-like diamagnetic complex containing two N-N linkages (**37**) and the mononuclear V(V) complex (**36**) are significantly higher. It may be concluded that in the former cases, the influence on the chemical shifts is dominated by a shielding effect, which is achieved by the particular arrangement of the three pyridyl rings bonded at each metal center, while the increase of the chemical shifts in the later cases simply results from the electronic effect (coordination effect).

6.5 Future work relevant to the transition metal polynuclear complexes involving open-chain diazine ligands

6.5.1 New homo- and hetero-polynuclear complexes

Because of their high flexibility, open-chain diazine bridges in polynucleating ligands have been proved to be of fundamental interest in many aspects e.g. magnetism, spectroscopy, electrochemistry through the research presented herein. In order to generate new homo- and hetero-polynuclear complexes containing open-chain diazine units from the available ligands studied in this thesis or relevant new ligands, several strategies, some of which have already been used in the work presented in this thesis, can be considered:

Strategy 1. Ligand exchange to make some dimetal complexes containing different diazine units , in order to tune the torsion angle between two metal magnetic planes.

E.g. Complex **4** (see Chapter2) + PYPZ (or PMHAP or PZHPZ)

Strategy 2. Using an asymmetric ligand to generate a partially coordinated (most likely mononuclear) complex which is further reacted with other metal centres to produce hetero-nuclear complexes. This method has been used to make the $Cu(II)_3Fe(III)$ complex **40**.

E.g. PHAAP + M^{n+} (Fe(III), VO^{+}, et al.) in 1:1 ratio then reacts with $\underline{M}^{m+}$

Strategy 3. Metal exchange. This method can be used to make hetero-polynuclear or homo-polynuclear complexes which cannot be made through a direct reaction of ligand with metal salt (e.g. $[(PAHAP)_2Ni_2(H_2O)_4]^{4+}$)

E.g. complex **37** reacts with M^{n+} in 1:1 ratio → $(PAHAP)_2CdM$ moiety then reacts with $\underline{M}^{m+}$ to produce $(PAHAP)_2M\underline{M}$ or directly reacts with M^{n+} in 1:2 ratio to produce $(PAHAP)_2M_2$

Strategy 4. Simple stoichiometric reaction to make spiral-like hetero-dinuclear complexes.

E.g. $3PAHAP + M^{n+} \rightarrow [(PAHAP)_3M]^{n+}$ then reacts with $\underline{M}^{m+}$

6.5.2 Magnetostructural correlations for the other first row transition metal polynuclear complexes bridged by open-chain diazine moieties

The first magneto-structural correlation for a dicopper system bridged by one N-N single bond has been successfully established, which might be extended to the dicopper system containing two N-N single bonds. However, because of the coordination geometry difference between copper(II) complexes (mostly 4- or 5-coordination) and the other first row transition metal complexes (usually 6-coordination), systematic variation of the torsion around the N-N single bond in the other first row transition metal polynuclear complexes is obviously difficult by using only the open-chain diazine ligands presented in this thesis. Even though the spiral-like dimanganese(II) and dinickel(II) complexes, which show a weak ferromagnetic coupling and no coupling at all respectively, seem to exhibit

very similar orthogonal torsion angles about the N-N single bond vector to those found in the dicopper system bridged by one N-N single bond, no further conclusions related to magnetic exchange properties in such systems could be made. Therefore, efforts to establish magnetostructural correlations for such systems should be towards the synthesis and designation of suitable new ligands and their complexes. To meet this purpose, the

Scheme 6-4

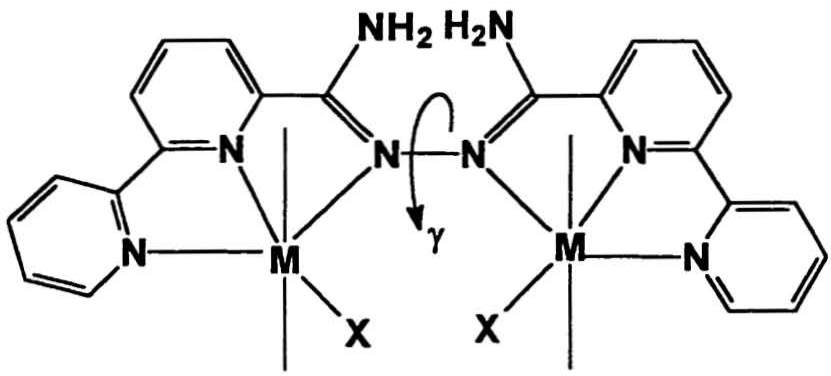

ligand shown in **Scheme 6-4** (or its modified ligands) and its complexes could be considered (in **Scheme 6-4**, the rotational angle γ will vary with the change of the co-ligand X).

References

1. O. Kahn, *Angew. Chem. Int. Ed. Engl.*, **24**, 834(1985).
2. P. W. Ball, *Coord. Chem. Rev.*, **4**, 361(1969).
3. a). M. Melnik, *Coord. Chem. Rev.*, **42**, 259(1982).

   b). M. Kato and Y. Muto, *Coord. Chem. Rev.*, **45**, 92(1988).
4. C. J. O'Connor, Prog. *Inorg. Chem.*, 29, 203(1983).
5. D. Gatteschi, J. S. Miller and F. Palacio, *Magnetic Molecular Materials;* Kluwer Academic: Dordrecht 1991.
6. D. Willett, D. Gatteschi and O. Kahn, *Magneto-Structural Correlations in Exchange systems,* D. Reidel Publishing Compaany, 1983.
7. O. Kahn, *Molecular Magnetism,* VCH Publishers: New York, 1993.
8. P. J. Hay, J. C. Thibeault and R. Hoffman, *J. Am. Chem. Soc.*, **97**, 4884(1975).
9. M. Park, *M. Sc. Thesis,* Memorial University of Newfoundland, 1997.
10. a). M. F. Charlot, S. Jeannin, Y. Jeannin, O. Kahn, A. J. Lucrece and F. J. Martin, *Inorg. Chem.*, **18,** 1675(1979).

    b). M. F. Charlot, O. Kahn, S. Jeannin and Y. Jeannin, *Inorg. Chem.*, **19,** 1410(1980).
11. O. Kahn, *Inorg. Chim. Acta.*, **62,** 3(1982).

12. O. Kahn , T. Mallah, J. Gouteron, S. Jeannin and Y. Jeannin, *J. Chem. Soc., Dalton Trans.*, 1117(1989).

13. P. J. van Koningsbruggen, *Ph.D. Thesis*, Leiden University, 1993.

14. M. F. Charlot, Y. Journaux, O. Kahn, A. Bencini, D.Gatteschi and C. Zanchini, *Inorg. Chem.*, **25**, 1060(1986).

15. L. K. Thompson, S. K. Mandal, S. S. Tandon, J. N. Bridson and M. K. Park, *Inorg. Chem.*, **35**, 3117(1996) and refs. therein.

16. S. K. Mandal, L. K. Thompson, M. J. Newlands, E. J. Gabe and F. L. Lee, *Inorg. Chem.*, **29**, 3556(1990).

17. O. Kahn, *Comments Inorg. Chem.* , **3**, 105(1984).

18. S. S. Tandon, L. K. Thompson and R. C. Hynes, *Inorg. Chem.*, **31**, 2210(1992).

19. L. K. Thompson, F. L. Lee and E. J. Gabe, *Inorg. Chem.*, **27**, 39(1988).

20. L. K. Thompson, S. K. Mandal, J. P. Charland and E. J. Gabe, *Can. J. Chem.*, **66**, 348(1988).

21. T. N. Sorrell, *Tetrahedron*, **45**, 3(1989).

22. S. J. Lippard and J. M. Berg, *Principles of Bioinorgnic Chemistry*, University Science Books: Mill-Valley, CA, 1994.

23. E. I. Ochiai, *Bioinorgnic Chemistry - An Introduction*, Allyn and Bacon, Inc.: Toronto 1977.

24. G. Challa, W. Chen and J. Reedijk, *Makromol. Chem., Macromol. Symp.*, **59**, 59(1992).

25. M. M. Rogic and T. R. Demmin, *J. Am. Chem. Soc.*, **100**, 5472(1978).

26. G. F. Endres, A. S. Hay and J. W. Eustace, *J. Org. Chem.*, **28**, 1300(1963).

27. H. C. Meinders, F. van Bolhuis and G. Challa, *J. Mol. Catal.*, **5**, 225(1979).

28. J. Reedijk, *Bioinorgnic Catalysis*, Marcel Dekker, New York, 1993.

29. J. H. van Vleck, *The Theory of Electronic and Magnetic Susceptibilities*, Oxford University Press: London, 1932.

30. A. Earnshaw, *An Introduction to Magnetochemistry*, Academic Press Inc.: New York, NY, 1968.

31. B. Bleaney and K. D. Bowers, *Proc. R. Soc. London Ser., A.* **214**, 451(1952).

32. O. Kahn, J. Galy, Y. Journaux, J. Jaud and I. Morgenstern-Badarau, *J. Am. Chem. Soc.*, **104**, 2165(1982).

33. I. V. Vasilevsky, R. E. Stenkamp, E. C. Lingafelter, V. Schomaker, R. D. Willett and N. J. Rose, *Inorg. Chem.*, **13**, 2619(1989).

34. S. K. Shakhatreh, E. G. Bakalbassis, I. Brüdgam, H. Hartl, J. Mrozinski and C. A. Tsipis, *Inorg. Chem.*, **13**, 2803(1991).

35. D. J. Hodgson, *Prog. Inorg. Chem.*, **19**, 1737(1975) and refs. therein.

36. V. H. Crawford, H. W. Richardson, J. R. Wasson, D. J. Hodgson and W. E. Hatfield, *Inorg. Chem.*, **15**, 2107(1976).

37. O. Kahn and B. Briat, *J. Chem. Soc., Faraday Trans.*, **72**, 268(1976).

38. O. Kahn and B. Briat, *J. Chem. Soc., Faraday Trans.*, **72**, 1441(1976).

39. L. Merz and W. J. Haase, *J. Chem. Soc., Dalton Trans.*, 875(1980).

40. S. Gehring, P. Fleischhauer, H. Paulus and W. Haase, *Inorg. Chem.*, **32**, 54(1993).

41. W. Haase and S. Gehring, *J. Chem. Soc., Dalton Trans.*, 2609(1985).

42. S. Gehring, H. Astheimer, and W. Haase, *J. Chem. Soc., Faraday Trans.*, II **83**, 347(1987).

43. S. Gehring, H. Paulus and W. Haase, E. Bill, A. X. Z. Trautwein, *Kristallogr.*, **186**, 83(1990).

44. G. Christou, S. P. Perlepes, E. Libby, K. Folting, J. C. Huffman, R. J. Webb and D. N. Hendrickson, *Inorg. Chem.*, **19**, 3657(1990).

45. J. Comarmond, P. Plumeré, J. -M. Lehn, Y. Agnus, R. Louis, R. Weiss, O. Kahn and I. Morgenstern - Badarau, *J. Am. Chem. Soc.*, **104**, 6330(1982).

46. O. Kahn, S. Sikorav, J. Gouteron, S. Jeannin and Y. Jeannin, *Inorg. Chem.*, **22**, 2877(1983).

47. S. Sikorav, I. Bkouche - Waksman and O. Kahn, *Inorg. Chem.*, **23**, 490(1984).

48. L. K. Thompson and S. S. Tandon, *Comments Inorg.Chem.*, **3**, 125(1996) and refs. therein.

49. S. S. Tandon, L. K. Thompson, M. E. Manuel and J. N. Bridson, *Inorg. Chem.*, **33**, 5555(1994).

50. L. K. Thompson, S. S. Tandon and M. E. Manuel , *Inorg. Chem.*, **34**, 2356(1995).

51. L. K. Thompson, S. S. Tandon and C. L. Sheppard, *unpublished results*.

52. L. K. Thompson, S. S. Tandon, F. Lloret, J. Cano and M. Julve, *Inorg. Chem.*, **36**, 3301(1997).

53. M. Y. Chow, Z. Y. Zhou and T. C. M. Mak, *Inorg. Chem.*, **31**, 4900(1992).

54. M. Inoue and M. Kubo, *Coord. Chem. Rev.*, **21**, 1(1976) and refs. therein.

55. T. Kamiusuki, H. Ōkawa, N. Matsumoto and S. Kida, *J. Chem. Soc., Dalton Trans.*, 195(1990).

56. J. C. Bayon, P. Esteban, G. Net, P. G. Rasmussen, K. N. Baker, C. W. Hahn and M. M. Gumz, *Inorg. Chem.*, **30**, 2572(1991).

57. J. Pons, X. López, J. Casabó, F. Teixidor, A. Caubet, J. Ruis and C. Miravitlles, *Inorg. Chim. Acta*, **195**, 61(1992).

58. A. Bencini, D. Gatteschi, C. Zanchini, J. G. Haasnoot, R. Prins and J. Reedijk, *Inorg. Chem.*, **24**, 2812(1992).

59. W. M. E. Koomen-van Oudenniel, R. A. G. de Graff, J. G. Haasnoot, R. Prins and J. Reedijk, *Inorg. Chem.*, **28**, 1128(1989).

60. P. J. van Koningsbruggen, D. Gatteschi, R. A. G. de Graff, J. G. Haasnoot and J. Reedijk and C. Zanchini, *Inorg. Chem.*, **34**, 5175(1995).

61. R. Prins, P. J. M. W. L. Birker, J. G. Haasnoot, G. C. Verschoor and J. Reedijk, *Inorg. Chem.*, **24**, 4128(1985).

62. P. M. Slangen, P. J. van Koningsbruggen, J. G. Haasnoot , J. Jansen, S. Gorter, J. Reedijk , H. Kooijman, W. J. J. Smeets and A. L. Spek, *Inorg. Chim. Acta*, **212**, 289(1993).

63. F. A.Abraham, M. Lagrenee, S. Sueur, B. Mernari and C. Bremard, *J. Chem. Soc., Dalton Trans.*, 1443(1991).

64. S. K. Mandal, L. K. Thompson, M. J. Newlands, F. L. Lee, Y. Lepage, J. -P. Charland and E. Gabe, *Inorg. Chim. Acta*, **122**, 199(1986).

65. L. Chen, L. K. Thompson and J. N. Bridson, *Inorg. Chem.*, **32**, 2938(1993).

66. S. S. Tandon, L. K. Thompson, M. E. Manuel and J. N. Bridson, *Inorg. Chem.*, **34**, 2356(1995).

67. P. J. van Koningsbruggen, J. G. Haasnoot R. A. G. de Graff, J. Reedijk and S. Slingerland, *Acta Crystallogr.*, **C48**, 1923(1992).

68. L. Chen, *Ph. D. Thesis*, Memorial University of Newfoundland, 1993.

69. T. Kamiusuki, H. Ōkawa, K. Inoue, N. Matsumoto, M. Kodera and S. Kida, *J. Coord. Chem.*, **23**, 201(1991).

70. P. M. Slangen, P. J. van Koningsbruggen, K. Goubitz, J. G. Haasnoot , and J. Reedijk , *Inorg. Chem.*, **33**, 1121(1994).

71. S. K. Mandal, L. K. Thompson, E. J. Gabe, J. -P. Charland and F. L. Lee, *Inorg. Chem.*, **27**, 855(1988).

72. D. Ajò, A. Bencini and F. Mani, *Inorg. Chem.*, **27**, 2437(1988).

73. W. J. Stratton and D. H. Busch, *J. Am. Chem. Soc.*, **82**, 4834(1960).

74. W. J. Stratton and D. H. Busch, *J. Am. Chem. Soc.*, **80**, 1286(1958).

75. W. J. Stratto and D. H. Busch, *J. Am. Chem. Soc.*, **80**, 3191(1958).

76. W. J. Stratton, P. J. Ogren, *Inorg. Chem.*, **9**, 2588(1970).

77. W. J. Stratton, M. F. Rettig and R. F. Drury, *Inorg. Chim. Acta*, **3**, 97(1969).

78. W. J. Stratton, *Inorg. Chem.*, **9**, 517(1970).

79. C. J. O'Connor, R. J. Romananch, D. M. Robertson, E. E. Eduok and F. R. Fronczek, *Inorg. Chem.*, **22**, 449(1983).

80. T. C. Woon, L. K. Thompson and P. Robichaud, *Inorg. Chim. Acta*, **90**, 201(1984).

81. A. W. Addison, T. N. Rao, J. Reedijk, J. van Rijn and G. C. Verschoor, *J. Chem. Soc. Dalton Trans.*, 1349(1984).

82. P. Souza, A. I. Matesanz and V. Fernández, *J. Chem. Soc., Dalton Trans.*, 3011(1996).

83. J. García - Jojal, J. García - Jaca, R. Cortés, T. Rojo, M. K. Urtiaga and M. I. Arriortua, *Inorg. Chim. Acta*, **249**, 25(1996).

84. F. Abraham, J. M. Capon, G. Nowogrocki, S. Sueur and C. Brémard, *Polyhedron*, **4**, 1761(1985).

85. J. García - Jojal, M. K. Urtiaga, R. Cortés, L. Lezama, M. I. Arriortua and T. Rojo, *J. Chem. Soc., Dalton Trans.*, 2233(1994).

86. A. Mangia, C. Pelizzi and G. Pelizzi, *Acta crstallogr.*, **B30**, 2146(1974).

87. A. Bonardi, S. Ianelli, C. Pelizzi and G. Pelizzi, *Inorg. Chem. Acta*, **187**, 167(1991).

88. A. Bacchi, A. Bonini, M. Carcelli, F. Ferraro, E. Leporati, C. Pelizzi and G. Pelizzi, *J. Chem. Soc., Dalton Trans.*, 2699(1996).

89. A. E. Koziol, R. C. Palenik and G. J. Palenik, *J. Chem. Soc. Chem. Commun.*, 650(1989).

90. M. Lagrenée, S. Sueur and J. P. Wignacourt, *Acta Crystallogr.*, **C47**, 1158(1991).

91. A. Bacchi, L. P. Battaglia, M. Carcelli, C. Pelizzi , G. Pelizzi, C. Solinas and M. A. Zoroddu, *J. Chem. Soc., Dalton Trans.*, 775(1993).

92. E. W. Ainscough, A. M. Brodie, J. D. Ranford and J. M. Waters, *Inorg. Chim. Acta*, **236**, 83(1995).

93. P. J. van Koningsbruggen, J. G. Haasnoot R. A. G. de Graff and J. Reedijk, *J. Chem. Soc., Dalton Trans.*, 483(1993), and refs. therein.

94. S. C. Chan, L. L. Koh, P. - H. Leung, J. D. Ranford and K. Y. Sim, *Inorg. Chim. Acta*, **236**, 101(1995).

95. P. Cheng, D. Liao, S. Yan, Z. Jiang, G. Wang, X. Yao and H. Wang, *Inorg. Chim. Acta*, **248**, 135(1996).

96. P. Iliopoulos, K. S. Murray, R. Robson, J. Wilson and G. A. Williams, *J. Chem. Soc., Dalton Trans.*, 1585 (1987).

97. X. Chen, S. Zhan, C. Hu, Q. Meng and Y. Liu, *J. Chem. Soc., Dalton Trans.*, 245(1997).

98. P. J. van Koningsbruggen, E. Muller, J. G. Haasnoot and J. Reedijk, *Inorg. Chim. Acta*, **208**, 37(1993).

99. D. S. Brown, V. H. Crawford, J. W. Hall and W. E. Hatfield, *J. Phys. Chem.*, **81**, 1303(1977).

100. F. H. Case, *Heterocyclic Chemistry*, **7**, 1001(1970).

101. F. H. Case, *J. Org. Chem.*, **30**, 931(1965).

102. C. J. Gilmore, *J. Appl. Cryst.*, **17**, 42(1984).

103. P. T. Beurskens, *DIRDIF: Technical Report 1984/1*, Crystallography Laboratory, Toernooiveld, 6525 Ed Nijmegen, Netherlands, 1984.

104. D. T. Cromer and J. T. Waber, *Internationational Tables for X-ray Crystallography*, Vol. IV. The Kynoch Press: Birmingham, United Kingdom, 1974; Table 2.2A.

105. J. A. Ibers and W. C. Hamilton, *Acta Crystallogr.*, **17**, (781)1974.

106. D. T. Cromer, *Internationational Tables for X-ray Crystallography*, Vol. IV. The Kynoch Press: Birmingham, United Kingdom, 1974; Table 2.3.1.

107. *Texsan-Texray Structure Analysis Package;* Molecular Structure Corporation: The Woodlands, Texas, 1985.

108. SMART: *Data Collection Software*, Version 4.050; Siemens Analytical X-ray Instruments Inc.: Madison, Wisconsin, 1996.

109. SAINT: *Data Reduction Software*, Version 4.050; Siemens Analytical X-ray Instruments Inc.: Madison, Wisconsin, 1996.

110. G. M. Sheldrick, *SHELXTL 5.04/VMS: An integrated system for solving, refining and displaying crystal structures from diffraction data*. Siemens Analytical X-ray Instruments Inc.: Madison, Wisconsin, 1995.

111. G. M. Sheldrick , *SADABS. Empirical Absorption Correction Program*. University of Göttingen: Göttingen, Germany, 1996.

112. A. B. P. Lever, E. Mantovani and B. S. Ramaswamy, *Can. J. Chem.*, **49**, 1957(1971).

113. a. C. L. Sheppard, *B. Sc. Thesis*, Memorial University of Newfoundland, 1998.

b. C. L. Sheppard, S.S. Tandon, L.K. Thompson, J.N. Bridson, D.O. Miller, M. Handa and F. Lloret, *Inorg. Chim. Acta*, **250**, 227(1996).

114. K. Nakamoto, *Infrared Spectra of Inorganic and Coordination Compounds*; Wiley-Interscience, New York, 1986.

115. K. Nakamoto, Y. Morimoto and A. E. Martell, *J. Am. Chem. Soc.*, **83**, 4528(1961).

116. K. Nakamoto and A. E. Martell, *J. Chem. Phys.*, **32**, 588(1960).

117. A. R. Katritzky and A. R. Hands, *J. Chem. Soc.*, 2202(1958).

118. W. E. Marsh, T. L. Bowman, C. S. Harris, W. E. Hatfield and D. J. Hodgson, *Inorg. Chem.*, **20**, 3864(1981).

119. B. E. Myers, L. Berger and S. J. Friedberg, *J. Appl. Phys.*, **40**, 1149(1969).

120. W. E. Marsh, K. C. Patel, W. E. Hatfield and D. J. Hodgson, *Inorg. Chem.*, **22**, 511(1983).

121. H. Oshio and U. Nagashima, *Inorg. Chem.*, **29**, 3321(1990).

122. Z. Xu, L. K. Thompson and D. O. Miller, *Inorg. Chem.*, **36**, 3985(1997).

123. L. K. Thompson, Z. Xu, A. E. Goeta, J. A. K. Howard, J. Clase and D. O. Miller, *Inorg. Chem.*, 1998, in press.

124. C. Mealli and D. M. Proserpio, *J. Chem. Ed.*, **67**, 399(1990).

125. P. J. Hay, J. C. Thibeault and R. Hoffmann, *J. Am. Chem. Soc.*, **97**, 4884(1975).

126. M. Ghedini, G. De Munno, G. Denti, A. M. Manotti Lanfredi and A. Tiripicchio, *Inorg. Chim. Acta*, **57**, 87(1982).

127. P. Dapporto, G. De Munno, G. Bruno and M. Romeo, *Acta Crystallogr., Sect C*, **39**, 718(1983).

128. G. De Munno, G. Denti and P. Dapporto, *Inorg. Chim. Acta*, **74**, 199(1983).

129. G. De Munno and G. Denti, *Acta Crystallogr.*, Sect C, 40, 616(1984).

130. G. De Munno and G. Bruno, *Acta Crystallogr.*, Sect C, 40, 2022(1984).

131. P. Dapporto, G. De Munno, A. Sega and C. Meali, *Inorg. Chim. Acta*, **83**, 171(1984).

132. W. Vreugdenhil, J. G. Hassnoot, M. F. J. Schoodergang and J. Reedijk, *Inorg. Chim. Acta*, **130**, 235(1987).

133. G. Vos, J. G. Hassnoot, G. C. Verschoor and J. Reedijk, *Inorg. Chim. Acta*, **102**, 187(1985).

134. L. R. Groeneveld, R. A. LeFebre, R. A. G. deGraaff, J. G. Hassnoot, G. Vos and J. Reedijk, *Inorg. Chim. Acta*, **102**, 69(1985).

135. F. S. Keij, R. A. G. deGraaff, J. G. Hassnoot and J. Reedijk, *J. Chem. Soc., Dalton Trans.*, 2093(1984).

136. L. Rosenberg, L. K. Thompson, E. J. Gabe and F. L. Lee, *J. Chem. Soc., Dalton Trans.*, 625(1986).

137. P. W. Ball and A. B. Blake, *J. Chem. Soc., Dalton Trans.*, 852(1974).

138. J. E. Andrew and A. B. Blake, *J. Chem. Soc., Dalton Trans.*, 1408(1969).

139. P. W. Ball and A. B. Blake, *J. Chem. Soc., Dalton Trans.*, 1415(1969).

140. A. Escuer, R. Vicente, B. Mernari, A. E. Gueddi and M. Pierrot, *Inorg. Chem.*, **36**, 2511 (1997).

141. T. Wen, L. K. Thompson, F. L. Lee and E. J. Gabe, *Inorg. Chem.*, **27**, 4190(1988).

142. C. Owens, R. S. Drago, I. Bertini, C. Luchinat and L. Banci, *J. Am. Chem. Soc.*, **108**, 3298(1986).

143. A. Dei, D. Gatteschi and E. Piergentili, *Inorg. Chem.*, **18**, 89(1979).

144. A. El-Dissouky and G. B. Mohamad, *Inorg. Chim. Acta*, **162**, 263(1989).

145. a). P. D. W. Boyd, M. Gerloch and G. M. Sheldrick, *J. Chem. Soc., Dalton Trans.*, 1097(1974).

b). J. Saroja, V. Manivannan, P. Chakraborty and S. Pal, *Inorg. Chem.*, **34**,3099(1995).

146. D. Philp and J. F. Stoddart, *Angew. Chem. Int. Ed. Engl.*, **35**, 1155(1996).

147. E. C. Constable, *Prog. Inorg. Chem.*, **42**, 67(1994).

148. E. C. Constable, A. J. Edwards, M. J. Hannon and P. R. Raithby, *J. Chem. Soc. Chem. Commun.*, 1991(1994).

149. M. Albrecht, H. Roettele and P. Burger, *Chem. Eur. J.*, **2**, 1264(1996).

150. E. C. Constable, S. M. Elder, M. J. Hannon, A. Martin, P. R. Raithby and D. A. Tocher, *J. Chem. Soc., Dalton Trans.*, 2423(1996).

151. E. C. Constable, M. J. Hannon , A. J. Edwards and P. R. Raithby, *J. Chem. Soc. Chem. Commun.*, 2669(1994).

152. J. -M. Lehn, *Supramolecular Chemistry - Concepts and Persperctives*, VCH, Weinheim 1995.

153. A. F. Williams, *Pure Appl. Chem.*, **68**, 1285(1996).

154. C. Piguet, G. Bernardinelli, B. Bocguet, A. Quattropani and A. F. Williams, *J. Am. Chem. Soc.*, **114**, 7440(1992).

155. M. Albrecht and R. Frohlich, *J. Am. Chem. Soc.*, **119**, 1656(1997).

156. Z. Xu, L. K. Thompson, D. O. Miller, J. Clase, J. A. K. Howard and A. E. Goeta, *Inorg. Chem.*, 1998, in press.

157. B. Kersting, M. Myer, R. E. Powers and K. N. Raymond, *J. Am. Chem. Soc.*, **118**, 7221(1996).

158. M. J. Hannon, C. L. Painting, A. Jackson, J. Hamblin and W. Errington, *J. Chem. Soc. Chem. Commun.*, 1087(1997).

159. N. Yoshida and K. Ichikawa, *J. Chem. Soc. Chem. Commun.*, 1091(1997).

160. L. J. Charbonnière, M. -F. Gilet, K. Berbauer and A. F. Williams, *J. Chem. Soc. Chem. Commun.*, 39(1996).

161. E. Fleischer and S. Hawkinson, *J. Am. Chem. Soc.*, **89**, 720(1967).

162. G. J. Palenik, D. J. Wester, U. Rychlewska and R. C. Palenik, *Inorg. Chem.* **15**, 1814(1976).

163. A. B. P. Lever, J. Lewis and R. S. Nyholm, *J. Chem. Soc.*, 1187(1964).

164. A. B. P. Lever, *Inorganic Electronic Spectroscopy*, Elsevier, New York, 1984.

165. O. Kahn, *Advances In Inorganic Chemistry*, **43**,179(1995).

166. V. L. Pecoraro, A. J. Stemmler, B. R. Gibney, J. J. Bodwin, H. Wang, J. W. Kampf and A. Barwinski, *Progress in Inorganic Chemistry*, **45**, 83(1997).

167. K. S. Murray, *Advances In Inorganic Chemistry*, **43**, 261(1995).

168. P. Knuuttila, *Inorg. Chim. Acta*, **58**, 201(1982).

169. L. K. Thompson, A. W. Hanson and B. S. Ramaswamy, *Inorg. Chem.*, **23**, 2459(1984).

170. C. G. Barraclough and M. L. Tobe, *J. Chem. Soc., 1993*(1961).

171. J. Korvenranta, *Suom, Kemistil. B*, **46**, 240(1973).

172. H. Endres, D. Nothe, E. Rossato and W. E. Hatfield, *Inorg. Chem.*, **23**, 3467(1984).

173. S. L. Lambert, T. R. Felthouse and D. N. Hendrickson, *Inorg. Chim. Acta*, **L223**, 29(1978).

174. H. Ōkawa, M. Koikawa and S. Kida, *J. Chem. Soc., Dalton Trans.*, 469(1990).

175. P. Chaudhuri, M. Winter, U. Flörke and H. -J. Haupt, *Inorg. Chim. Acta*, **232**, 125(1995).

176. C. Krebs, M. Winter, T. Weyhermüller, E. Bill, K. Wieghardt and P. Chaudhuri, *J. Chem. Soc. Chem. Commun.*, 1913(1995).

177. W. P. Griffith and T. D. Wickens, *J. Chem. Soc.*, A, 400(1968).

178. W. R. Scheidt, C. -C. Tsai and J. L. Hoard, *J. Am. Chem. Soc.*, **93**, 3867(1971).

179. R. R. Ryan, S. H. Mastin and M. J. Reisfeld, *Acta Crystallogr., Sect B*, **25**, 1270(1971).

180. F. A. Cotton and G. Wilkinson, *Advanced Inorganic Chemistry*, 4th Ed. Wiley, Toronto. 1980.

181. a). D. Clark, *J. Chem. Soc.*, 1615(1952).

b). N. N. Greenwood and A. Earnshaw, *Chemistry of the Elements*, Pergamon Press, 1984.

182. J. A. Real, M. Moller, R. Ruiz, J. Faus, F. Lloret, M. Julve and M. Philoche-Levisalles, *J. Chem. Soc., Dalton Trans.*, 1483(1993).

183. H. Okawa, N. Matsumoto, M. Koikawa and S. Kida, *J. Chem. Soc., Dalton Trans.*, 1383(1990).

184. Y. Journaux, O. Kahn, J. Zarembowitch, J. Galy and J. Jaud, *J. Am. Chem. Soc.*, **105**, 7585(1983).

185. I. Morgenstern-Badarau and H. H. Wickman, *Inorg. Chem.*, **24**, 1889(1985).

186. I. Morgenstern-Badarau , D. Laroque, E. Bill, H. Winkler, A. X. Trautwein , F. Robert and Y. Jeannin, *Inorg. Chem.*, **30**, 3180(1991).

187. G. P. Gupta, G. Lang, L. A. Koch, B. Wang, W. R. Scheidt and C. A. Read, *Inorg. Chem.*, **29**, 4234(1990).

188. D. B. Brown Ed., *Mixed-valance Compounds, Theory and Applications in Chemistry, Physics, Geology and Biology*, Reidel Publishing Co., Boston, 1980.

189. G. Blondin and J. J. Girerd, *Chem. Rev.*, **90**,1359(1990).

190. M. C. Feiters, *Comm. Inorg. Chem.*, 11, 131(1990).

191. E. I. Solomon, M. J. Baldwin and M. D. Lowery, *Chem. Rev.*, **92**, 521(1992).

192. K. Fukuyama, T. Hase, S. Matsumoto, T. Tsukihara, Y. Katsube, N. Tanaka, M. Kakudo, K. Wada and H. Matsubara, *Nature*, **286**, 522(1980).

193. R. H. Holm and J. A. Ibers, *Science*, **209**, 223(1980).

194. C. R. Kissinger, E. T. Adman, L.C. Sieker and L. H. Jensen, *J. Am. Chem. Soc.*, **110**, 8721(1988).

195. J. M. Berg and R. H. Holm, In "*Metal Ions in Biology*", T.G. Spiro Ed., Interscience, New York, 1988, Vol. 4, Chapter 2.

196. T. O'Sullivan and M. M. Millar, *J. Am. Chem. Soc.*, **107**, 4096(1985).

197. V. Papaefthymiou, M. M. Millar and E. Munck, *Inorg. Chem.*, **25**, 3010(1986).

198. G. W. Brudvig, W. F. Beck and J. C. de Paula, *Annu. Rev. Biophys. Chem.*, **18**, 25(1989).

199. G. N. George, R. C. Prince and S. P. Cramer, *Science*, **243**, 789(1989).

200. A. W. Rutherford, *Trends Biol. Sci.*, **14**, 227(1989).

201. J. B. Vincent and G. Christou, *Adv. Inorg. Chem.*, **33**, 197(1988).

202. M. B. Robin and P. Day, *Adv. Inorg. Chem. Radiochem.*, **10**, 247(1967).

203. S. Andersson and S. Jagner, *Acta Chem. Scand.*, **A42**, 691(1988).

204. W. Xukun, Z. Mingjie, W. Jitao, W. Ruji and Y. Xinkai, *J. Struct. Chem.*, **7**, 142(1988).

205. G. A. Bowmaker, A. Camus, B. W. Skelton and A. H. White, *J. Chem. Soc., Dolton trans.*, 727(1990).

206. S. Andersson and S. Jagner, *Acta Chem. Scand.*, **41A**, 230(1987).

207. A. Bencini and F. Mani, *Inorg. Chim. Acta*, **87**,L9(1984).

208. W. Clegg, J. R. Nichoson, D. Collison and C. D. Garner, *Acta. Crystallogr.*, **C44**, 453(1988).

209. B. Scott and R. Willett, *Inorg. Chem.*, **30**, 110(1991).

210. G. A.Nicholson, C. R. Lazarus and B. J. McCormick, *Inorg. Chem.*, **19**,192(1980).

211. H. Huang, F. Kai, Y. Asai, M. Hirohata and M. Nakamura, *Chem. Lett.*, 65(1991).

212. L. Cambi and L. Szego, *Ber. Dich. Chem. Ges.*, **64**, 2591(1931); **66**, 656(1933).

213. A. H. Eward, R. L. Martin, E. Sinn and A.H. White, *Inorg. Chem.*, **8**, 1837(1969).

214. K. Stahl and I. Ymén, *Acta Chem. Scand.*, **A37**, 729(1983) .

215. M. S. Haddad, W. D. Federer, M. W. Lynch and D. N. Hendrickson, *J. Am. Chem. Soc.*, **102**, 1468(1980).

216. M. S. Haddad, M. W. Lynch, W. D. Feddrer and D.N. Hendrickson, *Inorg. Chem.*, **20**, 123(1981).

217. M. S. Haddad, W. D. Federer, M. W. Lynch and D.N. Hendrickson, *Inorg. Chem.*, **20**, 131(1981).

Appendix L Variation of Cu-N-N-Cu Dihedral Angle in Model Complex 1

```
$ Cu2(pahap)cl4 rotate
 22  0DIST    2  7
60.,70.,80.,90.,100.,110.,120.
240.,250.,260.,270.,280.,290.,300.
0.,0.,0.,DU
 -1  1 N   0.715,180.,0.
 -1  2 N   0.715,0.,0.
  1  3CU   2.0,120.,0.
  2  4CU   2.0,120.,1000.
  3  5CL   2.25,180.,0.
  4  6CL   2.25,180.,180.
  3  7CL   2.25,90.,0.
  3  8 N   2.0,90.,180.
  4  9CL   2.40,90.,0.
  4 10 N   2.0,90.,180.
  1 11 C   1.3,120.,180.
  2 12 C   1.3,120.,2000.
 11 13 H   0.94,120,0.
 11 14 H   0.94,120,180.
 12 15 H   0.94,120,0.
 12 16 H   0.94,120,180.
  8 17 H   1.02,112.,180.
  8 18 H   1.02,112.,0.
  8 19 H   1.02,112.,90.
 10 20 H   1.02,112.,180.
 10 21 H   1.02,112.,0.
 10 22 H   1.02,112.,90.
```

Appendix II. Variation of Cu-N-N-Cu Dihedral Angle in Model Complex 2

```
$ Cu2(pahap)Br4 rotate
 22  0DIST    2  6
60.,70.,80.,90.,100.,110.
240.,250.,260.,270.,280.,290.
0.,0.,0.,DU
 -1  1 N   0.715,180.,0.
 -1  2 N   0.715,0.,0.
  1  3CU   2.0,120.,0.
  2  4CU   2.0,120.,1000.
  3  5BR   2.40,180.,0.
  4  6BR   2.40,180.,180.
  3  7BR   2.40,90.,0.
  3  8 N   2.0,90.,180.
  4  9BR   2.40,90.,0.
  4 10 N   2.0,90.,180.
  1 11 C   1.3,120.,180.
  2 12 C   1.3,120.,2000.
 11 13 H   0.94,120,0.
 11 14 H   0.94,120,180.
 12 15 H   0.94,120,0.
 12 16 H   0.94,120,180.
  8 17 H   1.02,112.,180.
  8 18 H   1.02,112.,0.
  8 19 H   1.02,112.,90.
 10 20 H   1.02,112.,180.
 10 21 H   1.02,112.,0.
 10 22 H   1.02,112.,90.
```

Appendix III. Variation of Cu-N-N-Cu Dihedral Angle in Model Complex 3

```
$ Cu2(pahap) rotate
 30  4DIST  0  0  0
0.,0.,0.,DU
 -1  1 N   0.715,180.,0.
 -1  2 N   0.715,0.,0.
  1  3CU   2.0,120.,0.
  2  4CU   2.0,120.,155.
  3  5 O   1.95,180.,0.
  4  6 O   1.95,180.,180.
  3  7 O   1.98,90.,0.
  3  8 N   2.0,90.,180.
  4  9 O   1.98,90.,0.
  4 10 N   2.0,90.,180.
  1 11 C   1.3,120.,180.
  2 12 C   1.3,120.,335.
 11 13 H   0.94,120,0.
 11 14 H   0.94,120,180.
 12 15 H   0.94,120,0.
 12 16 H   0.94,120,180.
  8 17 H   1.02,112.,180.
  8 18 H   1.02,112.,0.
  8 19 H   1.02,112.,90.
 10 20 H   1.02,112.,180.
 10 21 H   1.02,112.,0.
 10 22 H   1.02,112.,90.
  5 23 H   0.93,120.,45.
  5 24 H   0.93,120.,135.
  7 25 H   0.93,120.,45.
  7 26 H   0.93,120.,135.
  6 27 H   0.93,120.,45.
  6 28 H   0.93,120.,135.
  9 29 H   0.93,120.,45.
  9 30 H   0.93,120.,135.
```

Appendix IV. Magnetic Moment vs. Temperature Data of Complex 40

T(K)	μ(BM)
4.010492324829102	5.586578845977783
7.940032482147217	5.213029384613037
10.85771560668945	5.150508880615234
15.57092761993408	5.037305355072021
20.39982223510742	4.959061622619629
25.43278884887695	4.912238121032715
30.45068359375	4.873547554016113
35.16568374633789	4.850412368774414
39.9327507019043	4.829337120056152
44.71278762817383	4.819337368011475
49.43575286865234	4.809353351593018
53.20673370361328	4.804387092590332
58.02073669433594	4.799537181854248
62.82270050048828	4.794541358947754
67.63068389892578	4.798819065093994
72.45671844482422	4.797260761260986
77.27071380615234	4.802405834197998
82.10276794433594	4.810930252075195
90.50921630859375	4.827937602996826
100.7329483032227	4.843751430511475
110.9747314453125	4.851213932037354
121.1984710693359	4.862908840179443
131.4582977294922	4.878834247589111
141.6579742431641	4.895988464355469
160.9259948730469	4.925793647766113
181.3915252685547	4.942158222198486
201.8510131835938	4.961419105529785
222.3045043945312	4.989858150482178
242.7760314941406	4.988963603973389
263.2355346679688	5.003232955932617
283.111328125	5.02127742767334
295.1343078613281	5.021476745605469